AD NUMBER
AD377468
CLASSIFICATION CHANGES
TO: **UNCLASSIFIED**
FROM: **CONFIDENTIAL**
LIMITATION CHANGES
TO: **Approved for public release; distribution is unlimited.**
FROM: **Distribution authorized to U.S. Gov't. agencies and their contractors; Critical Technology; NOV 1966. Other requests shall be referred to Space Systems Division (SSD), Attn: SSBS, Los Angeles Air Force Station, Air Force Unit Post Office, Los Angeles, CA 90045. This document contains export-controlled technical data.**
AUTHORITY
AFRPL ltr dtd 7 May 1973 AFRPL ltr dtd 7 May 1973

GENERAL DECLASSIFICATION SCHEDULE

IN ACCORDANCE WITH
DOD 5200.1-R & EXECUTIVE ORDER 11652

THIS DOCUMENT IS:

Subject to General Declassification Schedule of Executive Order 11652-Automatically Downgraded at 2 Years Intervals- DECLASSIFIED ON DECEMBER 31, 1972

BY

Defense Documentation Center
Defense Supply Agency
Cameron Station
Alexandria, Virginia 22314

SECURITY MARKING

The classified or limited status of this report applies to each page, unless otherwise marked.
Separate page printouts MUST be marked accordingly.

THIS DOCUMENT CONTAINS INFORMATION AFFECTING THE NATIONAL DEFENSE OF THE UNITED STATES WITHIN THE MEANING OF THE ESPIONAGE LAWS, TITLE 18, U.S.C., SECTIONS 793 AND 794. THE TRANSMISSION OR THE REVELATION OF ITS CONTENTS IN ANY MANNER TO AN UNAUTHORIZED PERSON IS PROHIBITED BY LAW.

NOTICE: When government or other drawings, specifications or other data are used for any purpose other than in connection with a definitely related government procurement operation, the U. S. Government thereby incurs no responsibility, nor any obligation whatsoever; and the fact that the Government may have formulated, furnished, or in any way supplied the said drawings, specifications, or other data is not to be regarded by implication or otherwise as in any manner licensing the holder or any other person or corporation, or conveying any rights or permission to manufacture, use or sell any patented invention that may in any way be related thereto.

AFRPL-TR-66-315

TE2-237-11-6
Copy No. 20

DEVELOPMENT AND DEMONSTRATION OF AN OMNIAXIAL FLEXIBLE SEAL MOVABLE NOZZLE FOR THRUST VECTOR CONTROL (U)

QUARTERLY TECHNICAL REPORT NO. 1

CONTRACT AF 04(611)-11643

November 1966

Prepared for

AIR FORCE
ROCKET PROPULSION LABORATORY
RESEARCH AND TECHNOLOGY DIVISION
AIR FORCE SYSTEMS COMMAND
Edwards, California

THIOKOL CHEMICAL CORPORATION
WASATCH DIVISION
Brigham City, Utah

SPECIAL NOTICES

Qualified users may obtain copies of this report from the Defense Documentation Center.

Do not return this copy. When not needed, destroy in accordance with pertinent security regulations.

In addition to security requirements which must be met, this document is subject to special export controls and each transmittal to foreign nationals may be made only with prior approval of SSD (SSBS) Los Angeles Air Force Station, Air Force unit post office, Los Angeles, California, 90045.

AFRPL-TR-66-315 TE2-237-11-6

DEVELOPMENT AND DEMONSTRATION OF AN OMNIAXIAL FLEXIBLE SEAL MOVABLE NOZZLE FOR THRUST VECTOR CONTROL (U)

QUARTERLY TECHNICAL REPORT NO. 1

CONTRACT AF 04(611)-11643

November 1966

Prepared by

THIOKOL CHEMICAL CORPORATION
WASATCH DIVISION
Brigham City, Utah

C. G. Kennedy, Manager
Space Booster Development

Publications No. 1166-13094 0416-64-1103

FOREWORD

This quarterly technical report covers the work performed under Contract AF 04(611)-11643, "Development and Demonstration of an Omniaxial Flexible seal Movable Nozzle for Thrust Vector Control," for the period 11 Jul thru 31 Oct 1966.

This program is under the technical direction of John B. Schmuck, 1/LT, USAF, Project Engineer RPMMS, Air Force Rocket Propulsion Laboratory, Edwards AFB, California. Mr. Thomas Walker is the Wasatch Division Program Manager for Thiokol Chemical Corporation. Mr. Blen D. Nance is the Project Engineer for the Wasatch Division.

Publication of this report does not constitute Air Force approval of the report's findings or conclusions. It is published only for the exchange and stimulation of ideas.

TABLE OF CONTENTS

TABLE OF CONTENTS (Cont)

TABLE OF CONTENTS (Cont)

TABLE OF CONTENTS (Cont)

LIST OF ILLUSTRATIONS

LIST OF ILLUSTRATIONS (Cont)

LIST OF ILLUSTRATIONS (Cont)

LIST OF ILLUSTRATIONS (Cont)

LIST OF ILLUSTRATIONS (Cont)

LIST OF TABLES

SECTION I

INTRODUCTION AND SUMMARY

A. INTRODUCTION

This quarterly technical report reviews the effort accomplished by Thiokol Chemical Corporation between 11 Jul and 31 Oct 1966 for the Air Force Rocket Propulsion Laboratory under Contract AF 04(611)-11643. The primary objective of this program is the development and demonstration static test firing of an omniaxial flexible seal movable nozzle using a monolithic steel case, one million pound thrust class, 156 in. diameter motor, designated 156-9, as the test vehicle.

The flexible seal movable nozzle will consist of a fixed housing attached to the motor case and a movable housing interconnected by means of a flexible seal as shown in Figure 1-1. The flexible seal will be fabricated using two end rings connected by alternate layers of elastomer and steel shims.

The demonstration motor will incorporate a slotted, cylindrically perforated (CP) grain and a head end ignition system. The 156-9 motor is designed to operate for approximately 66 sec and produce a 67.7 x 10^6 lbf-sec of impulse.

This report presents a discussion of progress to date on the following major areas of the program.

1. Nozzle and flexible seal design and fabrication.
2. Motor design and fabrication, including liner and insulation, propellant and grain, ignition system, and TVC actuation system.

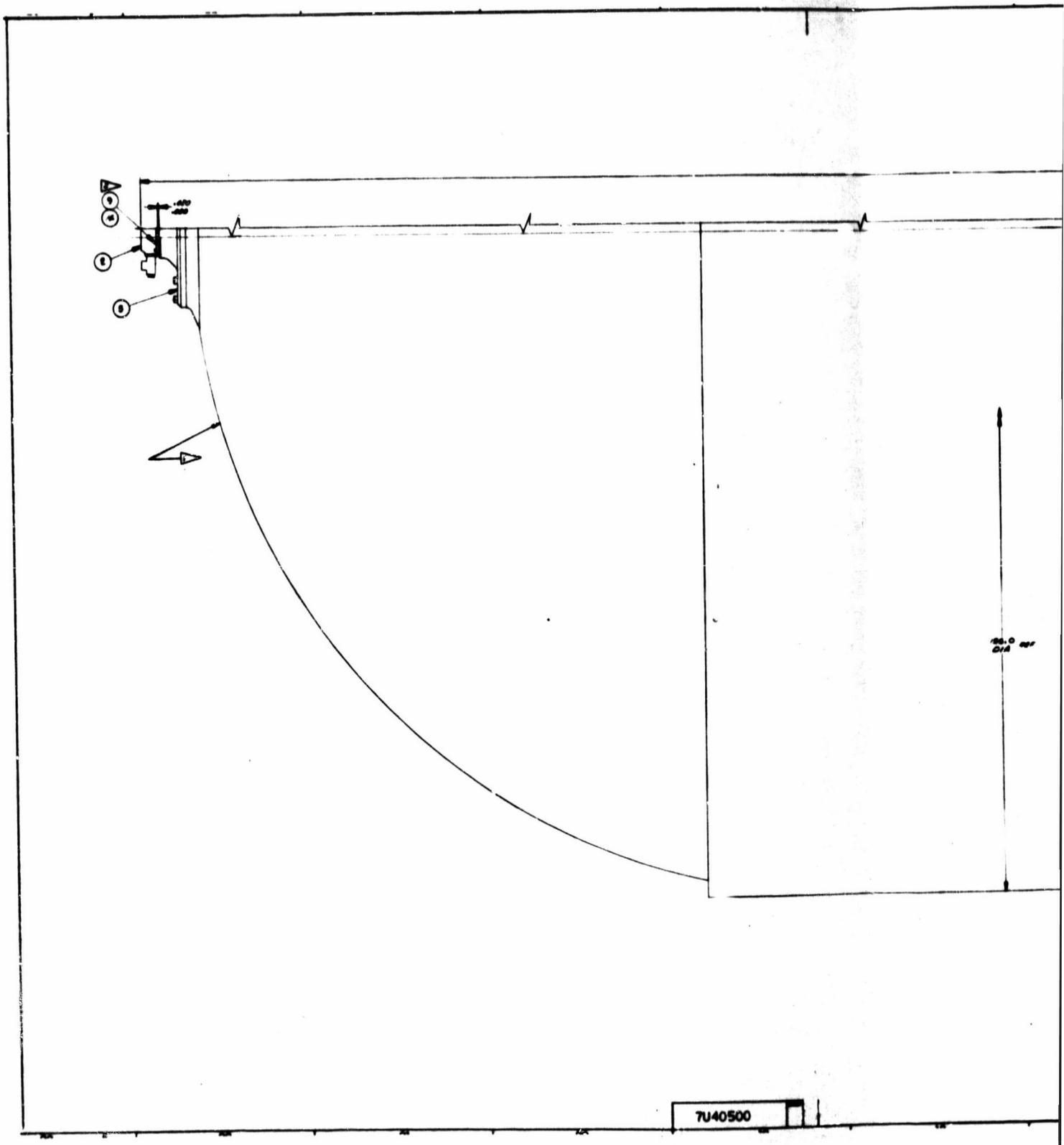
7U40500

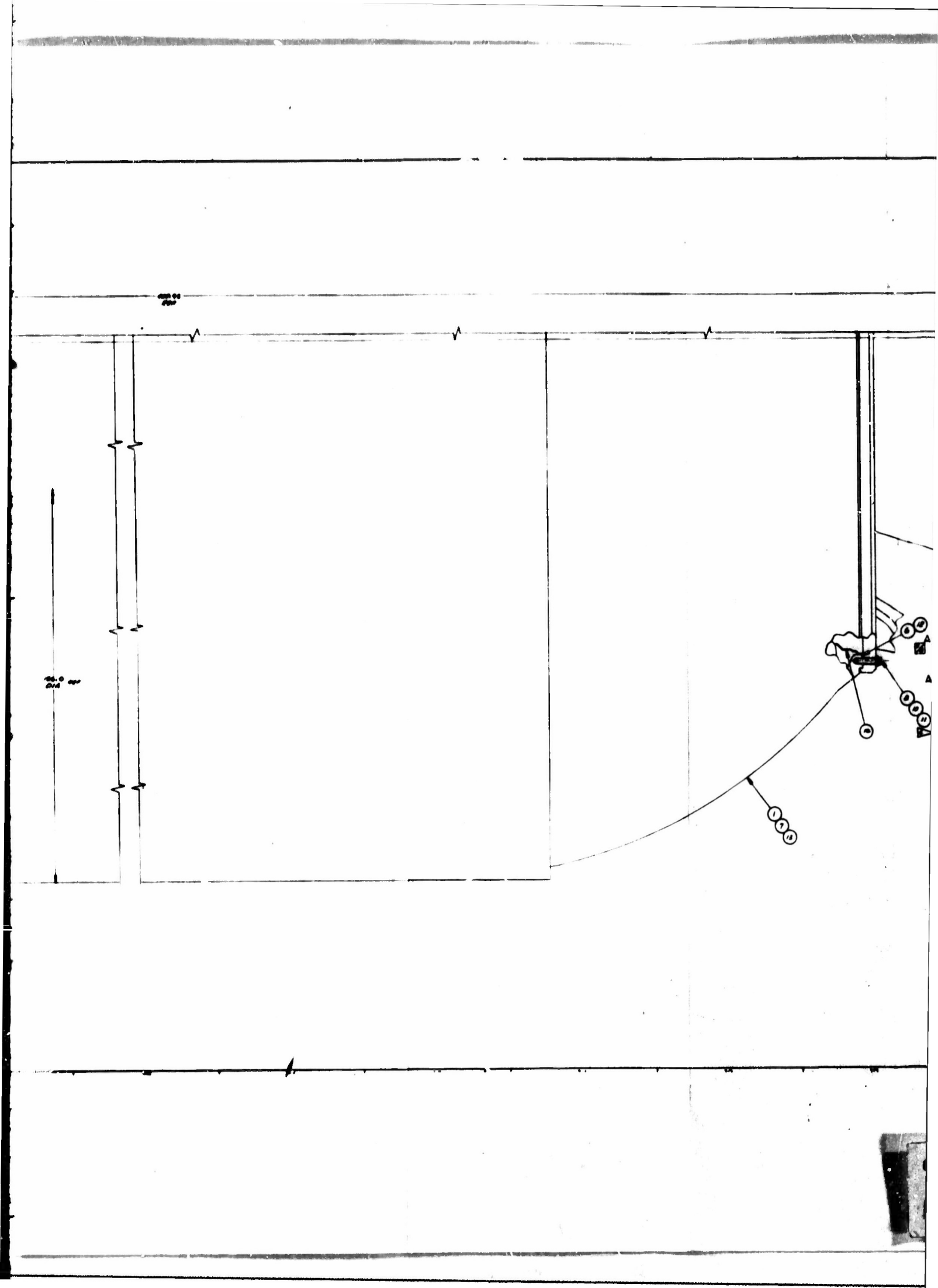

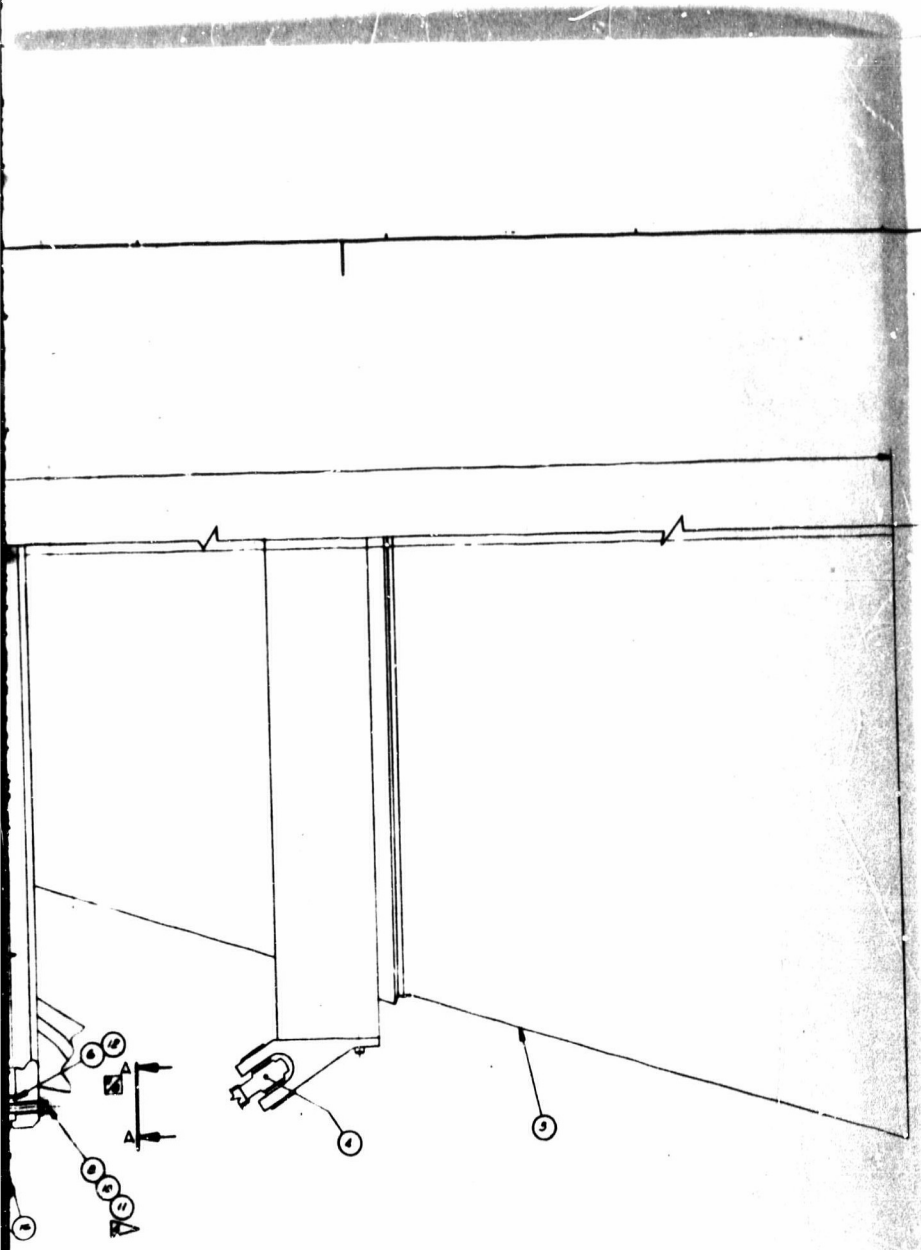

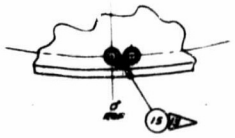

VIEW A-A

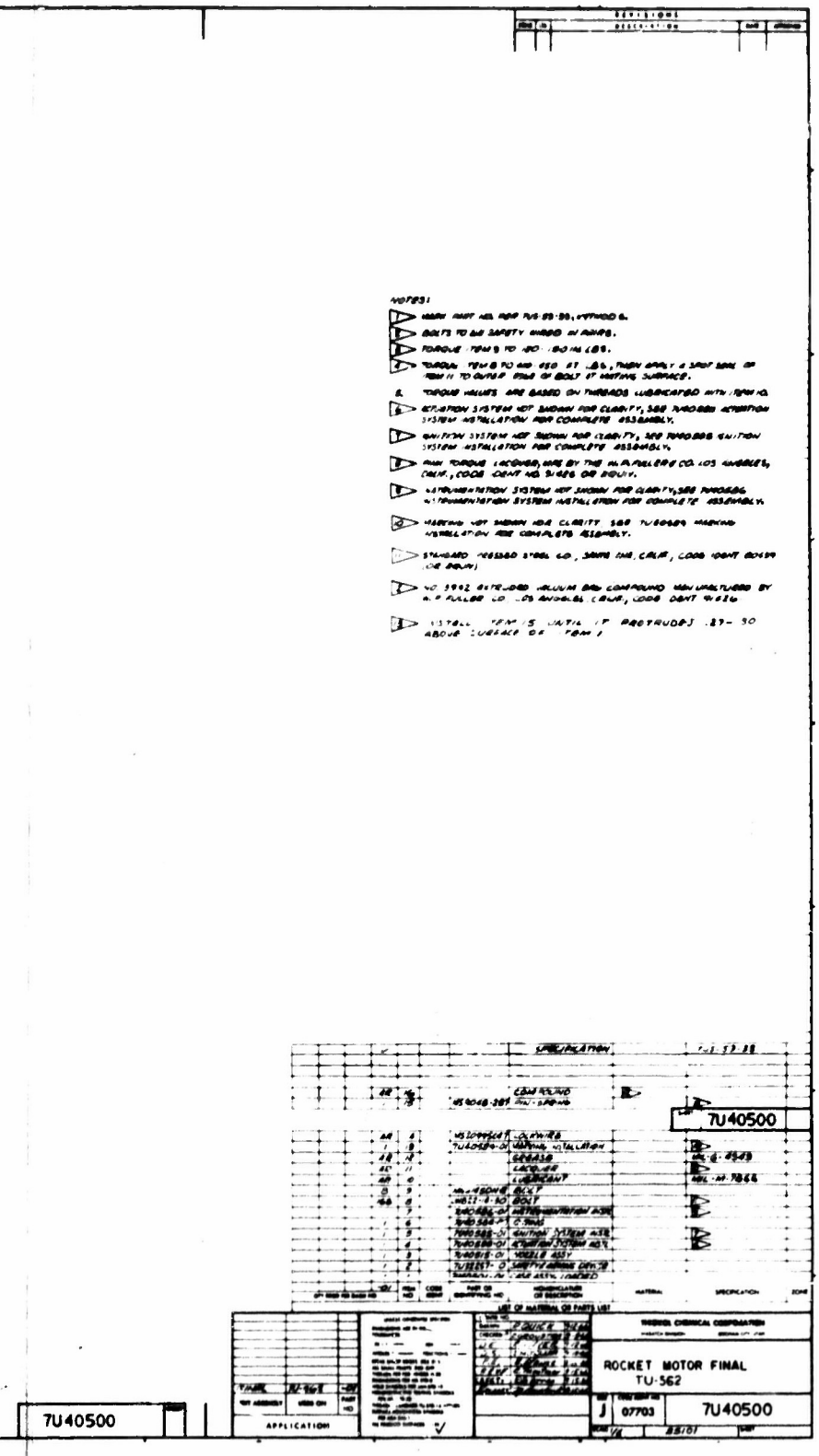

Figure 1-1. 156-9 Motor Design

B. SUMMARY

Work on major areas was completed during this quarter in accordance with the program schedule (Figure 11-1). Motor and component design documentation listed below was submitted to AFRPL during this report period for review and approval.

1.	156-9 Program Schedule	19 Aug 1966
2.	156-9 Nozzle Design	22 Sep 1966
3.	156-9 Grain/Propellant Design	22 Sep 1966
4.	156-9 Insulation and Flap Assembly Design and Liner Design	22 Sep 1966
5.	156-9 Nozzle Duty Cycle	26 Sep 1966
6.	156-9 Ignition System Design	30 Sep 1966
7.	156-9 Final Rocket Motor Design	22 Sep 1966
8.	Insulation Design Information	6 Oct 1966
9.	Liner and Insulation Verification Test Plan	11 Oct 1966
10.	Igniter System Test Plan	18 Oct 1966
11.	Ignition System Design Information	25 Oct 1966
12.	Flexible Seal Test Plan	26 Oct 1966
13.	TVC Actuation System Design	10 Nov 1966
14.	TVC Actuation System Test Plan	10 Nov 1966

The following design approvals were received during this reporting period:

1.	Nozzle, Exhaust, Rocket Motor, Drawing No. 7U40515	12 Oct 1966
2.	Propellant/Grain Design	17 Oct 1966
3.	Ignition System Design Drawing No. 7U40585	17 Oct 1966
4.	Insulation and Liner Design Drawing No. 7U40502	24 Oct 1966

This report reflects the nozzle material design change which was directed by AFRPL at the end of this report period.

In order that all approval submittals can be covered by this report, approval submittal of the TVC actuation system, which was actually completed in early November, has also been covered.

The nozzle design and performance analyses were completed and a nozzle fabrication contract was awarded to HITCO, Gardena, California. Nozzle design criteria included maximum utilization of 156-6 nozzle tooling, providing an envelope for the flexible seal installation, and insuring structural and thermal reliability. Analyses completed include aerodynamic, thermal, and structural. Material selection also was completed. The resulting nozzle has a 34.6 in. throat diameter, an overall length of 116.1 in. and an expansion ratio of 8.15 to 1. The total nozzle weight is calculated to be 13,517 pounds. Nozzle fabrication is on schedule with no problems encountered to date. Nozzle delivery to Thiokol is scheduled for February, 1967.

Flexible seal design effort to date has been directed toward Thiokol sponsored seal which will be fabricated and bench tested to destruction to obtain design data for the 156-9 motor seal. The seal design uses eighty-eight 0.036 in. thick stainless steel shims separated by 0.025 in. thick layers of polyisoprene rubber. The Thiokol sponsored seal end rings and shims are being fabricated. Ball bearing spacers and polyisoprene rubber have been ordered. Results of the Thiokol test plus data from tests on seals for a Thiokol 100 in. motor and POSEIDON motors will be used in the final design of the 156-9 motor seal.

The 156-9 motor case will be insulated with 3,059 lb of TI-H704B insulation, a Thiokol formulated mastic (asbestos filled HC polymer). A conservative insulation design performs its function by providing thermal protection to the case so the case material is not heated above ambient temperature during motor operation. The insulation design includes stress relief flaps at each end of the large forward portion of the propellant grain. The stress relief flaps are fiberglass fabric reinforced TI-H704B insulation.

The insulated case will be coated with 0.035 in. of TL-H714A liner and a carbon black filled HC polymer. This material uses the same binder as the insulation and the TP-H1115 propellant. Use of the common binder assures bond compatibility between the propellant grain and the insulation. A compatibility program is in progress to verify the bond adequacy.

A PBAA type propellant (designated TP-H1115) was selected for the 156-9 motor. The TP-H1115 propellant is essentially the same as propellant used extensively by Thiokol in large motor programs conducted to date. Propellant materials are inhouse and characterization is in progress. Target values for the propellant standardization are a modulus of 400 to 500 psi and a burning rate of 0.767 in./sec at 700 psia. The propellant grain is a 64 percent web fraction, slotted, cylindrically perforated design. This grain design is the same as that used in the 156-6 motor except that the aft port diameter has been increased to accomodate the submerged portion of the movable nozzle. The 277,775 lb of propellant will produce an average thrust of 999,020 lb for 66.6 sec at an average pressure of 687 psia. A total impulse of 66,534,800 lb/sec is predicted.

The ignition system for the 156-9 motor will be a head end PYROGEN igniter which is being developed for the 156-8 motor. An ignition system verification test will be conducted under the 156-8 motor program.

The 156-9 thrust vector control system consists of two specially adapted linear hydraulic servoactuators operated by a ground hydraulic power supply and an external electronic control system. The actuators are standard heavy duty industrial units modified to allow mounting of the servovalves and transducers. The servovalves are three stage industrial units with linear variable differential transformer (LVDT) feedback on the third stage spool. The manifold provides straight through porting to one side of the actuator and two hydraulic lines to the other. A standard LVDT is mounted inside the piston rod to insure minimum exposure hazard and to minimize the length of the assembly. The servoactuators are being assembled and checked out by Ling-Temco-Vought, Inc, Dallas, Texas.

Modification and fabrication of process and test tooling is in progress. Major items of process tooling include core modification, propellant casting aids, vacuum dome adapter, slot former and casting hopper adapter base. Test tooling required includes drill rings, an assembly fixture, a bench test fixture, an anti-flight system, and a post-test carbon dioxide quench system for the motor.

A summary of the 156-9 component weights is shown in Table 1-1.

TABLE 1-1

MASS PROPERTIES DATA

MASS PROPERTIES DATA TU562 DMN 9-20-66

	WEIGHT (LBS)	CENTER OF GRAVITY LONG.	CENTER OF GRAVITY LAT.	CENTER OF GRAVITY VERT.	MOMENT OF INERTIA PITCH	MOMENT OF INERTIA ROLL	MOMENT OF INERTIA YAW
CASE	22193.015	270.541	100.000	100.000	51635.873	25908.800	51635.873
INSULATION	3059.552	307.579	100.000	100.000	8612.874	3160.247	8612.874
LINER	367.295	261.618	100.000	100.000	1189.981	357.160	1189.981
FLAPS	216.089	263.611	100.000	100.000	890.381	175.613	890.381
IGNITION SYSTEM	691.175	113.761	99.999	99.998	23.988	7.696	23.983
NOZZLE	13517.466	427.446	99.925	99.483	4464.753	3590.433	4392.644
PRIMER	44.960	259.689	100.000	100.000	106.176	51.557	106.176
TOTAL INERTS	40089.554	323.439	99.975	99.826	119123.841	33252.029	119051.221
PROPELLANT	277773.398	261.679	100.000	100.000	456131.590	194399.939	456131.590
TOTAL MOTOR	317862.949	269.469	99.997	99.978	604097.367	227652.203	604024.516
MASS FRACTION	.874						

SECTION II

NOZZLE AND FLEXIBLE SEAL DESIGNS

A. NOZZLE DESIGN

Detailed design analyses have been conducted on the nozzle for the 156-9 demonstration motor. Design criteria included maximum utilization of 156-6 nozzle tooling, providing an envelope for the flexible seal installation, and insuring structural and thermal reliability. Completed to date are aerodynamic, thermal, structural and weight analyses and materials selection, configuration and nozzle fabrication technique studies. This section presents the results of these analyses for the design of the 156-9 nozzle.

In designing the 156-9 nozzle, maximum use of recent developments in analytical techniques and test results from recent firings, especially the 156-6, was made. The design analyses show that program design objectives are achieved and that the 156-9 nozzle design will perform successfully.

1. COMPONENT CONFIGURATION AND MATERIALS SELECTION

a. Component Configuration--The nozzle concept design for the 156-9 rocket motor is a submerged omniaxis movable flexible seal. The concept appears particularly attractive in reducing the weight of nozzles capable of producing omniaxial movement. The philosophy behind the design of the 156-9 nozzle has been to provide a minimum risk test vehicle for the flexible seal at a minimum cost. For this reason the 156-9 nozzle design is based primarily on the successfully tested 156-6 nozzle design. The aerodynamic configuration from the nosetip to the exit

plane is identical to the 156-6, thus permitting the reuse of existing tooling. Modifications have been made to the 156-6 design where necessary to incorporate the flexible seal and to provide for the different flow conditions resulting from incorporation of the movable flexible seal.

The 156-9 nozzle design is shown in Figure 2-1. The submerged movable nozzle is capable of a plus or minus 4 deg omniaxial vectoring motion through a flexible seal adjoining the fixed and movable sections of the nozzle. The nozzle is actuated by two linear servoactuators mounted between the nozzle fixed housing and exit housing. The actuators are 90 deg apart; one actuates pitch motion and the other yaw motion. Intermediate angles of vector are accomplished by simultaneous combination motions.

The throat and exit diameters of the nozzle are 34.54 in. and 98.64 in., respectively, corresponding to an initial expansion ratio of 8.15. The overall length of the nozzle assembly, 47 percent of which is submerged, is 116.1 inches. The aerodynamic design of the internal nozzle surface from the nosetip to the exit plane is identical to the 156-6 nozzle. The nosetip is defined by a radius of 1.62 inches. An 8.00 in. radius joins the tip radius to a 15.00 in. radius into the throat. The throat and the 17.5 deg exit cone are joined by a radius of 13.859 inches.

Structural integrity and maintenance of the aerodynamic contour are provided by a mechanical design consisting of steel structural components, reinforced plastic erosion liners, and thermal insulators. Nozzle structural and insulation subassemblies are fabricated independently and bolted or bonded to form the complete nozzle assembly.

The nozzle fixed housing assembly consists of a steel structure protected by silica cloth phenolic insulation. The steel consists of two forged flanges welded to a conical section of roll and weld construction. The silica at the small end of the housing has an outer surface which, in the pressurized condition, will be spherical about the flexible seal pivot point. This surface forms the fixed part of the secondary barrier gap which protects the flexible seal from direct radiant heating and sharply reduces convective flow. Ply orientation of the silica tape is parallel to the nozzle

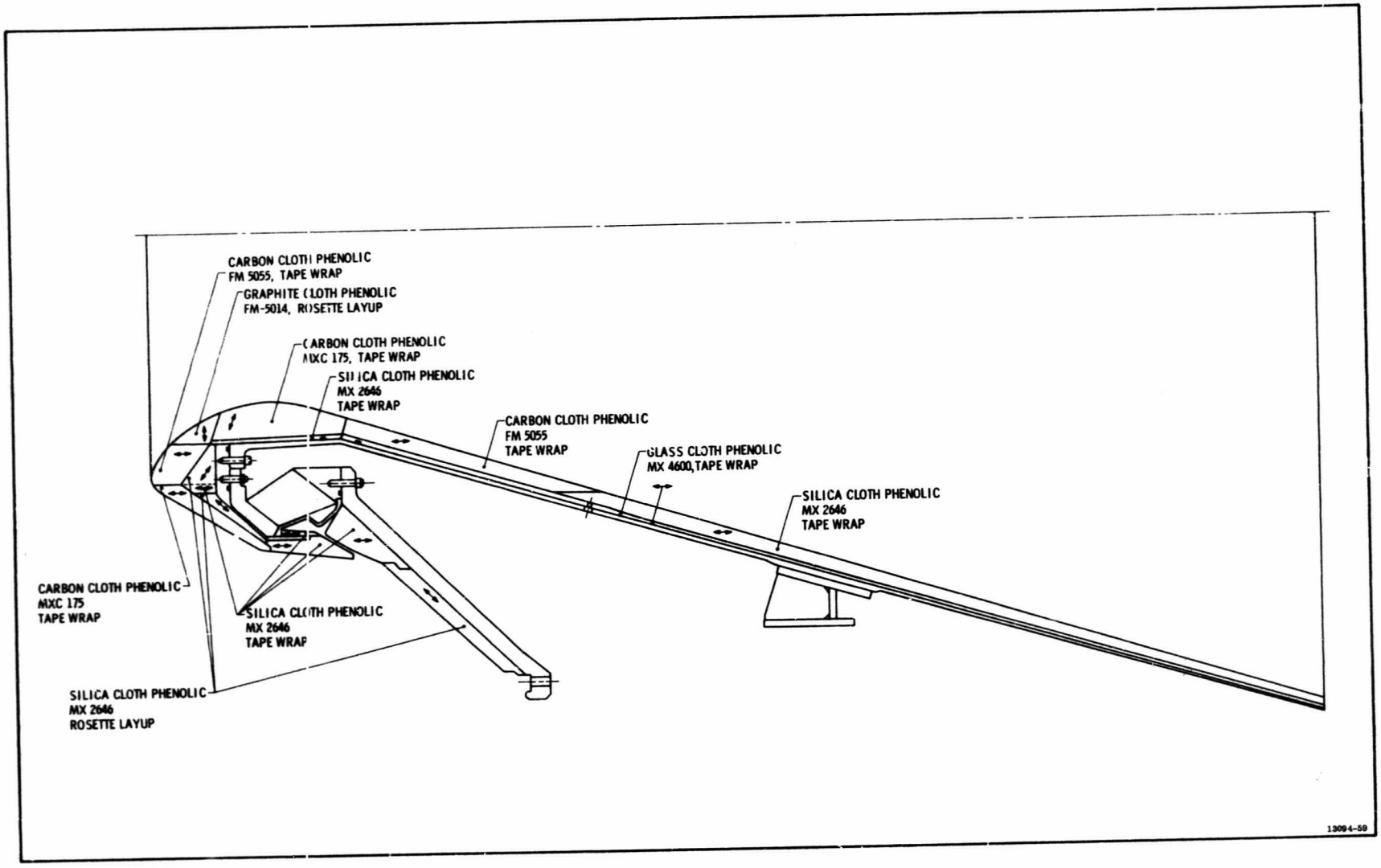

Figure 2-1. 156-9 Nozzle Design

centerline in order to provide a vent path between plies. The silica on the remainder of the exposed fixed housing surface is of rosette fabrication with the ply orientation parallel to the surface.

The two actuator support brackets bolt to clips on the fixed housing.

The movable part of the secondary barrier consists of a barrier assembly and a silica cloth phenolic ring which remains separate until assembly. The barrier assembly consists of a rolled and welded cylindrical steel ring and a silica cloth phenolic insulating ring bonded to its inner surface. The steel ring is attached to the seal forward end ring with set screws. Both the silica in the barrier assembly and the separate silica ring, which is bonded to the outer surface of the steel ring at final assembly, are tape wrapped parallel to the centerline.

The nose assembly consists of an entrance housing, two carbon cloth phenolic liners, a graphite cloth crossover ring, and two silica cloth phenolic insulators. The steel entrance housing is of roll and weld construction. The nose liner (backside or chamber side of the nose) is carbon cloth phenolic tape wrapped parallel to the centerline. Vent holes (proven helpful in the 156-7 and Thiokol TU-455-02 and TU-465) are provided on this surface. The entrance liner is also carbon cloth phenolic parallel to the centerline. The crossover ring is graphite cloth rosette with ply orientation 90 deg to the centerline. The silica cloth insulator behind the nose liner is a rosette layup with ply orientation parallel to the aft surface. The insulator behind the entrance liner is a combination of rosette layup and tape wrap, which enables the use of existing tooling.

The exit assembly consists of a steel shell, three liners, and two insulators. The forward ring of the shell is a ring forging; the remainder is of roll and weld fabrication. A reinforcing I-beam type structure girdles the aft exit cone to limit distortion during vectoring and distribute the actuator loads. The throat liner is a single piece carbon cloth tape wrap with ply orientation 70 degrees to the centerline. This is similar to the throats successfully tested on the 156-5, 156-7 and Thiokol TU-455.02 as well as the 260 Inch motor nozzles. An overwrap of silica phenolic tape insulates behind the throat liner.

The upper exit cone liner is carbon cloth phenolic tape wrapped parallel to centerline. This extends to an expansion ratio of 2.44 as in the 156-6 design. From this point to the exit the liner is silica phenolic tape, also wrapped parallel to centerline. Both liners are overwrapped with glass phenolic tape prior to final cure of the three components as an assembly. A row of retaining pins through the shell into the insulation is provided at an expansion ratio of 2.5 as a backup against bond failure.

b. Materials Configuration--The aerodynamic configuration of the 156-6 nozzle was selected for the 156-9 nozzle to provide a configuration proven reliable by test and almost identical environment. Materials to provide the aerodynamic contour, however, were not necessarily matched since a large number of materials have been qualified in large booster firings and similar environments. Therefore, selection was made from among all materials considered qualified in previous large booster firings.

Every material selected for use in the 156-9 nozzle has been qualified by previous successful static test in nozzles for motors having diameters of 120 in. or larger. Each material has been successfully tested with similar exhaust gas environment. Table 2-1 lists the materials selected for each nozzle component and the previous applicable experience.

All steel components are 4130 steel. This material was selected for its high strength, machinability, excellent welding properties, and heat treatment response.

Silica cloth phenolic has been selected as the liner material for the fixed housing and the projecting radiation barrier. Silica provides adequate erosion resistance in regions of moderate thermal severity and excellent insulation properties at a relatively low cost. The surfaces of the gap in the barrier are, therefore, also silica. Parallel-to-centerline orientation was selected for the silica on either side of the barrier gap to provide a large angle between the plies and the respective surfaces. Such an angle provides a natural out-gassing path which reduces blistering and

TABLE 2-1

MATERIAL USE HISTORY

Material	Vendor Designation	Use in TU-562	Previous Successful Experience
Carbon Cloth Phenolic	FM 5055	Upper exit liner	156-7, TU-465 Thiokol
		Entrance liner	
	MXC 175	Nose liner	156-5, 156-6
Graphite Cloth Phenolic	MXG 175	Throat liner	156-6
	FM 5014	Crossover ring	156-1, TU-465
Silica Cloth Phenolic	MX 2646	Fixed housing insulator	TITAN 3C Strap-on
		Barrier insulator	
		Nose insulator	
		Entrance insulator	
		Throat insulator	
		Lower exit cone liner	
Glass Cloth Phenolic	MXB 175-1584	Exit insulator	156-6

delamination of the surface to a minimum. The orientation of the silica on the remainder of the fixed housing is a rosette layup parallel to the housing surface.

Rubber insulators and mastic insulators were also analyzed for this application, but were found unsatisfactory due to high erosion rate predictions. Flow conditions in this region are more severe in the 156-9 design than the 156-6 because of the differing geometry which controls the flow patterns. The details of this tradeoff are contained in the aerodynamic analysis portion of Section II.

Fiberite Corporation MX 2648 silica cloth phenolic has been selected for the fixed housing and barrier plastic components. This material has been extensively tested in the Titan IIIC Program (Table 2-1) and it has performed successfully in all applications for which it is specified in the 156-9.

The relatively severe flow conditions on the chamber side of the nozzle also dictated the use of carbon cloth phenolic as the liner between the barrier and the tip of the nose. The thickness increases as the nosetip is approached reflecting the increasing flow velocities and resulting heat transfer. Carbon cloth provides excellent erosion resistance at moderate cost. Ply orientation is parallel to the centerline.

The entrance liner is of similar construction: carbon cloth phenolic oriented parallel to the centerline.

Fiberite MXC 175 has been selected for the nose liner; U. S. Polymeric FM-5055 has been selected for the upper exit cone liner. Both have substantial successful firing histories as given by Table 2-1.

The crossover ring which joins the entrance liner to the throat is graphite cloth phenolic, U.S. Polymeric FM 5014, fabricated in a rosette layup. This orientation, successfully tested in the 156-5, 156-6, 156-7 and the Thiokol TU-455 and TU-465 nozzles, provides desirable edge-orientation of plies to the gas stream along the entire exposed surface.

Carbon cloth phenolic, rosette layup, was also evaluated for the crossover ring. Graphite cloth phenolic was selected, however, because of the relatively poor performance of the carbon cloth rosette rings in the 156-5 and 156-6 programs. Graphite cloth rosette rings, by comparison, have performed well on the 156-1, 156-7, Thiokol TU-465 and TU-455 firings.

Silica cloth phenolic, Fiberite MX 2646, was selected for the insulators behind the nose and throat liners. This material combines excellent insulation properties with exceptionally high strength.

A single piece tape-wrapped throat was selected for the 156-9. A throat consisting of a series of rosette rings was also evaluated. The former design has been fired on the 156-5, 156-7, and the Thiokol TU-455.01. The latter design was utilized on the 156-6 and the Thiokol TU-455.02 and TU-465. The TU-465 throat performance was excellent and exhibited uniform, smooth, relatively low erosion. The other two rosette throats, however, exhibited gouging; high non-uniform erosion, and delamination. In contrast all three tape wrapped throats performed as well or better than the TU-465 rosette throat. The tape wrapped throat was, therefore, determined to be a more reliable design. The 70 deg to centerline angle used in the three listed firings was again selected. Graphite cloth was selected as the material for the throat based upon demonstrated successful performance in previous 156 Inch programs. MXG 175 graphite cloth phenolic was the particular material selected for the throat. MX 2646 silica cloth phenolic was selected as the insulator behind the throat.

The exit cone is identical to the 156-6 except for the increased thickness of liner adjacent to the throat. This increase, and the increase in thickness at the throat, resulted from higher erosion rates observed in the throat and upper exit cone of movable nozzles as compared to fixed nozzles. The transition from carbon cloth liner to silica cloth liner, both parallel to centerline, occurs at the same expansion ratio, 2.44. Glass cloth phenolic is also used as the insulator for the exit cone and is also parallel to centerline.

The particular materials selected for each component are U. S. Polymeric FM 5055 for the carbon cloth liner, Fiberite MX 2646 for the silica cloth liner, and Fiberite MXB 175-1584 for the glass cloth insulator. Table 2-1 indicates the qualification of each material.

2. FLEXIBLE SEAL LOCATION

The location of the flexible seal within the nozzle is significant. A thorough study of the optimum axial and radial location was conducted by Thiokol as part of the design studies for Project 3246 (100 inch motor) under Contract AF 04(694)-334. Various seal locations were investigated for a nozzle submerged 50 percent. The tradeoff study was among seal weight, seal torque, and fixed housing weight.

As the seal was moved closer to the throat, seal torque and weight were reduced, fixed housing weight increased. Results of the study for three locations are:

Seal Location	*Seal Torque (Percent)	*Total Nozzle Weight (Percent)
Throat	100	100
Midway	454	115
Case Flange	1,255	195

(*Seal torque and nozzle weight are given as percents of the value at the throat location.)

These comparisons and a study of the equations governing seal design and torque conclusively indicated that minimization of the seal diameter is desirable.

These studies indicate that the seal should be located immediately outside the nozzle throat at a point compatible with throat insulation and structural requirements and nozzle vectoring motions. The center of the seal should be as far upstream as is possible without increasing the size of the nose beyond that required for aerodynamic considerations.

Selection of the pivot location is the next step in design selection. The dynamics of a flexible seal require that an angle of 45 to 55 deg exist between the nozzle axis and the center of the seal cross section. This requirement forces the pivot to be either forward or aft of the throat on the nozzle axis. The choice must be made for each individual application based on vector angle requirements, depth of submergence, and case polar opening. Pivoting of the movable portion of the 156-9 nozzle was selected to be a point on the nozzle axis 25.50 inches aft of the throat. Location of the pivot in the exit cone aft of the throat presents the following advantages with a deeply submerged nozzle over the alternate location forward of the throat.

1. A smaller case polar opening is required for the same vector angle.
2. The aerodynamic forces always oppose the seal torque forces. (In the 156-9 design, elimination of aerodynamic torque reduced the maximum total torque by 500, 000 in. lb.)
3. The radiation barrier cap protecting the seal (Figure 2-3) can be located in a less severe environment.
4. A higher system steering angle results from a given nozzle vector angle, since the moment arm about the system center of gravity is greater with an aft pivot.
5. A highly reliable radiation barrier is obtainable with a smaller maximum nose outside diameter.

3. AERODYNAMIC ANALYSIS

An aerodynamic study has been conducted on the 156-9 motor to determine the nozzle and aft motor case wall heating environment and the eroded configuration of insulation materials. The aerodynamic nozzle geometry from the tip of the nose to the exit plane is identical to the 156-6 design. The aft part of the insulated case differs from the 156-6 only in the thickness of the case internal insulation which alters the flow geometry only slightly. The backside of the nozzle nose,

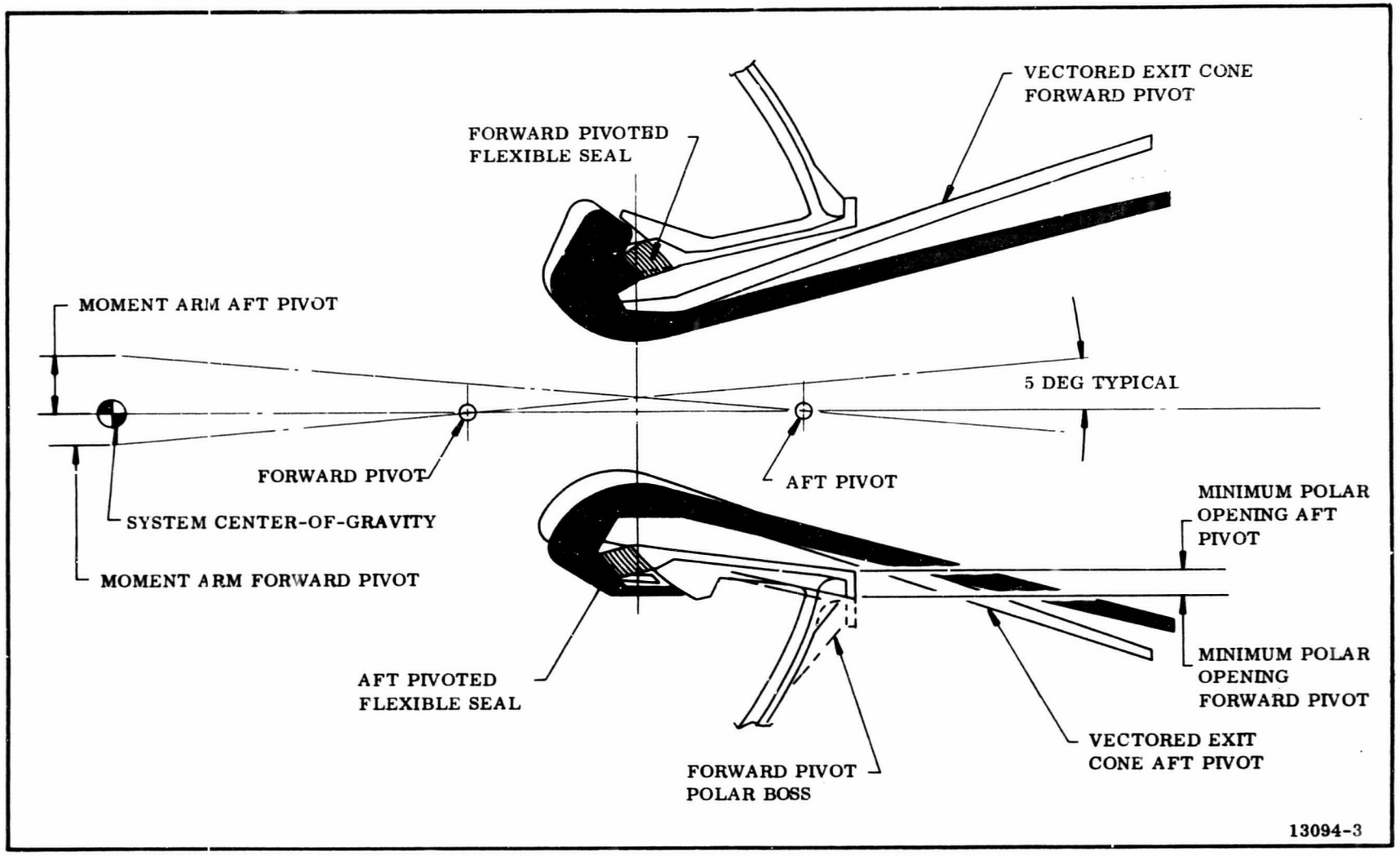

Figure 2-3. Comparison of Forward Pivoted and Aft Pivoted Seals

however, was modified to accommodate the flexible seal. The larger diameter of the nozzle backside changes flow conditions and thus affects the nozzle nose and aft case erosion.

The detailed flow analysis was conducted using a potential flow analogy programed on the IBM 7040 computer. This program calculates flow streamlines, Mach numbers, static temperatures, and static pressures in an axisymmetric, subsonic, compressible, potential flow field.

The potential flow properties are used to determine the boundary layer and the associated convective heat transfer coefficient on the entry. The heat transfer coefficient variation is then used to determine the erosion rate variation along the entry.

The erosion of graphite and graphite reinforced plastics in a solid propellant rocket motor primarily results from a diffusion limited chemical reaction occurring at the surface.* This erosion can be expressed as a function of the reacting species in the propellant combustion products (H_2O, CO_2, O_2, O and OH), the convective heat transfer coefficient, and the density of the carbonaceous material in the following manner:

$$\text{Erosion Rate } \left(\frac{\text{mils}}{\text{sec}}\right) = \frac{\beta\,(H/Cp)}{\rho}\quad (12 \times 10^3)$$

where β = blowing rate determined from the species in the propellant combustion products (dimensionless).

$$H/Cp = \frac{\text{Convective heat transfer coefficient}}{(Cp)\ \text{gas}}\left(\frac{\text{lbm}}{\text{sq ft - sec}}\right)$$

ρ = density of carbonaceous material (lbm/sq ft)

Measured erosion data are used to correlate with the theoretical parameter.

The analysis of silica base or asbestos base materials assumes they erode by melting. This heat of fusion is supplied by convection and radiation. Since the materials are not pure and the binder materials outgas and form a char layer,

*Erosion of Graphite in Solid Propellant Combustion Gases and Effects on Heat Transfer, A. M. McDonald, P. O. Hedman; AIAA Journal, Vol. 3, No. 7, July 1965.

the calculation is not exact and test data are used to relate erosion rate to total heat flux. The heat flux equation is:

$$Q_t = h\,(Taw - Tw) + K \epsilon\,(T^4 - Tw^4)$$

where

Q = total heat flux, Btu/sq ft sec

h = convective heat transfer coefficient, Btu/sq ft sec °R

Taw = Adiabatic wall temperature, °R

Tw = wall temperature, °R

K = Boltzmann's constant

ϵ = emissivity

T = free stream static temperature, °R

The parameters h, Taw, and T are calculated assuming no erosion and outgassing, the wall temperature is near the melt temperature of the primary material, the emissivity of each material represents the best correlation of erosion in motor headend stagnant flow (all radiation), subsonic flow, and supersonic flow (nearly all convective). All materials in the design have been tested in similar application and the erosion data correlated to predicted heat flux.

a. Nose--The final eroded nose configuration was determined using the above described techniques in the following manner.

1. The flow properties and heat transfer coefficient variations through the initial uneroded configuration were determined.
2. The erosion rates at the various locations on the nozzle entry are determined for the uneroded nozzle heating conditions and extrapolated over 15 seconds motor burning time to determine this intermediate configuration.
3. The flow properties and heat transfer coefficient for the 15 second configuration were calculated and compared with the initial calculations to determine

the error in extrapolation of the initially determined erosion rates. Because no large erosion rate changes occurred during the first 15 sec of burning time, the stepwise procedure was assumed adequate and no smaller increments of burning time were evaluated.

4. The process described in (3) is then repeated going to 38 sec, then 64.3 sec (web time).

The results of this erosion prediction are shown in Figure 2-4. The erosion along the nose is fairly uniform, about 0.60 inch. The heat transfer coefficient for the thermal analysis is shown in Figure 2-5.

b. Aft Case--The flow in the aft case area has been divided into two flow regions. For the first 30 percent of the web time a potential flow analysis was used, assuming the gas did not separate from the wall. After 30 percent of web time it was assumed the gas flow separates from the case wall at an axial station near the nose tip of the nozzle and leaves a separated area in the aft case. Analytical and cold flow studies have verified this assumption.* The separated type of flow is not amenable to analytical techniques which can describe the flow properties, heating rates and material erosion rates in a potential flow region. Therefore, prediction of these parameters must depend on a different technique.

Prediction of the erosion rates which will occur in the aft case area is achieved by equating the drag force driving the secondary flow and the wall drag length as shown in Figure 2-6. This relationship defines the velocities which occur on the backside of the nozzle nose and in the aft case. Using the velocities calculated in this manner, the boundary layer and heat transfer coefficients are determined.

*Investigation of Flow in the Aft Case of Motors with Submerged Nozzles, Thiokol Chemical Corporation, Wasatch Division, TWR-380; 22 Sep 1965.
Determination of Flow Properties in the Aft Chamber Region of the Poseidon C-3 First Stage Motor, Thiokol Chemical Corporation, Wasatch Division, TWR-1705; 24 Feb 1966.

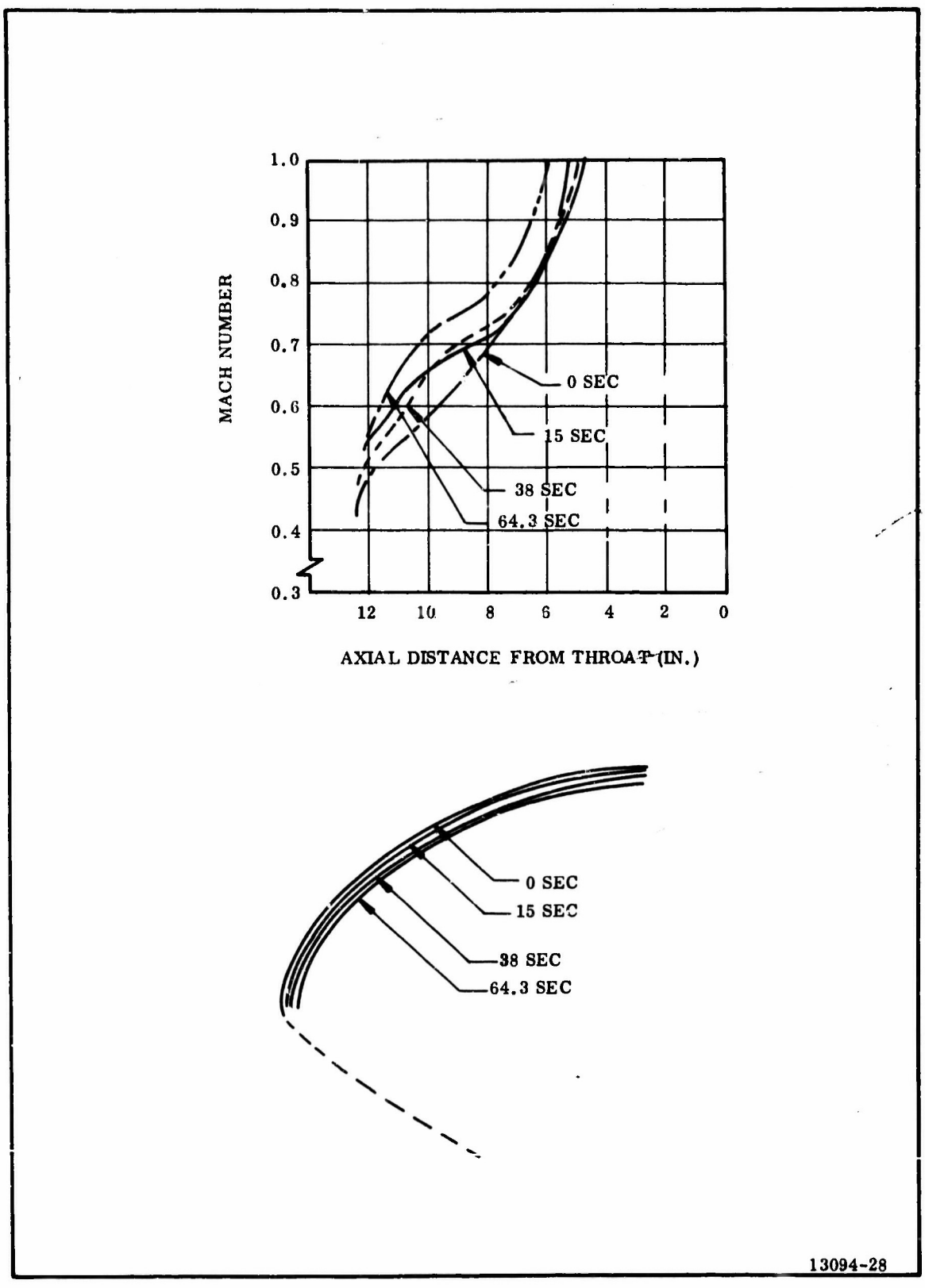

Figure 2-4. 156-9 Nozzle Nose Mach No. vs Axial Distance from Throat

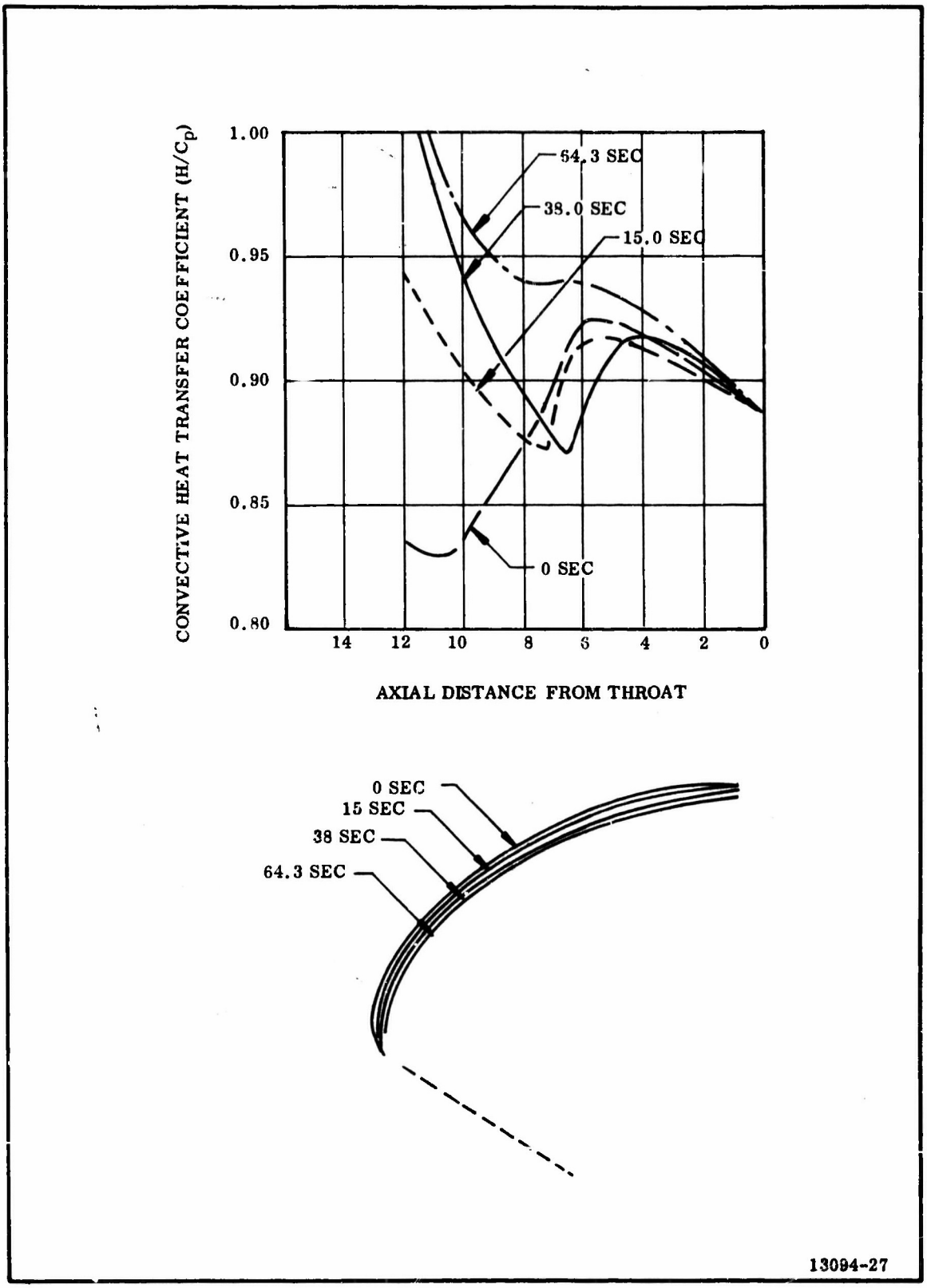

Figure 2-5. 156-9 Nozzle Nose Convective Heat Transfer Coefficient vs Axial Distance from Throat

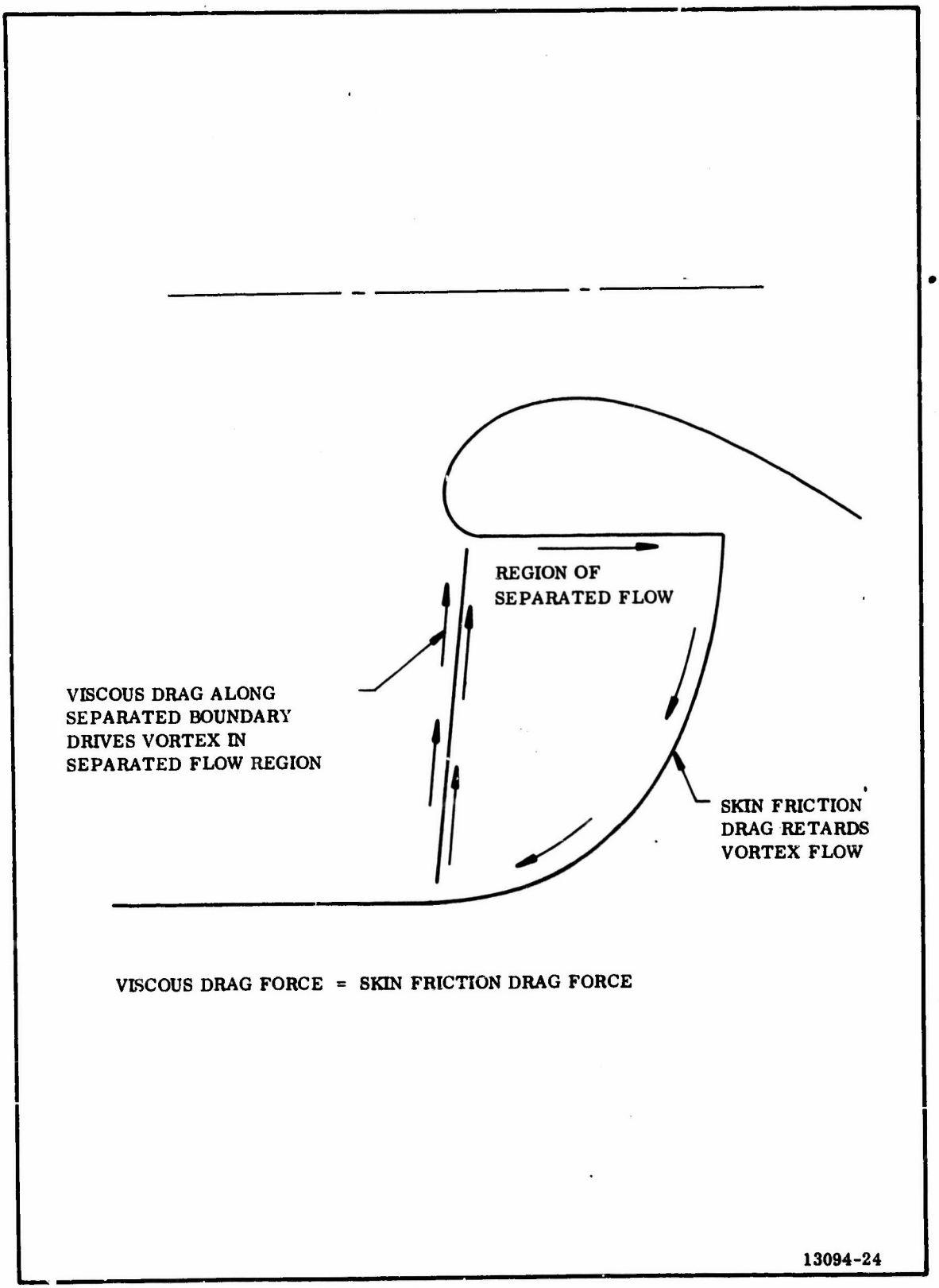

Figure 2-6. Description of Viscous and Skin Friction Drag Parameters

Existing correlations between heat transfer coefficients and material loss rates are used to determine the erosion profiles.

Aft case analysis differed somewhat from analysis of the nozzle backside because the propellant cover prevented erosion during this time.

Nozzle backside analysis assumed a potential flow moving forward along the surface as follows.

1. The same flow net for the 0 sec nose analysis defines the flow properties on the backside of the nozzle. The boundary layer was calculated from the nozzle case joint forward to the nozzle splitline, then reinitiated (started with a smaller momentum thickness) and continued to the nose tip.
2. The erosion rates for the nozzle backside are determined from the boundary layer results and the erosion predicted at 12.86 seconds.
3. The flow analysis was repeated at 12.86 sec and the heat transfer coefficients and heat fluxes were averaged between 0 sec and 12.86 sec to predict 19.3 sec erosion.
4. The flow net was used to determine the flow conditions along the assumed separated boundary in Figure 2-7. These flow Mach numbers define the viscous mixing drag forces and the flow conditions along the backside of the nozzle and aft case. This flow condition was analyzed at the 32 sec configuration and the erosion from 19.3 to 64.3 sec calculated on the nozzle backside and erosion rate calculated for the aft case. The exact erosion in the aft case is a function of the exposure time.

The final design of the nozzle backside is shown in Figure 2-8. The heat transfer coefficient is given along the carbon cloth and heat flux is given along the silica cloth because these parameters control erosion of the materials.

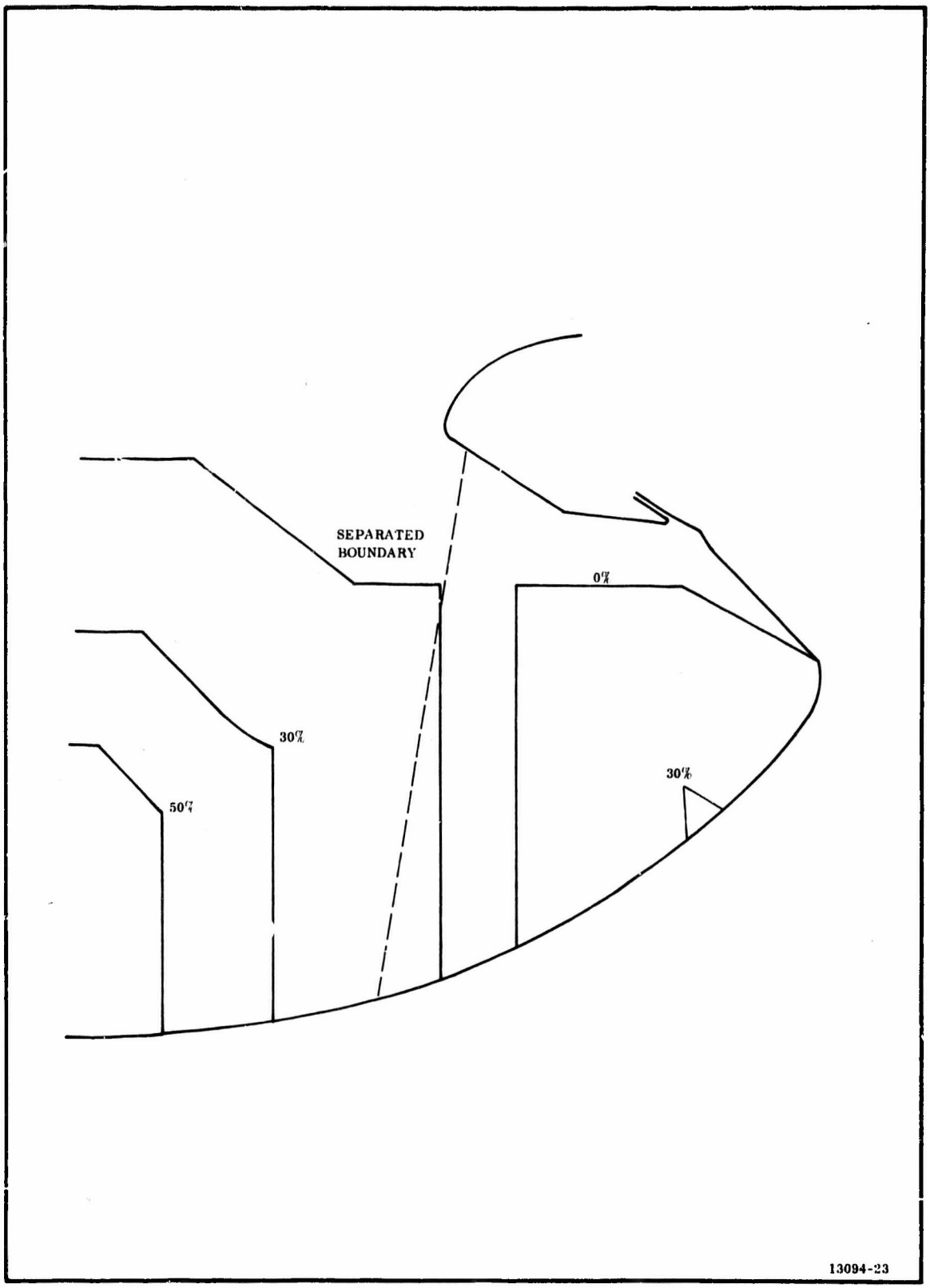

Figure 2-7. Aft Case Geometry and Grain Burnout

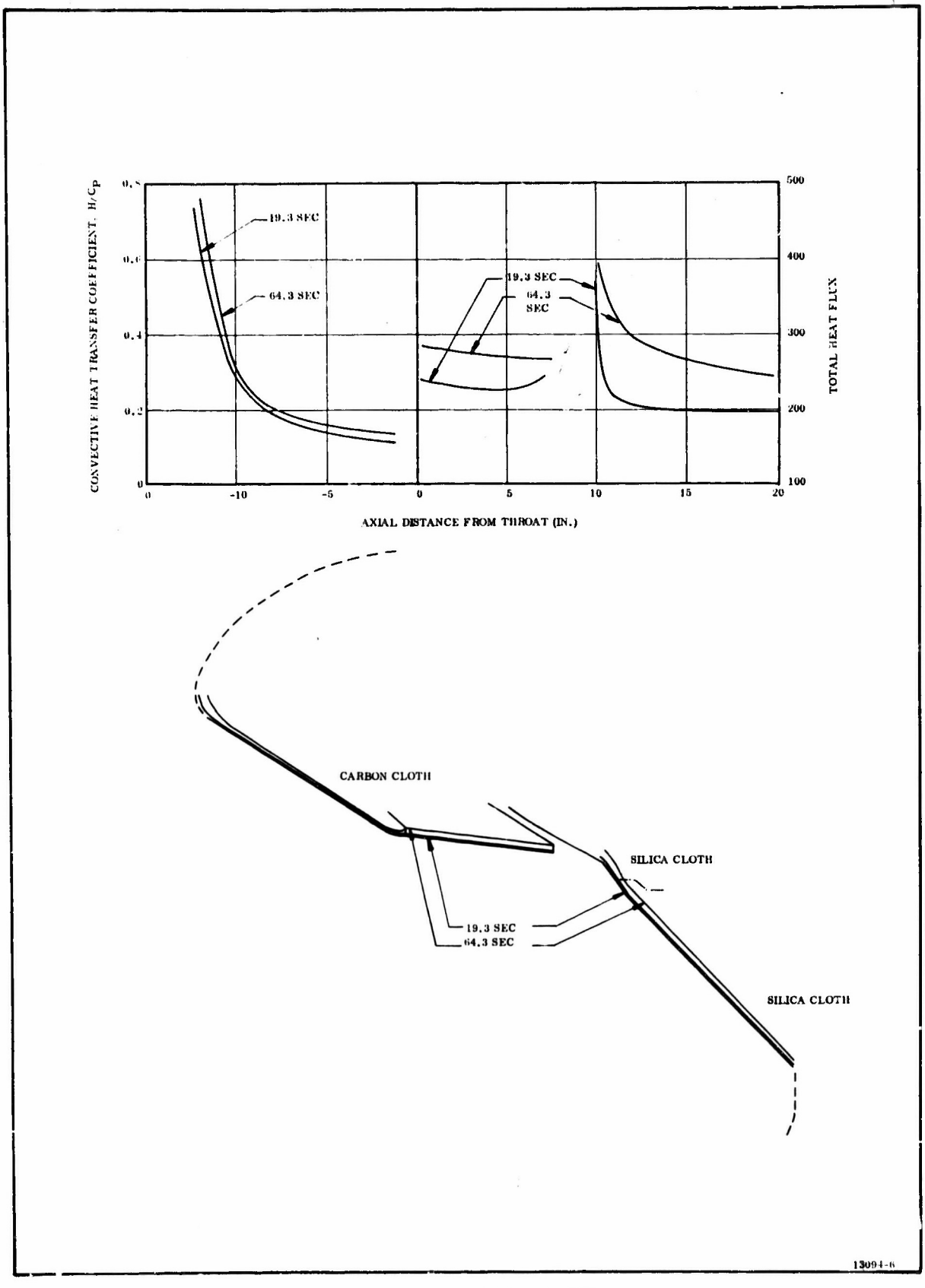

Figure 2-8. 156-9 Backside of Nozzle (Silica Cloth)

Other candidate materials, flow conditions and predicted erosion depths are shown in Figures 2-9 and 2-10.

c. Seal Region--The seal region of any movable nozzle must be designed to produce minimal gas velocities with resulting minimal convective heating for maximum reliability. The amount of radiant heating on the seal protective boot has been minimized in the 156-9 nozzle by covering the boot with a projecting insulation barrier, which prevents direct radiation to the boot. Nozzle movement is then allowed by providing a gap between the fixed and movable portions of the nozzle. If the boot is not protected from the radiant heat flux, the silicone rubber boot will erode at a rapid rate due to radiation.

A rubber boot directly exposed to chamber environment, as in the flexible seal nozzles tested thus far, * would be subject to direct convective heating, and would require prohibitive boot thickness to insure seal survivability.

The convective heating environment is much more severe in a large nozzle system, such as the one proposed, than in flexible nozzles tested thus far. The more severe environment occurs because of the larger flow velocities that occur in the separated region on the chamber side of the nozzle of the 156-9 motor than have occurred with the subscale nozzles of the tested end burning motors. These higher flow velocities result from gas generation aft of the nozzle nose in the separated region, a condition that did not occur in the subscale end burning designs.

Thiokol concluded that an unprotected boot design such as that used in the subscale tests would not survive in this more severe environment. Failure of the boot would result in the failure of the flexible seal.

Convective heating as well as radiation can be adequately reduced, however, by using the projecting barrier and gap design concept. With this design concept, the following mode of flow in the boot region occurs.

*Lockheed Propulsion Company: Development of an Elastomeric Seal for Omniaxial Movable Nozzles (Lockseal), Progress Report No. 3, Technical Report No. AFRPL-TR-65-243, November 1965.

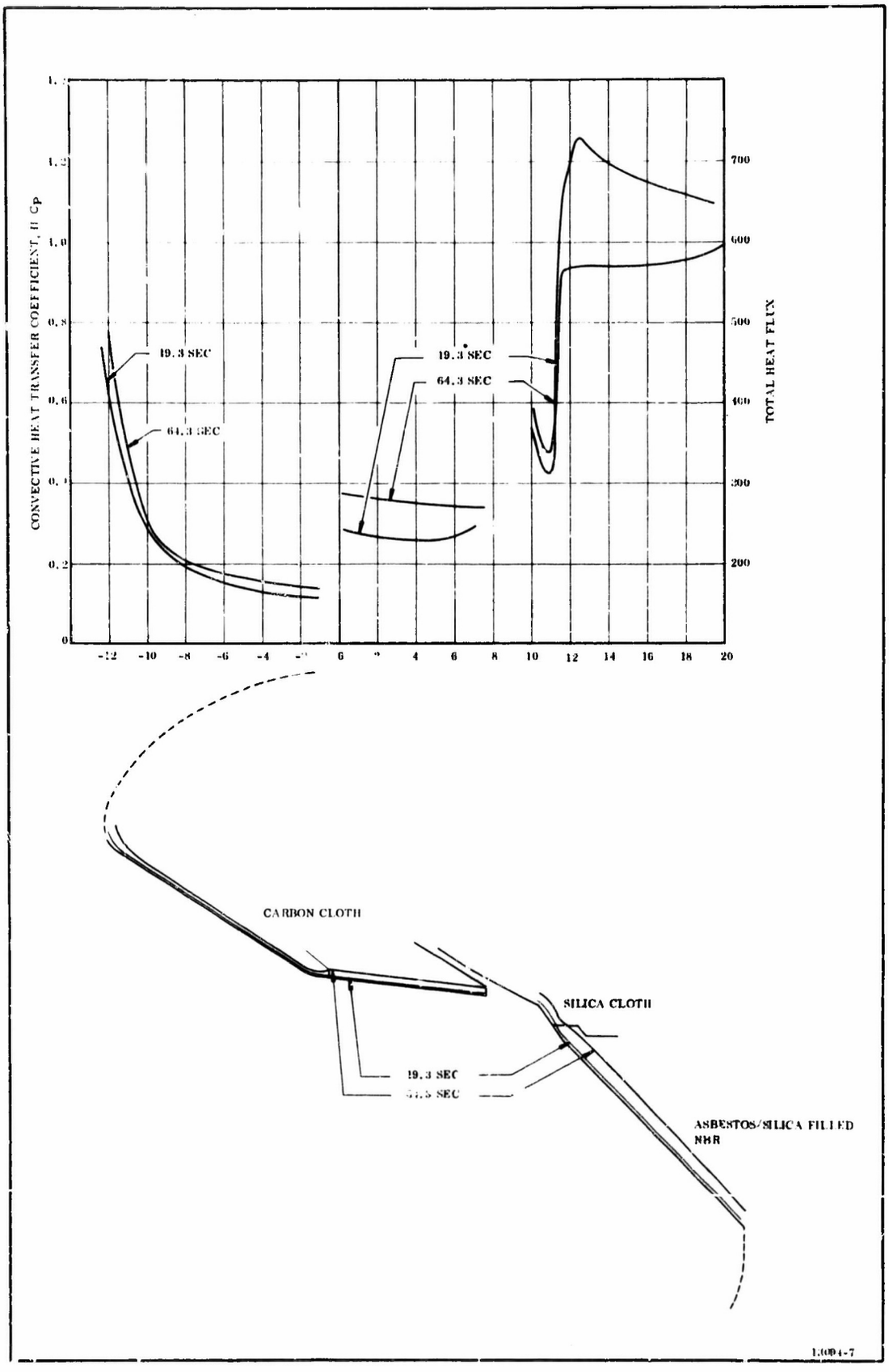

Figure 2-9. 156-9 Backside of Nozzle (Asbestos Filled NBR)

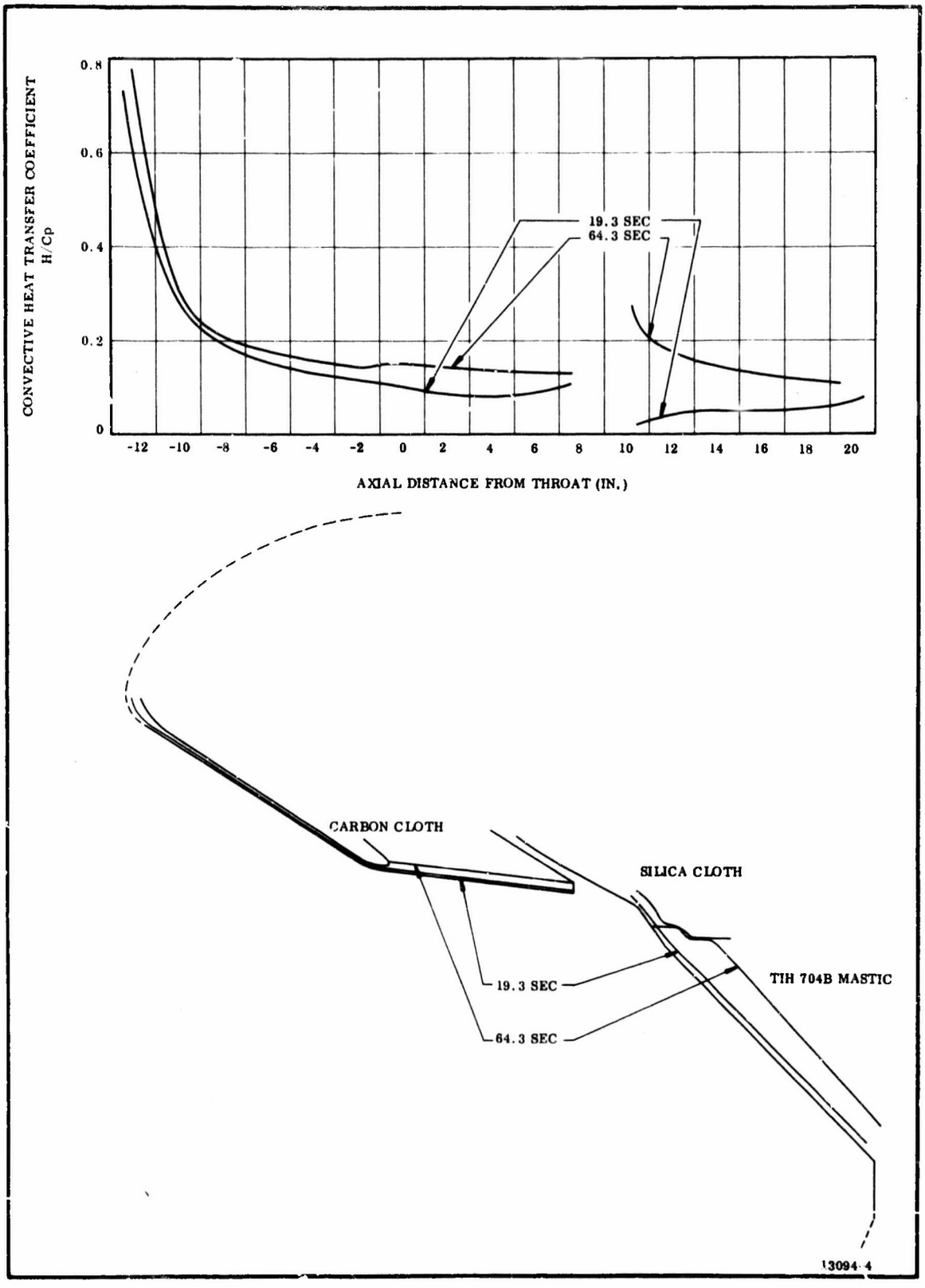

Figure 2-10. 156-9 Backside of Nozzle (TI-H704B Mastic)

At motor ignition, the flow from the aft surfaces is forward along the backside of the nozzle nose. When the nozzle is unvectored, the flow along the backside of the nozzle diffuses near the seal gap, separates across the gap, and reattaches on the forward side. This phenomena occurs symmetrically producing equal pressure in the gap around the periphery of the nozzle.

When the nozzle is vectored, the equality of pressure about the periphery of the seal gap is still maintained. Equal pressures are produced because the distance from flow separation to reattachment and the angle of reattachment are maintained at a nearly constant value about the nozzle periphery by the spherical ball surface (Figure 2-11). Therefore, with this flow mode no driving potential is produced to cause peripheral flow and large heating rates near the seal.

As burning time progresses, however, the basic mode of flow in the aft case near the backside of the nozzle is modified. Cold flow studies and static test firings of motors with submerged nozzles have indicated the flow pattern shown in Figure 2-6. With this type of flow the gas separates from the aft case wall just aft of the propellant surface. A separated flow is formed in the aft case region. The flow moves along with the separated boundary and reattaches to the nozzle near the tip of the nozzle entrance section. At the reattachment point, the flow divides with a portion of the flow moving aft along the backside of nozzle.

The flow moving aft along the backside of the nozzle nose thus approaches the seal region in a direction opposite to that which occurs at motor ignition. With this basic flow mode and the nozzle unvectored, the flow in the seal region occurs as shown in Figure 2-12. The flow separates from the nozzle wall, flows across above the seal gap, and reattaches to the downstream wall. Again in this case, the flow separation and reattachment occur symmetrically about the nozzle periphery. No driving force for circumferential flow under the separated boundary about the periphery of the seal exists, and seal survivability is assured. Nozzle vectoring does not change the symmetrical separation and reattachment because of the sphorical downstream surface.

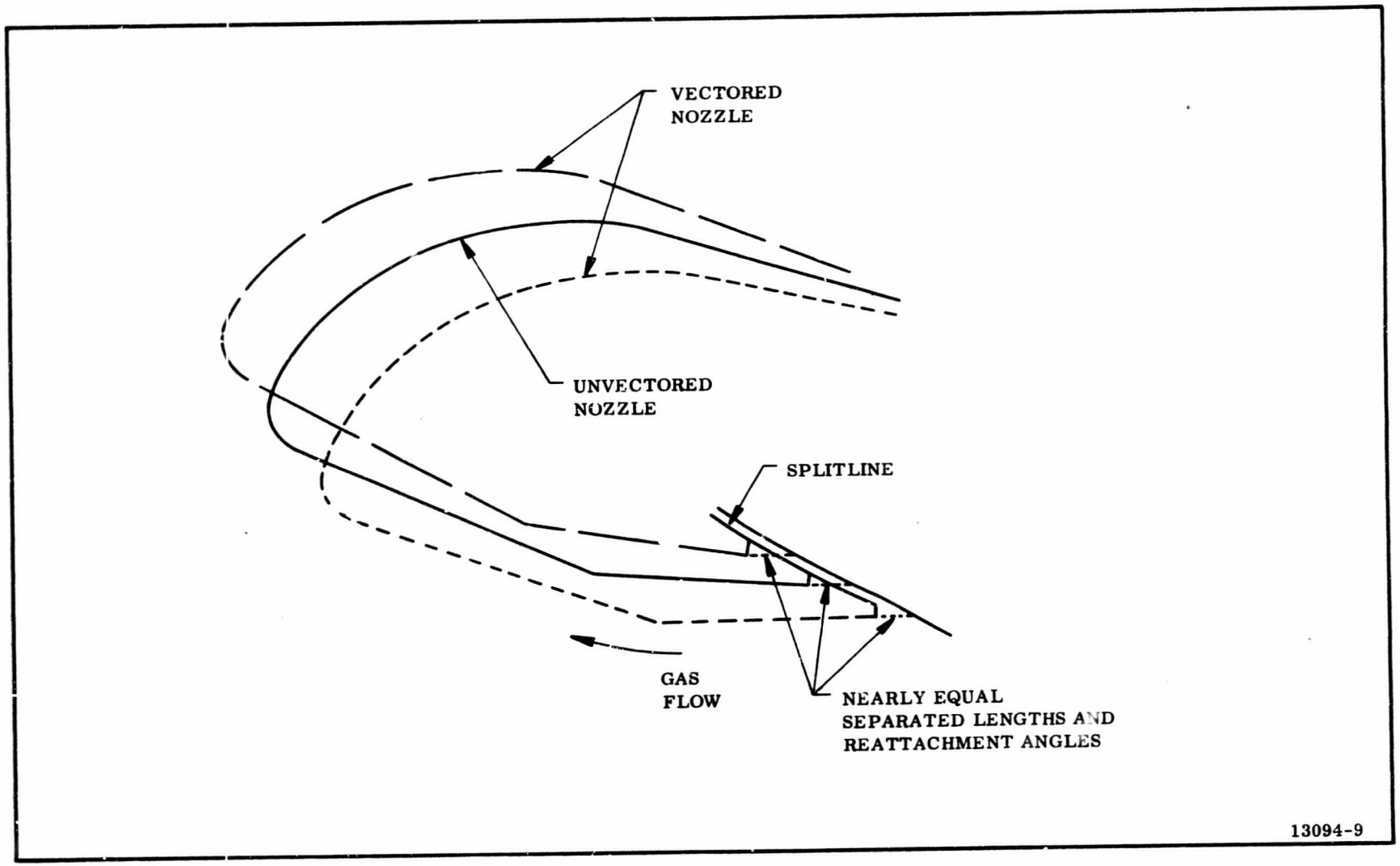

Figure 2-11. Motor Flow Near Splitline in Vectored Nozzle at Motor Ignition

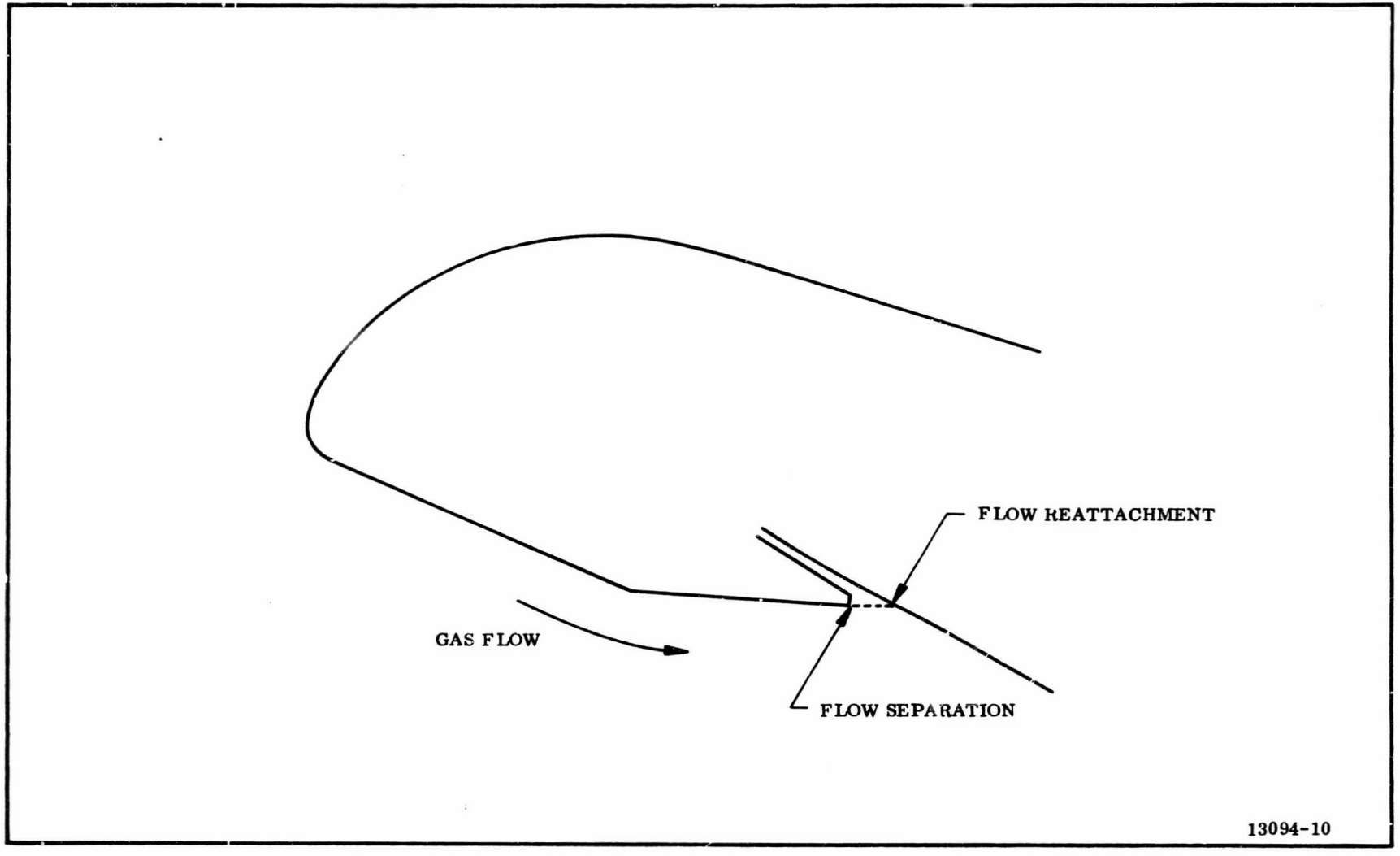

Figure 2-12. Mode of Flow Near Splitline

A series of cold flow tests in which the flow velocities were measured in the cavity near a flexible seal indicated that the flow Mach numbers near the boot protecting the flexible seal were less than 0.03 for both a null and a 5 deg vector position.

Therefore, the seal region will be exposed to nearly stagnant flow, and convective heating of the boot region is negligible throughout motor operation.

4. THERMAL ANALYSIS

A thermal analysis was conducted to insure that adequate material has been provided to allow for the anticipated losses (erosion-corrosion) and to adequately insulate the structural parts during firing.

The computer program determines the transient temperature response and surfaces-recession rates of a slab characterized by two receding surfaces.

The transient temperature response of the insulation and nozzle parts is a function of the thermal properties of the material and the internal environment to which the parts are subjected. The thermal properties are usually published values obtained from vendors and lab tests (Table 2-2).

The internal thermal environment of the motor is dependent on the composition of the propellant and the pressure at which combustion occurs. With these two parameters fixed, the combustion temperature, the enthalpy, the equilibrium composition of the combustion products, and the motor performance are calculated using an IBM 7040 computer. The computer program used simulates the isotropic gas expansion through the nozzle and calculates the static enthalpy of the gas at prescribed locations in the nozzle. From this information and a suitable recovery factor (a function of the Prandtl number), the recovery enthalpy may be determined from the following relationship.

TABLE 2-2

MATERIAL THERMAL PROPERTIES

Carbon Cloth Phenolic

Temperature (°F)	Density (lb/cu ft)	Thermal Conductivity (Btu/ft-hr-°F)	Specific Heat (Btu/lb-°F)
400	81	0.50	0.30
1,200	74	0.50	0.47
1,500	73	0.58	0.48
2,500	73	1.6	0.48
4,000	73	3.3	0.5
6,000	73	5.9	0.5

Silica Cloth Phenolic

Temperature (°F)	Density (lb/cu ft)	Thermal Conductivity (Btu/ft-hr-°F)	Specific Heat (Btu/lb-°F)
400	110	0.18	0.24
1,000	102	0.28	0.24
2,000	96	0.50	0.28
4,000	96	1.27	0.28
6,000	96	2.25	0.28

$$i_r = N_{r_f}(i_T - i_S) + i_S$$

where

i_r = recovery enthalpy (Btu/lb)

N_{r_f} = recovery factor (dimensionless, the cube root of the Prandtl number)

i_T = total (stagnation) enthalpy (Btu/lb)

i_S = static enthalpy (Btu/lb)

The recovery enthalpy represents the potential heat available for transmission across the boundary layer to the wall.

To determine the amount of heat actually transmitted across the boundary layer by convection, the enthalpy on the wall side of the boundary layer must also be known. This is obtained by a second computer program which is used to calculate gas equilibrium composition and enthalpy as a function of temperature and pressure. From these data and the recovery enthalpy, the difference across the boundary layer at any instantaneous set of conditions may be determined by the computer. This information, as well as the convective heat transfer coefficient, is needed to evaluate convective heat flux.

The simplified Bartz equation is used to calculate the convective heat transfer coefficients.

$$C_H = \frac{0.026}{(D_t)^{.2}\,(A/A^*)^{.9}} \left(\frac{(\mu)^{.2}}{(P_r)^{.6}}\right)_0 \left(\frac{(P_c)}{C^*}\right)^{.8}_0 \left(\frac{(D_t)}{r_c}\right)^{.1} \psi$$

where

C_H = heat transfer coefficient based on enthalpy difference (lb/sq ft/sec)

0.026 = a correlation constant derived by Bartz from turbulent boundary layer analyses

D_t = nozzle throat diameter (ft)

(A/A^*) = expansion ratio at the nozzle location under consideration

μ = viscosity at stagnation conditions (lb/ft-sec)

P_r = Prandtl number (c_p/k) (dimensionless)

P_c = chamber pressure (psia)

g = acceleration due to gravity (ft/sec^2)

C^* = characteristic gas velocity (ft/sec)

r_c = throat radius of curvature (ft)

ψ = dimensionless factor accounting for variation of ρ (gas density) and μ (gas viscosity) across the boundary layer

Transport properties appearing in the Bartz equation are calculated with a computer program based on the kinetic theory of gases. The latest thermochemical data are used in this program and its predictions compare well with available experimental data.

Heat transfer coefficients are determined as a function of wall temperature and nozzle expansion ratio.

Having obtained the foregoing information, the convective heat flux may be calculated according to the following equation.

$$Q_{conv} = C_H (i_r - i_w)$$

where:

C_H = convective heat transfer coefficient (lb/ft^2-sec)

i_r = recovery enthalpy of the combustion gases (Btu/lb)

i_w = static enthalpy of the gases on the wall side of the boundary layer (Btu/lb)

Conventional techniques are used to determine the net radiant heat flux to the wall. The net radiant heat flux may be expressed as:

$$Q_{rad} = \epsilon_w^1 \sigma \left[\epsilon_g T_g^4 - \alpha_g T_w^4\right]$$

where:

ϵ_w = effective wall emissivity

ϵ_g = gas emissivity

α_g = gas absorptivity

T_g = temperature of the gas (°K)

T_w = temperature of the wall (°K)

σ = Boltzmann's constant

The emissivity (absorptivity of a particle laden gas at any particular temperature) may be expressed as:

$$\epsilon_g = 1 - (e)^{-NAL}$$

where:

N = particle number density (number/cu cm)

A = condensed particle cross-sectional area (cu cm)

L = mean radiation beam length (cm)

The computerized thermal analysis requires an input erosion rate as a function of time. The predicted erosion rates for the nozzle exit cone were obtained using an empirical procedure which has been developed as a result of analyzing static test data. This procedure consists of correlating nozzle exit cone erosion rates with convective heat transfer coefficients. Erosion data obtained in numerous firings with propellant formulation very similar to that proposed for the 156-9 motor have shown good correlation with convective heat transfer coefficients.

The relationships between the exit cone erosion rate and convective heat transfer coefficient are shown in Figures 2-13 and 2-14 for carbon cloth phenolic and silica cloth phenolic. These data are for the conditions of the test, i.e., the chamber pressure, nozzle configuration, and the exhaust gases of the proposed 156-9 motor.

The assumption implicit in the use of the correlation is that erosion is primarily a reaction of certain chemical species in the combustion gases with the nozzle material. Furthermore, it is assumed that the material is at a sufficiently

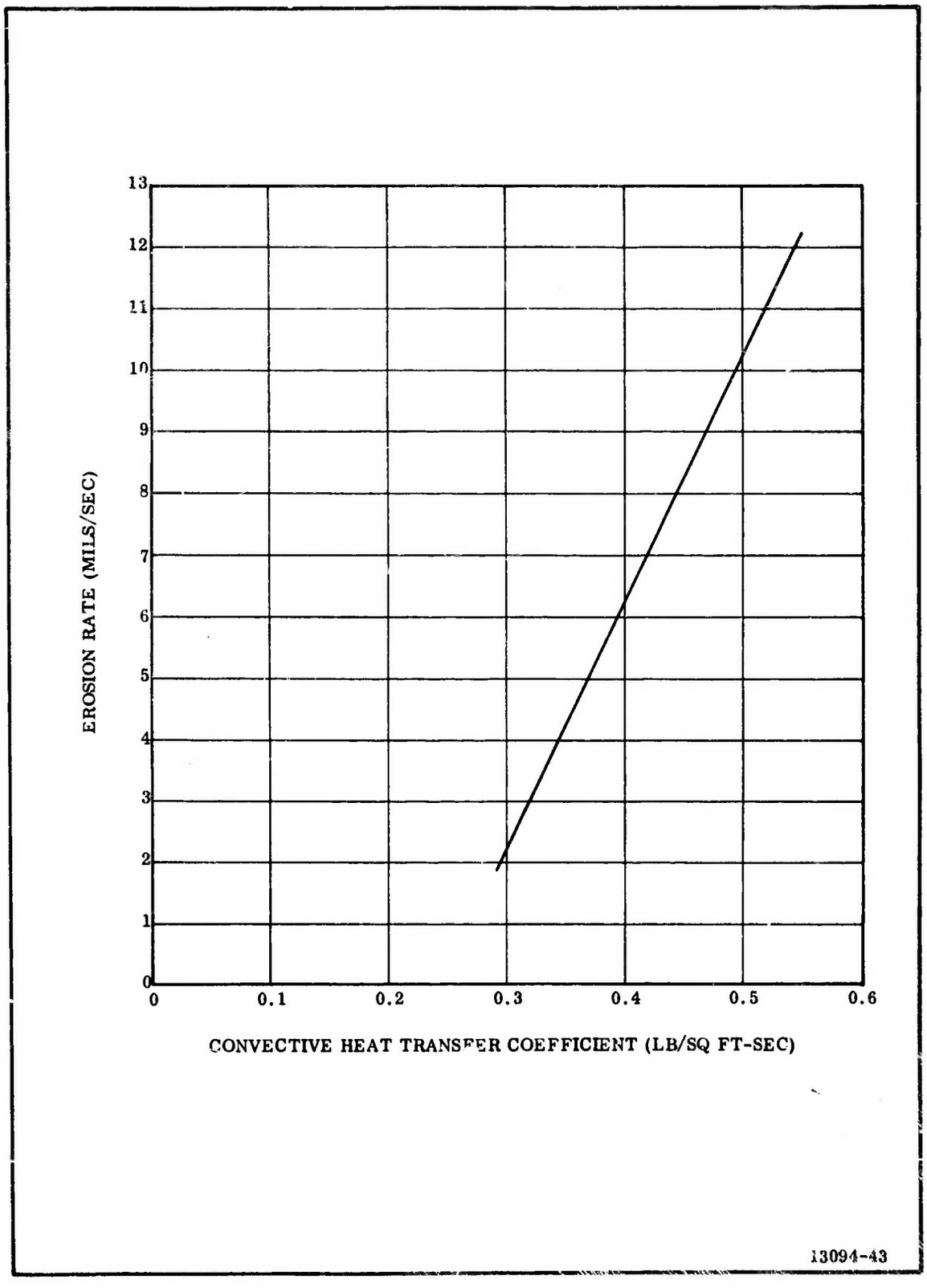

Figure 2-13. Convective Heat Transfer Coefficient vs Erosion Rate, Carbon Cloth

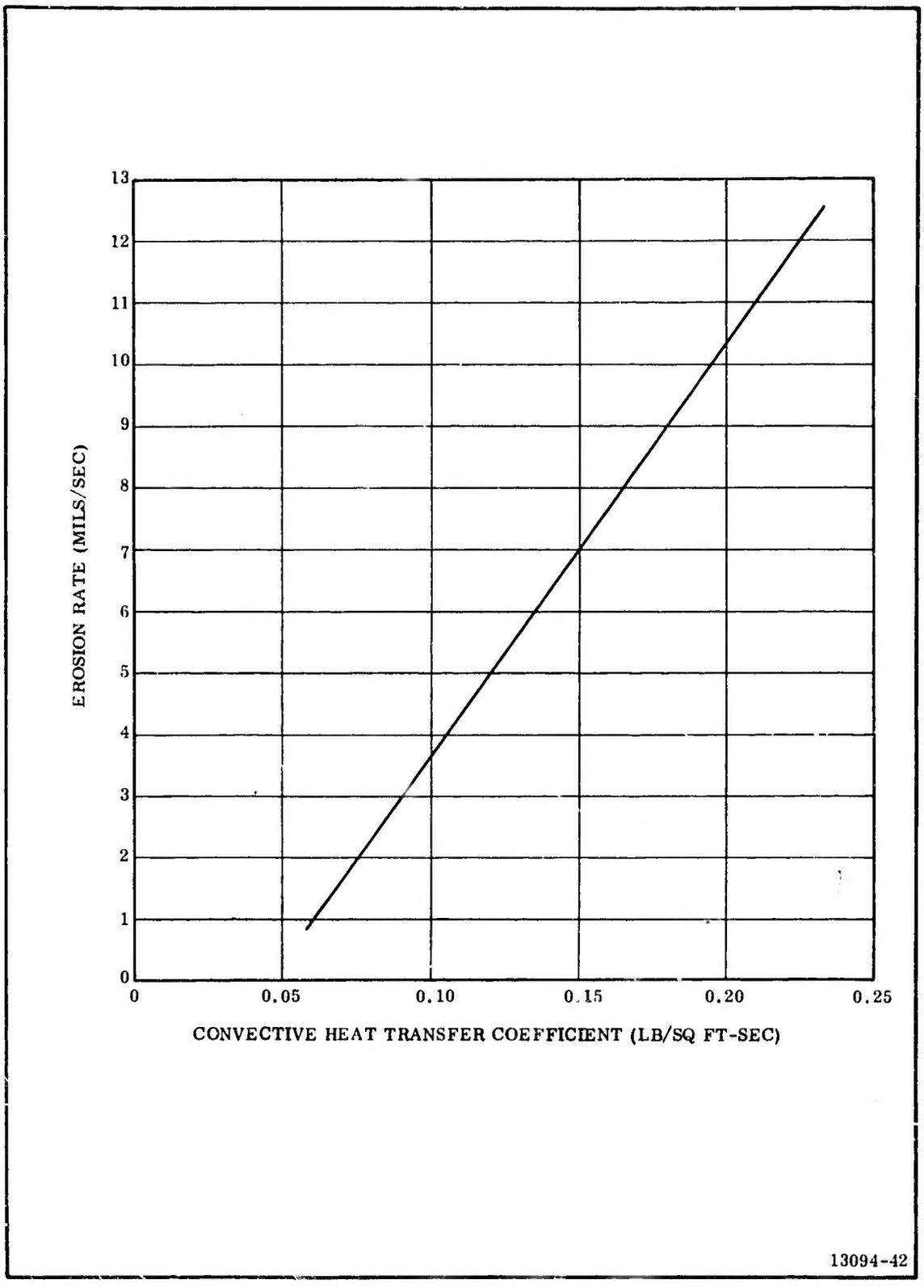

Figure 2-14. Convective Heat Transfer Coefficient vs Erosion Rate, Silica Cloth

high temperature so that the reaction rate of the reacting species and the wall material is infinite and that the overall rate of erosion (corrosion) is determined only by boundary conditions which control the transport rate of reactants and reaction products. These controlling boundary conditions are satisfactorily defined by the convective heat transfer coefficient.

It is recognized that this approach is somewhat specious with silica cloth since physical changes (melting, vaporization) controlled by environmental temperature play a more prominent role here than do chemical reactions. The correlation has, however, been found to yield dependable design data in applications and under conditions similar to those under which the reference test data was obtained.

This empirical technique somewhat circumvents uncertainties in the heat transfer coefficient calculation. The same method for computing this coefficient is used both to set up the correlation and to read values out of it. Uncertainty in the heat transfer coefficient is thus cancelled out.

It has been shown that the erosion of a graphite containing material is primarily the result of a chemical reaction occurring at the material surface.* The magnitude of this effect is dependent upon the quantity of oxygen containing species in the propellant combustion gas and is defined by a parameter called the blowing coefficient (β). Since different propellant formulations have different blowing coefficients, the resulting erosion of a carbon containing material will depend on the propellant formulation selected.

This blowing coefficient analysis is not applicable to plastic materials with siliceous reinforcement because corrosion is not the primary cause of material loss in this case. The char formed with this material is lost primarily by vaporization.

*McDonald, A. J., and Hedman, P. O., "The Determination of the Mechanism of Erosion of Graphite in Solid Propellant Combustion Gases and Resulting Effects on Heat Transfer Phenomena," January 1964.

Separate correlations are used for the nose region and the nozzle exit because the convective heat transfer coefficients are calculated by different methods in the two cases.

The predicted erosion rates for the nozzle entrance or nose section are not as easily obtained as those for the exit cone. The nozzle inlet configuration may cause non-uniform acceleration of the gases into the throat resulting in high local velocities in the supersonic range. Subsequent deceleration to subsonic velocities will set up a shock pattern making a reliable estimate of convective heat transfer coefficients impossible. Hence, to predict erosion rates for the inlet section where the flow is supersonic, predicted convective heat transfer coefficients were extrapolated between the points of known flow conditions.

The convective heat transfer coefficients were obtained by determining the Mach number profile around the inlet section of the nozzle up to the point of sonic flow. Output from this computer program included predicted material erosion rates which are dependent upon flow conditions and the composition of the combustion gases. The Mach numbers were converted to effective area ratios using one-dimensional flow assumptions. The resulting area ratios and corresponding gas dynamic properties of the combustion products were used as input to the Bartz equation to calculate the convective heat transfer coefficient.

The erosion rates at various locations throughout the nozzle as determined by the methods previously discussed were used as input to the thermal program. The computer program handles the erosion as a function of the convective heat transfer coefficient with the nodal thickness being reduced with time. The predicted nozzle erosion and char profiles are shown in Figure 2-15. The predicted temperature profiles for the locations indicated are presented in Figures 2-16 thru 2-20.

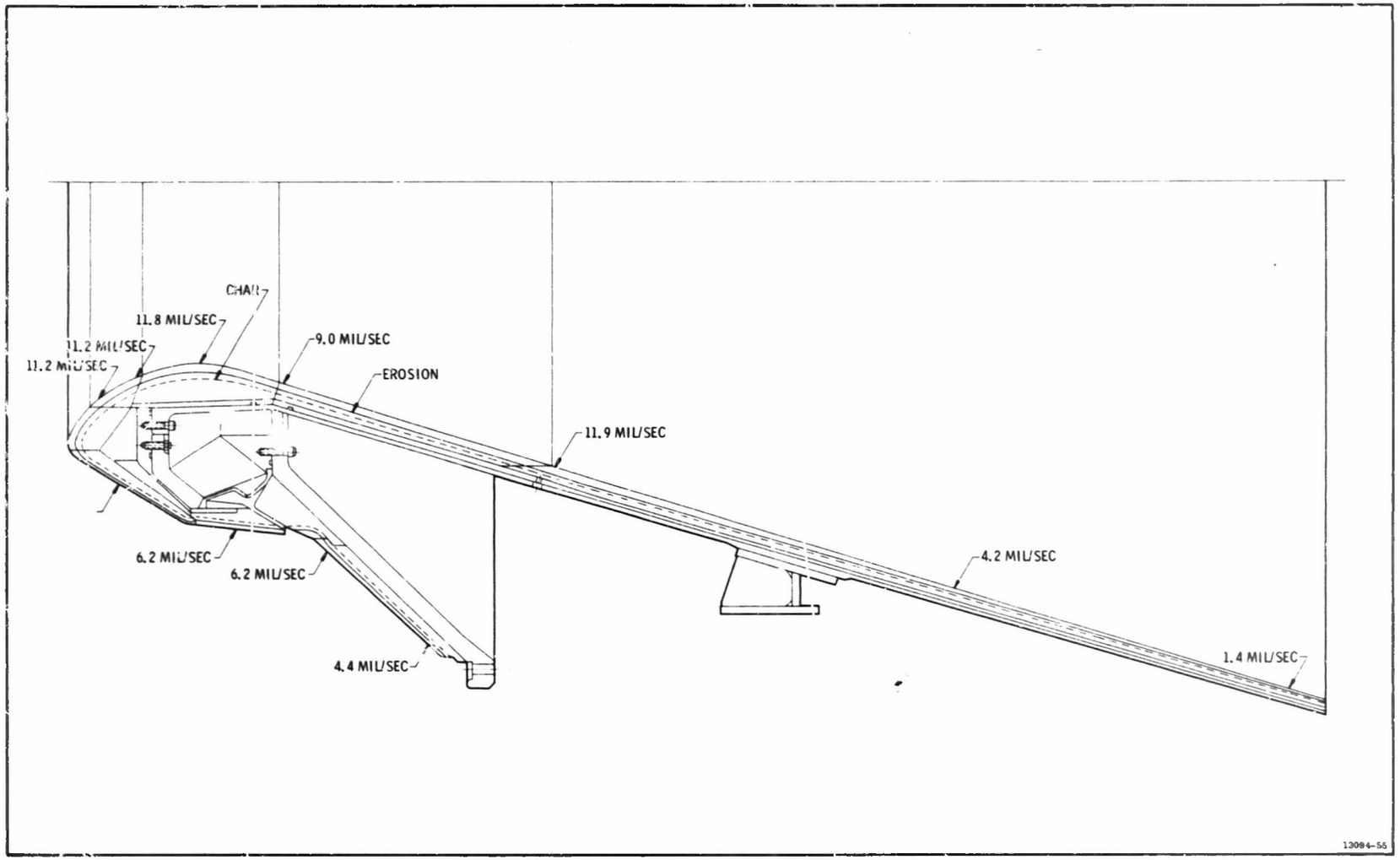

Figure 2-15. 156-9 Predicted Erosion and Char (Maximum)

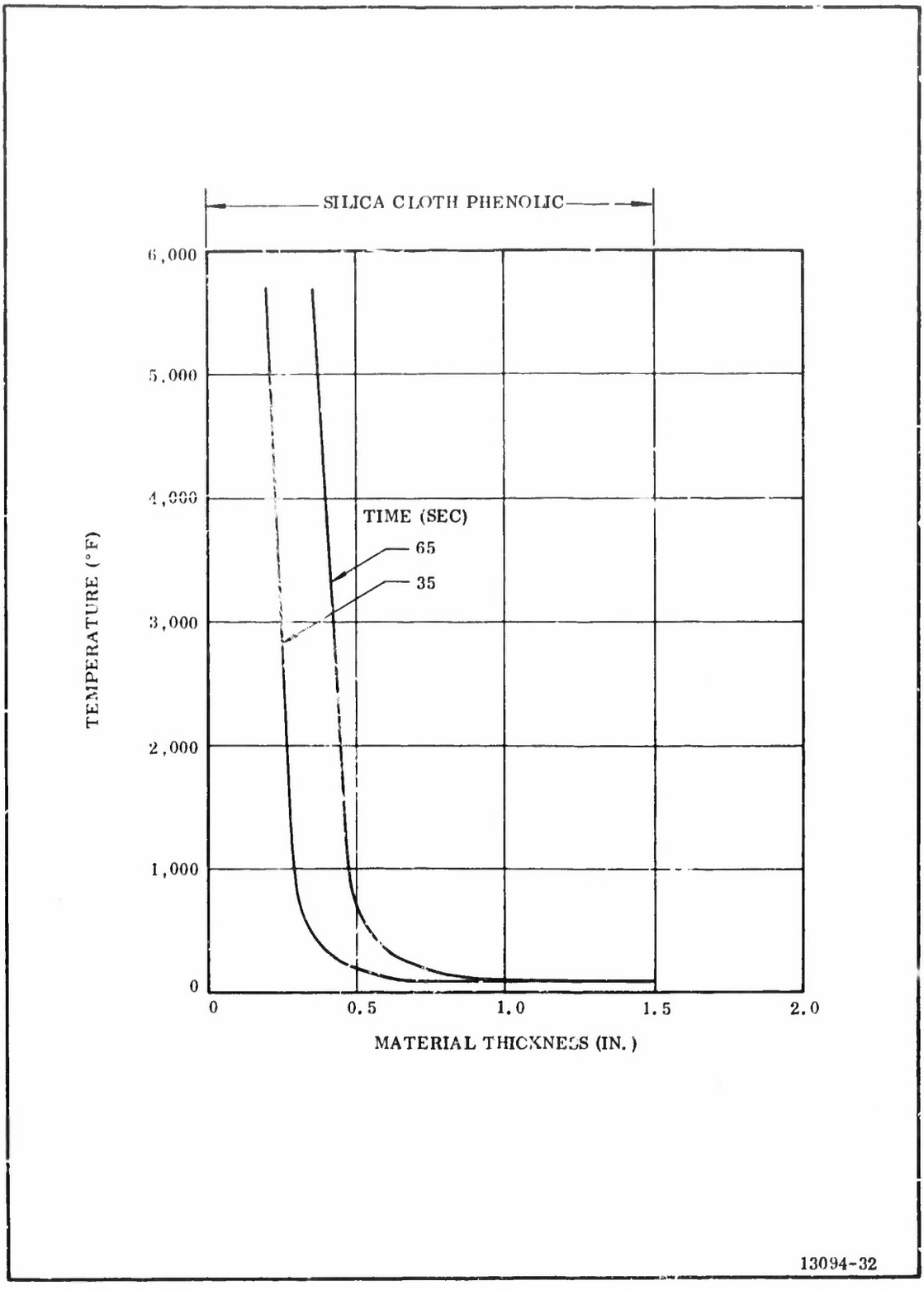

Figure 2-16. 156-9 Nozzle Entrance Temperature Profile, $A/A^* = 3.88$ (Backside)

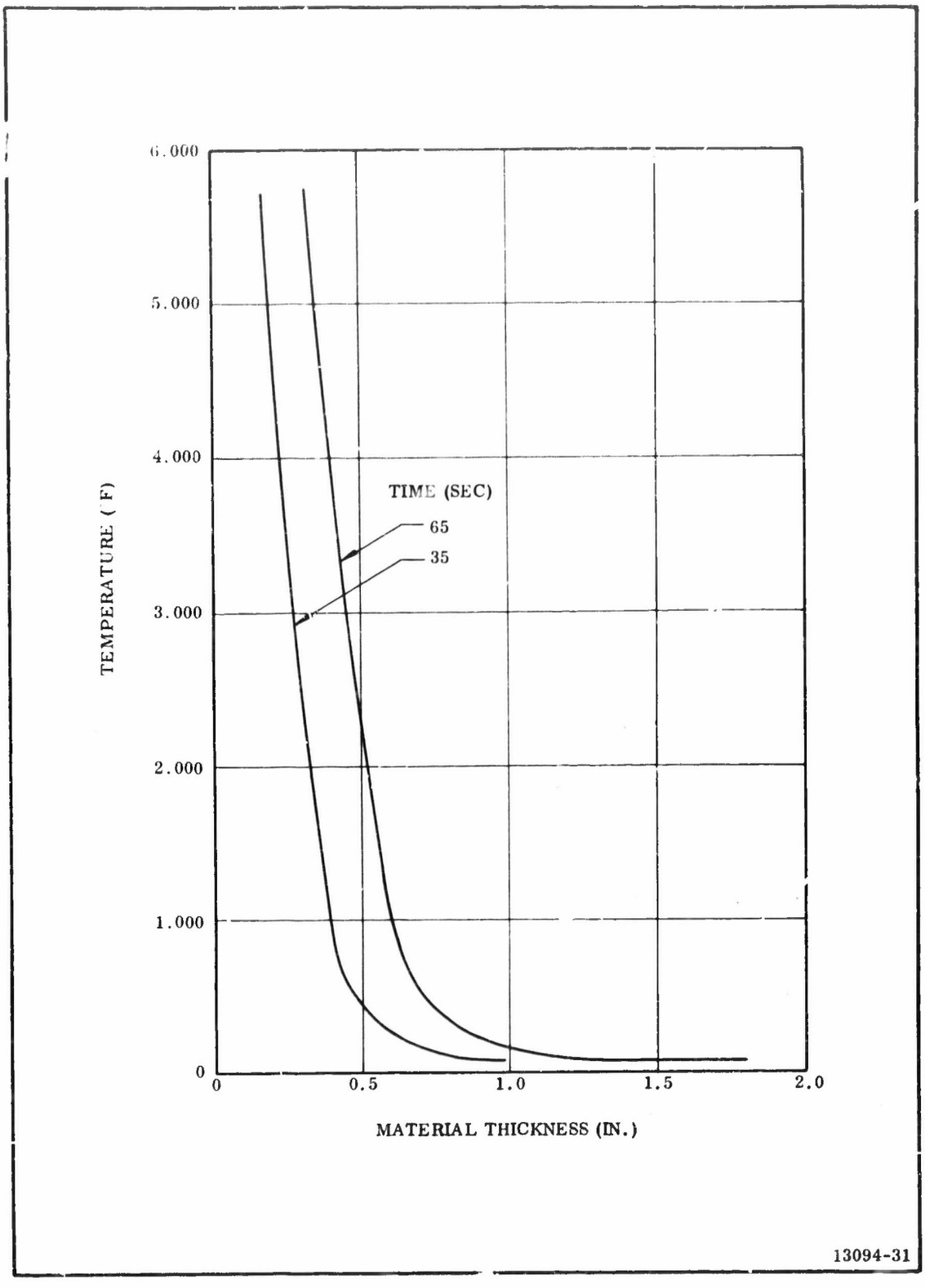

Figure 2-17. 156-9 Nozzle Entrance Temperature Profile, A/A* = 2.52 (Back Side) Carbon Cloth

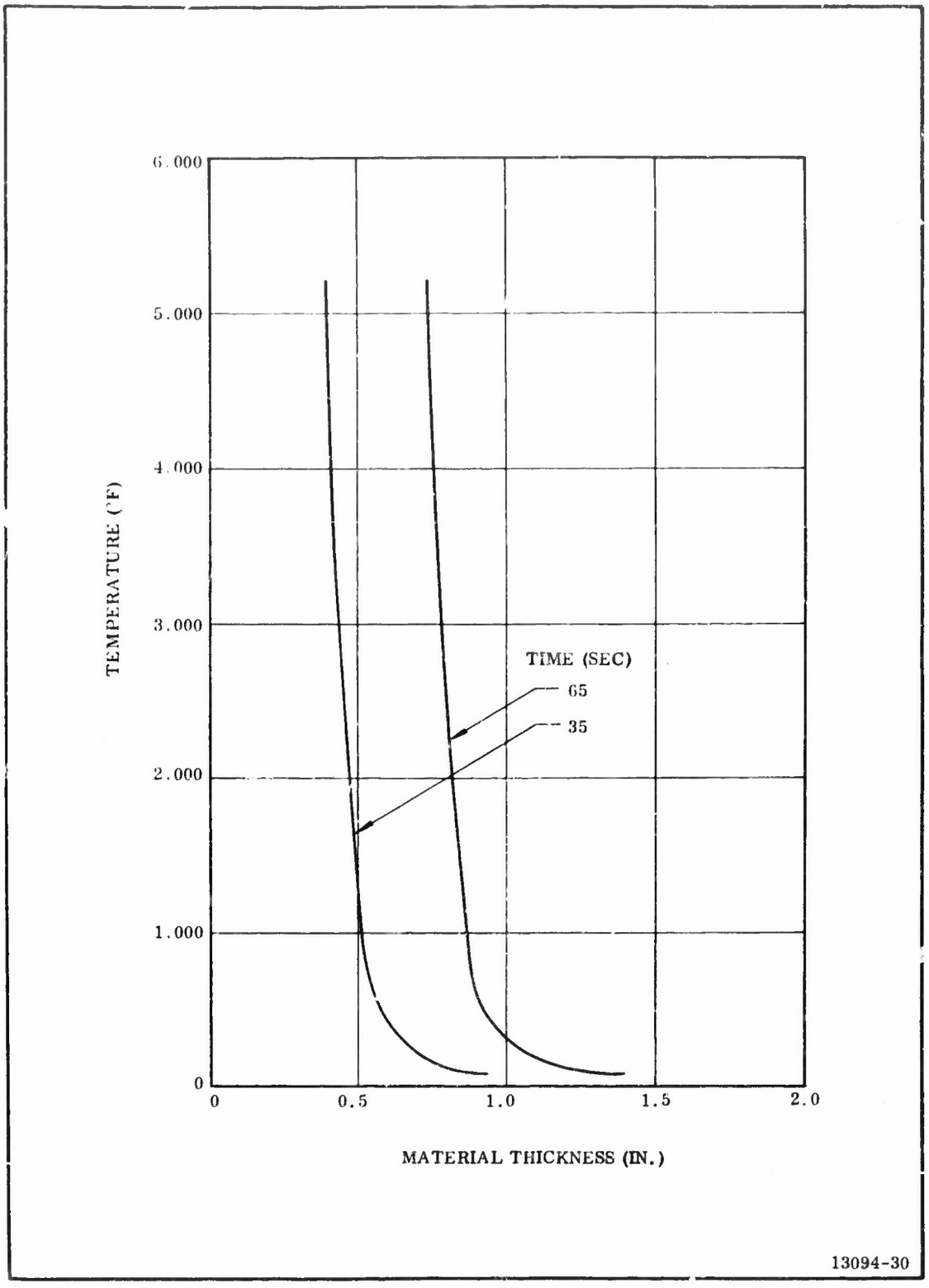

Figure 2-18. 156-9 Nozzle Entrance Temperature Profile, A/A* = 1.17 Carbon Cloth

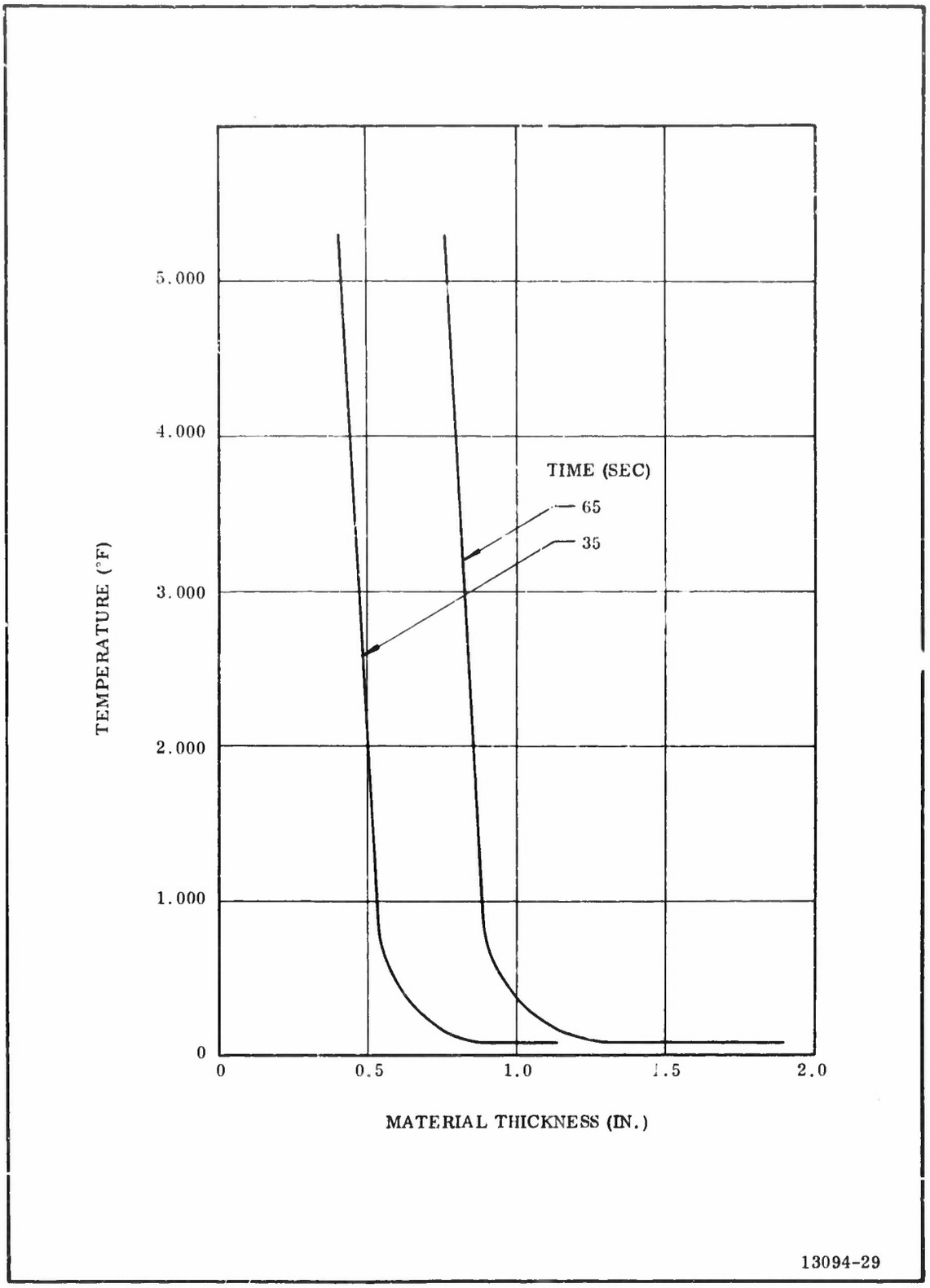

Figure 2-19. 156-9 Nozzle Temperature Profile,
A/A* = 1.0 Carbon Cloth Phenolic

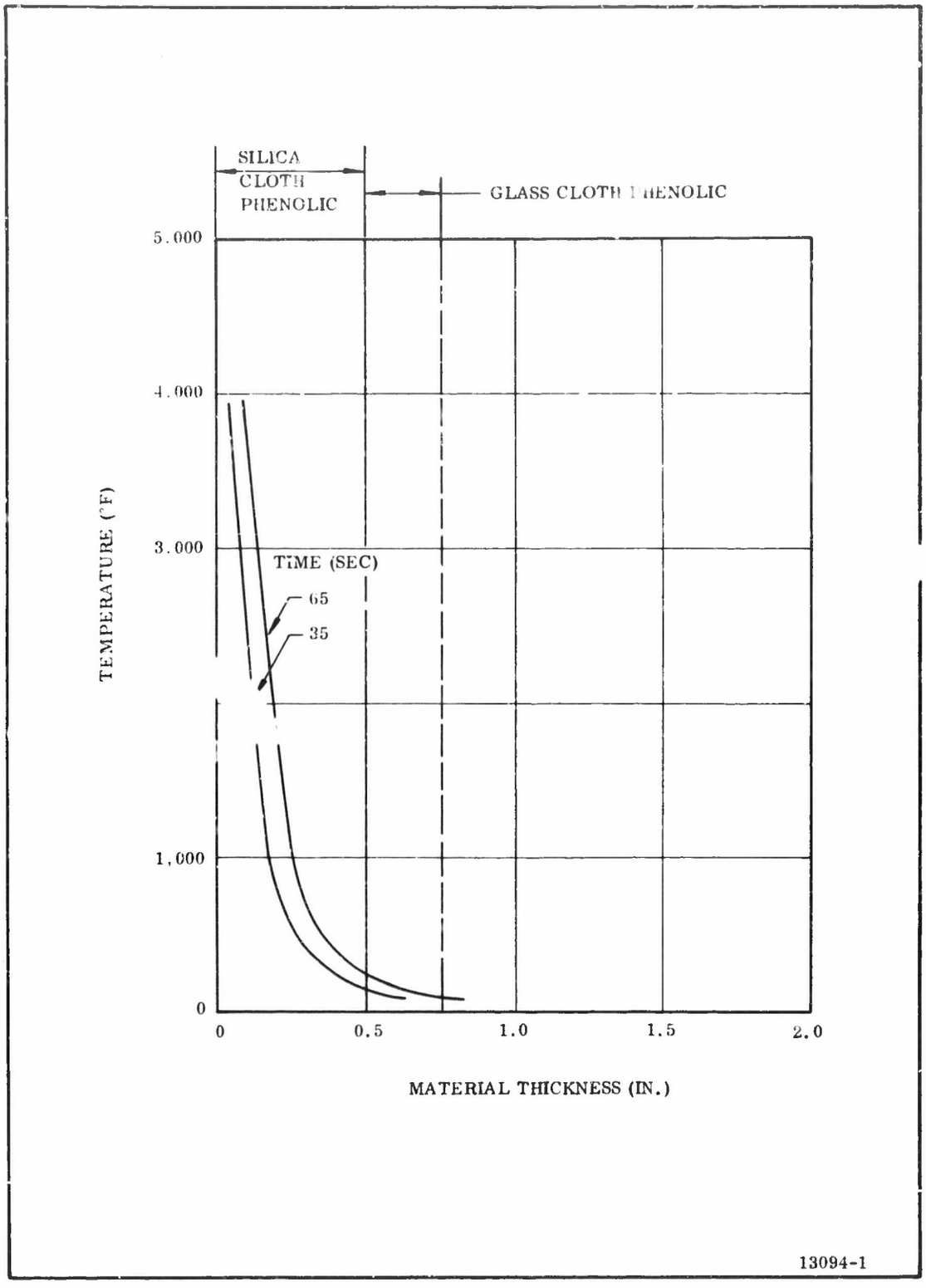

Figure 2-20. 156-9 Nozzle Exit Cone Temperature Profile, $A/A^* = 8.16$

5. STRUCTURAL ANALYSIS

This section presents the results of the structural analysis of the 156-9 nozzle structural body, fixed housing and associated actuator brackets. The analysis was conducted to verify the structural integrity of the fixed housing and nozzle at a maximum expected operating pressure of 830 psig, and to analyze the nozzle actuator brackets to determine structural integrity at an actuator stall load of 70,097 pounds.

The minimum ultimate tensile strength of the materials for the various components is shown in Figure 2-21. The ultimate bolt strengths were selected insure a 0.25 minimum margin of safety.

The structural analysis was conducted at a case pressure of 830 psig, which is the maximum expected operating pressure. The stresses that result from MEOP case pressure, or the stresses in the various components which result from actual predicted applied loads, are defined as limit stresses (σ).

The margins of safety presented here exist between limit stresses and ultimate strength capability or between limit stresses and critical buckling capability.

A basic design criteria for the various components dictated that a margin of safety of at least 0.25 be maintained in all areas during the most severe loading condition to be encountered during static firing.

The target margin of safety was not attained in the aft end of the case membrane adjacent to the fixed housing and case joint. The margin of safety in this area is 0.185. The case is already in existence and does not lend itself to redesign or modification in order to increase this margin. The stresses occurring in this area are basically due to discontinuity bending due to the reversed direction of the fixed housing which was necessitated by the submerged nozzle. However, it is doubtful that this would result in a premature case rupture.

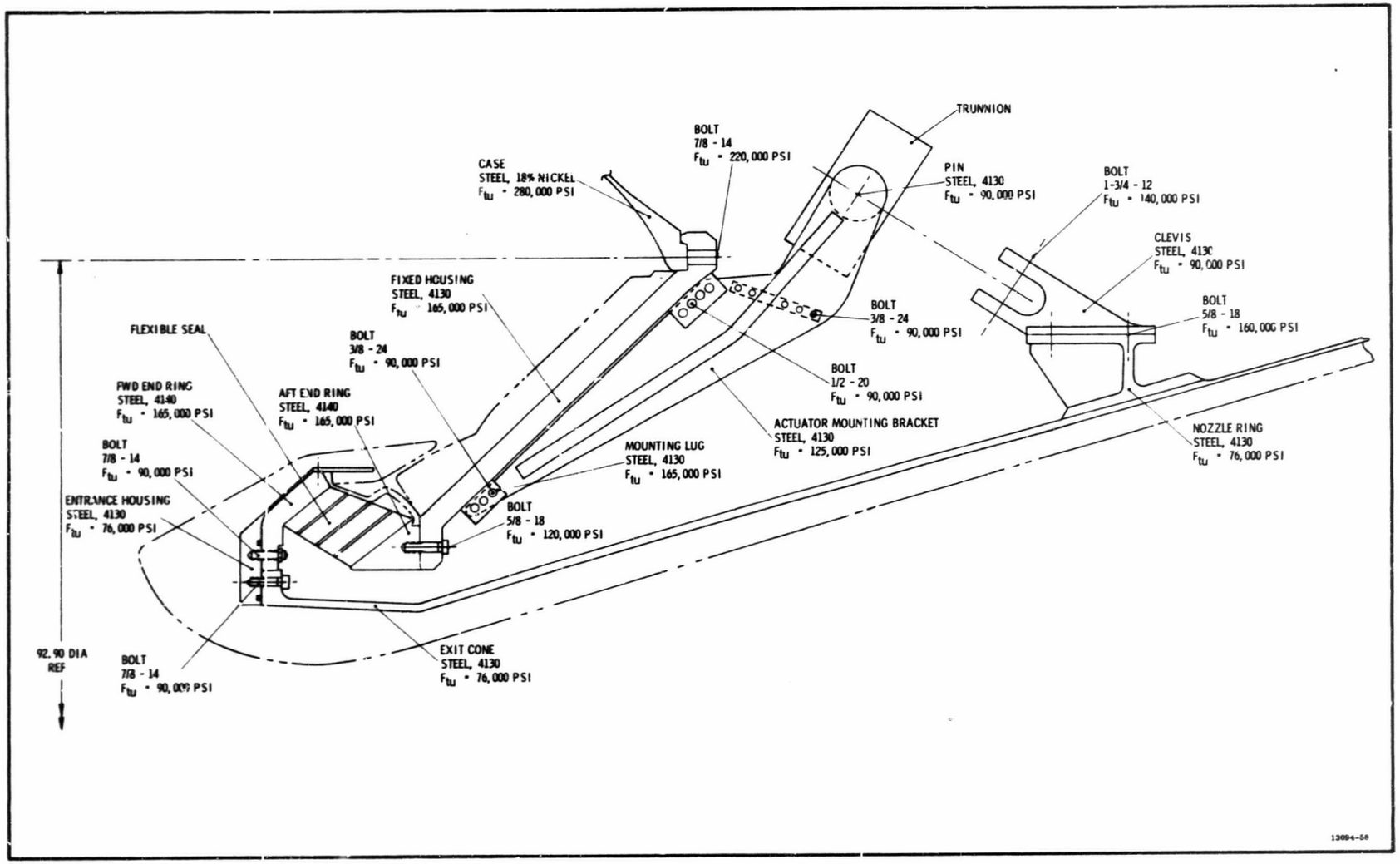

Figure 2-21. Summary of Materials and Minimum Ultimate Strengths

The area with the next lowest margin of safety is the bolts which attach the fixed housing to the case. The margin of safety for the bolt tension is 0.28 which is above the minimum requirements. Margins of safety for various areas are listed in Table 2-3. The various components analyzed will, therefore, withstand the maximum anticipated loads or pressures.

Computer runs used in the analysis are included in Section V. The free body sketches of the geometrical shapes shown on the computer runs reflect the positive direction for the moment, shear, and axial loads.

Four basic components of the 156-9 nozzle are considered here. They are fixed housing, nozzle body, actuator mounting bracket, and nozzle ring and actuator attach bracket.

a. Fixed Housing--The fixed housing is a heavyweight design, 1.55 in. thick, which is considerably thicker than required to withstand the internal case pressure. The extra thickness was included to facilitate fabrication of the unit. The maximum stress is located at a radius of approximately 45 in. from the centerline of the part. This area is adjacent to the housing-to-case attachment ring. The area has a stress level of 78, 599 psi and a margin of safety of 1.1.

b. Nozzle Body--The nozzle body analysis includes the flexible seal end rings, the entrance housing ring, and the nozzle exit cone attachment ring. This analysis assumes that the flexible seal will transfer axial loads only and will not add significantly to the rigidity of the end rings or induce appreciable moments or shear into the rings. The maximum stresses induced in the flexible seal end rings occur in the forward ring. However, this stress is only 14,403 psi with a margin of safety of 10.45.

TABLE 2-3

SUMMARY OF MINIMUM MARGINS OF SAFETY

Number	Component	Minimum M.S.
1	Case	0.185
2	Bolt (Case to fixed housing)	0.28
3	Fixed Housing	1.10
4	Bolt (Fixed housing to flex seal)	0.54
5	Flex Seal, Forward end ring	10.45
6	Bolt (Flex seal to entrance housing)	2.32
7	Bolt (Entrance housing to exit cone)	2.18
8	Exit Cone	2.04
9	Nozzle Ring	1.31
10	Bolt (Nozzle ring to clevis)	0.31
11	Clevis	0.58
12	Actuator Bracket	0.47
13	Bolts (Actuator bracket to fixed housing lugs)	0.46

c. Actuator Mounting Bracket--The actuator mounting bracket, trunnion, and mounting bracket to fixed housing lugs, were designed to sustain an actuator axial stall load of 70,097 pounds. The maximum stress in these three components occurs in the actuator mounting bracket and is 84,517 psi and results in a margin of safety of 0.47. This area is approximately midway down the bracket arm and is in the area directly over the mounting lugs closest to the actuator.

d. Nozzle Ring and Actuator Attach Clevis--The nozzle ring is used to distribute the actuation loads into the nozzle exit cone and reduce the deflection and stresses in the cone as a result of the point actuation loads. The ring is assumed to be loaded radially at two locations, 0 and 90 degrees. One load is applied toward the center of the ring and the other outward from the center of the ring. This load pattern is used to simulate the most severe anticipated actuation condition. The maximum deflection was 0.96 in. outward from the centerline. The maximum shear load is 25,338 lb at the 90 deg station and the maximum tensile stress is 32,846 psi at the 90 deg station. The minimum margin of safety is 1.31 at the 90 deg station. This analysis assumes that the total actuator loads are reacted by the ring only and does not include the rigidity or stiffness of the exit cone which will in actual application complement the ring structure. The load distribution summary is shown in Figure 2-22.

6. TORQUE ANALYSIS

To move the nozzle mechanically in accordance with the specified dynamic requirements, the loads resisting nozzle deflection must be accurately defined. For convenience, these loads are normally expressed in terms of the torque produced about the pivot axis. The application of the results of the torque analysis and the design of other motor components is shown in the design of the nozzle actuation system presented in Section VII of this report.

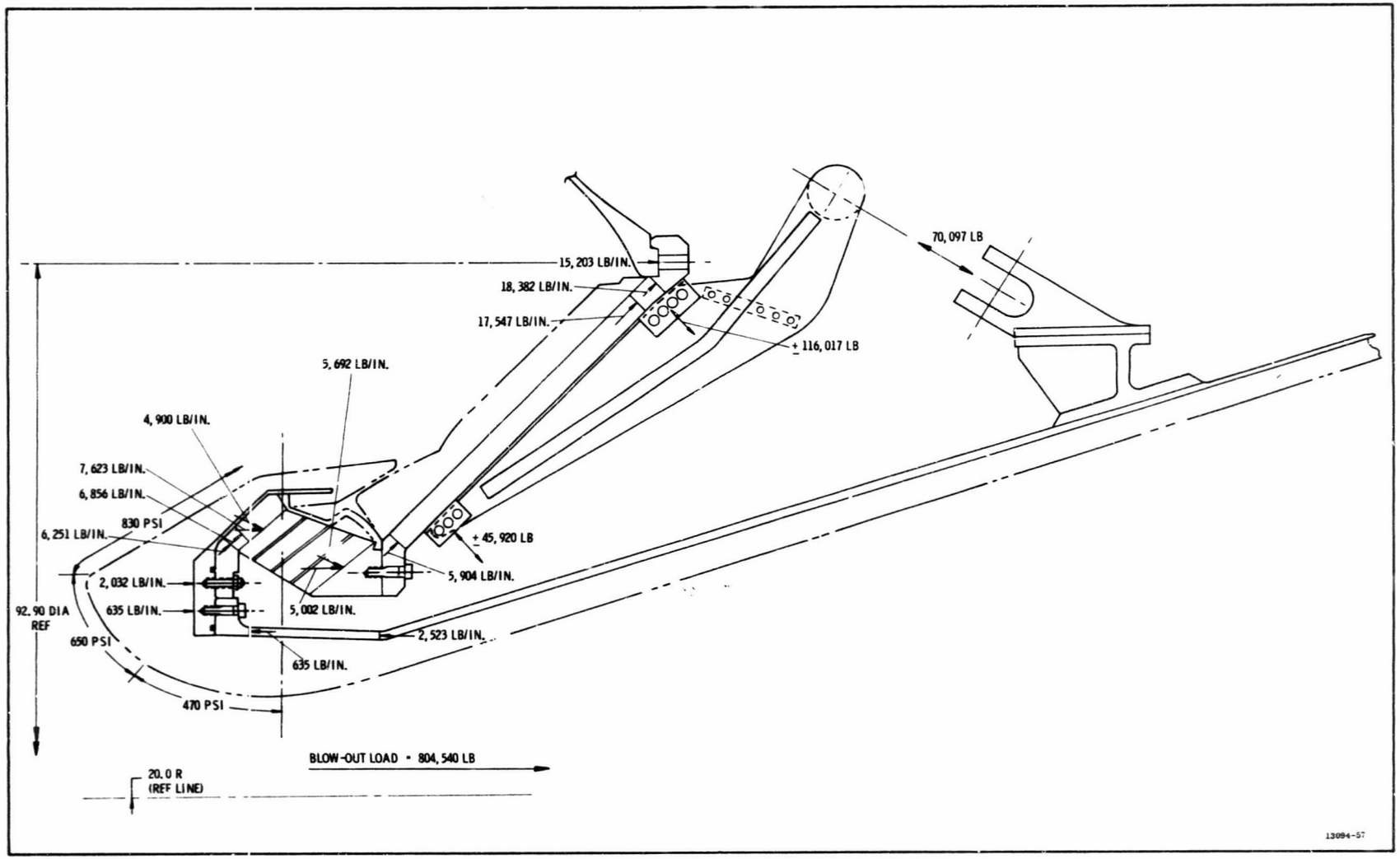

Figure 2-22. Load Distribution Summary

Total torque is a summation of all contributing factors and is a direct function of the mechanics of the design and internal and external aerodynamics. For the 156-9 nozzle, the following major torque components must be considered.

1. Dynamic spring torque.
   (1) Flexible seal spring torque.
   (2) Internal aerodynamic torque.
2. Frictional torque.
3. Offset torque.
4. Inertial torque.
5. Gravitational torque.

External aerodynamic torque is essentially nonexistent in static test applications. Coriolis torque (effect of earth's rotation on nozzle motion) also is of a very small magnitude and will not be considered in this analysis.

The flexible seal torque and aerodynamic torque vary almost linearly with nozzle position and will be expressed as a spring rate in units of in.-lb/degrees. These components are otherwise unrelated and are analyzed individually.

The gravity torque is maximum for a static firing condition when the motor is in the horizontal position, as will be the case for the 156-9.

The inertial torque is maximum during flight where the angular and lateral acceleration contribute appreciably to this component. However, missile accelerations produce inertial loads that are in the opposite direction to the spring torque, thus reducing the total torque. Static firing conditions will, therefore, produce a larger total torque than flight conditions. Hence, in the torque analysis static test conditions will be assumed for each torque component, and the torque prediction will, therefore, be conservative for flight conditions.

Individual analysis of each torque component provides a convenient method for establishing the design level torque. Definition of each component also is necessary to evaluate the performance characteristics of the TVC system.

The spring torque in the nozzle affects the response of the actuation system. An increase in spring torque produces a decrease in the damping ratio and, for large vector angles, results in a reduction in the system response. The steady state error as measured in vector angle will increase with increased spring rate.

The damping or viscous friction torque in the nozzle tends to stabilize the system. If the amount of damping is increased, the system becomes less oscillatory and if increased sufficiently the system will become overdamped, hence exhibiting zero overshoot.

The effect of increased inertia in the nozzle causes the system to become more oscillatory. This requires increased damping to stabilize the system. Offset and gravity torque will not affect the system stability but will contribute to the steady state error.

The following paragraphs present a brief discussion of the methods used in defining the torque characteristics of the 156-9 nozzle.

a. Flexible Seal Spring--The torque produced by the flexible seal can be established by summing the incremental forces around the periphery of the seal multiplied by the moment arms of these forces about the pivot axis.

As illustrated in Figure 2-23, the force acts in the plane of the seal at point A and acts normal to the seal plane at point B. The deflection in the seal as well as the length of the moment arm also vary from point A to point B. It was, therefore, necessary to define these variables so the summation of the incremental torques around the seal could be accomplished.

The following paragraphs present the derivation of the seal torque expression. Since the seal deflects in the same manner in all four quadrants, this derivation will consider only a single quadrant of the seal.

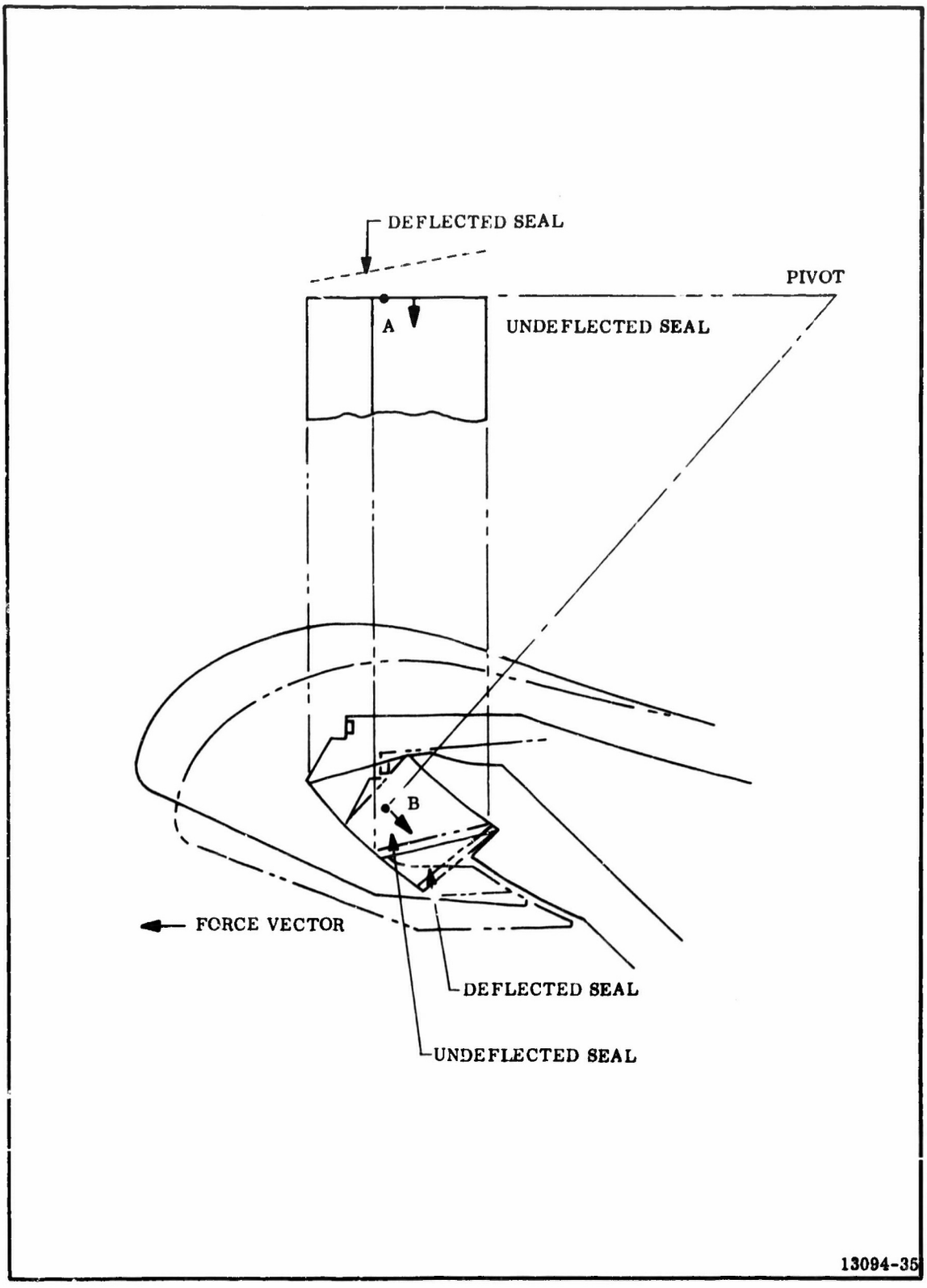

Figure 2-23. Flexible Seal Deflection

The general expression for seal torque is:

$$T = \sum_{o}^{\pi/2} F_i \bar{l}_i$$

where: F = force,

$\bar{l}$ = moment arm.

The incremental force in the seal then can be expressed in terms of seal deflection, shear modulus of the rubber, and seal geometry.

$$F_i = \frac{\delta_i G \, dA}{n t_r}$$

where: δ_i = seal deflection,

G = shear modulus,

dA = incremental cross-sectional area,

n = number of rubber laminates,

t_r = thickness per laminate.

The seal deflection is simply $\bar{l}\,\theta$ where $\bar{l}$ is the moment arm and θ is the nozzle deflection angle (Figure 2-24). The general expression for the moment arm length is:

$$\bar{l} = \bar{r} \, (\mathrm{Sin}^2 \beta \, \mathrm{Sin}^2 \Phi + \mathrm{Cos}^2 \beta)^{1/2}$$

where: $\bar{r}$ = radius of curvature,

β = angle between seal axis and the mean radius of the seal.

The incremental area also is:

$$dA = (\bar{r} \, \mathrm{Sin} \, \beta \, d \, \Phi) \, W.$$

The width (w) can now be expressed in terms of β_1 and β_2, the angles measured between the seal centerline, and the inside and outside radii of the seal, respectively, so that

$$w = \bar{r} (\beta_2 - \beta_1),$$

β_2 and β_1 expressed in radians.

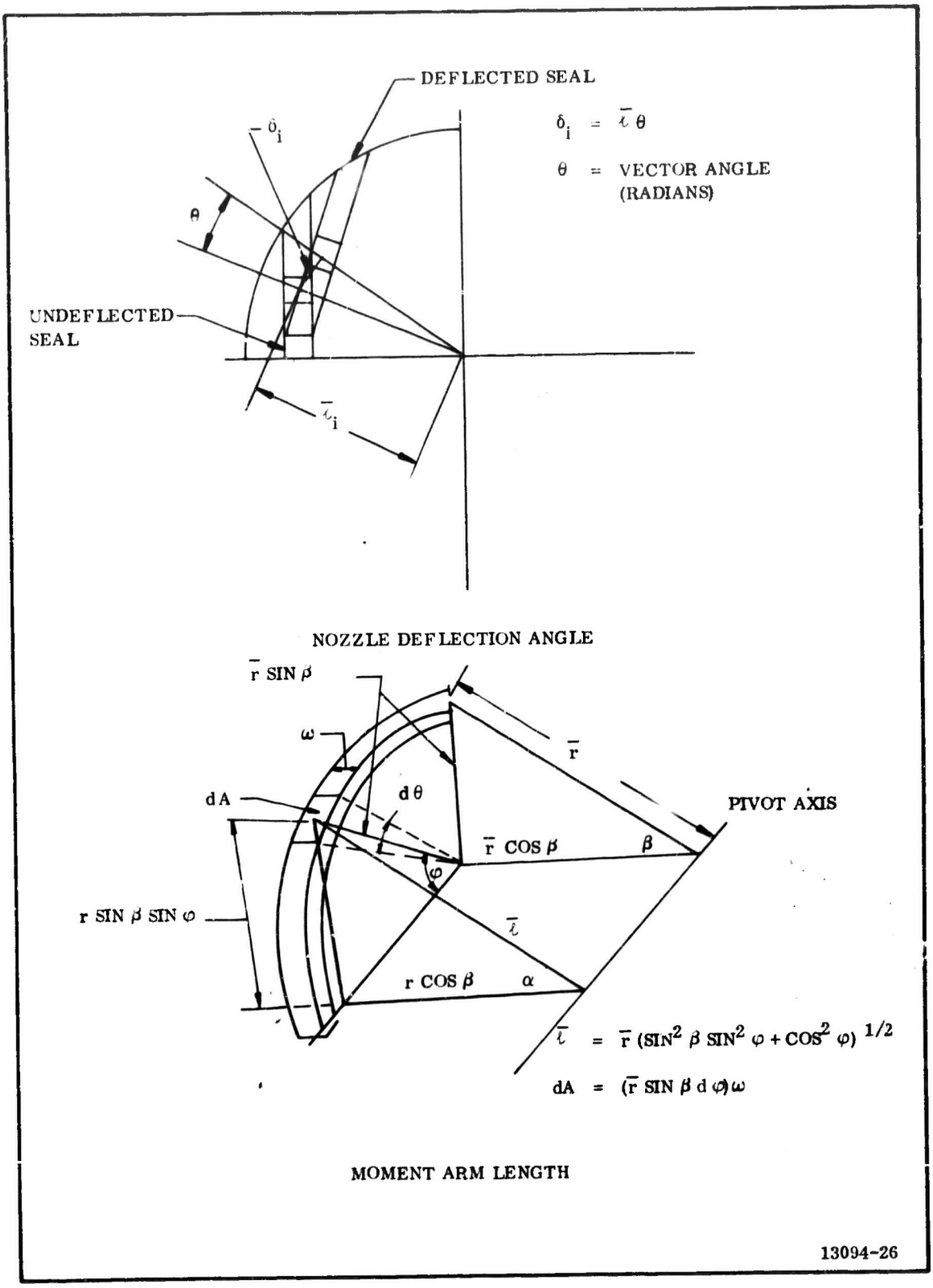

Figure 2-24. Determination of Moment Arm

The force in the seal thus becomes

$$F_i = \frac{G}{nt_r} r^3 \text{ Sin } \beta \left(\text{Sin}^2 \beta \text{ Sin}^2 \Phi + \text{Cos}^2 \beta\right)^{1/2} \left(\beta_2 - \beta_1\right) d\Phi.$$

The torque for the entire seal can then be determined from the integral

$$T = 4 \int_0^{\pi/2} \bar{1} \, F_i = 4 \int_0^{\pi/2} \frac{G}{nt_r} r^4 \text{ Sin } \beta \left(\text{Sin}^2 \beta \text{ Sin}^2 \Phi + \text{Cos}^2 \Phi\right) \left(\beta_2 - \beta_1\right) d\Phi.$$

Performing the integration and converting all angles from radians to degrees:

$$T = \frac{G \pi^3}{3.24 \times 10^4 nt_r} \bar{r}^4 \text{ Sin } \beta \left(1 + \text{Cos}^2 \beta\right) \left(\beta_2 - \beta_1\right).$$

Since the seal torque is linear with deflection angle, expression of this component is more convenient as torque per degree of vector. Hence,

$$\frac{T}{\theta} = \frac{G \pi^{3-4} \text{ Sin}}{3.24 \times 10^4 nt_r} \left(1 + \text{Cos}^2 \beta\right) \left(\beta_2 - \beta_1\right).$$

In Figure 2-25, the theory is compared with Lockheed test data.* The theory predicts torque slightly lower than data recorded at zero chamber pressure and slightly higher than the data from 600 psi testing. The predicted curve was calculated using the shear modulus quoted for the zero pressure condition. There is less than 10 percent error in the data and the error appears to be linear with position. The shear modulus appears as a linear function in the torque equation, leading to the conclusion that the shear modulus was in error.

*Lockheed Propulsion Co, Development of an Elastomeric Seal for Omniaxial Movable Nozzles (Lockseal), Progress Report No. 2, Technical Report No. AFRPL-TR-65-173. August 1965.

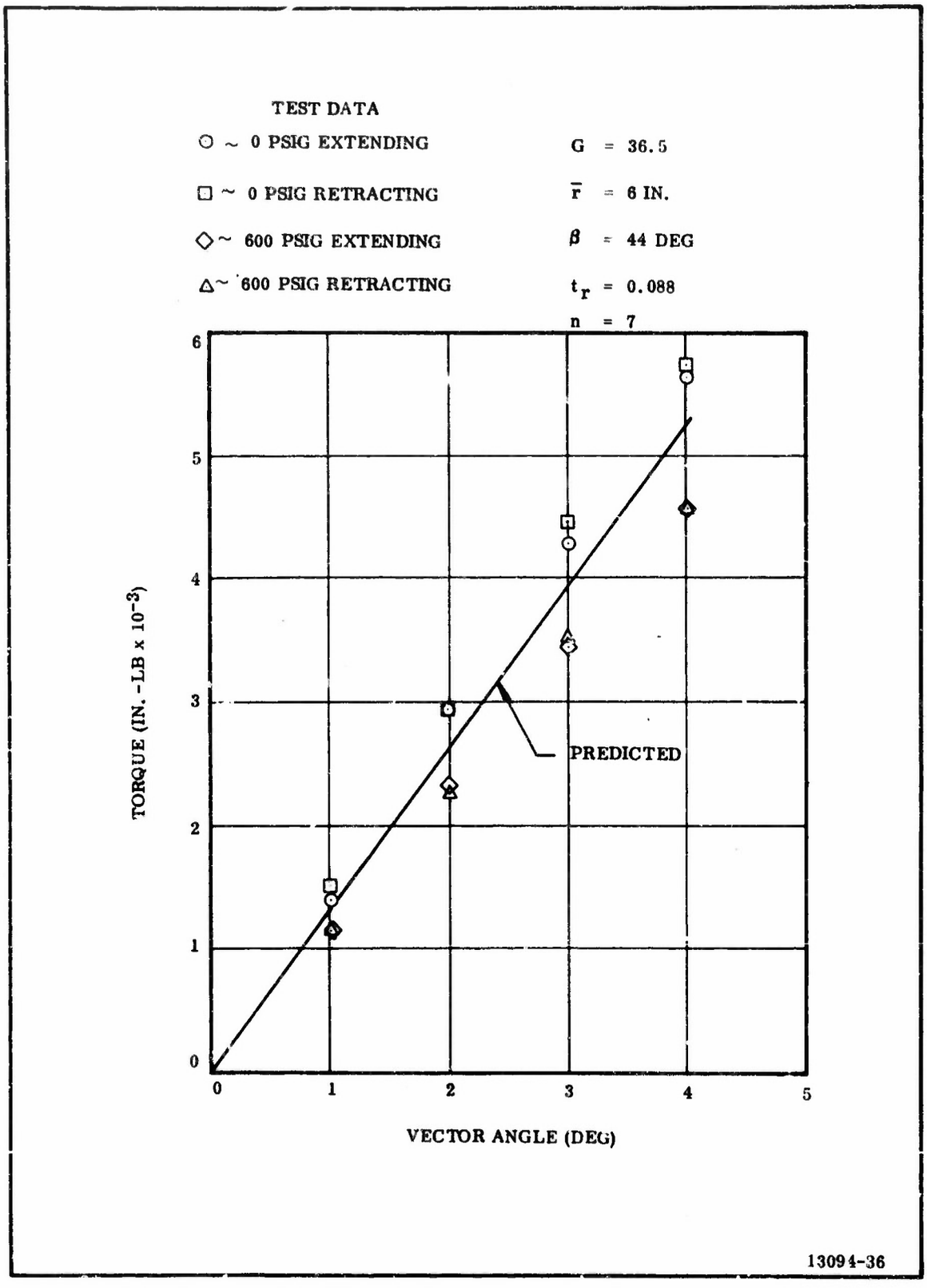

Figure 2-25. Seal Torque vs Vector Angle

The above derivation is for a spherical shim seal. However, the 156-9 seal design has conical shims. Derivation of an equation to define the torque in a conical seal has not been accomplished. However, bench test data for a conical shim seal have been compared with predicted values obtained using the above equation. These data are presented in Figure 2-26. Test data shows good agreement with predicted values at low pressures. However, an increase in pressure results in an increase in the seal spring rate. This effect is opposite to that experienced with the Lockheed seal. It has not been determined whether the increase in torque with pressure is due to a change in the shear modulus of the rubber, or if this variation is characteristic of the conical shim seal. However, at the design pressure (MEOP = 830) the torque is approximately 50 percent higher than predicted. Therefore, a 50 percent factor was applied to the 156-9 predicted torque obtained with the spherical shim equation. This prediction is presented in Figure 2-25 as nominal value. The maximum value shown was determined by applying a 25 percent factor to account for variation in rubber properties.

b. Internal Aerodynamic Spring--The internal aerodynamic torque acting on a submerged movable nozzle is the result of unsymmetrical flow in the vectored nozzle, thus producing a pressure differential in the actuation plane. Aerodynamic torque is normally linear with deflection angle and reacts as spring torque.

The aerodynamic torque can be calculated by summing the components of force produced by pressure acting on the nozzle wall multiplied by the perpendicular distance from the force to the nozzle pivot. The general equation describing the aerodynamic torque may be written as:

$$T_a = \int_{X_1}^{X_2} \int_0^{2\pi} \rho \sin\theta \, (rX + r^2 \tan\alpha) \, d\theta \, dx$$

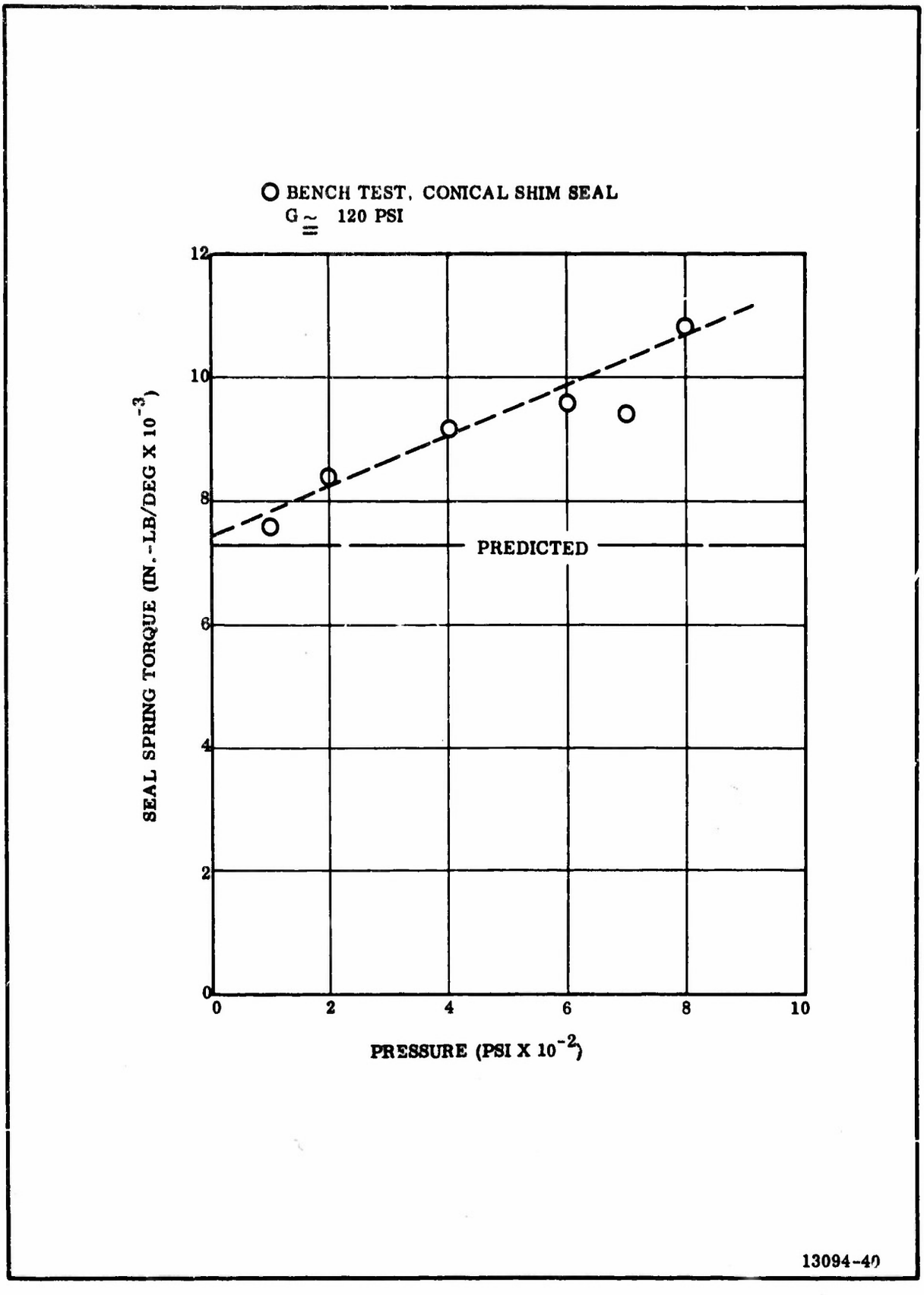

Figure 2-26. Seal Spring Rate vs Chamber Pressure

where: θ = azimuthal angle (radians),

T_a = total aerodynamic torque about the pivot axis (in. - lb),

r = nozzle radius at point of force application,

x = axial distance from pivot to point of calculation in the nozzle (in.)

p = static pressure,

α = nozzle wall slope.

This equation requires knowledge of the wall static pressure and the pressure differentials which exist in the nozzle. Two procedures are available for developing internal wall pressure in a vectored nozzle. They are air flow simulation tests (cold flow) and a two dimensional method of characteristics solution.

The axial location (x) may be expressed as a function of the throat radius and the aerodynamic torque may be expressed as a function of chamber pressure and the cube of the throat diameter. This relationship may be used for scaling of geometrically similar nozzles.

The effect of nose design and propellant configuration on submerged movable nozzle torque was determined by cold flow testing. These data were used to predict the aerodynamic torque. The grain configuration has a major influence on aerodynamic torque. In the 0 sec web time configuration, the gas has a relatively high velocity at the aft end of the grain and turning of the gas through the nozzle results in a nozzle wall pressure differential in the plane of actuation. However, as the propellant burns out a large plenum of low velocity gas is created. Therefore, vectoring the nozzle does not significantly alter the nozzle pressure distribution late in the firing. For this reason the aerodynamic torque for submerged nozzles decreases significantly with firing time.

Since the pivot location may vary considerably on submerged nozzles, it was necessary to investigate this effect of varying the pivot location. This was accomplished by analytically varying the pivot in the preceding equation. This

technique assumes that pressure distribution in the nozzle is not altered when the pivot location is moved relative to the nozzle throat. Figure 2-27 presents the aerodynamic spring rate divided by chamber pressure and the cube of the throat diameter versus pivot location. Curves are shown for the 0 sec grain and burned out grain configuration.

As indicated in Figure 2-27 the present configuration produces nonrestoring aerodynamic torque which opposes the torque of the seal, thus reducing the total torque during the early portion of the firing.

Placing the pivot forward of the throat would produce a restoring torque which increases total torque. A forward pivot increases the moment arm through which the asymmetric forces act, thus the magnitude of the torque increases. Placing the pivot an equal distance forward of the throat on the 156-9 would increase the maximum total torque prediction by 500,000 inch pounds. The results of the aerotorque prediction are given in Table 2-4.

Aerodynamic torque, however, becomes less significant as the firing progresses. Although total torque is reduced early in firing by the aerotorque, it was assumed to be zero throughout firing since it approaches zero late in the firing. This imparts further conservatism to the actuation system design since the maximum vector angle on a flight version of the 156-9 will probably be required early in the firing when the aerotorque is diminishing the total predicted torque value.

c. Frictional--Frictional torque in conventional movable nozzles is the result of sliding surfaces such as bearings, O-rings, etc. Since there are no sliding surfaces in the flexible seal nozzle, the coulomb friction torque normally associated with movable nozzles does not exist.

Elimination of friction torque is one of the outstanding advantages of the flexible seal. Friction torque has two major disadvantages.

1. Friction torque is notoriously variable and therefore unpredictable with the desired accuracy.

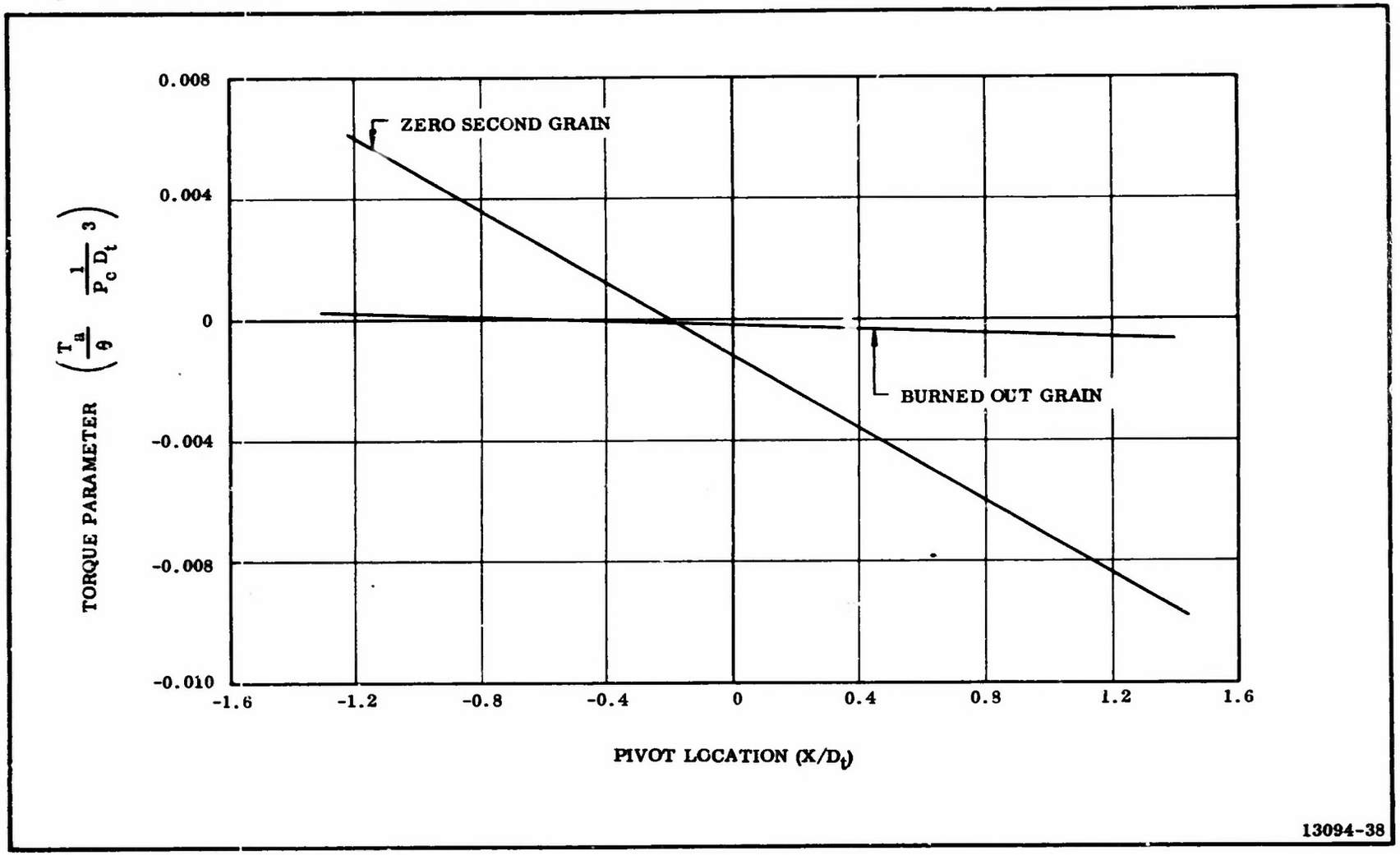

Figure 2-27. Aerodynamic Spring Rate vs Pivot Location

TABLE 2-4

156-9 TORQUE PREDICTION

	Torque Component	Predicted Spring Constant (in.-lb/deg) Nominal	Predicted Spring Constant (in.-lb/deg) Maximum	Predicted Torque (in.-lb) Nominal	Predicted Torque (in.-lb) Maximum (Worst-on-Worst)
1.	Dynamic Spring	--	--	320,000	1,356,000
	Seal Component	271,700	339,000	806,800	--
	Aerodynamic Component	-70,000	0	--	--
2.	Seal Viscous	--	--	125,000	250,000
3.	Offset	--	--	103,000	171,000
4.	Gravitational	--	--	188,000	188,000
5.	Inertial	--	--	117,300	117,300
				1,338,100	2,080,000

$$\text{Actuation Design Factor of Safety} = \frac{2,080,000}{1,338,100} = 1.55$$

2. Friction torque is the major source of steady state error in the servocontrol system.

Friction torque varies widely since it depends on surface conditions, lubricant condition, gap width, and applied load. There is also a variation from static friction to sliding friction which produces a "breakaway" peak in torque.

On Stage I MINUTEMAN motors, friction torque variations of 100 percent among the four nozzles on the same motor have been observed, and as high as 400 percent variations from motor to motor. Friction torque on these nozzles tends to increase with motor age. An average friction torque increase of 50 percent occurs in a three year storage period, probably resulting from lubricant and O-ring aging.

Elimination of the unpredictable friction torque thus reduces actuation system weight by reducing the statistical upper design limit.

Reducing steady state error simplifies the control system and improves the accuracy of the guidance. By reducing flight time spent off the flight path (by improving accuracy), the range is increased. Thus, eliminating friction torque improves the range and accuracy of a missile system while reducing cost.

The viscoelastic properties of the rubber produce a torque which is a function of the nozzle actuation rate. This torque is defined as viscous friction torque, which can be expressed as:

$$T_V = C \frac{d}{dt}$$

where:

C = damping coefficient of the seal

It is apparent that for the normal sinusoidal actuation this component does not contribute to the maximum total torque since this term is a maximum when the nozzle is at zero position and zero when the nozzle is fully vectored. This component, however, contributes to the stability of the TVC system and, therefore, must be thoroughly analyzed.

Amplitude decay tests were performed on a spherical shim bearing to determine the damping characteristics of the proposed seal. This seal has a radius of curvature of 7.6 in , 81 shims and a total rubber thickness of 0.567 inch. The shear modulus of the rubber was determined to be approximately 120 psi. Figure 2-28 shows a typical transient response curve obtained from this test program. This system appears to have a damping ratio of approximately 0.2. This value was used to determine the nominal viscous torque for the 156-9 seal. Viscous torque values are presented in Table 2-4.

Viscous damping is also an important consideration in determining the stability characteristics of the TVC system. An analog simulation study is presently being performed at TCC. The damping requirement of the 156-9 TVC system will be determined from this study.

d. Offset--Offset torque is considered to be the zero position aerodynamic torque resulting from asymmetrical flow in the unvectored nozzle. Therefore, it can be scaled in the same manner as aerodynamic torque.

Comparisons were made of cold flow data and hot firing data from four Thiokol submerged nozzle firings. It was determined that for all firings, scaling of the cold flow data resulted in overprediction of the offset torque. Therefore, to insure a conservative maximum offset torque prediction, the cold flow data were scaled directly. Offset torque is presented in dimensionless form as a function of pivot location in Figure 2-29. The predicted offset torque for the design configuration is presented in Table 2-4.

e. Inertial--The inertial torque imposed on the nozzle during static firing is simply that torque resulting from accelerations produced by the actuator. Assuming a sinusoidal actuation, the maximum acceleration and the maximum inertial torque can be determined as:

$$\ddot{\theta} = \dot{\theta} \times 2\pi f$$

$$T_{inertial} = \frac{\pi J}{180} \ddot{\theta}\ Max$$

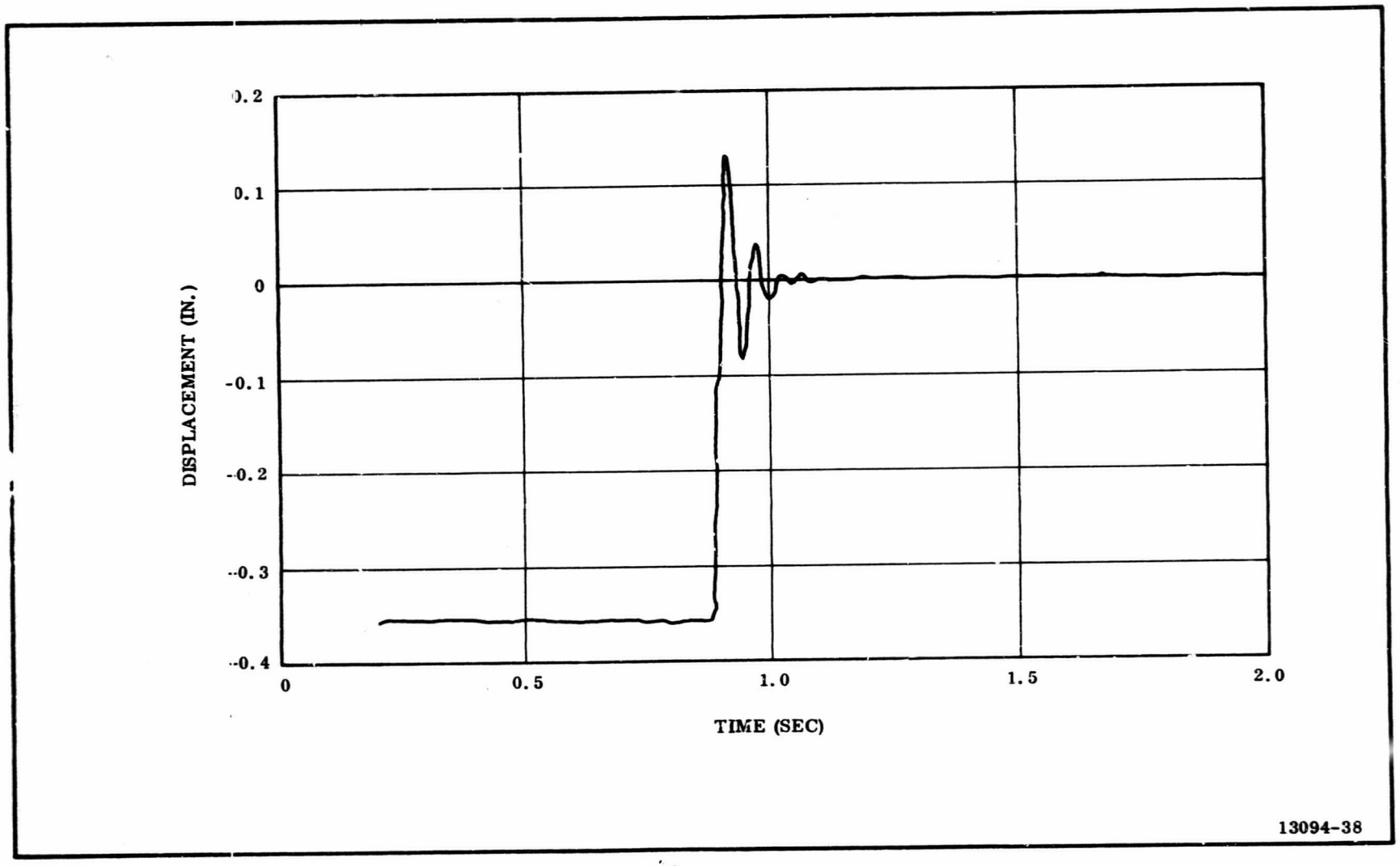

Figure 2-28. Flexible Seal Transient Response, MRC-2A

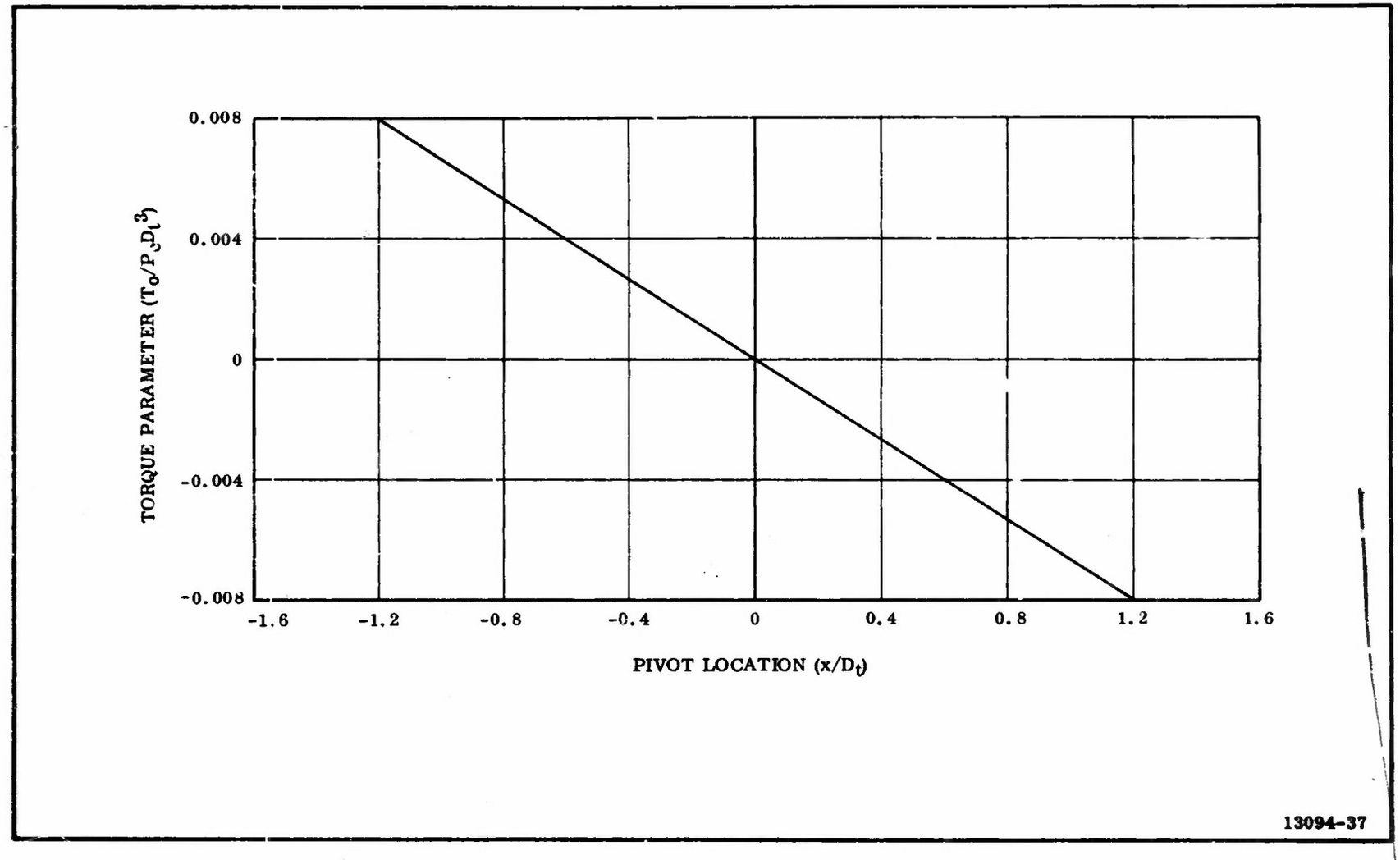

Figure 2-29. Offset Torque vs Pivot Location Zero Second Grain

where:

J = mass moment of inertial (in. lb-sec^2)

$\ddot{\theta}$ Max = maximum angular acceleration (deg/sec^2).

Table 2-4 shows the predicted maximum inertial torque.

f. Gravitational--The moment produced by gravity is simply the nozzle weight multiplied by the distance from pivot to the center of gravity. The maximum gravity torque that will be experienced by the nozzle will occur when the nozzle is in the horizontal position. This distance will vary slightly with nozzle deflection. However, the maximum torque will occur with the nozzle in the zero position. Therefore a zero position nozzle was assumed for this prediction.

Missile attitude also affects the magnitude of the gravity torque component. For design purposes the missile was assumed to be in the horizontal position. This results in a conservative prediction since the minimum angle between the missile centerline and the horizontal axis is approximately 20 deg for normal flight conditions.

g. Total--Total torque can be expressed with the following general expression.

$$T_t = J\ddot{\theta} + C\dot{\theta} + K\theta + T_o + T_G$$

where:

J = mass moment of inertia,

C = damping coefficient,

K = combined seal plus aerodynamic spring rate,

T_o = offset torque,

T_G = gravity torque,

θ = nozzle vector angle for sinusoidal motion,

$\theta = \theta_{max} \text{ Sin } 2\pi \text{ ft}$,

$\dot{\theta} = 2 \text{ ft } \theta_{max} \text{ Cos } 2\pi \text{ ft}$,

$\ddot{\theta} = (2\pi f)^2 \theta_{max} \text{ Sin } 2\pi \text{ ft}$.

Since

$$t = \frac{1}{2\pi f} \left(\text{Sin}^{-1} \frac{\theta}{\theta_{max}}\right),$$

the following expression is readily obtained.

$$T_t = -J(2\pi f)^2 \theta + C(2\pi f)(\theta^2_{max} - \theta^2)^{1/2} \frac{\dot{\theta}}{|\dot{\theta}|} + K\theta + T_o + T_G$$

For the sine wave actuation at the maximum required rate, the total torque has been calculated as a function of nozzle position using the equation above.

The predicted total torque as well as the various components are presented in Table 2-4.

This number represents the maximum expected total torque for a sinusoid actuation. To determine the worst condition value, the conservative upper limit predicted values for each component occur simultaneously in the same direction. This is a hypothetical condition since the maximum spring torque, inertial torque, and viscous torque cannot occur physically simultaneously in the same direction.

7. WEIGHT ANALYSIS

Total weight of the 156-9 nozzle assembly is 13,102 lb of which 7,667 lb is contained in the movable portion, 3,894 lb in the fixed portion, and 1,541 lb in the flexible seal. The seal weight is preliminary and can be expected to change as the seal design is finalized.

In the weight analysis (Table 2-5) the nozzle is divided into movable, fixed, and bearing or seal portions. Each component is identified by drawing and item number. A format of title identations is followed in the subtotals. The weights of items whose titles are indented are summed in the weight column for the title preceding the indentation. This format is continued up through the subassemblies to the complete nozzle assembly.

TABLE 2-5

MASS PROPERTIES DATA

NOZZLE-TU-562 7U40515 JW 8-11-66

	WEIGHT (LBS)	CENTER OF GRAVITY LONG.	LAT.	VERT.	MOMENT OF INERTIA PITCH	ROLL	YAW
TOTAL NOZZLE 7U40515	13517.466	427.446	99.925	99.483	4464.753	3590.433	4392.644
MOVABLE PORTION	7666.900	440.662	100.000	100.000	2852.195	2022.153	2845.259
METAL PARTS	4494.807	444.248	100.000	100.000	1582.542	1271.918	1575.608
ENTRANCE HOUSING7U40521	420.491	392.551	100.000	100.000	29.010	57.847	29.011
ITEM 1 SHELL	36.509	395.264	100.000	100.000	3.567	7.127	3.567
ITEM 2 PLATE	383.983	392.293	100.000	100.000	25.380	50.720	25.381
EXIT HOUSING 7U40522	4015.642	450.329	100.000	100.000	1246.304	1201.794	1239.370
ITEM 1 FLANGE	172.626	393.929	100.000	99.997	9.424	18.823	9.426
ITEM 2 RING	198.059	400.001	100.000	100.000	10.135	19.632	10.135
ITEM 3 FWD CONE	819.381	426.521	100.000	100.000	93.524	140.449	93.524
ITEM 4 AFT CONE	1659.685	473.334	100.000	100.000	421.516	643.400	421.516
ITEM 5 STIFFENER RING	462.606	451.769	100.000	100.000	66.920	132.455	66.920
ITEM 6 PLATE	182.570	452.651	100.000	100.000	29.781	59.559	29.781
ITEM 7 MOUNTING RING	491.801	450.280	100.000	100.000	89.835	178.236	89.835
ITEM 8 GUSSETS (8)	28.915	449.169	100.000	100.000	8.106	9.241	1.169
BARRIER HOUSING 7U40526	58.673	398.540	100.000	100.000	6.157	12.277	6.157
PLASTICS	3122.833	435.552	100.000	100.000	1238.278	750.235	1238.278
NOSE ASSEMBLY 7U40516	487.327	390.175	100.000	100.000	35.780	70.201	35.780
ITEM 2 LINER-OUTER-CC	163.715	390.927	100.000	100.000	14.676	28.718	14.676
ITEM 3 LINER-NOSE -CC	110.749	387.650	100.000	100.000	6.529	12.978	6.529
ITEM 4 RING -CC	45.769	389.936	100.000	100.000	2.039	4.054	2.039
ITEM 6 INSUL-INNER-SC	100.578	390.223	100.000	100.000	6.466	12.904	6.466
ITEM 5 INSUL-OUTER-SC	66.516	392.621	100.000	100.000	5.812	11.547	5.812
MOVABLE HOUSING 7U40520	2424.712	447.723	100.000	100.000	828.667	633.183	828.667
ITEM 2 INSULATOR -CC	234.418	397.676	100.000	100.000	9.977	18.726	9.977
ITEM 3 INSULATOR -GLC	56.164	397.390	100.000	100.000	2.827	5.313	2.827
ITEM 4 INSULATOR -CC	289.514	416.904	100.000	100.000	20.460	34.621	20.460
ITEM 6 INSULATOR -SC	1354.650	464.223	100.000	100.000	337.893	439.647	339.893
ITEM 7 INSULATOR -GLC	489.117	450.110	100.000	100.000	158.115	134.796	158.115
ITEM 9 O-RINGS	.849	403.933	100.000	100.000	.040	.081	.040
BARRIER HOUSING	210.794	400.449	100.000	100.000	23.651	46.851	23.651
ITEM 6 INSULATOR -SC	29.515	399.579	100.000	100.000	3.009	6.002	3.009
ITEM 7 LINER -SC	181.279	400.590	100.000	100.000	20.637	40.849	20.637
ATTACH BOLTS + PINS	49.260	437.466	100.000	100.000	1.186	.000	1.186
ITEM 19 SET SCREWS	5.700	465.780	100.000	100.000	.000	.000	.000
ITEM 20 SOC HD CAP SCRS	24.000	436.180	100.000	100.000	.000	.000	.000
ITEM 22 SET SCREWS	1.700	433.630	100.000	100.000	.000	.000	.000
ITEM 23 STUDS	16.800	430.480	100.000	100.000	.000	.000	.000
ITEM 24 NUTS	1.060	431.180	100.000	100.000	.000	.000	.000
FIXED PORTION	3893.998	414.597	99.941	99.941	638.804	1212.519	638.804

TABLE 2-5 (Cont)

MASS PROPERTIES DATA

NOZZLE-TU-562 7U40515 JW 8-11-66

	WEIGHT (LBS)	CENTER OF GRAVITY LONG.	LAT.	VERT.	MOMENT OF INERTIA PITCH	ROLL	YAW
METAL PARTS	3348.267	415.166	99.932	99.932	556.017	1056.603	556.017
FIXED HOUSING 7U40528	3348.267	415.166	99.932	99.932	556.017	1056.603	556.017
ITEM 1 LOWER FLANGE	750.245	422.893	100.000	100.000	170.776	341.310	170.776
ITEM 2 CONE	2280.030	414.003	100.000	100.000	342.558	665.097	342.558
ITEM 3 UPPER FLANGE	305.711	404.805	100.000	100.000	23.204	46.380	23.204
ITEM 4 - CLIPS	5.107	408.137	85.471	85.471	.234	.466	.234
ITEM 5 - CLIPS	7.174	423.055	78.400	78.400	.725	1.447	.725
PLASTICS	545.731	411.105	100.000	100.000	81.117	155.915	81.117
ITEM 17-INSULATOR -SC	226.315	405.913	100.000	100.000	24.217	48.101	24.217
ITEM 18-INSULATOR -MAS	319.416	414.784	100.000	100.000	54.649	107.814	54.649
FLEXIBLE BEARING 7U40530	1807.361	398.506	100.000	100.000	147.808	287.907	147.808
ITEM 1 FWD END RING	524.973	394.796	100.000	100.000	44.959	89.569	44.959
ITEM 2 AFT END RING	448.260	402.171	100.000	100.000	31.513	62.768	31.513
ITEM 3 STABILIZER PLATE	.000	.000	100.000	100.000	.000	.000	.000
ITEM 4 STABILIZER PLATE	.000	.000	100.000	100.000	.000	.000	.000
ITEM 5 STABILIZER PLATE	.000	.000	100.000	100.000	.000	.000	.000
ITEM 6 ELASTOMER	84.720	398.766	100.000	100.000	6.905	13.692	6.905
ITEM 7 SHIMS	721.851	398.766	100.000	100.000	58.837	116.658	58.837
BOOT	27.558	401.980	100.000	100.000	2.650	5.220	2.650
BRACKET ASSY	149.207	434.234	94.773	54.731	4.716	1.768	3.893
ACTUATOR BRACKET	57.712	424.989	91.643	58.713	1.081	.497	.649
TRUNNION ASSY	50.368	434.393	94.921	48.908	.226	.225	.130
TRUNNION PIN	5.084	435.680	91.773	48.803	.002	.003	.004
CLEVIS	35.418	448.682	100.000	57.360	.071	.040	.087
BUSHINGS	.624	444.680	100.000	55.590	.000	.000	.000

8. NOZZLE ASSEMBLY

The sequence of nozzle assembly is shown in Figure 2-30.

The protective rubber boot will be bonded to the seal end rings to form the seal assembly. The barrier assembly will be positioned around the seal and the set screws installed. Adhesive will be applied to the silica and boot interface prior to mating of the subassemblies. The barrier liner will be dry fit and then bonded to the barrier assembly.

The resulting assembly will then be mated with the fixed housing assembly, bolts installed and torqued to predetermined values. The nose assembly will then be bolted and bonded to the assembly.

The final step is the fitting, bonding, and bolting of the exit assembly. Three tapered pins will be provided on the entrance housing to aid in the alignment of the exit housing.

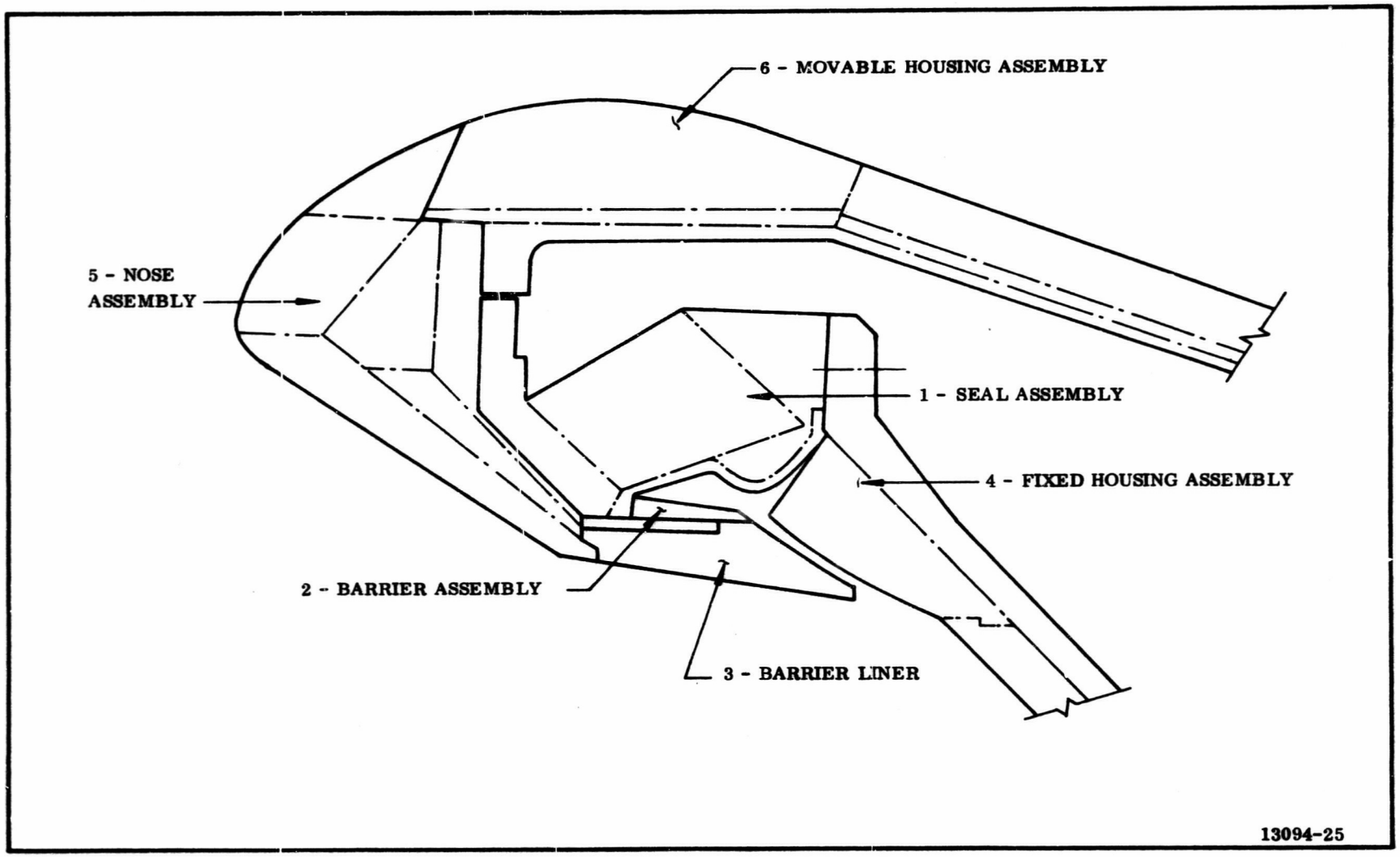

Figure 2-30. 156-9 Nozzle Assembly Sequence

B. SEAL

1. CONFIGURATION

Data from testing completed to date was used to modify the equation for critical pressure. The two major revisions are:

1. Value of n = 0.25 has been replaced by a curve of n as a function of the ratio of radius to shim thickness (a/t_m);
2. The relation between rubber shear modulus and buckling pressure has been revised.

The equation for critical pressure as it has been modified is:

$$P_{cr} = K_1 \frac{E_M}{2(1-\mu^2_M)}\left(\frac{t_M}{\bar{a}}\right)^2 \left[1 - \frac{R_i^2}{R_o^2}\right] \left[1 + \frac{(G_R)^{0.25} W}{t_R} C_1 \left(\frac{\bar{a}^2}{E_M t^2_M}\right)^n\right]$$

Where:

E_M	=	Elastic Modulus of Metal Shims
K_1	=	Constant for Flat Washer*
μ_M	=	Poisson's Ratio of Metal Shim
t_M	=	Metal Shim Thickness
$\bar{a}$	=	Average Spherical Radius
R_i	=	Inside Radius at $\bar{a}$
R_o	=	Outside Radius at $\bar{a}$
G_R	=	Shear Modulus of Rubber
t_R	=	Rubber Layer Thickness
W	=	Width of Shim at $\bar{a}$
C_1	=	Constant = 24.2
n	=	Buckling Constant

*Roark, "Formulas for Stress and Strain," page 315. McGraw Hill, 1954.

Figure 2-31 shows the buckling constant as a function of the radius to shim thickness ratio. The available data are rather limited and two curves have been fitted through the data in an attempt to define an upper and lower limit on the critical pressure. As n decreases, the critical pressure increases.

Figure 2-32 shows curves of critical pressure as a function of shim thickness for various values of shim to rubber layer thickness ratios. Two sets of curves are shown to represent the two plots from Figure 2-31. Based on these curves, a shim thickness of 0.036 in. was selected for the Thiokol flexible seal assembly.

Figure 2-33 shows how torque, critical buckling pressure and critical pressure based on material yield strength vary for a shim thickness of 0.036 in. as a function of rubber layer thickness. The minimum required pressure and maximum allowable torque are indicated on the graph. A rubber layer of 0.025 in. was selected for the Thiokol seal, resulting in an acceptable value of torque and a high structural factor of safety. The buckling equation will be re-evaluated following the bench test of the first seal for the 100 in. program and, if any revisions are required, the 156 in. flexible seal design will be re-evaluated.

2. TESTS

Table 2-6 summarizes the seal work completed by Thiokol and shows the fabrication and testing planned for other programs. Figure 2-34 shows the relative size of the flexible seals that have been or will be tested by Thiokol.

The completed, refined 156 in. flexible seal design is shown in Figure 2-35. Detailed parts of the seal are shown in Figures 2-36, 2-37 and 2-38.

3. SHIM THICKNESS

Note that the design is based on using 88 stainless steel shims of a nominal 0.036 in. thickness. If the actual thickness of the shims exceeds 0.036 in., fewer will be needed. If actual thickness is less than 0.036 in., more will be needed.

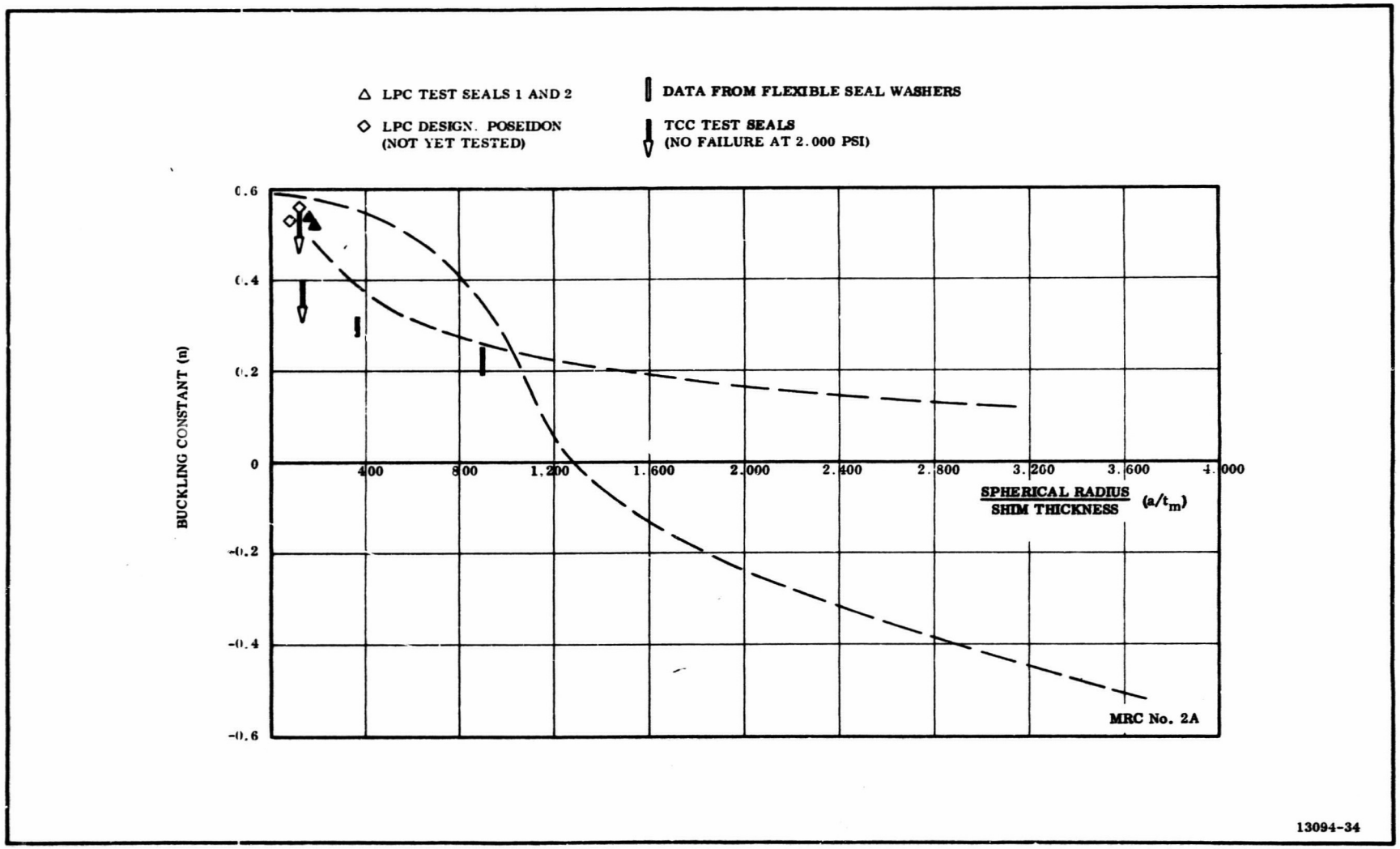

Figure 2-31. Buckling Constant as a Function of Spherical Radius to Shim Thickness Ratio

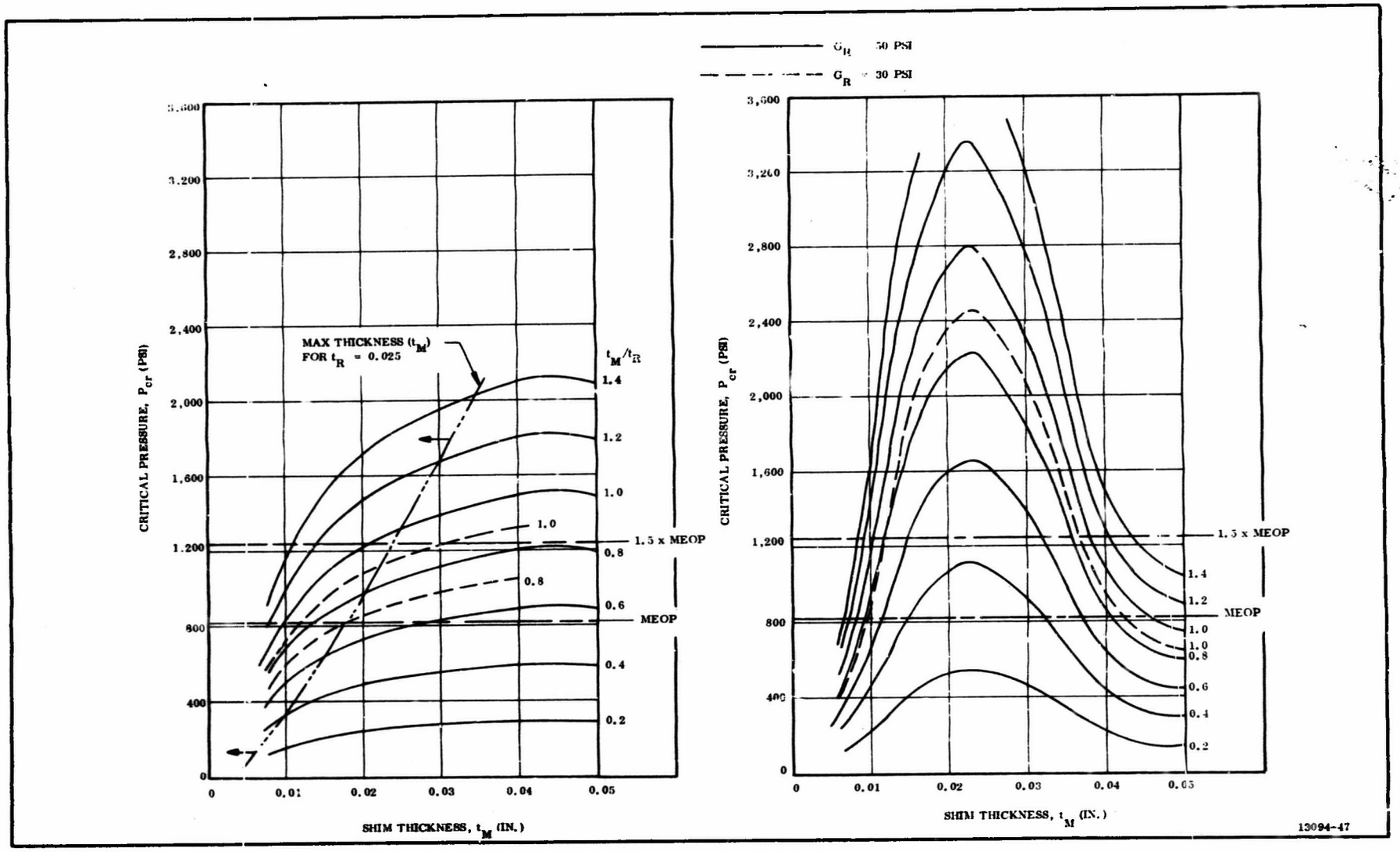

Figure 2-32. 156 In. Nozzle Flexible Seal Critical Pressure vs Shim Thickness for Varying t_M/t_R Ratios

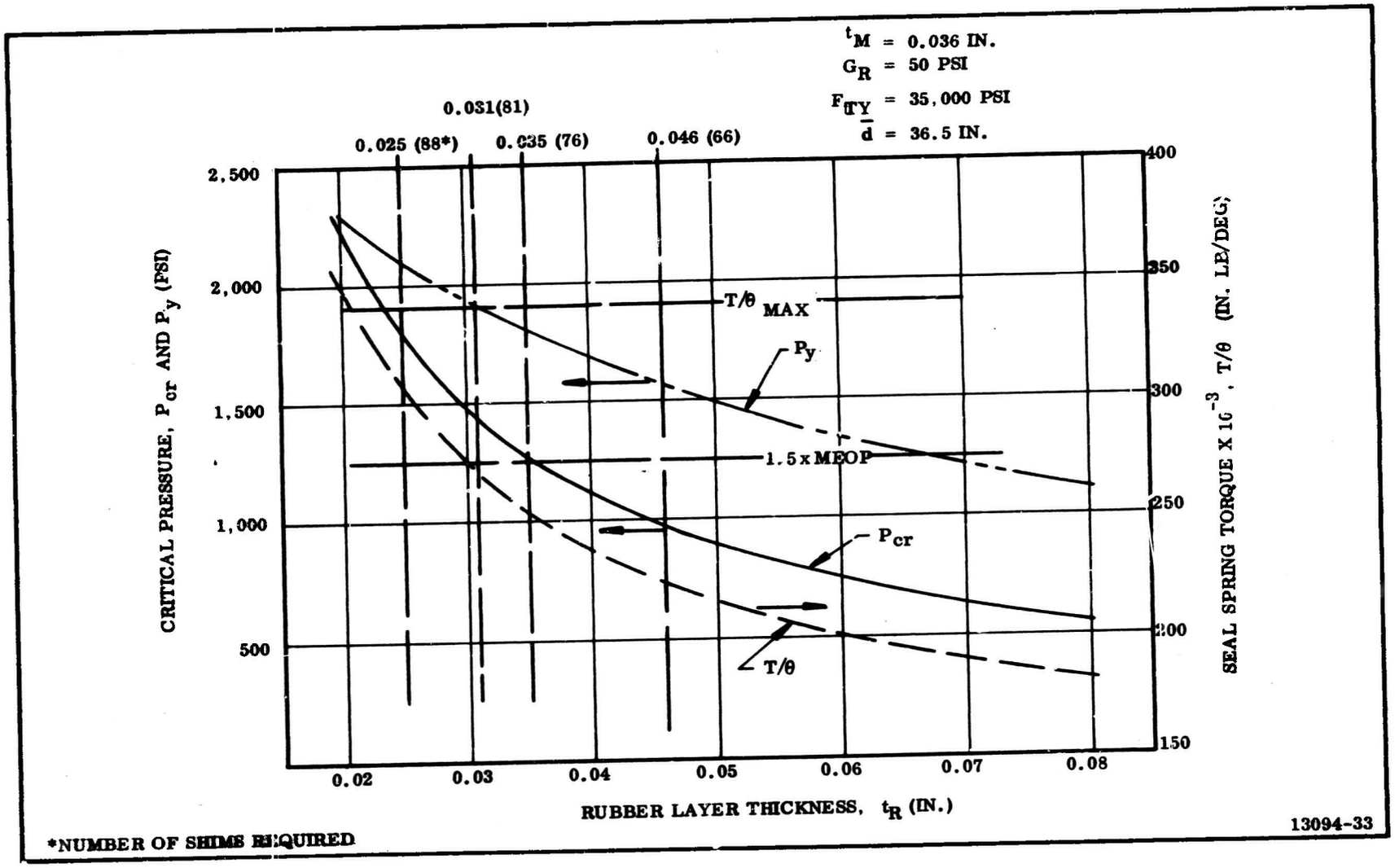

Figure 2-33. 156 In. Motor - Flexible Seal Critical Pressure and Torque vs Rubber Layer Thickness

TABLE 2-6

FLEXIBLE SEAL CONFIGURATION

Program	Serial No.	Vector Angle (deg)	Elastomer: Material and Method of Application	Elastomer: No. of Plys and Thickness (in.)	Elastomer: Shear Modulus (psi)	Shim: Material and Configuration	Shim: Shim Thickness (avg)	Test Results: Spring Rate (in.-lb/deg)	Test Results: Pressure Test (psig)	Remarks
Flat Washer	1 thru 16	--	Silastic Screeded	15 - 0.004 30 - 0.008	--	Stainless - Brass - Flat - Continuous	0.002 0.008	--	1,000 7,000	Buckling tests
IR & D	MRC-1	3	DC 86571 Screeded	81 - 0.007	130	SS 302 Buttons	0.002	--	--	Not tested, unbonded
	MRC-2A	3	86571/15 Screeded	81 - 0.007	105	SS 302 Split Spherical	0.002	10,000 at 800 psig	1,500	Failed at 1,500 psig at 3 deg deflection
	MRC-2B	3	DC 86571/15 Spray	81 - 0.007	105	SS 302 Herringbone	0.002	--	--	Bond failure
	MRC-3	8	DC 86571/15 Screeded	158 - 0.007	40	SS 302 Split Conical	0.002	--	--	In fabrication, test 1 Nov
	MRC-4	2.25	DC 86571/15 Screeded	93 - 0.007	105	SS 302 Split Spherical	0.002	11,000 at 800 psig	800	Slipped shim
	MRC-5	2.25	DC 86571/15 Spray	94 - 0.007	40	SS 302 Laboratory Formed Spherical	0.002	--	--	Shims fabricated, 15 Nov
	MRC-2C	3	DC 86571/15 Spray	89 - 0.007	40	SS 302 Laboratory Formed Spherical	0.002	--	--	Shims fabricated, 1 Dec
	TCC-1	3	Goodyear 357-2 Polyisoprene Calendered	7 - 0.046	97	SS 304 Laboratory Formed Spherical	0.060	15,400 at 800 psig	800	Leaked at pressure
	TCC-2	3	Goodyear 357-2 Polyisoprene Calendered	7 - 0.046	97	SS 304 Laboratory Formed Spherical	0.060	9,000 at 800 psig	2,000	Did not fail at 2,000 psig at 30 deg deflection
	TCC-3	5	Shell Modified Polyisoprene Calendered	7 - 0.046	38	SS 304 Laboratory Formed Spherical	0.060	800 at 800 psig	1,200	Extruded shim at 56% psig
	TCC-4	2.25	Goodyear 357-2 Polyisoprene Calendered	7 - 0.046	97	SS 304 Laboratory Formed Spherical	0.060	5,500/8,800*	800	
	TCC-5	3	Goodyear 357-2 Polyisoprene Calendered	5 - 0.130	97	SS 304 Laboratory Formed Spherical	0.060	--	2,000	Did not fail at 2,000 psig at 3 deg deflection
	TCC-6	2.25	Goodyear 357-2 Polyisoprene Calendered	7 - 0.046	97	SS 304 Laboratory Formed Spherical	0.060	8,550/7,000*	800	To be tested on motor
BSD 100 In.	TCC-1	5	Goodyear 357-11 Polyisoprene Calendered	34 - 0.046	50	SS 302 Laboratory Formed Spherical	0.038	--	--	In fabrication, test 15 Dec
	TCC-2	5	Goodyear 357-11 Polyisoprene Calendered	34 - 0.046	50	SS 302 Laboratory Formed Spherical	0.038	--	--	To be tested on motor
	TCC-3	5	Goodyear 357-11 Polyisoprene Calendered	34 - 0.046	50	SS 302 Laboratory Formed Spherical	0.35	--	--	To be tested on motor
	MRC-1	5	DC 86571/15 Silastic - Spray	98 - 0.017	50	SS 302 Hydroform Spherical	0.011	--	--	In fabrication, test 5 Nov
156-9	TCC-1	4	Goodyear 357-11 Polyisoprene Calendered	75 - 0.031	50	SS 302	0.038	--	--	IR & D design finished, materials procured
	TCC-2	4	Goodyear 357-11 Polyisoprene Calendered	75 - 0.031	50	SS 302	0.038	--	--	First program seal
	TCC-3	4	Goodyear 357-11 Polyisoprene Calendered	75 - 0.031	50	SS 302	0.038	--	--	To be tested on 156-9

*With boot.

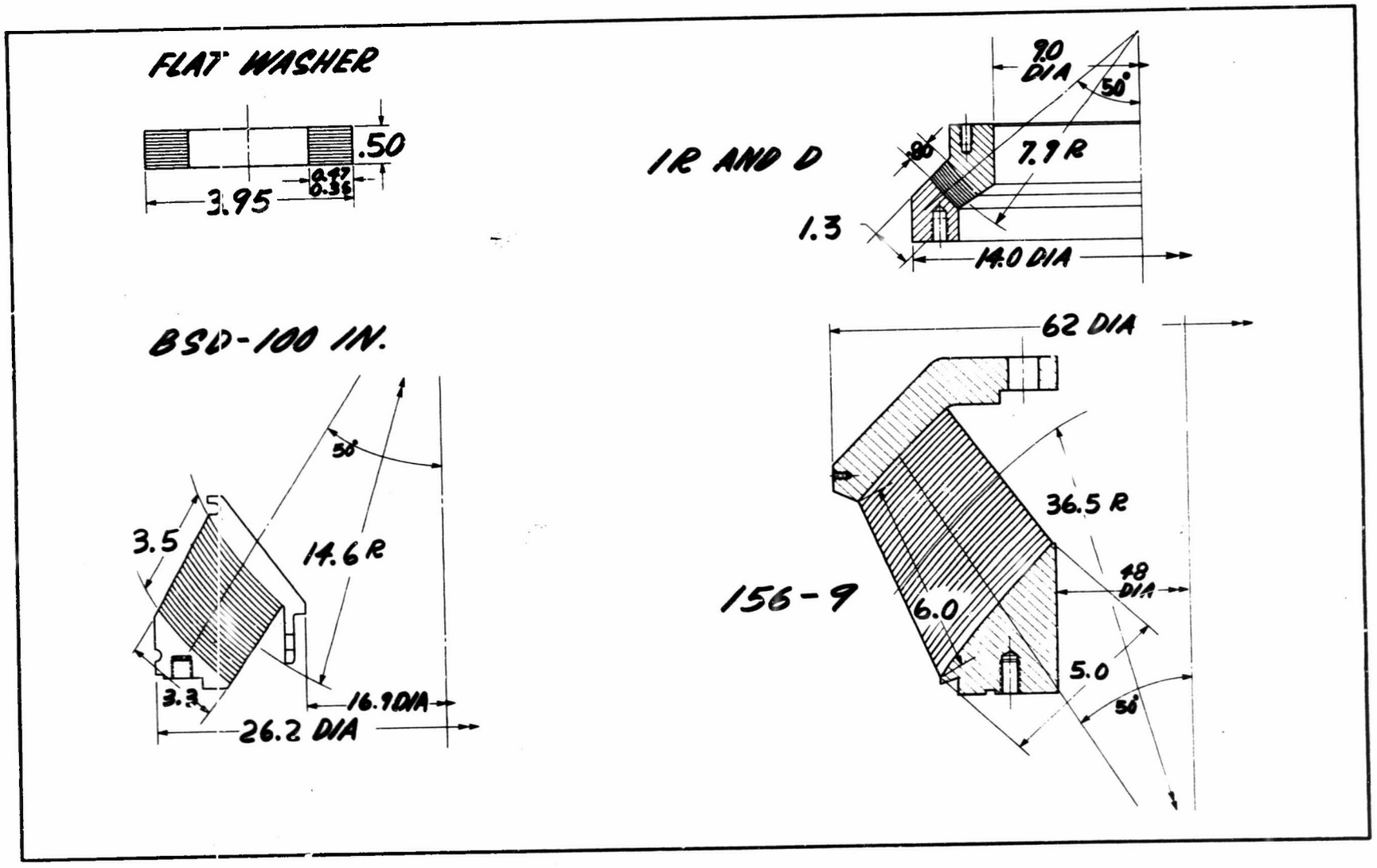

Figure 2-34. Flexible Seal Programs

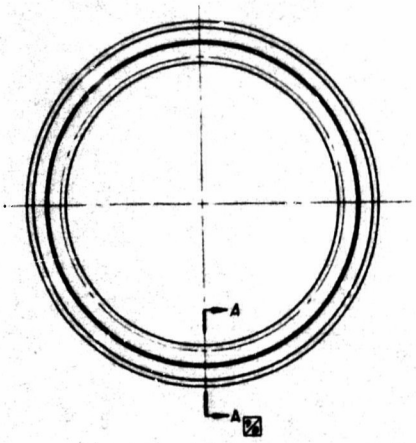

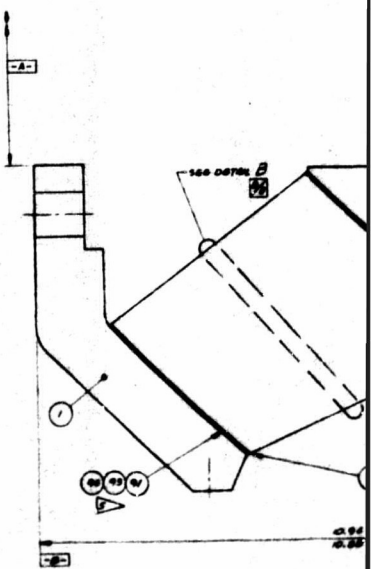

SECTION A-A
SCALE : 1/1

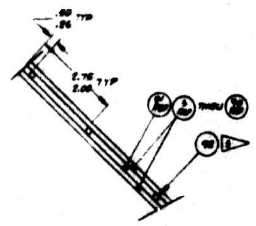

DETAIL B
SCALE: NONE

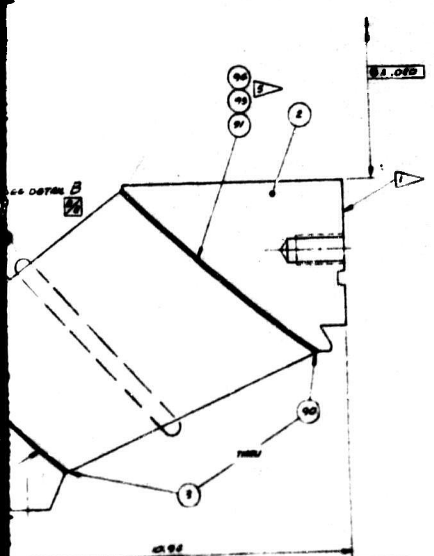

SECTION A-A
SCALE 1/1

NOTES:

1. MARK PART NO. PER TUS-[illegible]-38 METHOD [illegible].
2. MATERIAL: POLY-ISOPRENE PER STW4-[illegible] SHEAR MODULUS 60-90 PSI AT 50-100% STRAIN
3. CIRCUMFERENTIAL LOCATION 8.0-10.0 [illegible] TYP EACH LAYER
4. HIGH CARBON-CHROME STEEL BALL .0248-.0252 DIA
5. SAND BLAST BOTH SIDES OF ITEMS [illegible]-90 & THE MATING SPHERICAL SURFACES OF ITEMS [illegible] & [illegible]. COAT ALL SAND BLASTED SURFACES WITH ITEMS 95 & 96.
6. LAYUP UNCURED RUBBER (ITEM 91) ON ITEMS [illegible]-90. APPLY ITEM [illegible] [illegible] REQUIRED [illegible] PRESSURE & TEMPERATURE TO ASSURE REQUIRED RUBBER LAYER THICKNESS & VULCANIZATION OF RUBBER TO ITEMS [illegible]-90.
7. MAY BE PURCHASED FROM HUGHSON CHEMICAL CORP, ERIE PA.

7U40678

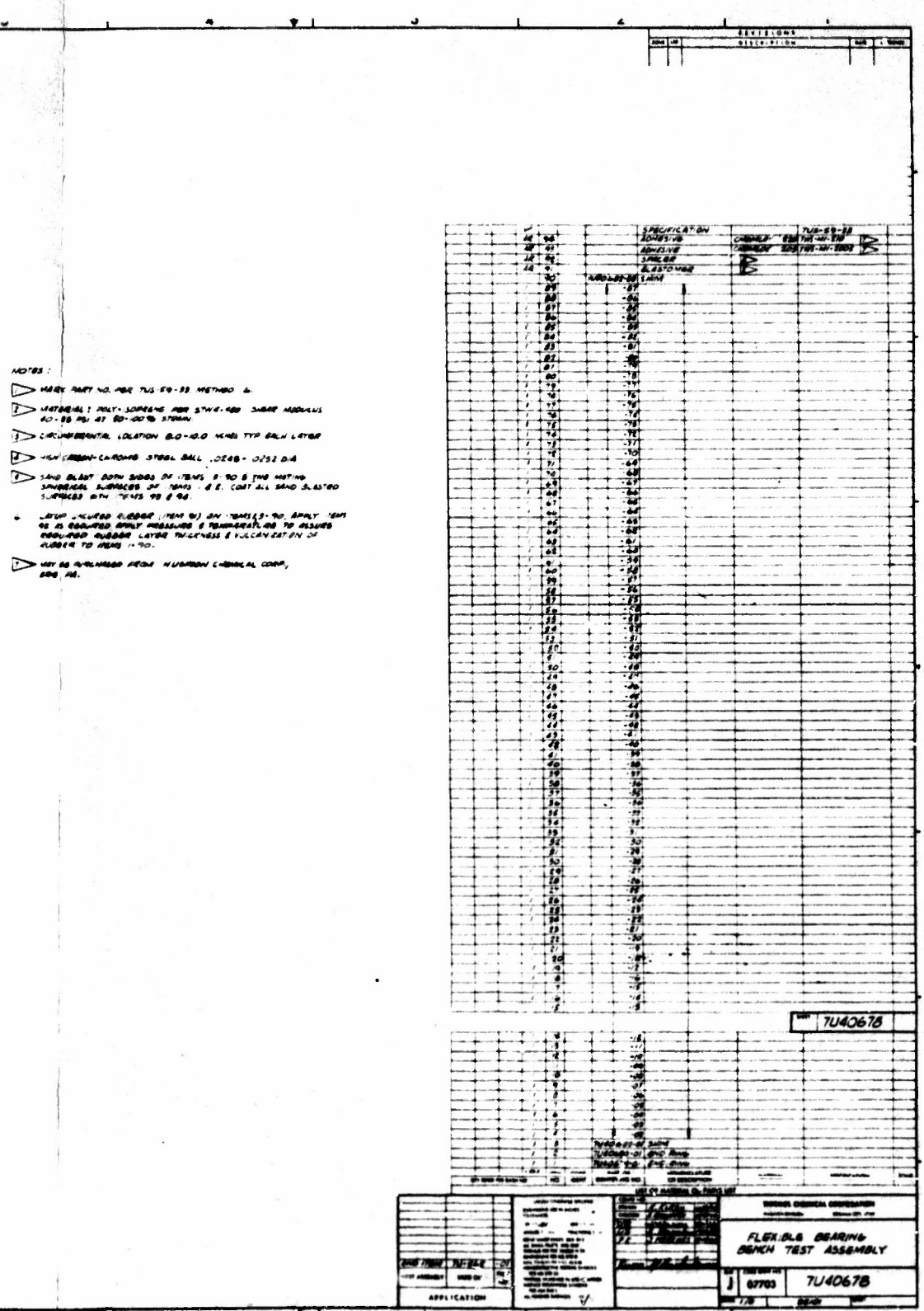

Figure 2-35. 156 In. Flexible Seal Design

3

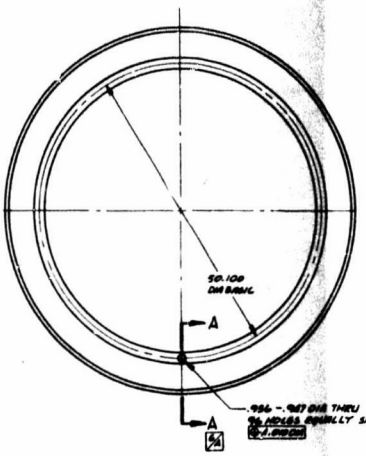

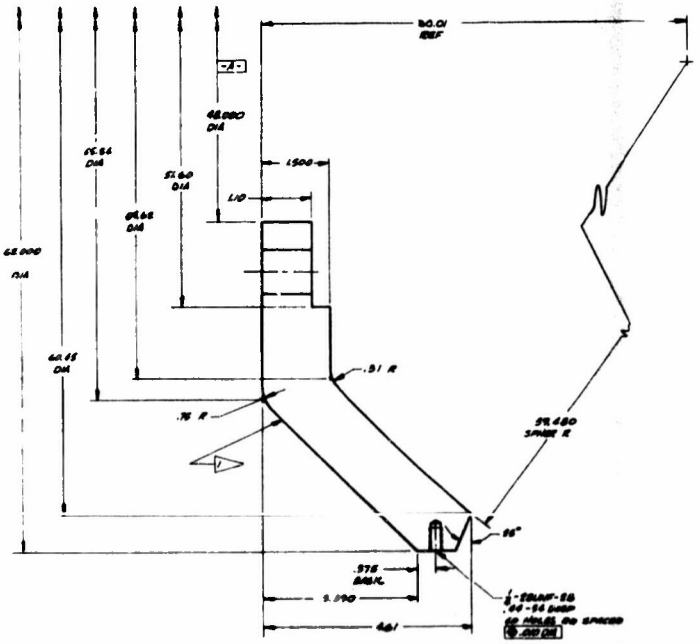

SECTION A-A
SCALE 1 : 1

APPLICATION

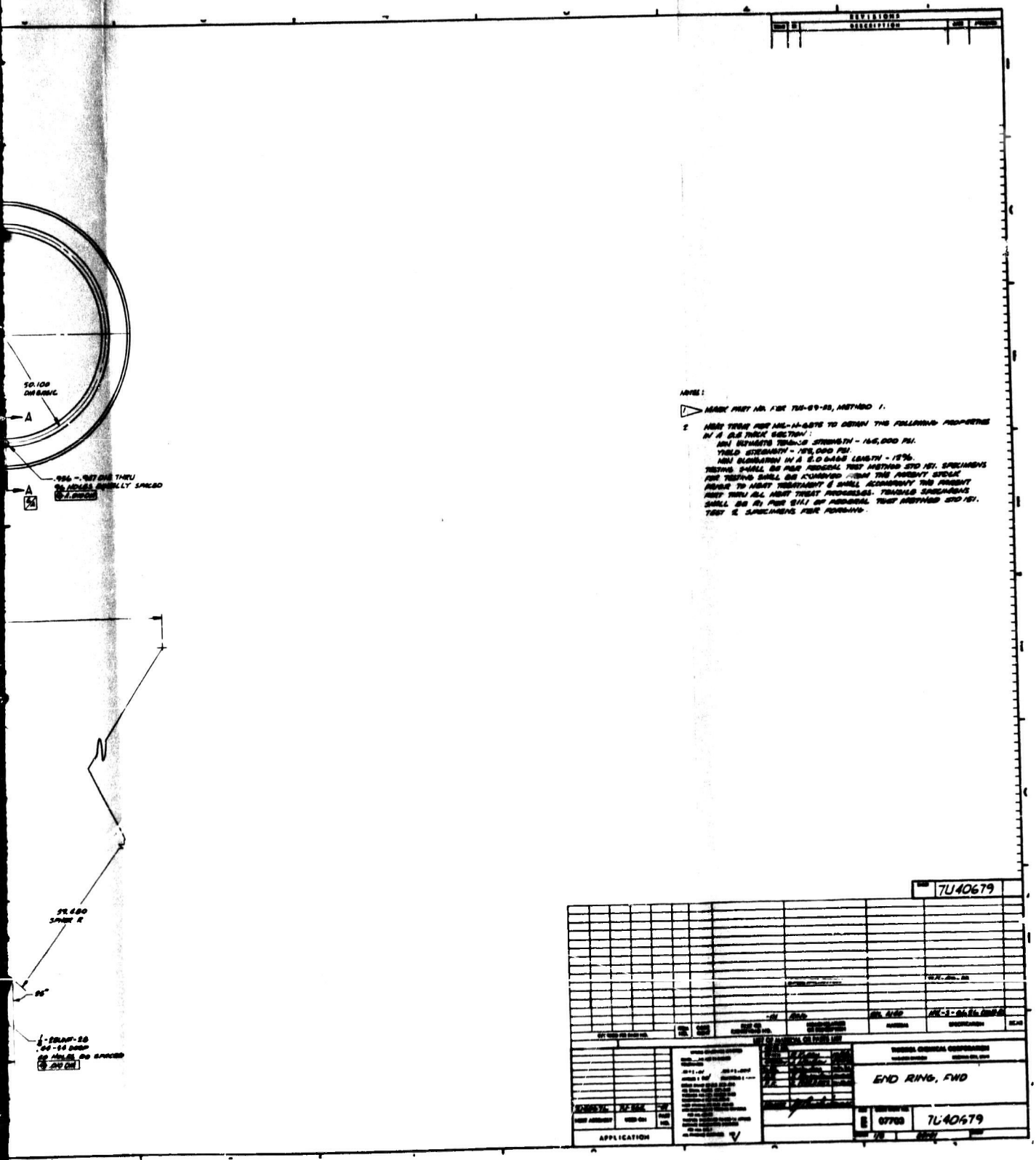

Figure 2-36. Forward End Ring

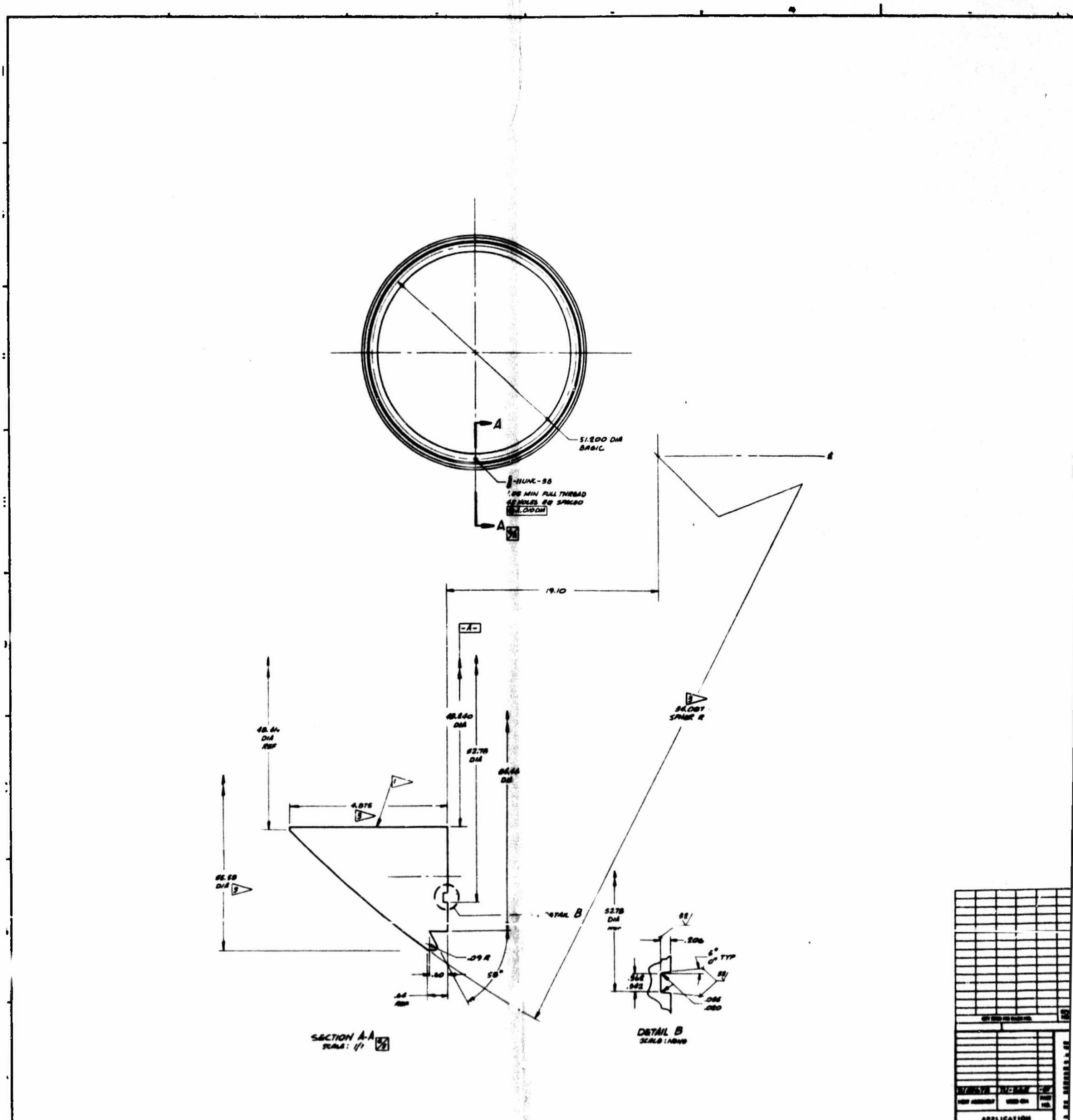

51.200 DIA BASIC
1.88 MIN FULL THREAD
A
A
19.10
-A-
48.64 DIA REF
4.875
36.087 SPHER R
52.78 DIA
52.78 DIA
DETAIL B
.09 R
58°
.206
6° TYP
.095
.080
SECTION A-A SCALE: 1/1
DETAIL B
APPLICATION

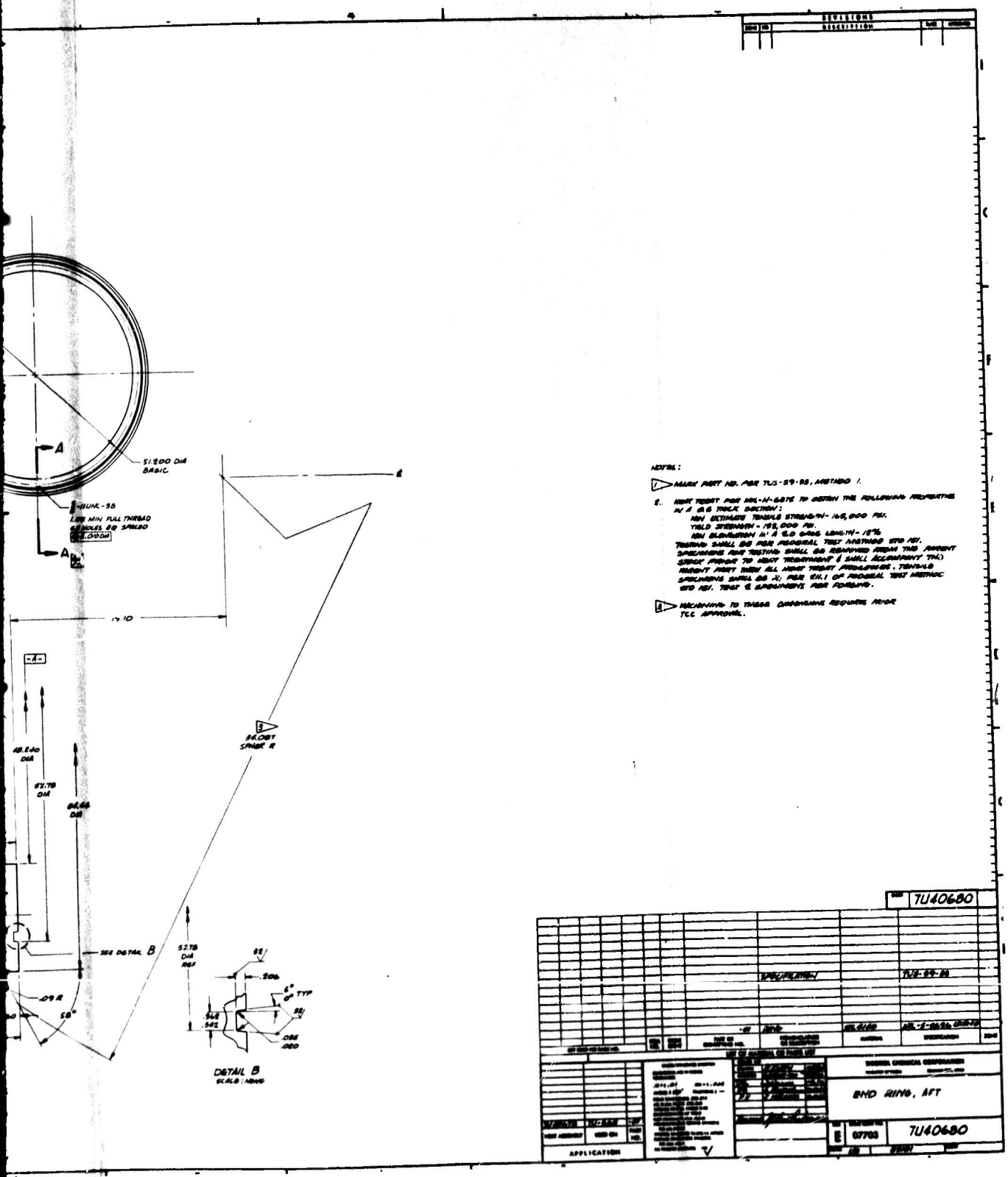

Figure 2-37. Aft End Ring

DASH NO.	A SPHER R ±.005	B DIA +.01 -.00	C DIA ±.01
[illegible]	[illegible]	[illegible]	[illegible]

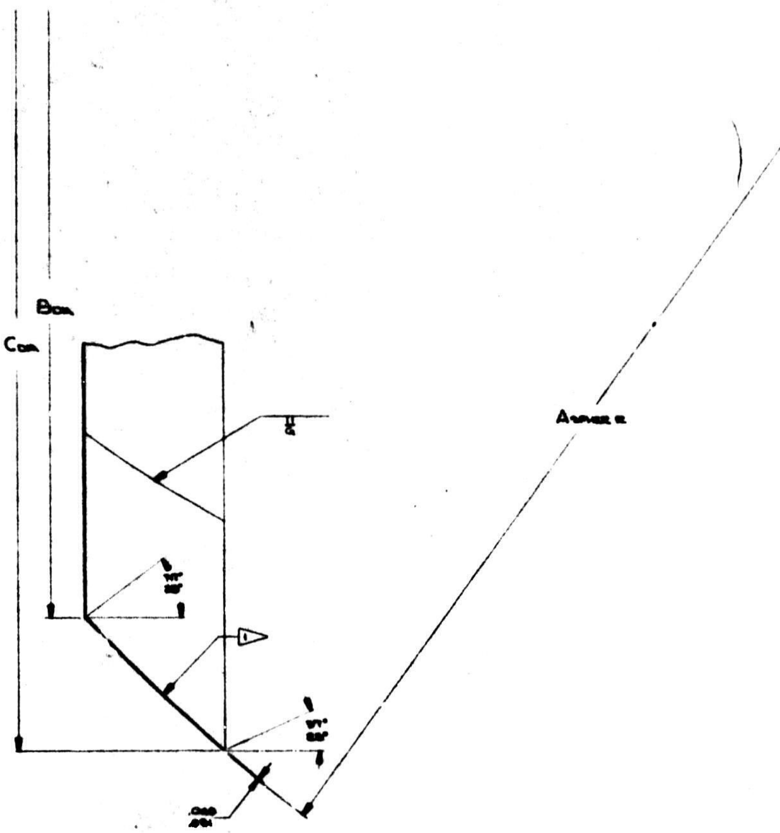

7U40682

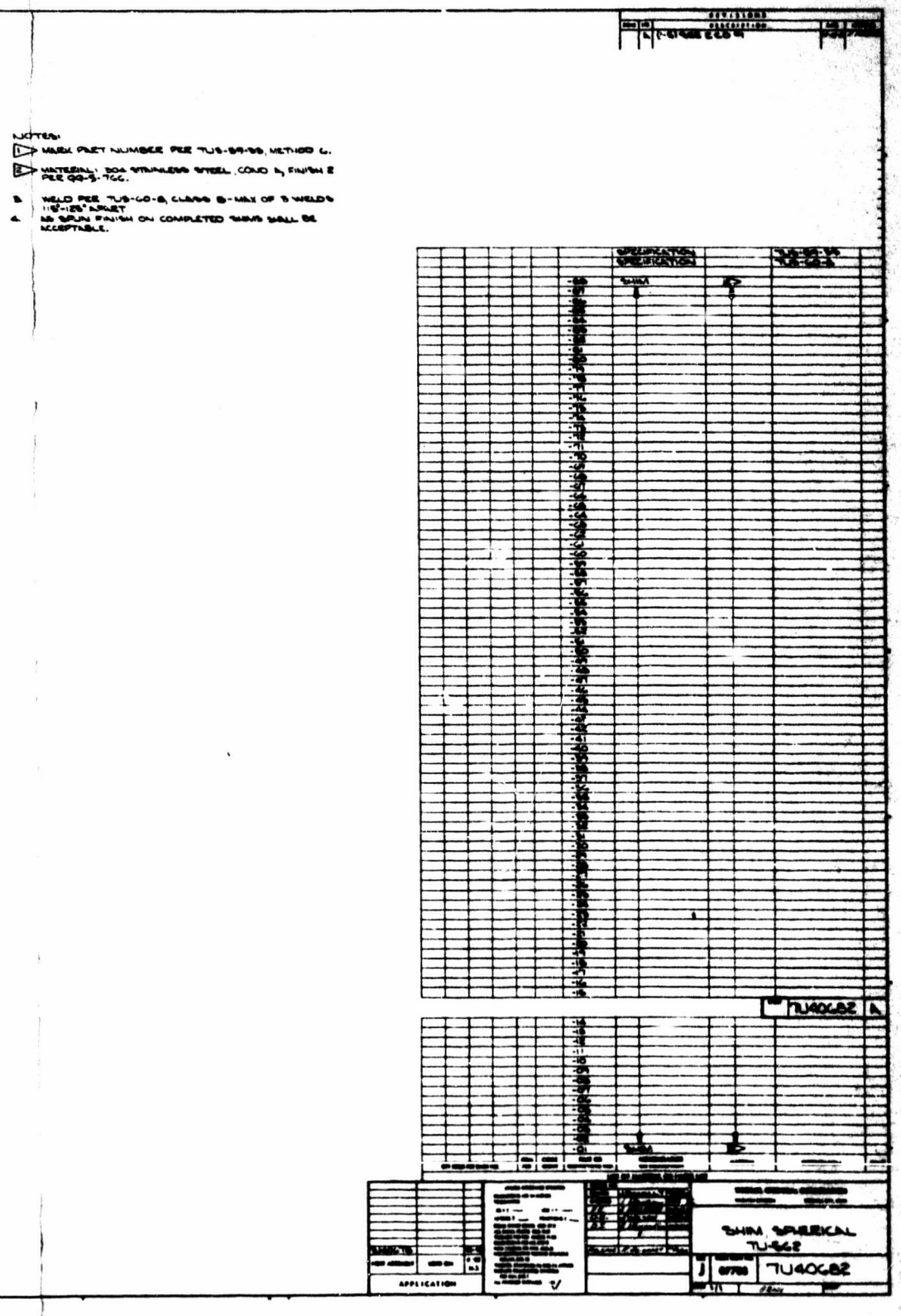

Figure 2-38. Spherical Shim

This is so because overall seal length and end ring to end ring concentricity must be held in order to assure the designed physical relationship between fixed and movable portions of the nozzle. Thus, by design, the shape and location of the first and last shims are fixed.

If, for example, 82 shims were used the ID of shim No. 82 would be greater than that of No. 88. Therefore, the point at which the seal inner surface contacts the aft end ring would move outboard (Figure 2-35). Conversely, if 96 shims were used, the ID of shim No. 96 would be less than shim 88 and the point at which the inner surface of the seal contacts the aft end ring would move inboard. Thus, the angle formed by the conical inner surface with respect to the nozzle centerline will vary significantly as a function of shim thickness.

4. PLANNED EFFORT

Figure 2-35 will be revised when the precise thickness of shims making up the pack is known. Manufacturing planning is predicated on receiving a revised seal drawing at a later date.

5. FABRICATION

The 156 inch seal fabrication effort at Marlin-Rockwell has been canceled. The last Thiokol seal and both seals required by this program will be fabricated by Thiokol with assistance from other vendors. The status and planning of this new effort is outlined below.

a. End Rings--Forgings for these end rings were procured by Marlin-Rockwell under their contract to Thiokol. These are available and are presently at Excelco Developments Inc, Silver Creek, New York. Excelco was under contract to machine these forgings to a Marlin-Rockwell configuration (rough machined). Thiokol will use these forgings but have them machined to Drawings 7U40679 and 7U40680

(Figures 2-36 and 2-37), respectively. The completely machined forgings will be delivered to Haveg Industries Inc, Reinhold Aerospace Division, Santa Fe Springs, California. *

b. Shims--During the fabrication of POSEIDON and the 100 inch flexible seals, Thiokol developed a shim forming technology called "lab form." This process involves clamping a sheet of stainless steel in a fixture and admitting inert gas under the sheet. The gas pressure blows the sheet into an almost hemispherical shape. From the section thus formed, a spherical shim is cut.

This lab form process may be compared to rolling and welding a conical preform (from patterns cut from sheet stock) and then shear spinning to a finished spherical shim. Because of the high energy involved and other hazards associated with lab forming, the shims will be shear spun.

A contract is pending with Precision Sheet Metal Inc, (PSM), Los Angeles, California, for three sets of spherical shims. Upon contract award, PSM will procure a stainless steel coil which will be accurately measured for thickness and thickness variation. The seal drawing (Figure 2-35) will then be revised to reflect the known steel thickness. Figure 2-36 will also be revised and PSM will begin fabrication of the quantity of shims determined necessary by this redesign effort. The completed shims will be delivered to Reinhold.

c. Spacers--Precision ground ball bearings have been ordered for delivery to Thiokol during the first week in November 1966. These spacers are accurately ground on modern centerless grinding machines. Diameter variation is small indeed and tolerance stackup is negligible in the shim/rubber pack buildup. Spherical spacers will be handcarried by Thiokol to Reinhold for seal manufacture.

d. Elastomer--Formulation of the selected elastomer is defined by STW4-488. The ingredients for this polyisoprene elastomer have been ordered and will be delivered

*Thiokol will contract with Reinhold on a time and materials basis to provide facilities and assistance during actual seal fabrication.

to Rubber Engineering Co in Salt Lake City. In November 1966, Thiokol will authorize Rubber Engineering to mix the rubber and calender it to 0.028 inch. The rolls of calendered rubber will be delivered to Thiokol and handcarried to Reinhold by Thiokol personnel.

e. Seal Assembly--During the fabrication of POSEIDON and the 100 inch flexible seals, technology and manufacturing techniques were developed which have produced satisfactory seals. The same technology will be applied to the fabrication of a 156 in. flexible seal. However, the equipment and facilities available at Thiokol Wasatch are inadequate to perform the full scale work. Large furnaces, autoclaves, and huge presses will be rented to maintain proven manufacturing techniques. A time and materials type contract with Reinhold is planned for this effort. Thiokol will provide a team to do most of the engineering work and direct the actual seal assembly. Reinhold will provide the facilities, technicians and labor force, i.e., forklifts with operators, press operators, etc. Reinhold will also provide engineering consultation services to assist Thiokol in the design of a curing mold and to obtain optimum cure of the rubber.

The Thiokol team will arrive at Reinhold near the end of December and will remain at Reinhold until the seal is completed (approximately two weeks). Seal components, an assembly fixture and other needed items will be delivered to Reinhold prior to or concurrent with the arrival of Thiokol personnel. A manufacturing plan, outlining the detailed processing steps to be followed, will also be prepared for use at Reinhold. Actual inspection at critical stages of the processing will be performed and signed off by qualified Reinhold inspectors. A general outline of the manufacturing process follows.

1. Dryfit shims over assembly fixture.
2. Sandblast shims.
3. Clean with MEK.
4. Apply Koropon bonding agent.
5. Lay uncured polyisoprene over each shim.
6. Stack shims in proper order over assembly fixture.

7. Debulk as required during layup of shim/rubber pack.
8. Install mold cover.
9. Press seal to mold dimensions.
10. Clamp mold.
11. Place in furnace for cure.

During assembly of the seal, accurate records will be kept of each operation performed from which detailed special processing instructions, shop travelers, and other manufacturing and inspection paper will be prepared. Assembly sequence and procedures thus developed will be used during fabrication of the second two seals, which are Air Force funded.

The Reinhold/Thiokol team will deliver a completed seal to Thiokol Wasatch where a complete dimensional inspection will be performed.

The remaining Thiokol test seal will be tested in two modes. One will be an extremely high pressure mode to assure that the vulcanized rubber will not blow out between shims and the other will be a complete functional check at a pressure equivalent to the MEOP during firing. These tests will be performed in a test fixture. The planned testing will not destroy this Thiokol seal which will be retained as a spare to back up the Air Force seals.

The second fabricated seal will be delivered to Thiokol Wasatch, dimensionally inspected and functionally tested. It will be inspected and bought off as an assembly and will then be tested to destruction. The third seal will be fabricated by the same documented procedures. It will be installed in the nozzle and test fired on the 156-9 motor.

f. Boot--An insulation boot will be fabricated at the Wasatch Division by Thiokol's materials laboratory. This boot will be made of a silicon rubber hand laid up over a male mandrel. The mandrel will likewise be fabricated by Thiokol's materials laboratory personnel. This layup of uncured silicon rubber is done while spinning

the mandrel in much the same fashion as pottery is made. After layup, the boot will be cured while still on the mandrel. Three such boots will be fabricated and functionally tested on each of the three seals.

SECTION III

INSULATION AND LINER DESIGNS

A. INSULATION

1. DESIGN CRITERIA

The internal case insulation must insure that the original structural integrity of the pressure vessel is not degraded by thermal effects throughout the duration of the motor operation. A conservative insulation design performs its function by providing thermal protection to the case so that the case material is not heated above ambient temperature during motor operation.

2. INSULATION DESIGN AND FORMULATION

The purpose of the 156-9 motor is to test the flexible seal movable nozzle; therefore, the insulation is designed to minimize risk to the test vehicle. No attempt was made to optimize material thickness and conservative safety factors were applied. The insulation selection is based on proven materials and manufacturing techniques.

The internal case insulation is TI-H704B (asbestos filled HC polymer). The insulation materials composition is shown on Table 3-1.

The insulation design includes stress relief flaps at each end of the large forward portion of the propellant grain. The stress relief flaps are fiberglass fabric reinforced TI-H704B insulation. By using TI-H704B flaps, compatibility between insulation and flap material is assured. This concept has been proven during the programs listed in Table 3-2.

TABLE 3-1

INSULATION, TI-H704B

Composition (percent)	
HC Binder and Curing Agents	45
XL-434 Polymeric (HC) HX-760 HX-740	
Asbestos	30
Carbon Black	15
Dibasic Ammonium Phosphate	10
Physical Properties	
Density (lb/cu ft)	75
Ultimate Stress Minimum Allowable (psi)	175
Ultimate Strain (in./in.)	150
Hardness (Shore A)	70
Tensile Adhesion to Steel Case (psi)	80
Thermal Properties	
Specific Heat (cal/gm-°C)	0.325
Thermal Conductivity (cal/cm-sec-°C)	9.15×10^{-4}
Thermal Diffusivity (sq cm/sec)	2.35×10^{-3}
Processing Properties	
Pot Life at 135°F (hr)	1.5 - 2.0
Cure at 135°F (day)	5

TABLE 3-2

PREVIOUS USAGE OF TI-H704B AND TL-H714A INSULATION LINER SYSTEM

Motor	Case Size (in.)	Propellant	Average Chamber Pressure During Web Time (psia)	Area of Use
156-2C-1	156	TP-H8163 16% Al/85% Solids HB Polymer	668	Case forward dome, cylinder and aft dome
TU-455.01	65	TP-H1096 16% Al/85% Solids HB Polymer	734	Case forward dome and cylinder
TU-455.02	65	TP-H1096 16% Al/85% Solids HB Polymer	714	Case forward dome and cylinder
TU-418.01	65	TP-H8163 16% Al/85% Solids HB Polymer	598	Case forward dome and cylinder
TU-418.02	65	TP-H8163 16% Al/85% Solids HB Polymer	640	Case forward dome and cylinder and nozzle inlet

The insulation configuration is shown in Figure 3-1 . The predicted material loss and the insulation design criteria are shown in Figure 3-2 . The predicted material loss rate was based primarily on results reported for the 156-6 motor. When the 156-6 case is received at Thiokol, the fired insulation will be removed. Additional thickness measurements will be taken with a micrometer, and the results will be compared to those previously reported. Should local areas of high material loss be discovered, the 156-9 insulation design thickness will be increased to insure thermal protection to all areas of the case. No thermal protection to the case is attributed to the liner.

3. PREVIOUS EXPERIENCE

Past performance of TI-H704B insulation is shown in Table 3-2. Results from the test motors shown on this table and insulation performance from the 156-7 motor were used in predicting insulation performance for the 156-9.

4. WEIGHT ANALYSIS

The insulation weight is calculated to be 3,059 pounds. The stress relief flaps will weigh 367 pounds.

5. INSTALLATION TECHNIQUE

The TI-H704B insulation will be installed using a pneumatic extrusion process. The material will be inserted into a cartridge which will be placed into a pneumatic installation tool. As pressure is applied to the cartridge, the insulation will be extruded through a nozzle which is manually rotated around the case. Overlaps between passes with the extrusion nozzle will be hammered in place using a pneumatic hammer. Following material installation and cure, a vacuum test will be conducted on the insulated case assembly to insure that entrapped air voids come to the surface.

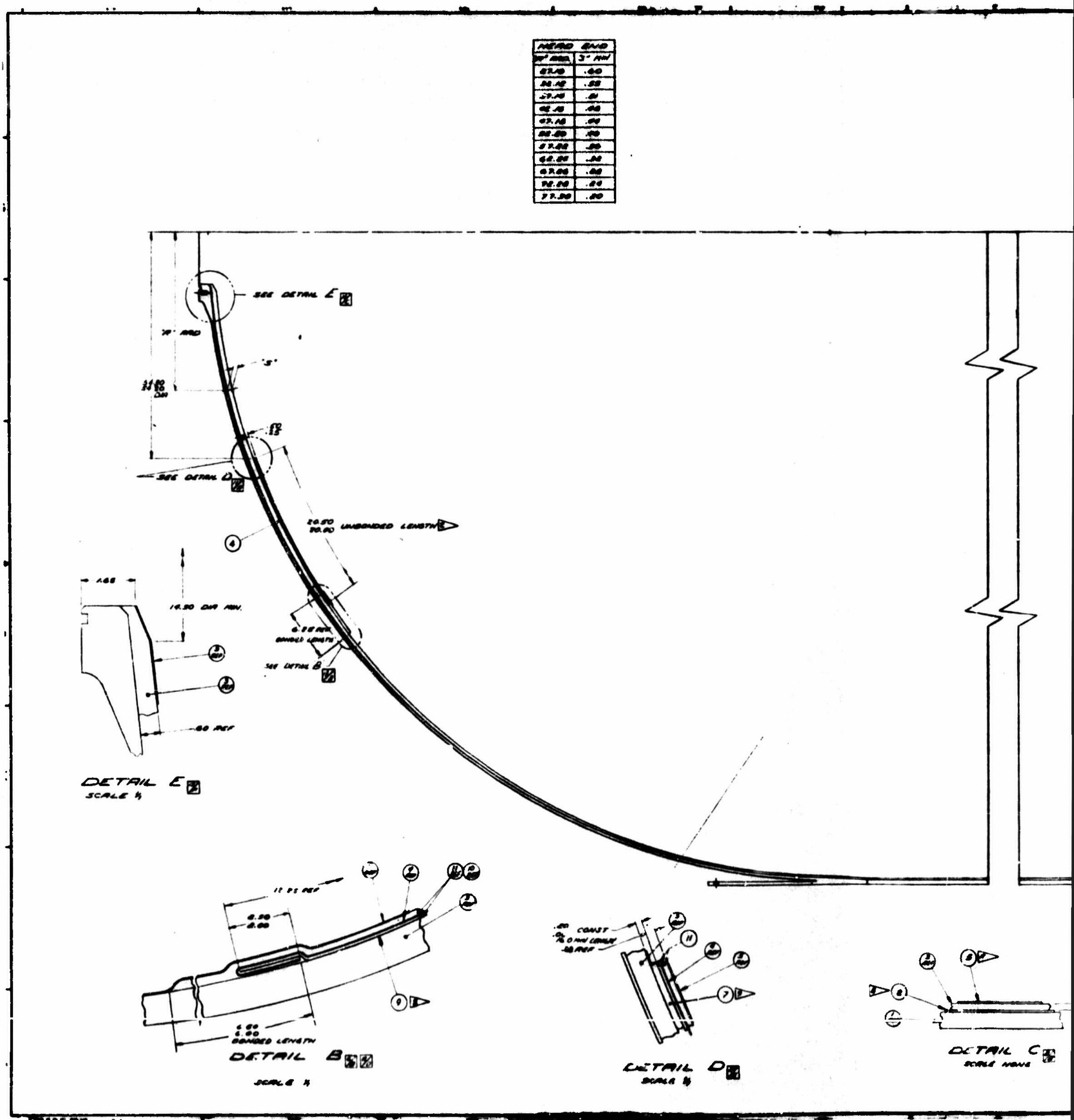

HEAD END
SEE DETAIL E
SEE DETAIL D
UNBONDED LENGTH
SEE DETAIL B
BONDED LENGTH
14.50 DIA MIN.
.60 REF
DETAIL E
SCALE ½
11.75 REF
DETAIL B
SCALE ½
CONST
DETAIL D
SCALE ½
DETAIL C
SCALE NONE

AFT END	
"X"	Y min
5.00	.00
10.00	.00
20.00	.01
30.00	.04
40.00	.11
45.00	.18
50.00	.40
55.00	.52
60.00	.64
65.00	.80
70.00	.90
75.00	.96
80.00	1.00

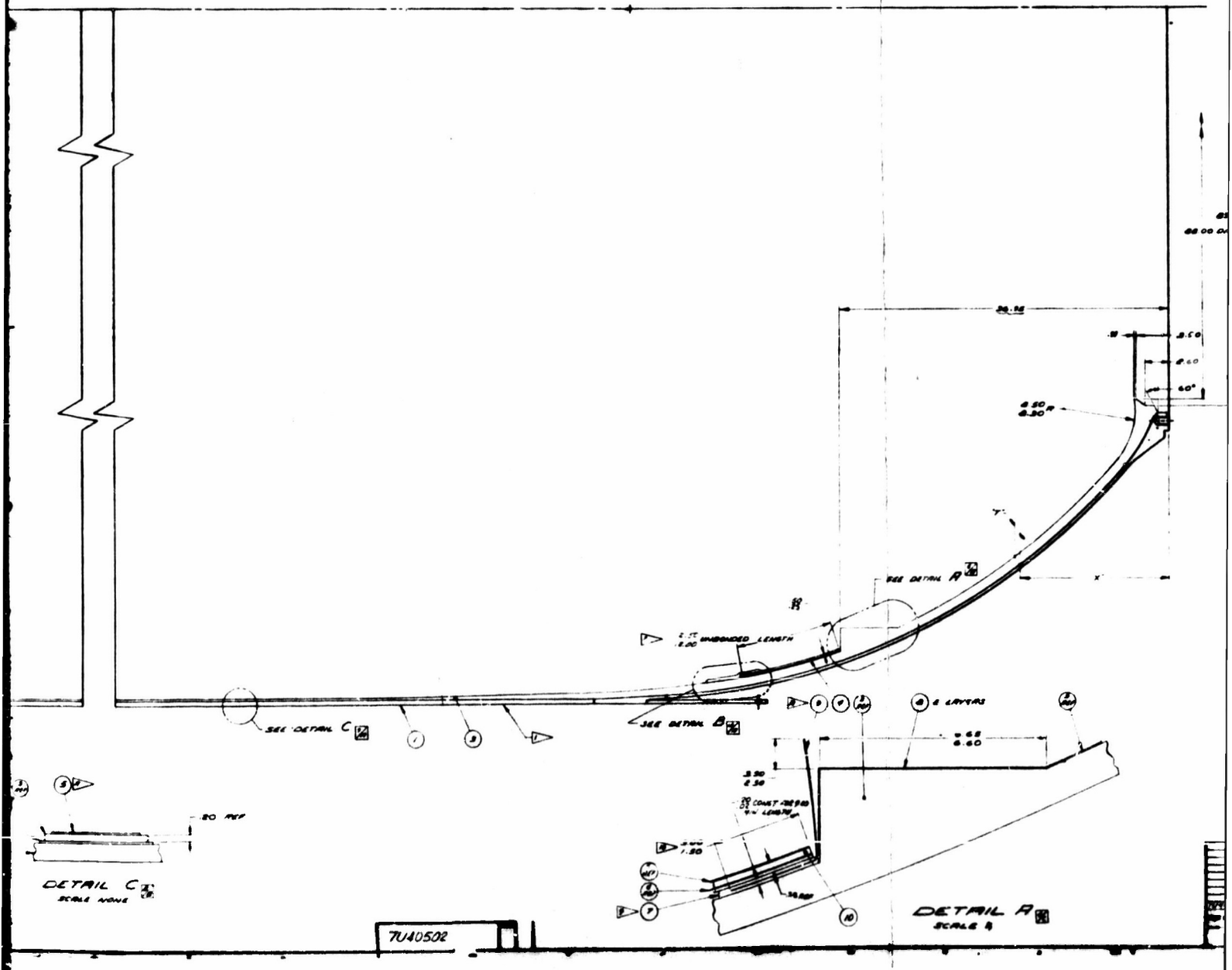

2

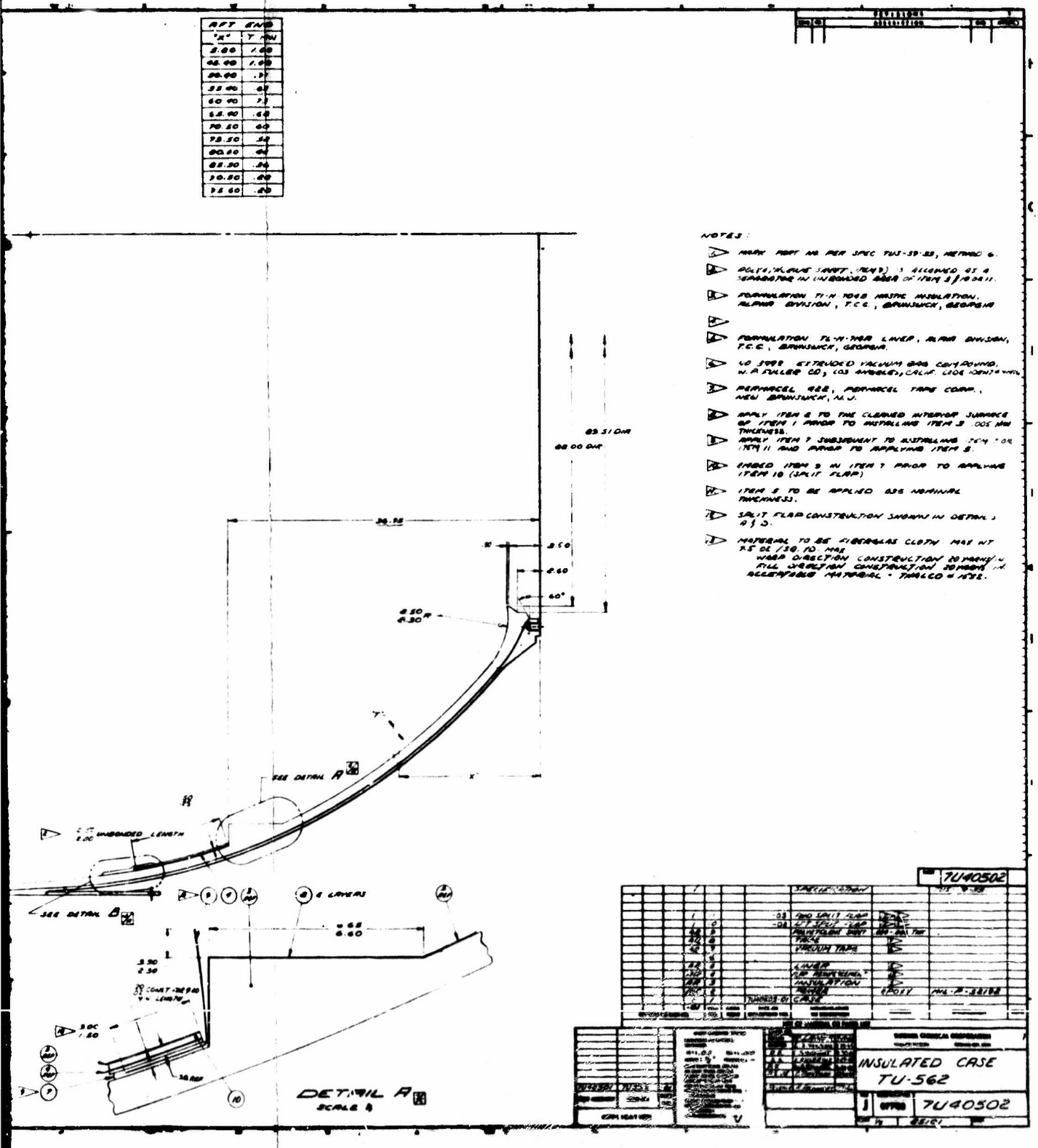

Figure 3-1. 156-9 Insulated Case

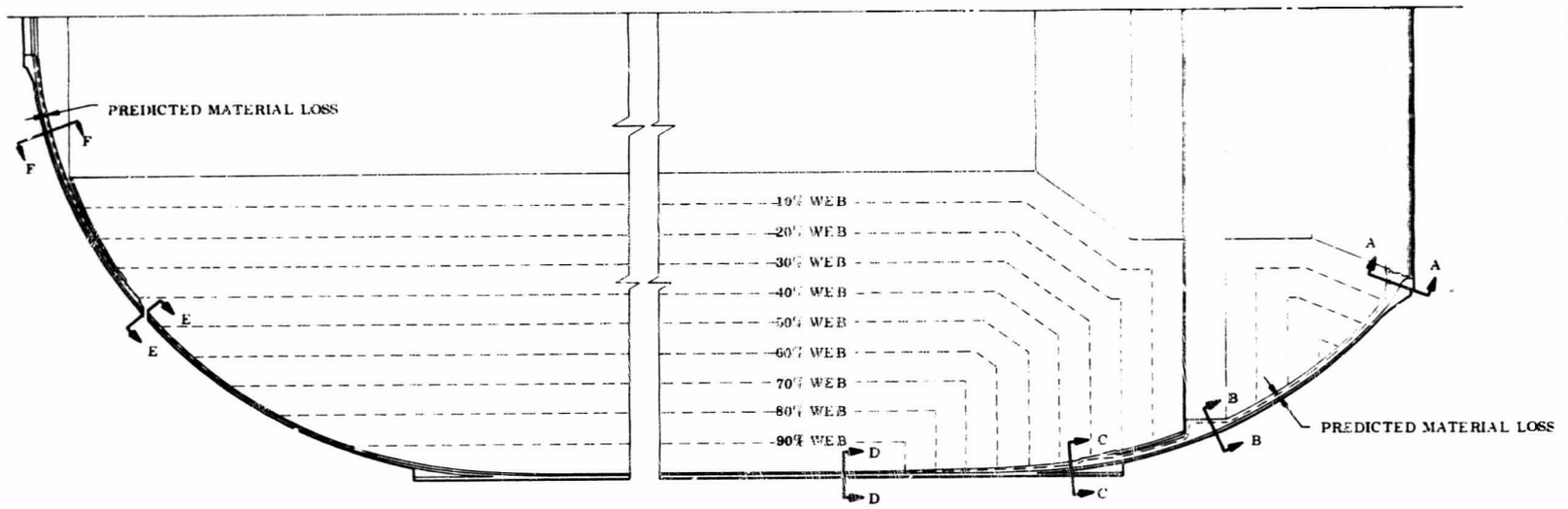

SECTION	PREDICTED EXPOSURE TIME (SEC)	PREDICTED MATERIAL LOSS RATE (MIL/SEC)	PREDICTED THICKNESS FOR EROSION (IN.)	ADD FOR SAFETY FACTOR	THERMAL PROTECTION (IN.)	TOTAL THICKNESS REQUIRED (IN.)	DESIGN THICKNESS (IN.)
A-A	65	8.0	0.520	0.260	0.200	0.980	2.40
B-B	65	8.0	0.520	0.260	0.200	0.980	1.00
C-C	42	8.0	0.336	0.168	0.200	0.704	0.83
D-D	--	--	--	--	0.200	0.200	0.20
E-E	36	4.0	0.144	0.072	0.200	0.316	0.42
F-F	65	4.0	0.260	0.130	0.200	0.590	0.60

13094-5

Figure 3-2. Insulation Design Information

Void areas will be repaired by hand trimming and hand installation of additional TI-H704B insulation.

B. LINER

1. LINER DESIGN AND FORMULATION

The liner material selected is TL-H714A, carbon black filled HC polymer. This material uses the same binder as both the TI-H704B insulation and the TP-H1115 propellant. This common binder assures bond compatibility between the propellant grain and the insulation. The liner formulation is shown in Table 3-3. The liner thickness is 0.035 in. and no thermal protection to the case is attributed to the liner.

2. PREVIOUS EXPERIENCE

This liner has been used extensively with the insulation system selected for use in this motor. Past history for the insulation liner system is shown on Table 3-2.

3. WEIGHT ANALYSIS

The calculated liner weight is 367 pounds.

4. APPLICATION TECHNIQUE

The interior case area will be sling lined except for the extreme forward and aft domes and other peripheral areas which will be lined by the brush application technique.

TABLE 3-3

TL-H714A LINER

Composition (percent)	
HC Binder and Curing Agents	70
XL-434 Polymeric (HC) HX-760 HX-740	
Carbon Black	30
Physical Properties	
Density (lb/cu ft)	69
Ultimate Stress Minimum Allowable (psi)	175
Ultimate Strain (in./in.)	200
Hardness (Shore A)	40
Tensile Adhesion to Insulation (psi)	80
Tensile Adhesion to Propellant (psi)	80
Thermal Properties	
Specific Heat (cal/gm-°C)	0.375
Thermal Conductivity (cal/cm-sec-°C)	6.28×10^{-4}
Thermal Diffusivity (sq cm/sec)	1.52×10^{-3}
Processing Properties	
Cure Time at 135°F (day)	6

With the motor case aligned vertically in the casting pit the sling liner will be positioned directly over the case, concentric and parallel to the axis of the case, on a platform supported at the outer edges of the pit.

The liner will be pumped from a container on the scale to a rapidly rotating slinger disc which will apply it evenly to the TI-H704B insulation surface while traversing the motor case interior. Following ambient gel time the liner will be cured at 135 $\pm$ 10°F.

C. COMPATIBILITY TESTING

1. INTRODUCTION

To insure a successful bond of the propellant to the case wall in the 156-9 motor, a series of tests will be conducted prior to, and during propellant casting. These tests will verify the design, processes, and the product, and will utilize standard testing procedures and equipment.

The primary objective is to verify the ability of the insulation to liner to propellant bond system to meet the minimum design criteria. Bond strength at all interfaces will be determined and compared with the design requirements of the motor.

The secondary objective is to determine whether the scheduled processes and materials contain any elements detrimental to motor construction. Any interfering reactions will be isolated by these tests.

Physical tests will be conducted to verify bond strengths of the interfaces at:

1. Insulation to Koropon to steel,
2. Liner to insulation,
3. Propellant to liner.

Interface bond strengths will be evaluated by 180 deg peel, and tensile adhesion tests In addition, tensile adhesion tests will be conducted on composite insulation to liner to propellant specimens. The type of failure plus strengths will be evaluated.

2. TEST SCHEDULE

Tests will be conducted in accordance with the schedule indicated in Table 3-4.

3. DESCRIPTION OF PHYSICAL TESTS AND APPARATUS

Five types of standard physical tests are used in insulation to liner to propellant compatibility verification. They are:

1. Peel, 180 deg;
2. Tensile adhesion, steel cup to steel disc;
3. Tensile adhesion, tenshear;
4. Adhesion cup;
5. Lap shear.

a. 180 Degree Peel Test--This test is used to determine the comparative peel or stripping characteristics of adhesives. Results are expressed in average load per unit width of bond required to separate one material from the adhered surface at a separation angle of approximately 180 degrees. Units are pounds per linear inch. The test specimen consists of a piece of flexible material which is bonded to a steel plate or to a slab of insulation or propellant by the formulation under test. Testing is completed in a power driven machine which can apply tension at a uniform rate and can record the applied load. The apparatus and test is detailed in Federal Test Standard No. 175 (Figure 3-3).

TABLE 3-4

COMPATIBILITY TEST SCHEDULE

	Phase	Weeks After Go-Ahead 0–1	1–2	2–3	3–4	4–5	5–6
I.	Insulation-Steel	XXXX	XXXX				
II.	Insulation to Liner to Propellant	XXXX	XXXX	XXXX	XXXX		
III.	Liner Cure Time vs Bond Strength	XXXX	XXXX	XXXX	XXXX	XXXX	
IV.	System Compatibility	XXXX	XXXX	XXXX	XXXX	XXXX	XXXX
V.	Data Analysis and Report			XXXX	XXXX	XXXX	XXXX

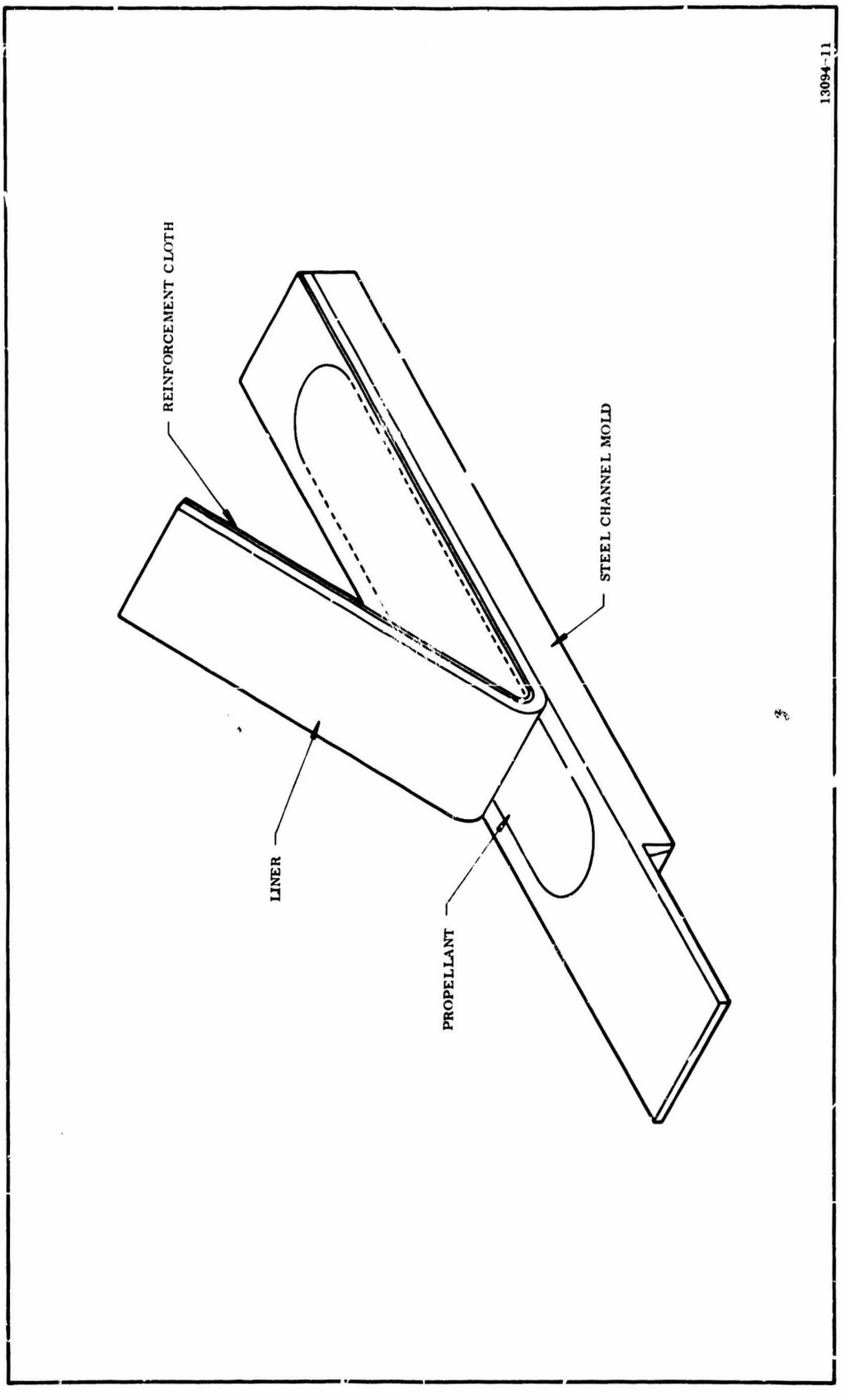

Figure 3-3. 180 Deg Peel Test Specimen

b. Tensile Adhesion, Steel to Steel Disc--In this test, two steel discs are bonded together with a fixed surface area and fixed glueline thickness. Force is applied by an Instron tensile tester and the force required to separate the discs is recorded. Results are expressed in pounds per square inch (Figure 3-4).

c. Tensile Adhesion, Tenshear--In this test, two steel plates(2 by 4 in.) are bonded together with a fixed area and fixed liner, propellant, glueline thickness. Testing is completed using an Instron tensile tester and the force required to separate the plates is recorded (Figure 3-5).

d. Adhesion Cup--This specimen consists of a 2 by 2 in. steel plate to which liner, insulation, or other substrate materials are applied. A Teflon spacer is placed on the plate to circumscribe a definite area of adhesion. A two inch diameter steel tube is placed on the Teflon spacer and filled with propellant or other adherent. Force is applied by an Instron tensile tester and the amount required to separate the tube from the plate is recorded (Figure 3-6).

e. Lap Shear--This test specimen consists of two 1 by 4 in. steel plates overlapping each other at 180 degrees. The adherent is placed on the last inch of the overlapping plates. The double lap shear consists of a third 1 by 4 in. plate placed above and parallel to the bottom plate (Figure 3-7).

f. Test Apparatus--Tenshear and peel test apparatuses are shown in Figures 3-8 and 3-9.

4. TEST PROCEDURES

The specimens for this program are specified in Tables 3-5 thru 3-8 . Requirements for detailed processing and formulation variables are included.

General specimen process requirements will simulate predicted processing of the 156-9 motor except where specified otherwise in Tables 3-5 thru 3-8 . Predicted motor processing is as follows.

1. Prime steel with two coats of Koropon.
2. Cure for 24 hr min at 80 (± 20)°F.

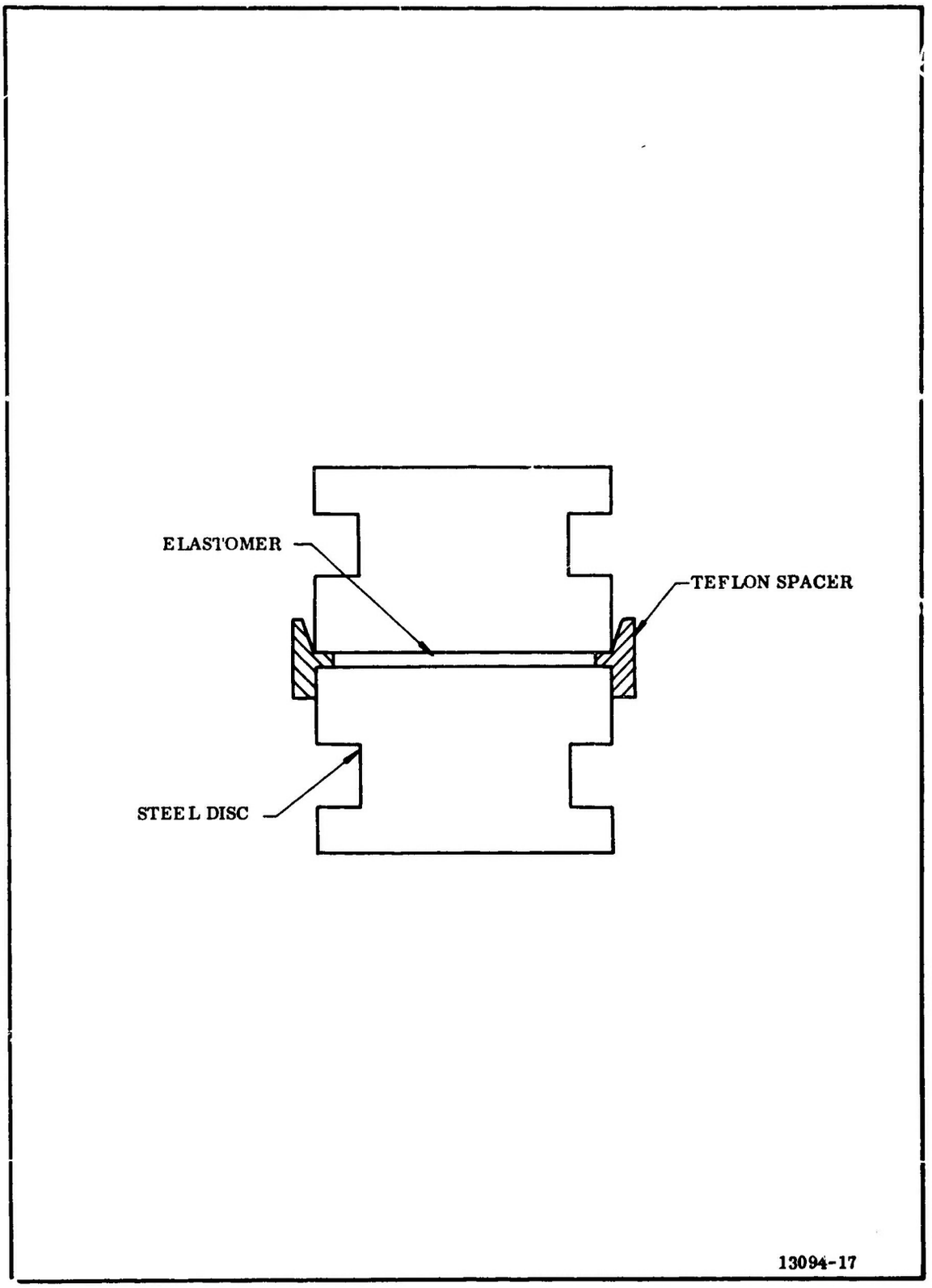

Figure 3-4. Tensile Adhesion, Steel to Steel Disc

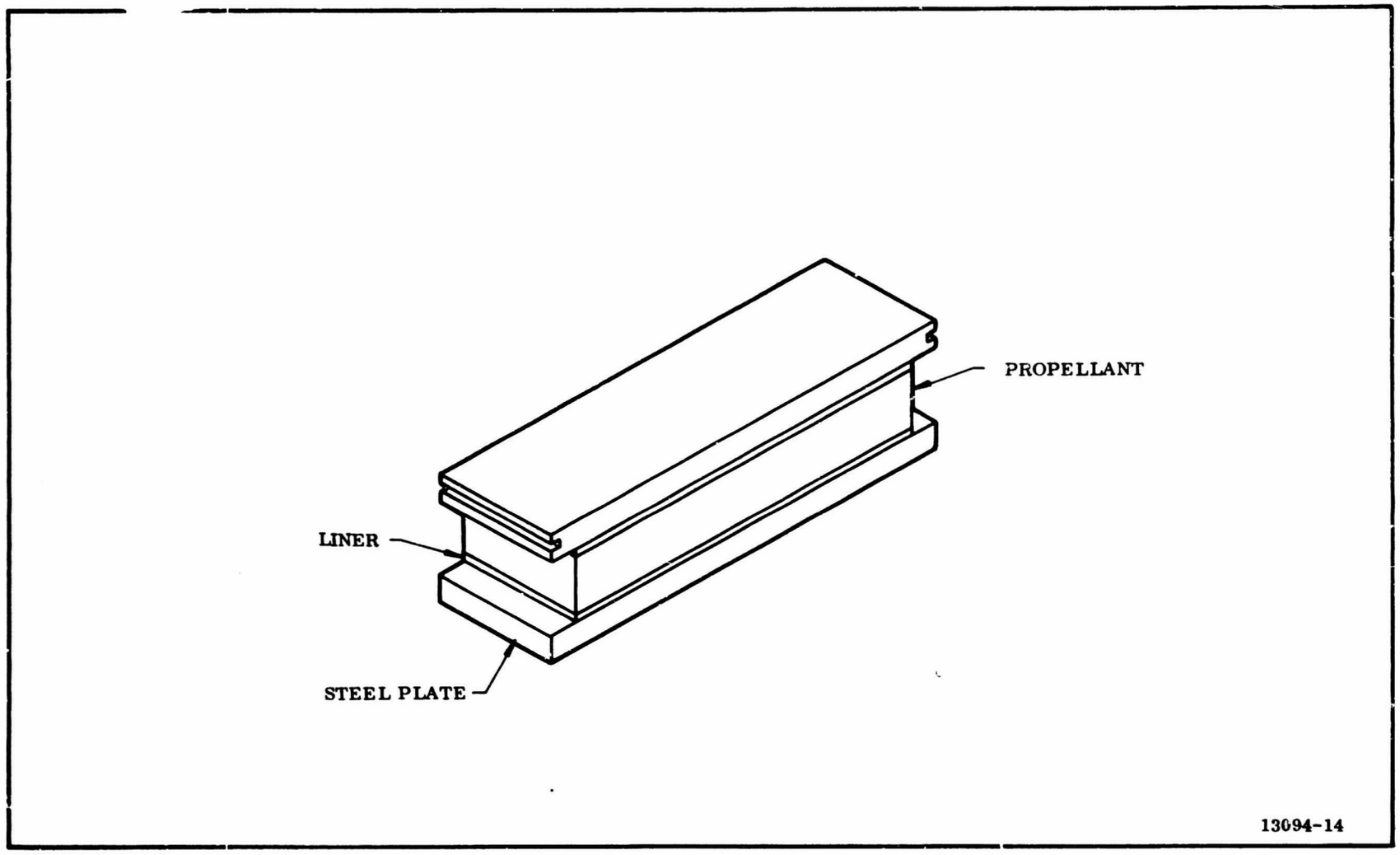

Figure 3-5. Tensile Adhesion, Tenshear

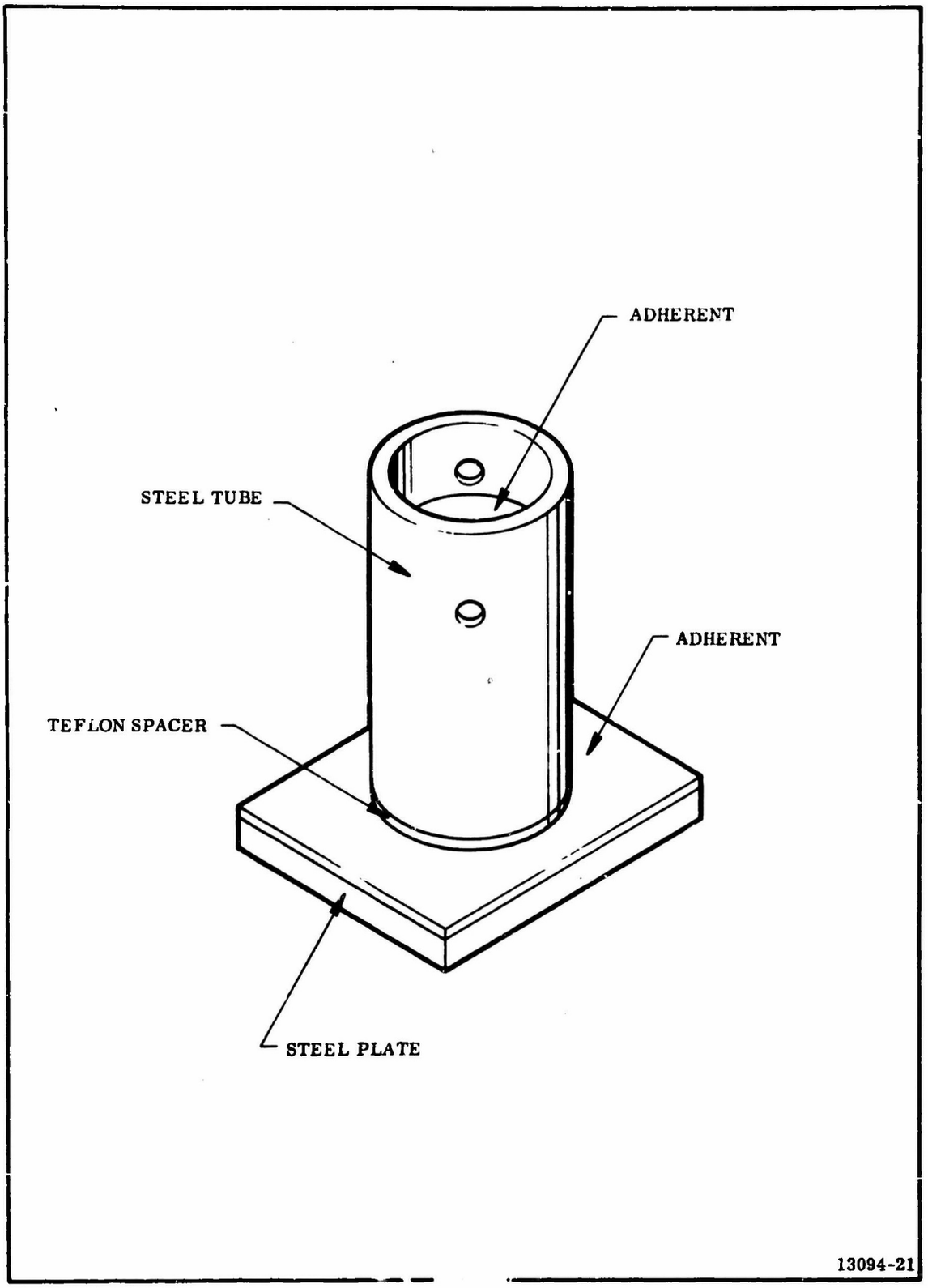

Figure 3-6. Ac .ı Cup Test Specimen

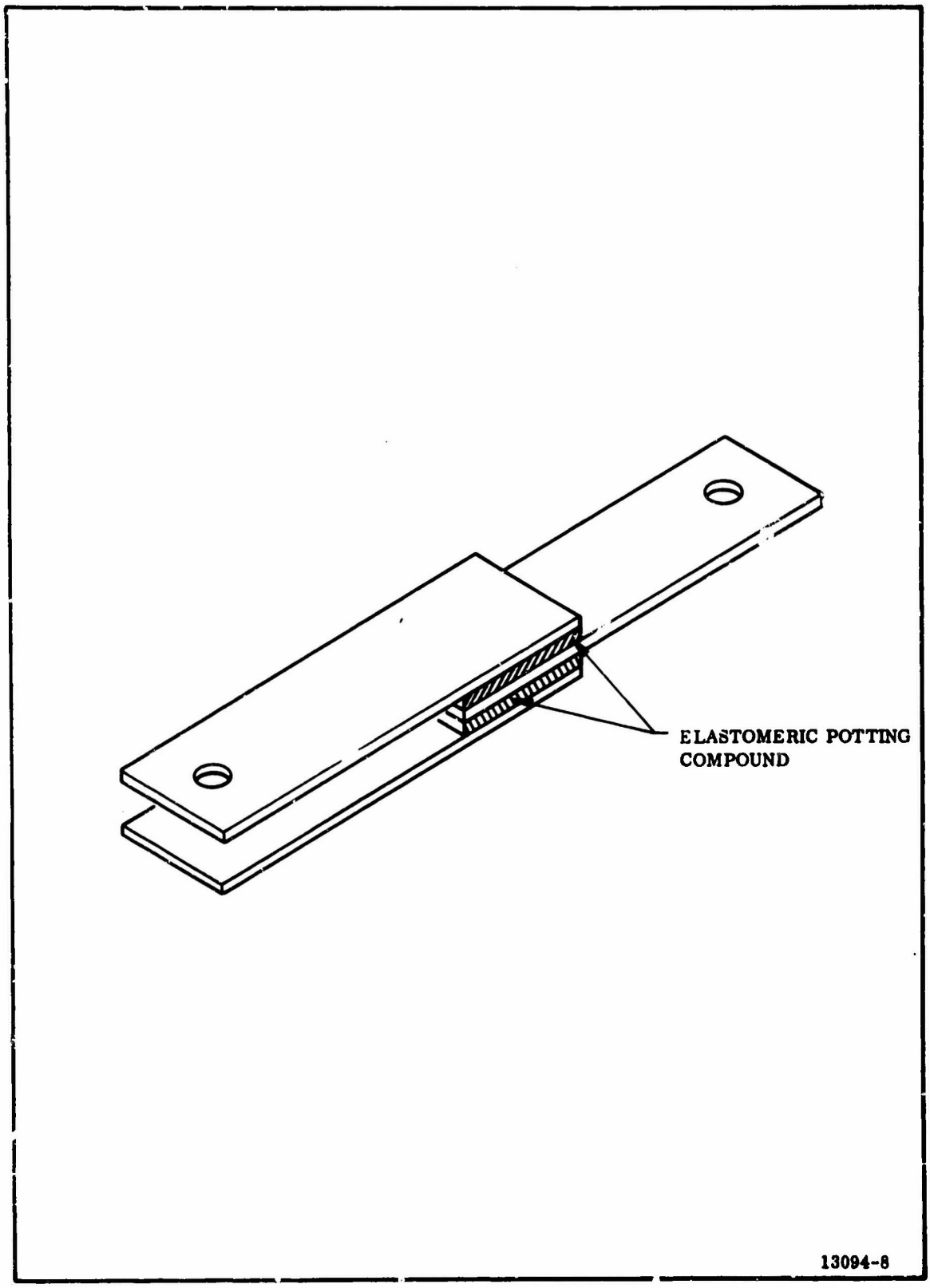

Figure 3-7. Lap Shear Adhesion Test Specimen

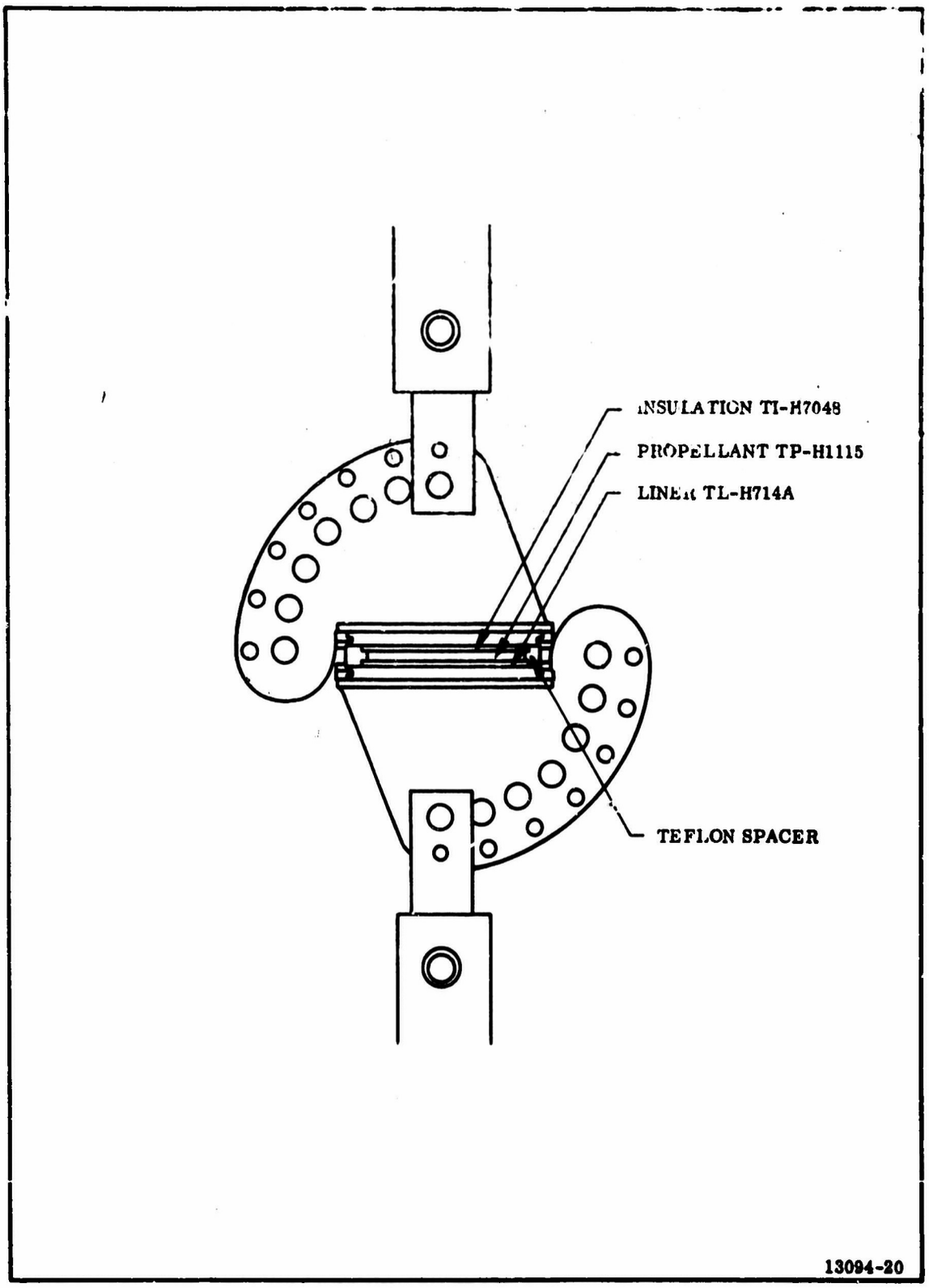

Figure 3-8. Tenshear Test Apparatus

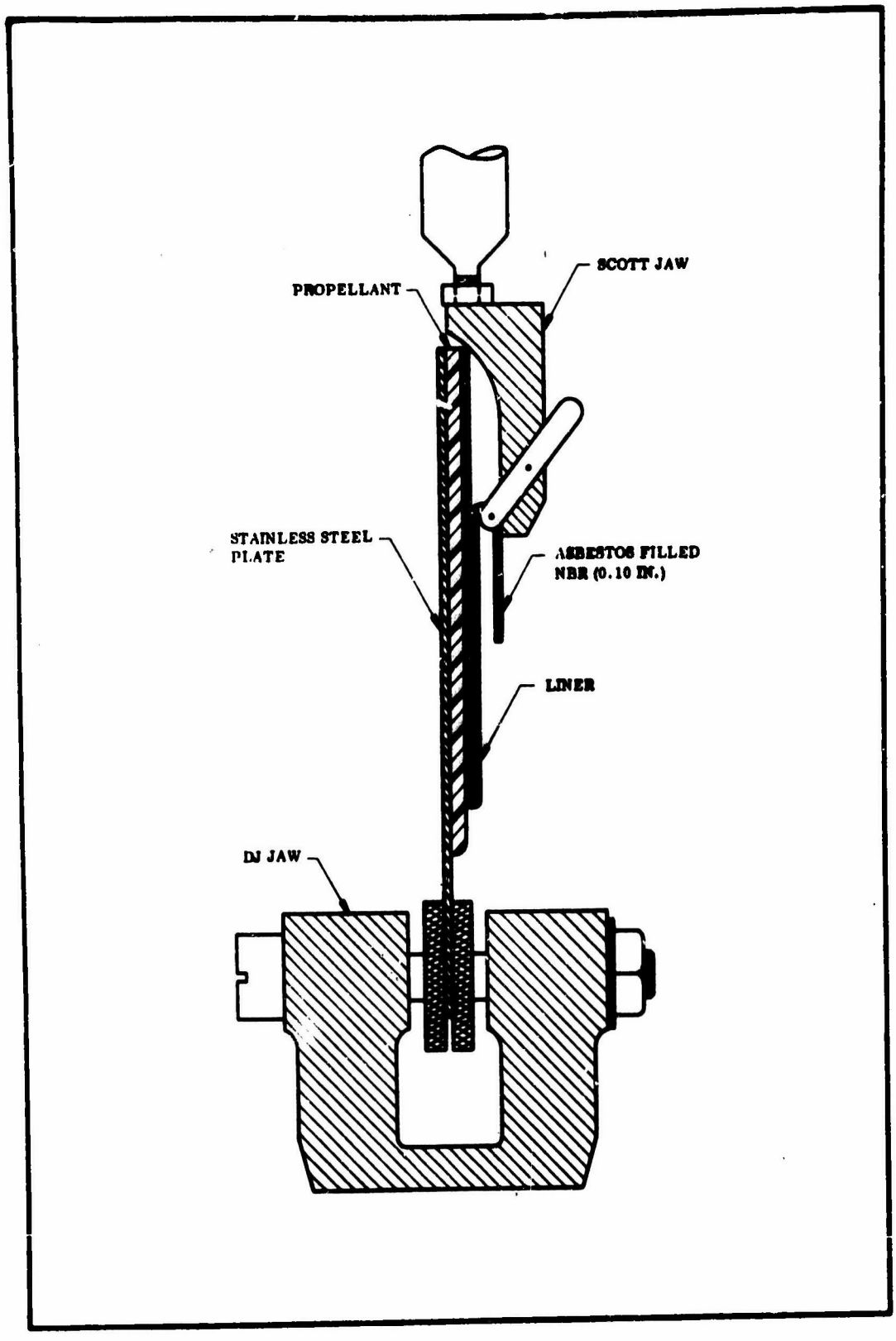

Figure 3-9. 180 Deg Peel Test Specimen and Arrangement

TABLE 3-5

BOND STRENGTH, PHASE I

Determining bond strength of TI-H704B at steel interface under motor conditions.

INTERFACE MATERIAL	Steel	Steel
Primer	Koropon	
Insulation	TI-H704B	TI-H704B
Conditions	Prime Steel Plate with Koropon; Apply 0.15 in. thick layer of TI-H704B and cure	Apply 0.15 in. thick layer of TI-H704B and cure

Tests 5 Adhesion cup
5 Lap shear

Total Tests 20

Peel and tenshear tests will be conducted in the peel and tensile apparatus shown in Figures 3-8 and 3-9 (Reference Phases II, III and IV).

TABLE 3-6

BOND STRENGTH, PHASE II

Determining bond strength of insulation liner propellant.

Insulation	TI-H704B
Condition	Cured
Liner	*TL-H714A
Condition	Cured
Propellant	TP-H1115

Tests 4 180 deg peel
5 Tenshear
5 Adhesion cup

*Liner TL-H714A to Propellant 180 deg peel.

TABLE 3-7

BOND STRENGTH, PHASE III

Determining effects of liner cure upon liner bond strength.

Insulation	TI-H704B				
Condition	Cured				
Liner	TL-H714A				
Cure condition at 135°F prior to casting	48	72	120	144	200 Hr
Propellant	TP-H1115				
Tests	4 180 deg peel 5 Tenshear				
Total Tests	50				

TABLE 3-8

BOND COMPATIBILITY, PHASE IV

Determining the compatibility of the insulation to liner to propellant bond.

Substrate		Steel	
Primer		Koropon	
Insulation		TI-H704B	
Liner		TL-H714A	
Cast Conditions	5 Hr at 1 in. Hg	50 Hr at 1 in. Hg	50 Hr at 1 in. Hg
Propellant	TP-H1115	TP-H1115	
Cure Condition			3 days at 170°F
Propellant			TP-H1115

Tests 4 180 deg peel
5 Adhesion cup

3. Apply TI-H704B mastic insulation.
4. Cure 4 days min at 80 (± 20)°F.
5. Apply liner by sling lining.
6. Cure for 24 hr at 135°F
7. Preheat 10 hr at 135°F.
8. Cast 50 hr max under vacuum at 135°F, with TP-H1115 propellant.
9. Cure 6 days at 135°F.

5. PREDICTED RESULTS

Since the insulation, liner, and propellant are comprised essentially of the same materials that have been used in previous motors, test results are expected to verify the design and processes with no modification. Variables to be considered are limited to changes in propellant formulation to obtain requisite burning rate, and modification of liner to insure compatibility.

SECTION IV

PROPELLANT DESIGN

A. FORMULATION AND PHYSICAL PROPERTIES

The propellant to be used in the 156-9 motor utilizes a polybutadiene acrylonitrile tripolymer (HB polymer) binder, ammonium perchlorate oxidizer, and aluminum metal additive. This propellant, designated TP-H1115, has a Class 2 explosive hazards classification. The propellant composition and theoretical, physical, and ballistic parameters are shown in Table 4-1. Standardization of this propellant is in progress. Target values for the propellant standardization are a modulus of 400 to 500 psi and a burning rate in the 156-9 motor of 0.767 in./sec at 700 psia.

B. PREVIOUS EXPERIENCE

The TP-H1115 propellant is essentially the same as propellant used extensively by Thiokol in large motor programs conducted to date. The propellant has been used in four Stage I MINUTEMAN size motors and the 156-2C-1 motor tested by the Thiokol Alpha Division. The only modification in the propellant formulation is the addition of five micron size oxidizer to increase the propellant burning rate to the desired level.

TABLE 4-1

PROPELLANT CHARACTERISTICS
TP-H1115

Formulation	Percent
HB/ECA Binder and Curing Agent	11
Aluminum Fuel	18
Ammonium Perchlorate Oxidizer	68
Dioctyl Adipate Plasticizer	2
Iron Oxide Burning Rate Catalyst	1
Theoretical Physical and Ballistic Parameters	
Density (lb/cu in.)	0.065
Characteristic Velocity (ft/sec)	5,187
Ratio of Specific Heats, Chamber	1.13
Ratio of Specific Heats, Exit	1.18
Temperature, Chamber (°F)	6,000
Temperature, Throat (°F)	5,635
Temperature, Exit (°F)	3,708

C. WEIGHT ANALYSIS

The calculated weight of propellant to be contained in the 156-9 motor is 277,775 pounds.

D. MIXING AND CASTING TECHNIQUES

The 600 gal. vertical mixer will be used to manufacture the propellant for the TU-562 motor. This mixer has a working capacity of approximately 6,000 lb of TP-H1115 propellant with a complete mix cycle of 1 hr and 15 min per mix. The expected total mix time for the motor, therefore, would be 61 hours. This is equal to the casting rate during the TU-412 (156 in. segmented) motor casting when 4,400 lb of propellant were delivered every 55 min using three 300 gal. ABW horizontal mixers. Use of the vertical mixer rather than the horizontal mixers is estimated to result in a savings of approximately 0.001 manhours per pound of propellant produced or approximately 300 manhours for the TU-562 motor.

A bimodal oxidizer formulation will be used containing approximately 45 percent special fine ground oxidizer (5 micron) and 55 percent Type 1 unground oxidizer. Should undue agglomeration occur because of the relatively large amount of special fine oxidizer required, an adjustment in storage and mixer feeding techniques may be necessary. Experience indicates that the tote bins, which were modified for the TU-312 motor casting, will accommodate the quantity of oxidizer needed for the TU-562 mixes. The mix may have to be reduced in size to match the amount of oxidizer that can be placed in the tote bins. This will be investigated as soon as the new 300 lb per hour fluid energy mill has been installed for oxidizer grinding.

Aluminum, dioctyl adipate (DOA), iron oxide (Fe_2O_3), HB polymer, and Epon 828 will be premixed in the vertical mixer immediately prior to adding the oxidizer. The aluminum and HB will be weighed directly into the mixer change can

at Building M-120. The DOA, Fe_2O_3, and Epon 828 will be weighed in separate containers and dumped into the mixer change can after the aluminum and polymer have been added. No separate premixing operation will be performed at the premix area, but the weighed up raw materials will be delivered to the mixer building in the mixer change can where they will be mixed for approximately five minutes before the oxidizer is added.

The mixed propellant will be delivered to the casting site in the mixer change can, and poured into the casting hopper with the aid of a breakover stand. The propellant will be vacuum cast to preclude a separate deaeration step and insure a superior quality grain.

SECTION V

GRAIN DESIGN

A. BALLISTIC DESIGN

The 156-9 motor contains a 64 percent web fraction slotted cylindrically perforated propellant grain. This grain design is the same as that used in the 156-6 motor except that the aft port diameter has been increased to accommodate the submerged portion of the movable nozzle. The motor case is a monolithic structure. The propellant grain is cast in two operations separated by the installation of slot formers in the aft grain. Unrestricted burning is permitted on all exposed propellant surfaces. The core diameter is 54.2 in. in the motor forward end and 77.25 in. in the vicinity of the submerged nozzle (motor aft end). After grain shrinkage, an average grain ID of 55.39 in. is predicted. The case has a very conservative insulation design resulting in a propellant web thickness of 49.57 inches. The 156-9 loaded case design is shown in Figure 5-1.

The 156-9 grain design was based upon the use of existing motor hardware and tooling while achieving contractually required motor performance. Major design considerations were maximum expected operating pressure (MEOP), aft grain limitations imposed by the configuration of the submerged nozzle, and chamber pressure vs time neutrality. The slot location was selected to facilitate motor manufacture and to maximize use of existing hardware. The 6.5 in. slot width was selected to provide high propellant weight without causing the local high gas velocity that is associated with a very narrow slot.

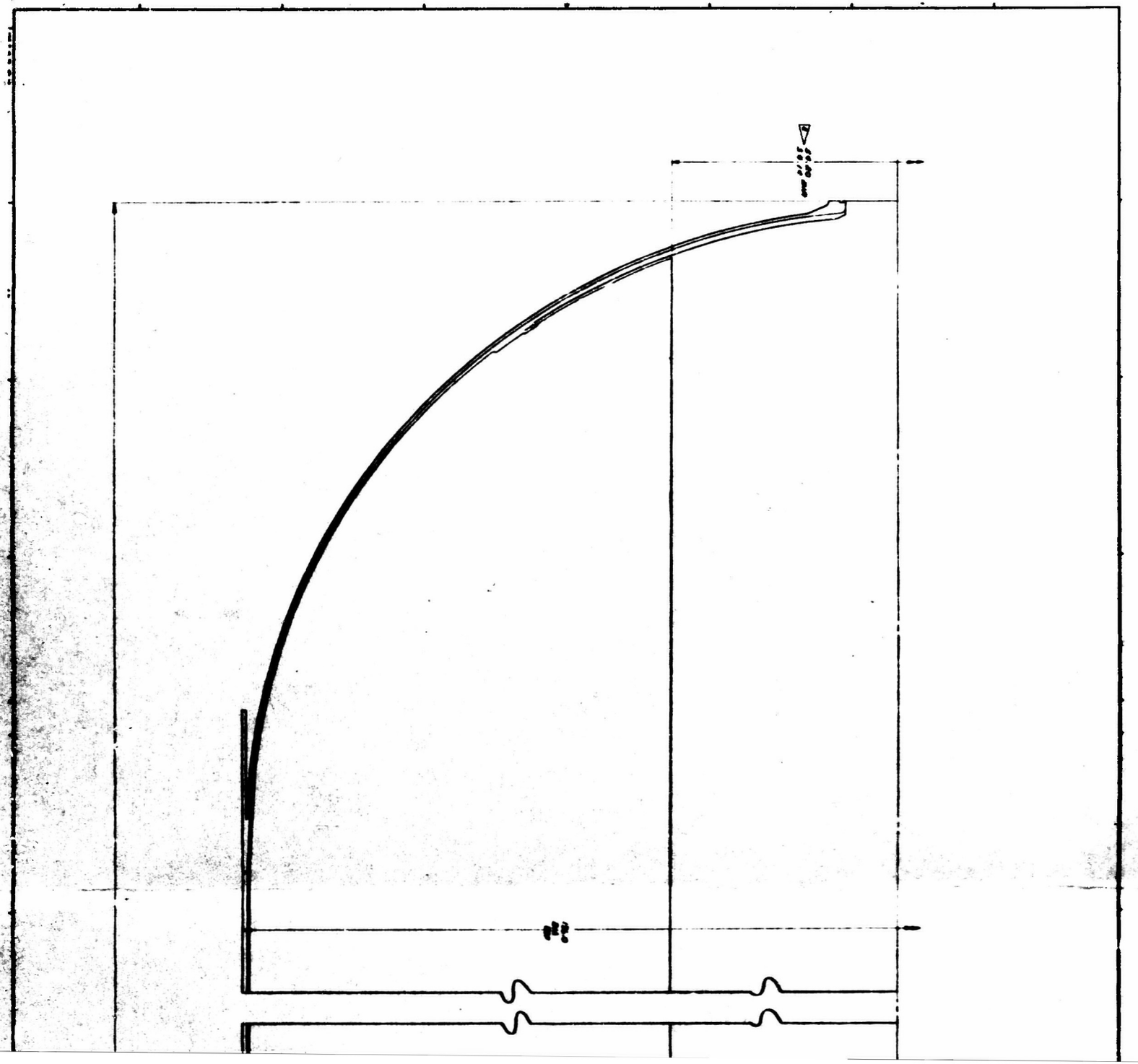

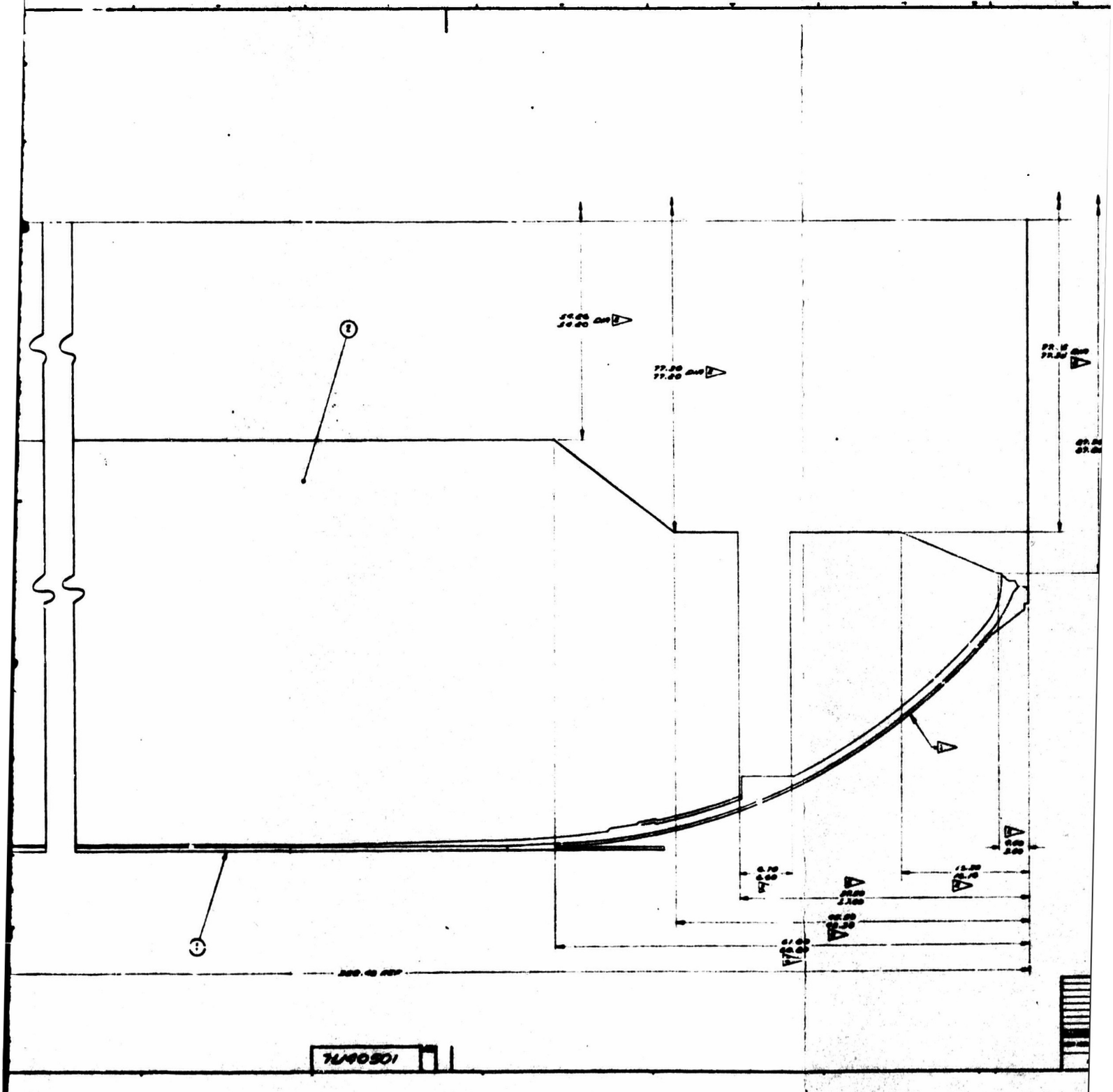

Figu

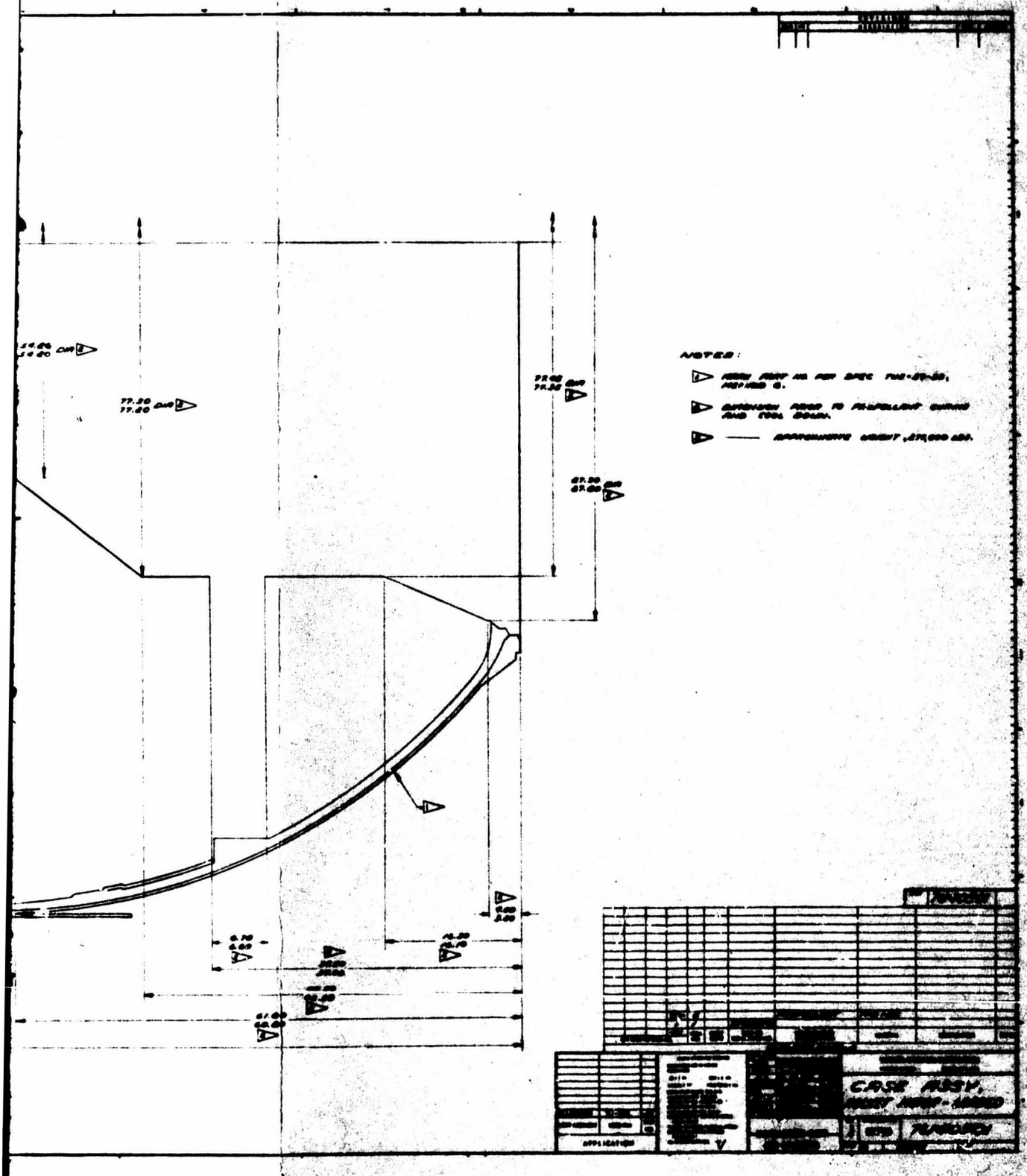

Figure 5-1. 156-9 Loaded Case

1. PREDICTED PERFORMANCE

The 156-9 motor predicted performance (Table 5-1), satisfies the performance requirements to the extent possible using existing motor hardware.

2. PRESSURE AND THRUST VERSUS TIME

The predicted chamber pressure and thrust vs time traces are shown in Figure 5-2 . The pressure trace shows the neutrality achieved with the 156-9 grain design.

3. GAS FLOW CHARACTERISTICS

The 156-9 motor (Lockheed) and the 156-9 motor (Thiokol) are designed to use the same basic core to form the internal grain configuration. Use of a submerged nozzle on the 156-9 motor, however, necessitates a change in the nozzle cutout grain geometry. The initial flow conditions have been compared to show that the 156-9 motor grain design results in more conservative gas velocities in the motor aft plenum chamber than was predicted for the successfully tested 156-6 motor.

A sketch of the aft grain configurations of the 156-6 and 156-9 motors is shown in Figure 5-3 with the approximate nozzle envelope of each motor. The flow analysis of the 156-9 motor was made with the nozzle in the vectored position (4 deg) resulting in additional conservatism in the analysis. The aft slot location and configuration in both motors are similar, with the design slot width being approximately 6.5 inches. The nozzle in the Lockheed 156-6 motor extended farther over the aft slot than in the 156-9 motor.

A comparison of pertinent parameters of the two motors at the various locations in the aft plenum identified in Figure 5-3 is presented in Table 5-2 . A comparison at Stations 3, 4, and 5 reveals that the one dimensional Mach numbers, and thus velocities, in the 156-9 motor are less than in the 156-6 motor.

TABLE 5-1

PREDICTED MOTOR PERFORMANCE

Web Time Parameter	
Burning Time (sec)	64.6
Average Pressure (psia)	701
Maximum Pressure (psia)	761
MEOP (psia)	822
Total Impulse, sea level (lbf-sec)	65,942,500
Average Thrust, sea level (lbf)	1,020,723
Maximum Thrust, sea level (lbf)	1,127,000
Propellant Burning Rate, at P_{cb} (in./sec)	0.767
Target TU-131 Burning Rate, at 700 psia (in./sec)	0.717
Burning Rate Scale Factor	1.07
Propellant Weight Expended (lbm)	274,292
Maximum to Average Pressure Ratio	1.086
Action Time Parameters	
Action Time (sec)	66.6
Average Pressure (psia)	687
Total Impulse, sea level (lbf-sec)	66,534,800
Average Thrust, sea level (lbf)	999,020
Sea Level Specific Impulse (lbf-sec/lbm)	239.9
Thrust Coefficient (γ = 1.18. λ = 0.9769)	1.5174
Motor Coefficient (C_m)	0.981
Propellant Weight Expended (lbm)	277,344

TABLE 5-1 (Cont)

PREDICTED MOTOR PERFORMANCE

Nozzle Parameters	
Average Throat Area (sq in.)	976
Average Throat Diameter (in.)	35.3
Average Exit Area (sq in.)	7642
Average Exit Diameter (in.)	98.6
Initial Throat Diameter (in.)	34.5
Average Expansion Ratio	7.83
Throat Erosion Rate (in./sec)	0.011
Effective half angle (deg)	17.5
Effective λ	0.9769
Grain Design Parameters	
Grain Outside Diameter (in.)	154.5
Grain Inside Diameter (in.)	55.39
Cross-sectional Loading Density (percent)	0.87
Port Area (sq in.)	2437
Initial Port/Throat Area Ratio ($\frac{1}{J}$)	2.6
Web Thickness (in.)	49.57
Web Fraction (percent)	0.64
Slot Width at Bore (in.)	6.65
Slot Angle to Motor $\mathbb{Q}$ (deg)	90

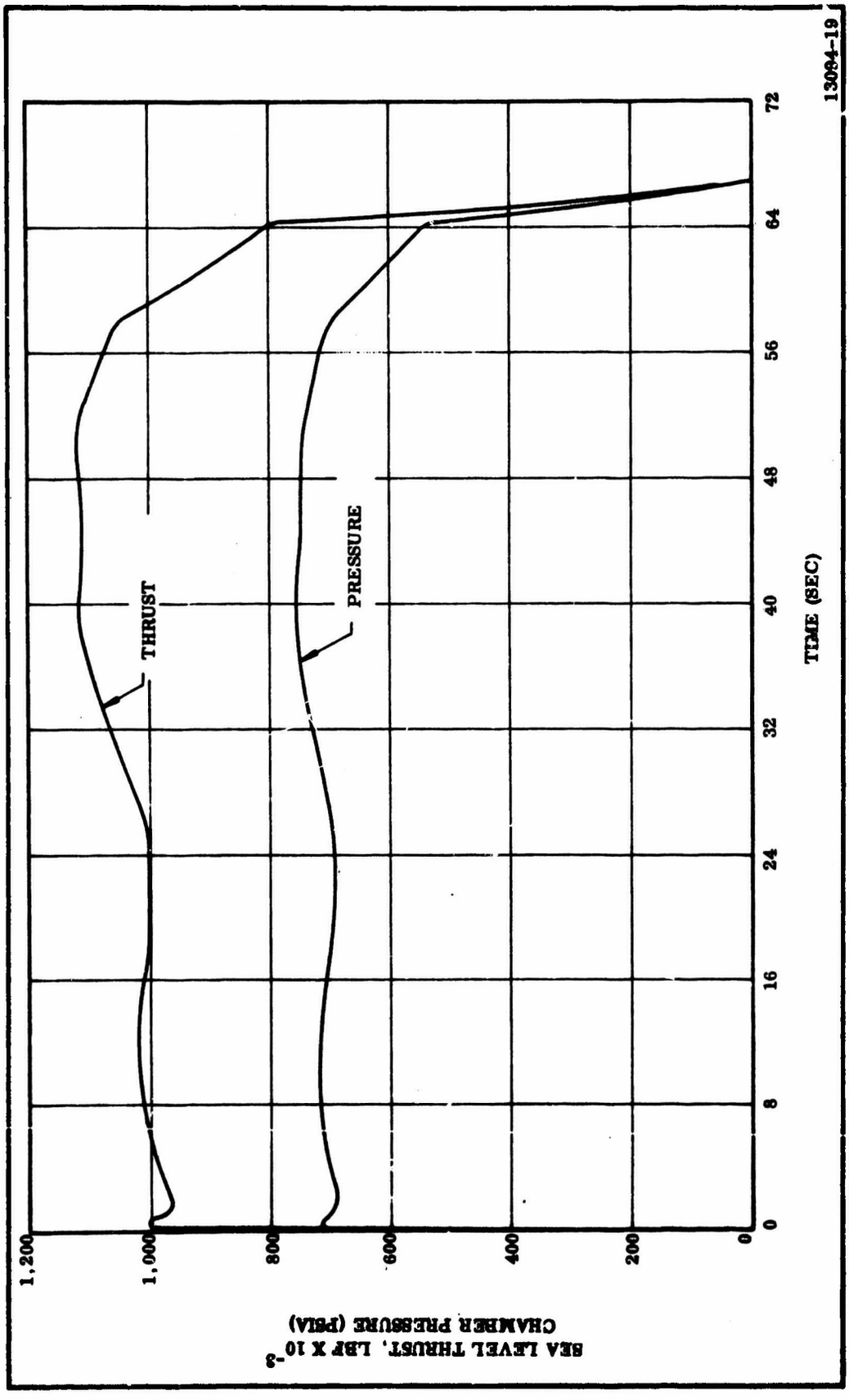

Figure 5-2. Predicted Chamber Pressure and Sea Level Thrust vs Time at 80°F

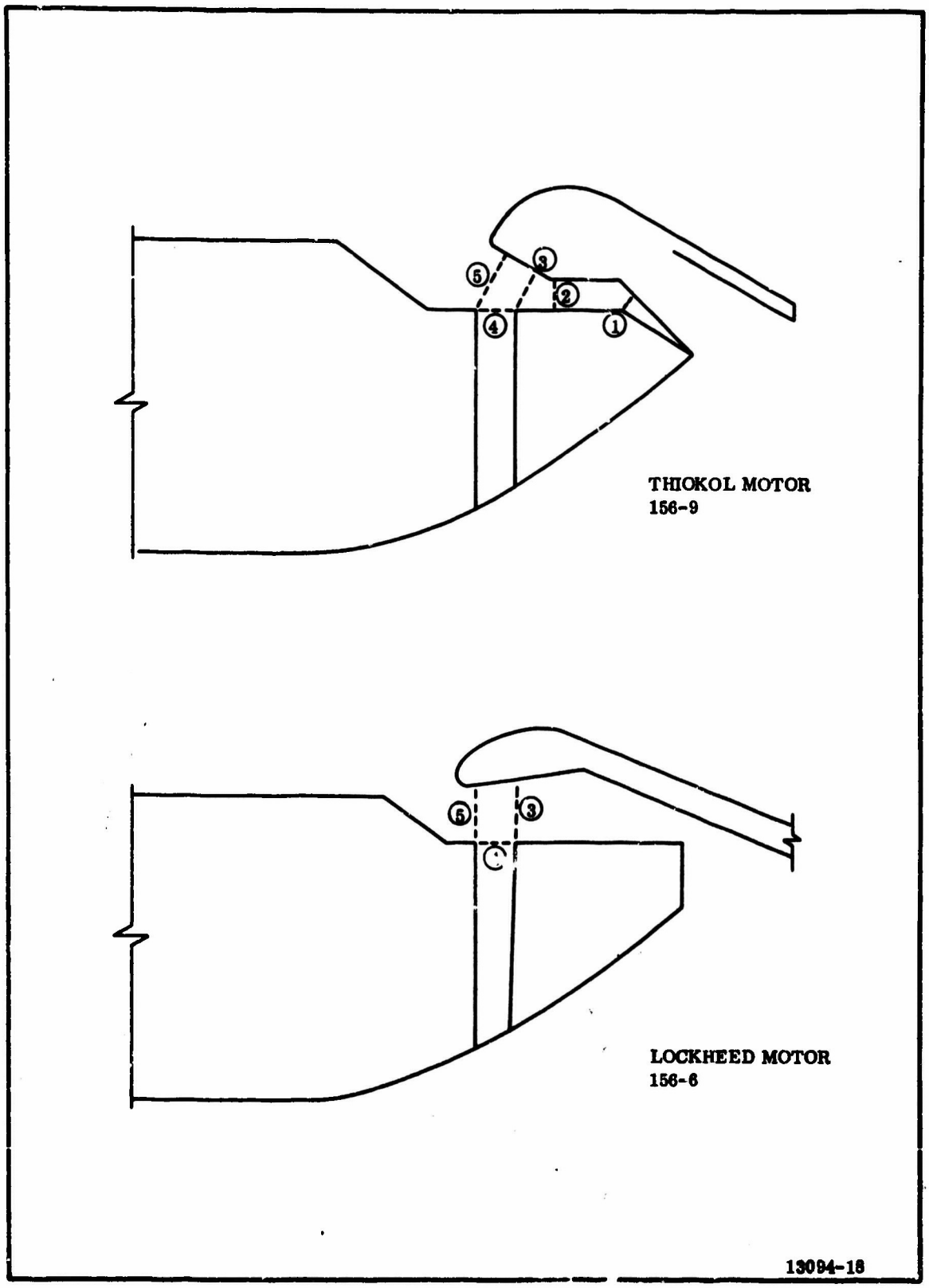

Figure 5-3. Aft Plenum Initial Flow Characteristics, 156-6 and 156-9

TABLE 5-2

AFT PLENUM INITIAL FLOW CHARACTERISTIC COMPARISON

	Lockheed 156-6*	Thiokol 156-9
Surface Area Aft of Station No. (sq in.)		
Station 1	--	3,765
Station 2	--	5,782
Station 3	8,314	7,240
Station 4	22,660	20,526
Station 5	30,974	27,766
Local Flow Areas (sq in.)		
Station 1	--	1,003
Station 2	--	1,004
Station 3	1,663	1,471
Station 4	1,465	1,615
Station 5	1,663	2,113
Local A_s/A_t Ratio		
Station 1	--	3.8
Station 2	--	5.6
Station 3	5.0	4.9
Station 4	15.5	12.7
Station 5	18.6	13.1
Local Mach No.		
Station 1	--	0.026
Station 2	--	0.041
Station 3	0.04	0.036
Station 4	0.11	0.090
Station 5	0.13	0.094
Local Velocity (ft/sec)		
Station 1	--	90
Station 2	--	142
Station 3	138	124
Station 4	380	311
Station 5	449	325

*Technical Report No. AFRPL-TR-65-212
156 Inch Diameter Motor Liquid Injection TVC Program,
Lockheed Propulsion Company, October 1965

The Lockheed final program report* revealed that after cure shrinkage and grain slumpage, the slot width at the slot exit was approximately 8.77 inches. Other grain dimensions around the nozzle remained essentially the same. This increase in slot width reduced the theoretical Mach number at Station 4 (Figure 5-3 in the 156-6 motor to 0.05, with a velocity of 173 f /sec. Grain shrinkage also will tend to increase the slot width and reduce the gas velocity at the slot exit below the 311 ft/sec indicated.

It can be concluded that the grain configuration in the aft plenum chamber of the 156-9 motor is satisfactory and that the backside of the nozzle will not be subject to velocities significantly greater than already experienced in the 156-6 motor. The predicted one dimensional Mach number at the end of the grain of the 156-9 motor is 0.137 (velocity = 473 ft/sec). Propellant erosive burning will, therefore, not be significant in predicting motor performance.

B. STRUCTURAL DESIGN

A comprehensive stress analysis of the propellant grain of the 156-9 motor has been completed. The analysis was based on an axisymmetric elastic stiffness matrix method that was developed at Redstone Arsenal Research Division of Rohm and Haas Company. The stress and strain patterns for conditions of cure thermal shrinkage and pressurization have been calculated and compared to the failure criteria. The failure criteria used was the Smith failure boundary derived from uniaxial tests of the propellant. The analysis showed satisfactory margins between the calculated imposed loads and the failure boundary in all cases.

---

*Technical Report No. AFRPL-TR-66-109 156-Inch Diameter Motor Liquid Injection TVC Program, Volume 1, Book 1. Lockheed Propulsion Company, July 1966

1. GRAIN CONFIGURATION

The 156-9 is a 156 in. diameter steel case motor with a slotted cylindrically perforated propellant grain (Figure 5-4). Although the grain consists of two separate sections, the stress study considers them as one body. The main grain web fraction is 64.0 percent, and the length to diameter ratio is 1.68. The loading conditions considered are cure and thermal shrinkage to +60°F and ignition transient pressurization of 682 psia.

2. STRUCTURAL ANALYSIS

The stress analysis of the 156-9 rocket motor grain was performed using a computer program developed at the Redstone Arsenal Research Division of Rohm and Haas Company.* This program uses the "finite element" method of solution which is based on the direct stiffness analysis of structural mechanics. The direct stiffness method constitutes a procedure for applying the classical Rayleigh-Ritz method of structural mechanics. The method involves idealizing the continuum (propellant grain) and shell (case) structures by a set of finite elements which are geometrically triangular and rectangular, respectively. By using a simple finite element for which the stiffness or approximate stiffness is known, a system of equations relating the displacements at the corners of each element to the forces at these same locations can be constructed. Hence, the problem is reduced to a simple mathematical model involving the algebraic solution of a large set of simultaneous equations whose coefficient matrix is better known as the stiffness matrix. The principle of minimum potential energy may be stated as follows. If the potential energy of the body in question is expressed as a functional of the displacement field within the body, the

*Becker, E. B. and Brisbane, J. J. Special Report No. S-76, Application of the Finite Element Method of Stress Analysis of Solid Propellant Rocket Grains, Rohm and Haas Company, Redstone Arsenal Research Division, Huntsville, Alabama, November 1965

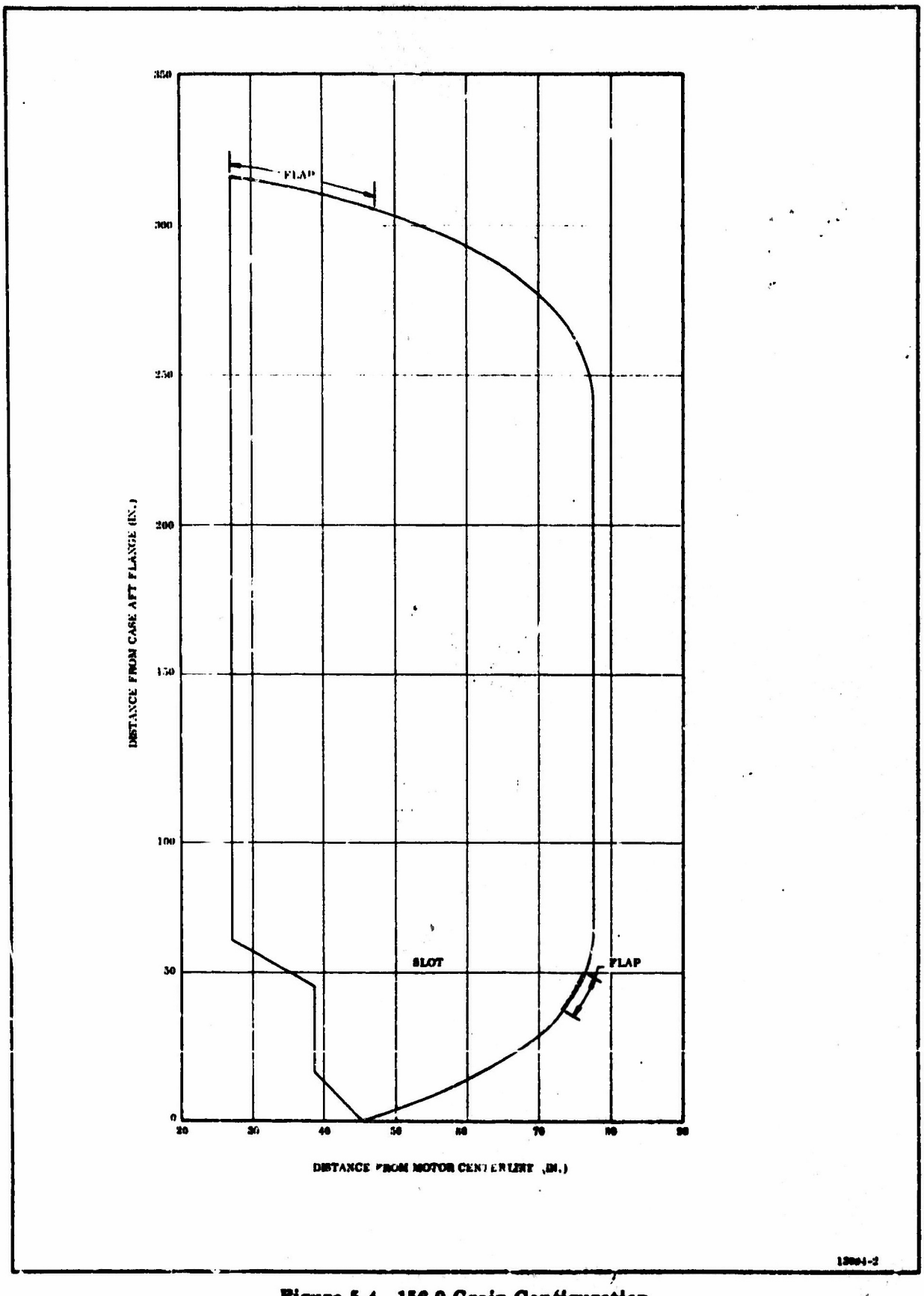

Figure 5-4. 156-9 Grain Configuration

displacement field which satisfies the boundary conditions and the equilibrium equations also minimizes the functional. To this point the stiffness method is exact in theory. However, to apply it to a practical analysis problem requires that a form of the displacement field must be assumed which satisfies the condition of compatibility of displacements for each finite element. If the displacement field within each element is assumed to vary linearly with the coordinates, the potential energy functional will become a quadratic form of the coordinates which, when minimized, will yield the system of alegebraic equations mentioned previously. The solution of this set of equations results in the coefficients of the assumed displacement field, providing the strain and stress fields through the strain-displacement relations and the stress-strain equations, respectively.

The foregoing statement of the direct stiffness or equilibrium method may be summarized by the following characteristics.

1. Displacements are taken as unknowns.
2. Compatibility requirements are satisfied initially for all displacement fields assumed.
3. A number of independent conditions (equations) equal to the number of degrees of freedom of the structure are established.
4. Displacements are computed which provide equilibrium.

The program is written around a reformulation of the field equations, making the quality of the solution independent of Poisson's ratio. Many of the older finite element analyses were based on the usual formulation of the field equations which develops a singularity at Poisson's ratio equal to 0.5 and presents a doubtful solution at values of Poisson's ratio approaching 0.5.

Since Thiokol propellant exhibits almost incompressible behavior under most motor rates, the ability to consider high values of Poisson's ratio becomes important. This becomes particularly significant when considering the effect of Poisson's ratio on induced bore tangential strain. The present programs include the ability of adding

the case stiffness to that of the propellant, providing a solution to the real case-grain situation. Prior stress analysis programs had to handle the case-propellant interaction in an artificial manner through displacement boundary conditions applied to the propellant.

The input data of the program includes description of geometry, material properties, and boundary conditions (both displacement and tractions). The program output consists of displacement of the element corners, and stress and strain over the elements. In addition, an auxiliary program permits the plotting of stress and strain contours, in addition to displacement grids.

As discussed, the computer analysis is based on elastic theory; therefore, a viscoelastic analysis per se is not possible. A pseudo-viscoelastic analysis can be obtained by making repeated computer runs in which time dependent propellant properties are varied. Consequently, for long time associated phenomena, the propellant equilibrium modulus as a function of temperature would be used. For short time occurrences, the stress relaxation modulus for the appropriate time of the event would be used.

a. Input Parameters--Accurate material properties are essential in conducting useful or dependable stress analyses. The time history of the various loading conditions also must be known. TP-H1115 propellant has not been characterized; however, under cognizance of the POSEIDON and Large Booster Programs, TP-H1096, TP-H1114, and TP-H8163 have been characterized and their actual properties are considered in this report as experimental data.

The significant material properties are stress relaxation modulus (E_R) as a function of temperature, thermal coefficient of linear expansion (TCLE) as a function of temperature, coefficient of cure shrinkage ($\emptyset_R$) and Poisson's ratio. The time to soak and the pressure vs time history data were derived from theoretical calculations.

The propellant stress relaxation curve vs time and temperature that was utilized is shown in Figure 5-5 . This curve was obtained from broad spectrum data reduction techniques. The long time or equilibrium modulus approaches 200 psi.

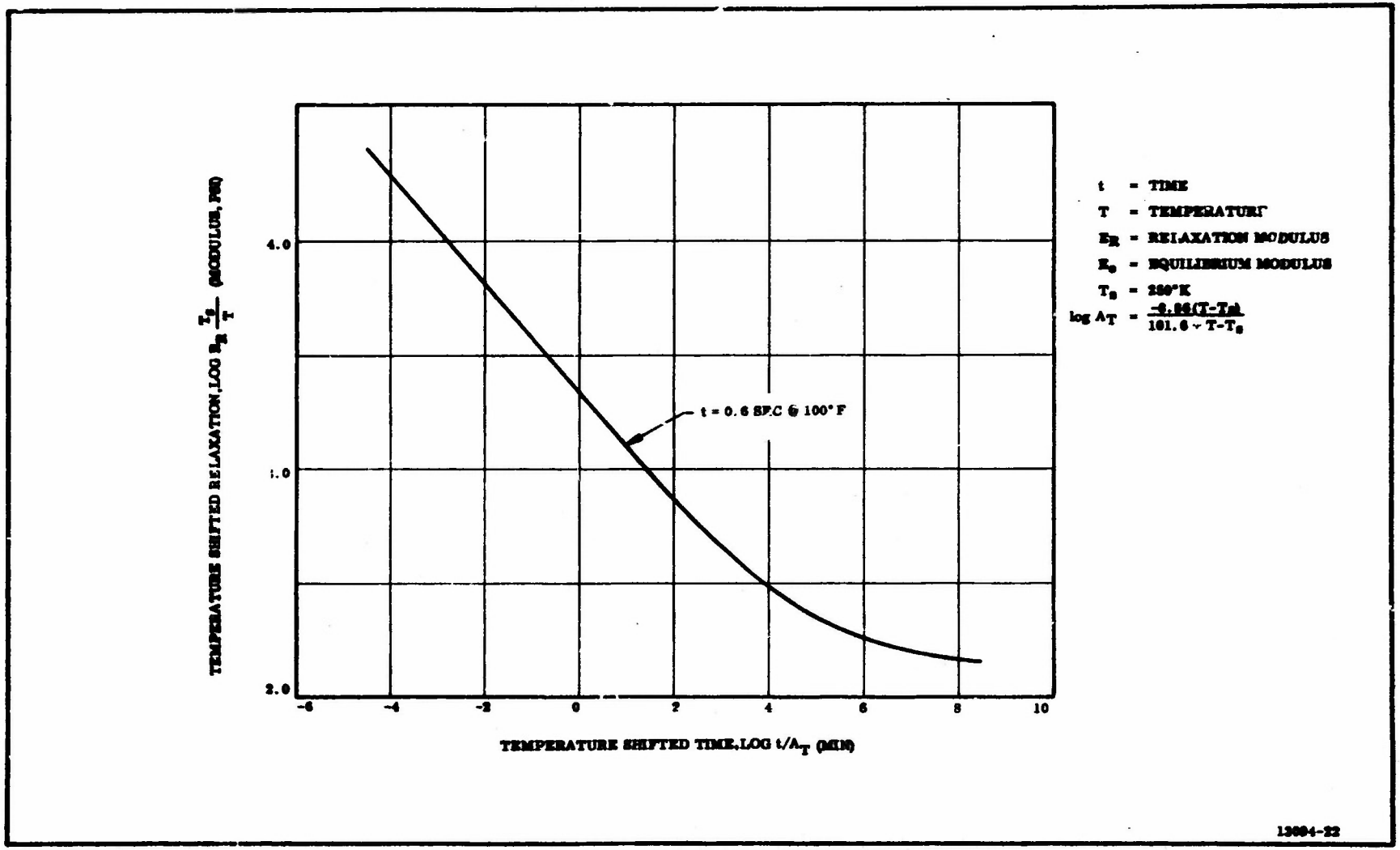

Figure 5-5. Propellant Stress Relaxation Modulus

The thermal coefficient of linear expansion was taken from propellant experimental data. The TCLE vs temperature has an inflection point at approximately 0°F. Above and below this point, the value is 6.26×10^{-6} and 6.67×10^{-5} in./in./°F. For conservatism, the average of these was used in the analysis.

The amount of cure shrinkage is difficult to ascertain, particularly because motor size affects the total shrinkage. Stress inducing cure shrinkage may range as high as 0.8 percent in very small motors and as low as 0.1 percent in very large motors.* A conservative value of 0.4 percent was used in this study. In a recent small analog motor containing 10 lb of propellant, the stress inducing cure shrinkage factor was determined to be less than 0.4 percent. The Thiokol computer program cannot calculate the cure shrinkage factor directly, so this factor is translated to an increment of temperature as a function of the thermal coefficient of linear expansion. Figure 5-6 illustrates the relationship between the cure shrinkage factor, thermal coefficient of linear expansion, and increment temperature. As noted in the figure, 20.5°F is the exact increment of temperature for a $\emptyset_R$ of 0.4 percent and the average TCLE temperature used in the analysis was 21°F to insure conservatism.

All computer runs were based on a Poisson's ratio input of 0.5. The rationale for this selection is based on experimental data. For cure and thermal shrinkage conditions (i.e. very low strain rate), experimental evidence indicates that Poisson's ratio is indeed 0.5. Also, as Poisson's ratio decreases from 0.5, the bore strains decrease. Therefore, if the exact value is less than 0.5, this approach is conservative. For pressurization conditions, the elastic relationships between bulk and Young's modulus and Poisson's ratio perhaps should be used, but for a lightly loaded motor like the 156-9, no significant difference will be seen. Hence, a Poisson's ratio of 0.5 was considered best for end result accuracy.

*Nelson, J. M., Special Report, Improvement of the Elastic Analysis Method of Predicting Low Temperature Operational Capability of Solid Propellant Motors (U), Thiokol Chemical Corporation, Alpha Division Huntsville Plant, 27 Nov 1963.

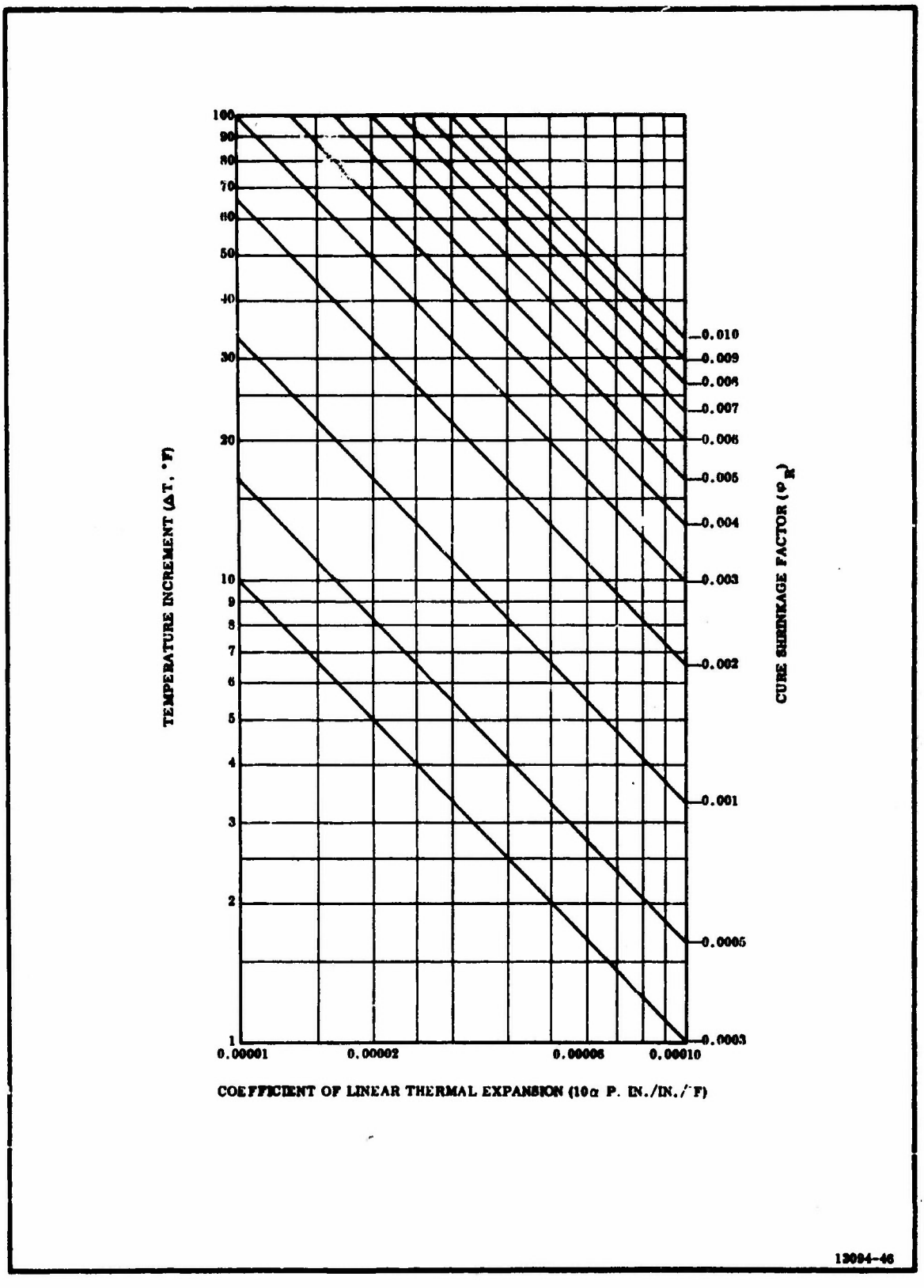

Figure 5-6. Design Curves for Selecting Temperature Increment Equivalent to the Cure Shrinkage Factor

The computer runs for this study had to be completed before the propellant data became available. Experience suggested the selection of 1,000 psi as an effective modulus for the pressure runs. Figure 5-5 indicates that for a time of 0.6 sec and a temperature range of 60 to 100°F, the lowest modulus would exceed 1,000 psi by at least 33 percent. Since the previously selected number would result in a higher induced bore strain, the original computer runs were not changed.

In addition to the mechanical properties parameters discussed earlier, material capability limits are required to determine the failure boundary. As determined experimentally, the propellant is the weak link in the 156-9 insulation to liner to propellant bond system. Therefore, propellant capability should be the limiting factor. The combined stress-strain capability of TP-H1115 was selected as a failure boundary. Figure 5-7 is a plot of the maximum corrected principal stress vs the maximum principal strain for uniaxial specimens tested over a wide range of temperatures and strain rates. For strain oriented failure, the lower value of strain was assumed to be 0.16 in./in.

The grain geometry used in the program assumed that the grain was one continuous body. The effects of split flaps and the slot are accounted for by inputting fictitious properties for the grid elements involved. The numbers used were 1.0 and 0.01 for modulus and Poisson's ratio, respectively.

b. Failure Criteria--Many different strain and stress inducing conditions are involved in the 156-9 study and no single failure criterion is adequate for all loads. Also, a wide diversity of opinions are extant within the solid propellant industry about which failure criteria are the most realistic. Thiokol has been using stress-strain boundary failure criteria as shown in Figure 5-7 . The boundary to be used is determined by whether the failure is dilatational or distortional. For dilatational failure, the boundary used is the sum of the principal stresses vs the maximum principal strain. For distortional failure, the boundary is the maximum deviatoric stress vs the maximum principal strain.

Justification of the dilatational failure criteria is realistically based on experimentation. Failure of a time dependent material must consider both stress and strain.

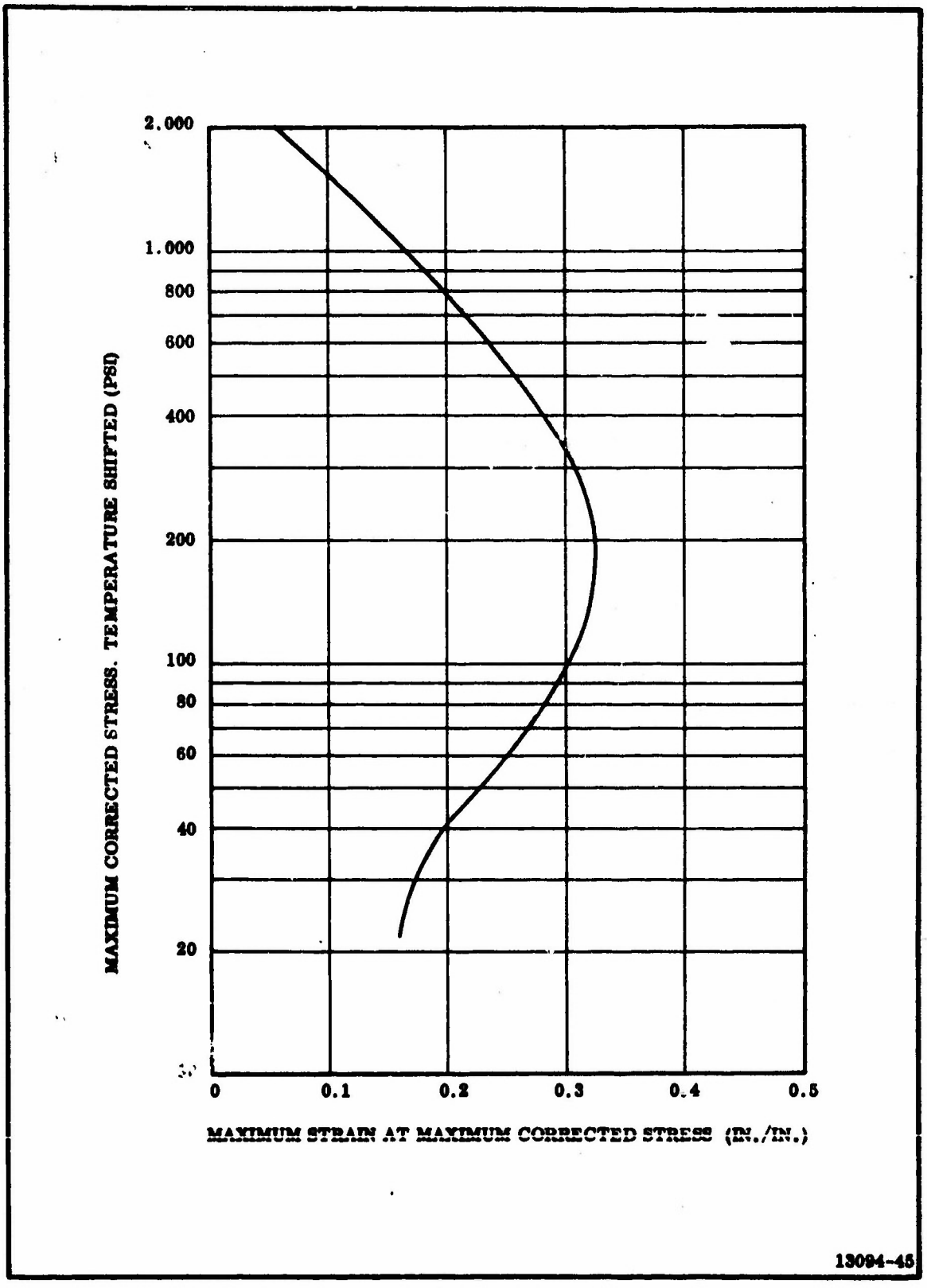

Figure 5-7. Failure Boundary Selected for the 156-9 Study

Exclusively independent stress or strain failure theory is not possible. Looking at all possibilities, at least three principal stresses and three principal strains must be considered. The sum of the principal stresses is a constant which defines the all tensile stress octant failure surface, as has been shown experimentally. Experimentally, the strain octant failure surface is defined by the maximum principal strain. The obvious question at this point is why not the sum of principal strains rather than the maximum? The solution is just as obvious, when the material in question is considered essentially incompressible and, therefore, the sum of principal strains is zero or insignificant. Experimentally, the strain sum cannot be ascertained. No motor design predicted to be structurally adequate based on this failure criterion has been known to fail. On the SAM-D program the Thiokol Huntsville Division correlated small scale TX-318 motor data with the failure boundary as shown in Figure 5-8. Based on these results, Huntsville concluded that the failure boundary approach was indeed very realistic.

Justification of the distortional failure criteria is no more complex than for the dilatational type. Experimental results have shown that in a distortional condition, i.e., elongation in hydrostatic compression, a limiting difference exists between principal stresses beyond which failure occurs. The maximum deviatoric stress is a logical measure of the limiting stress difference. Little difference occurs between this stress limit and the maximum stress difference, but there is a distinction between the two stress limits. The latter one is a measure of shear rather than tensile capability. Carefully controlled experimentation has revealed that shear failures are extremely rare in Thiokol propellants. Therefore, the deviatoric stress limit is used in preference to the stress difference. Again the stress octant failure surface has been defined. Maximum principal strain is used for the strain failure surface in both dilatational and distortional failure criteria. But for an incompressible material, the maximum deviatoric and principal strain essentially are identical. The Thiokol Wasatch and Huntsville divisions have determined that some H series propellants similar to TP-H1115 show a marked improvement in propellant distortional capability as a function of superimposed pressure in uniaxial tests. On the HiPads Program, the Huntsville Division determined that the improvement is realized in the motor.

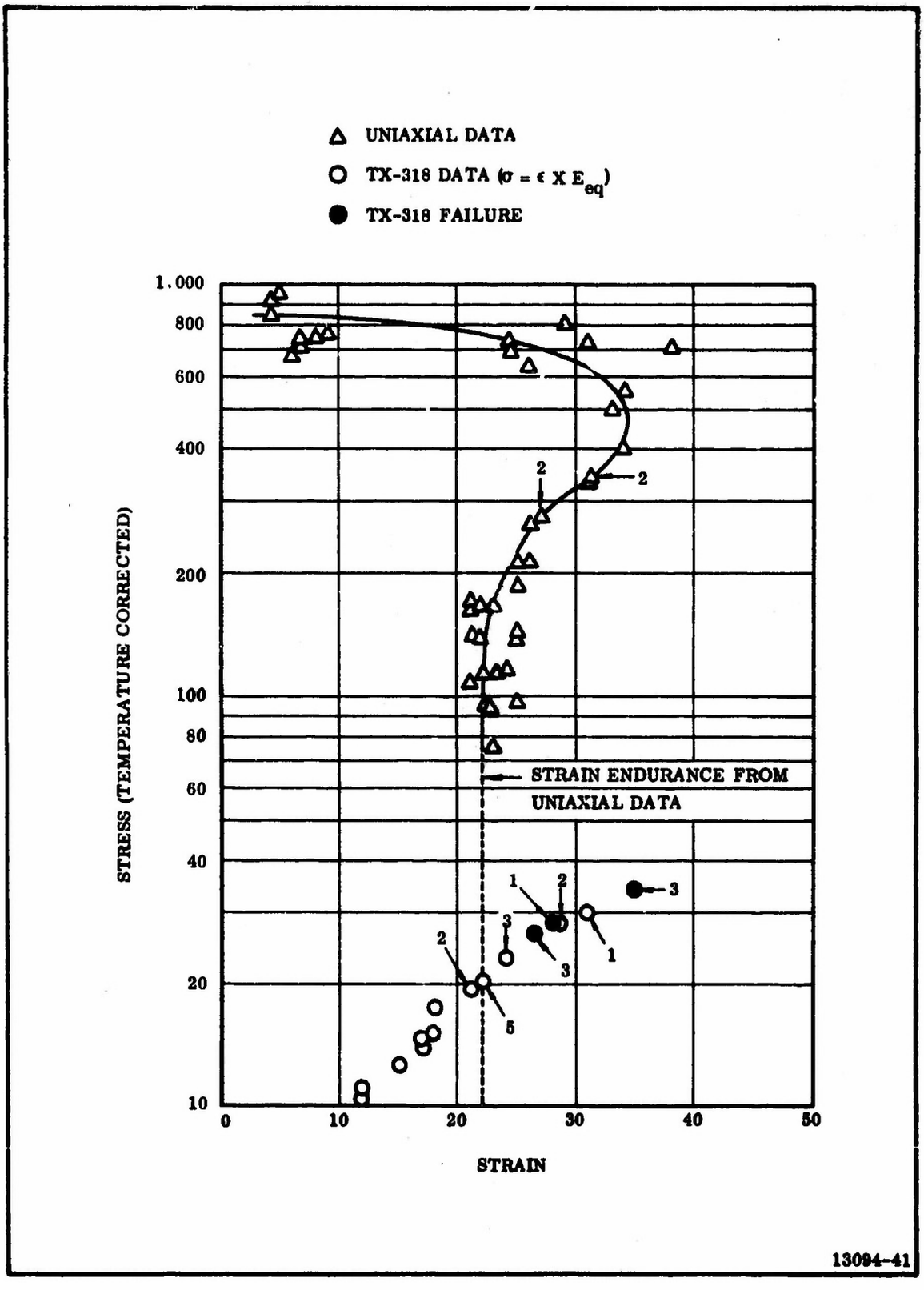

Figure 5-8. Comparison of Dilatational Failure of Uniaxial Tensile Specimens and Multiaxial Motor Grains, TP-H7034 High Solids HC

Further, a Castor II motor was successfully fired recently for which the sum of the inner bore hoop strain due to shrinkage and pressure significantly exceeded the propellant capability in an unpressurized state. If the unpressurized failure boundary is used, it must be concluded that the motor is indeed safe. To date, a satisfactory means of determining a margin of safety has not been developed for the stress-strain boundary. The interpretation of safety for the stress-strain boundary is merely the stipulation that the end point of the condition under consideration be inside the boundary, and in such a position, that stress decay will not result in the trace crossing the boundary. Further, if statistical limits for batch to batch variability and age are used to reduce the boundaries, then determination of a margin should be unnecessary.

c. Stress Analysis and Failure Criteria Results--In general, the 156-9 stress analysis studies have defined for the stress inducing loads considered:

1. Grain deformations,
2. Stress-strain contours throughout the grain,
3. Worst grain stress-strain conditions compared to propellant capability limits.

The first two limits may be illustrated by plots obtained from the original computer output. The grain deformations due to cure and thermal shrinkage to +60°F and ignition transient pressure to 682 psi are presented in Figures 5-9 and 5-10, respectively. The computer plotting program does not obtain contours of the failure criteria stress parameters of interest (i.e. the sum of the principal stress and the maximum deviatoric stress for dilatational and distortional failures, respectively). These data are only evaluated at the worst conditions. However, the maximum principal strain and stresses are available and are presented in Figures 5-11 thru 5-20.

Both the maximum principal and tangential strains are presented as the larger magnitude strain varies between the two. Hence, at the propellant to liner bond interface, the former will be predominant, while in the bore, the latter one will. Figures 5-11, 5-12, 5-16, and 5-17 show that large strains are in the vicinity of the slots. This occurs because the fictitious low modulus material used in the slot incurs large deformations. The plot program then reports the resulting strain. However, these strains must be neglected in the failure criteria analysis.

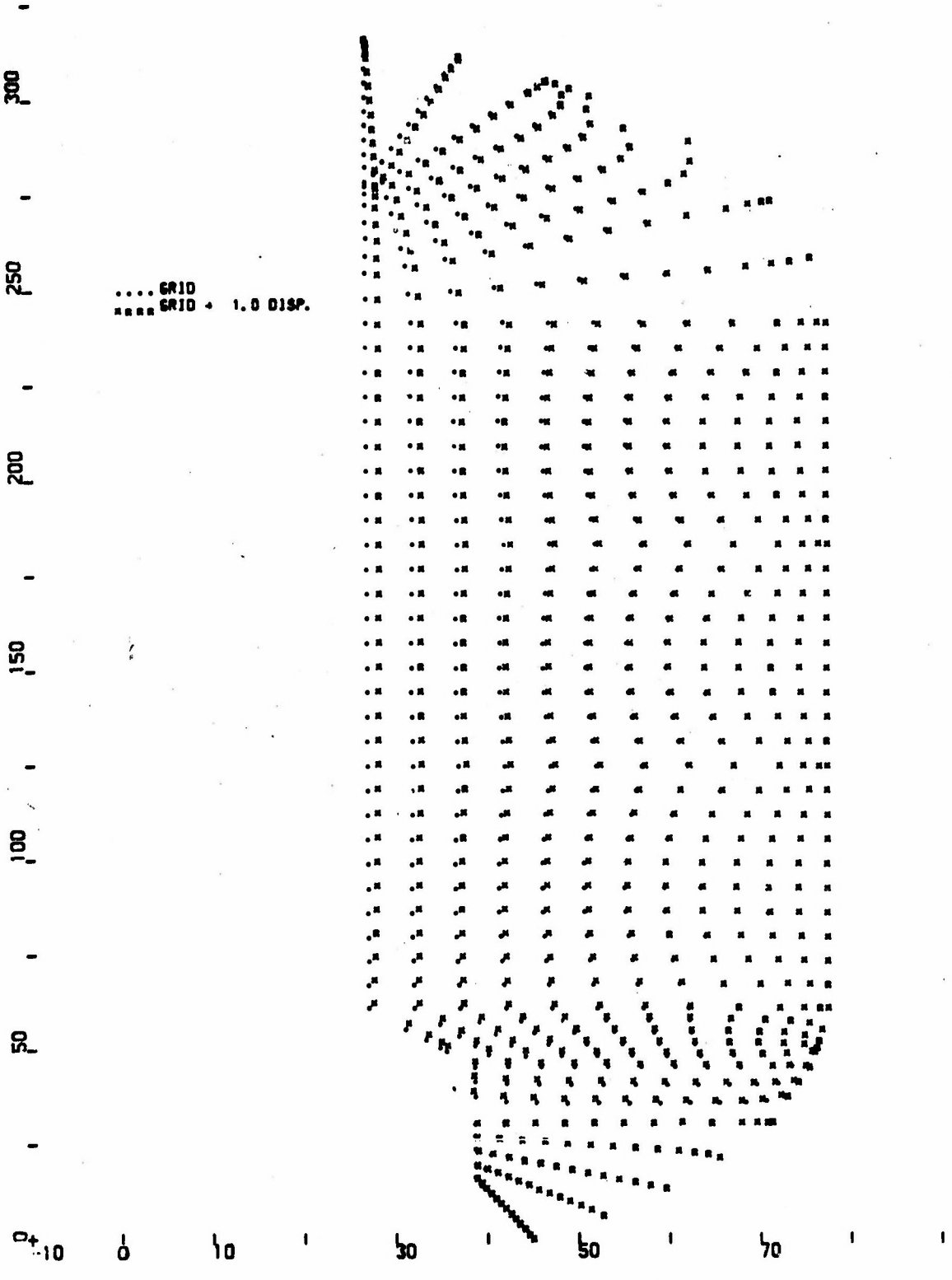

Figure 5-9. 156-9 Cure-Thermal Shrinkage Stress Analysis Grain Deformation

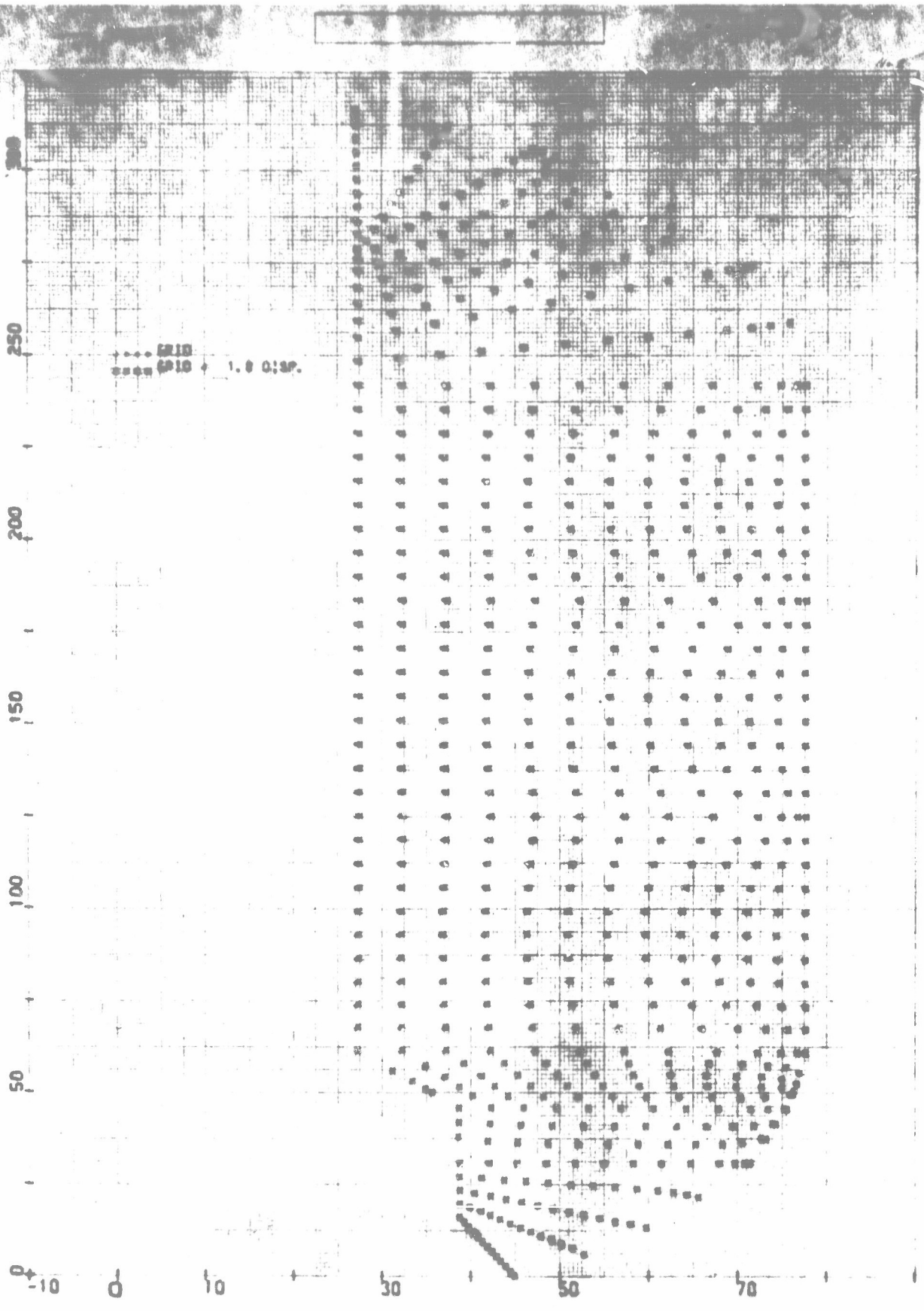

Figure 5-10. 156-9 Ignition Pressure 682 psi Stress Analysis Grain Deformation

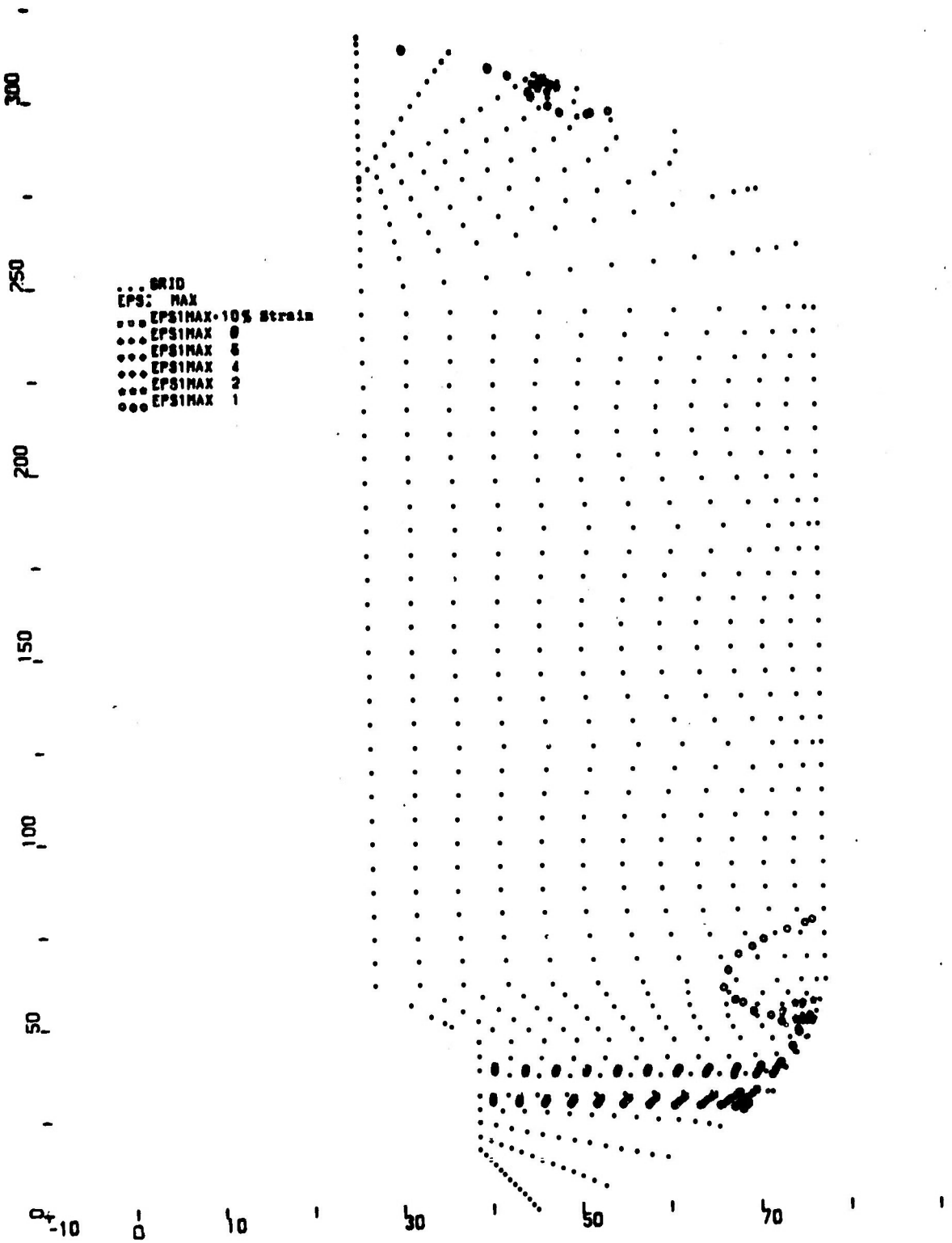

Figure 5-11. 156-9 Cure-Thermal Shrinkage Stress Analysis
Maximum Principal Strain (EPSI Max)

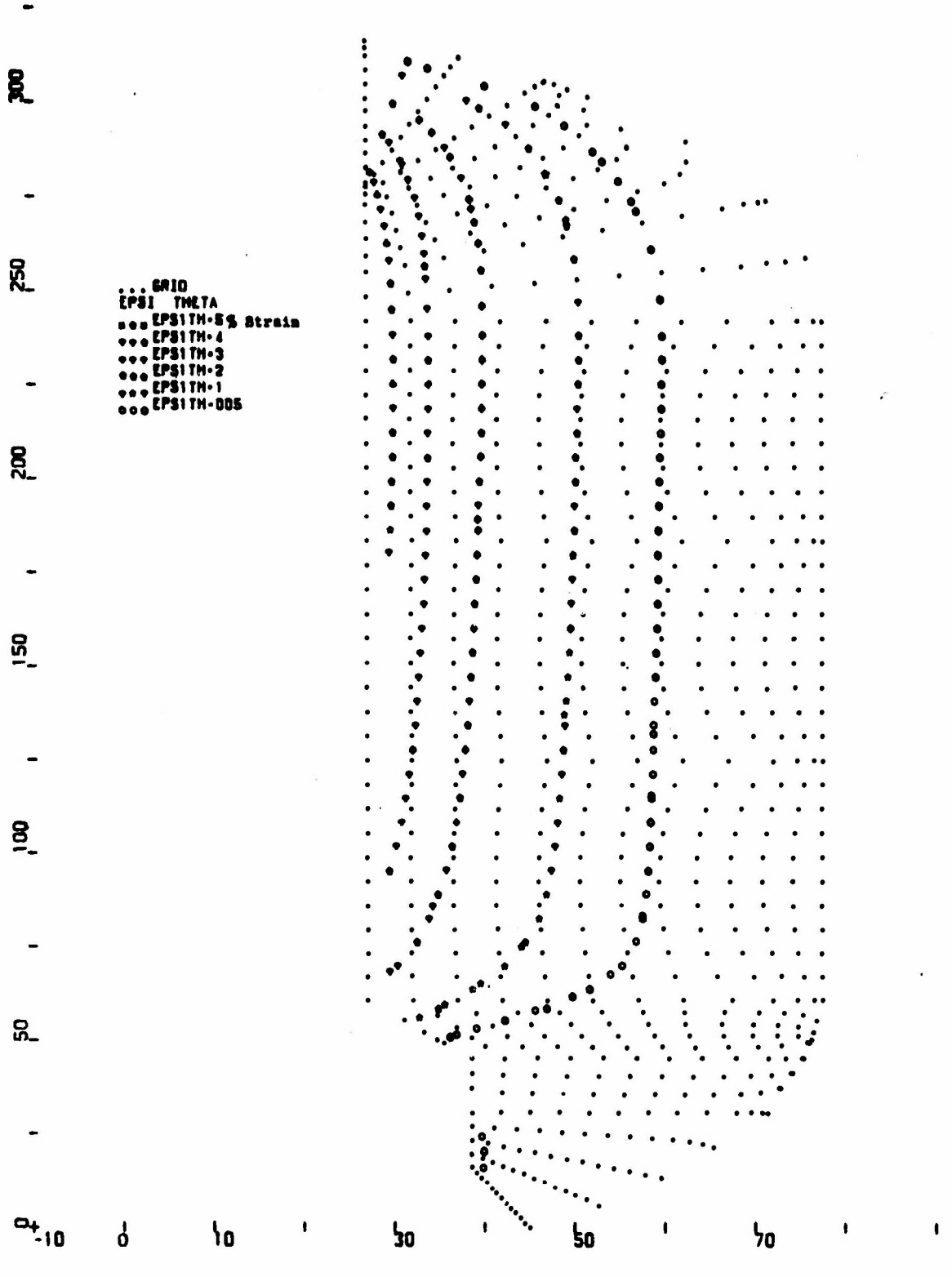

Figure 5-12. 156-9 Cure-Thermal Shrinkage Stress Analysis
Tangential (Principal) Strain (EPSI Theta)

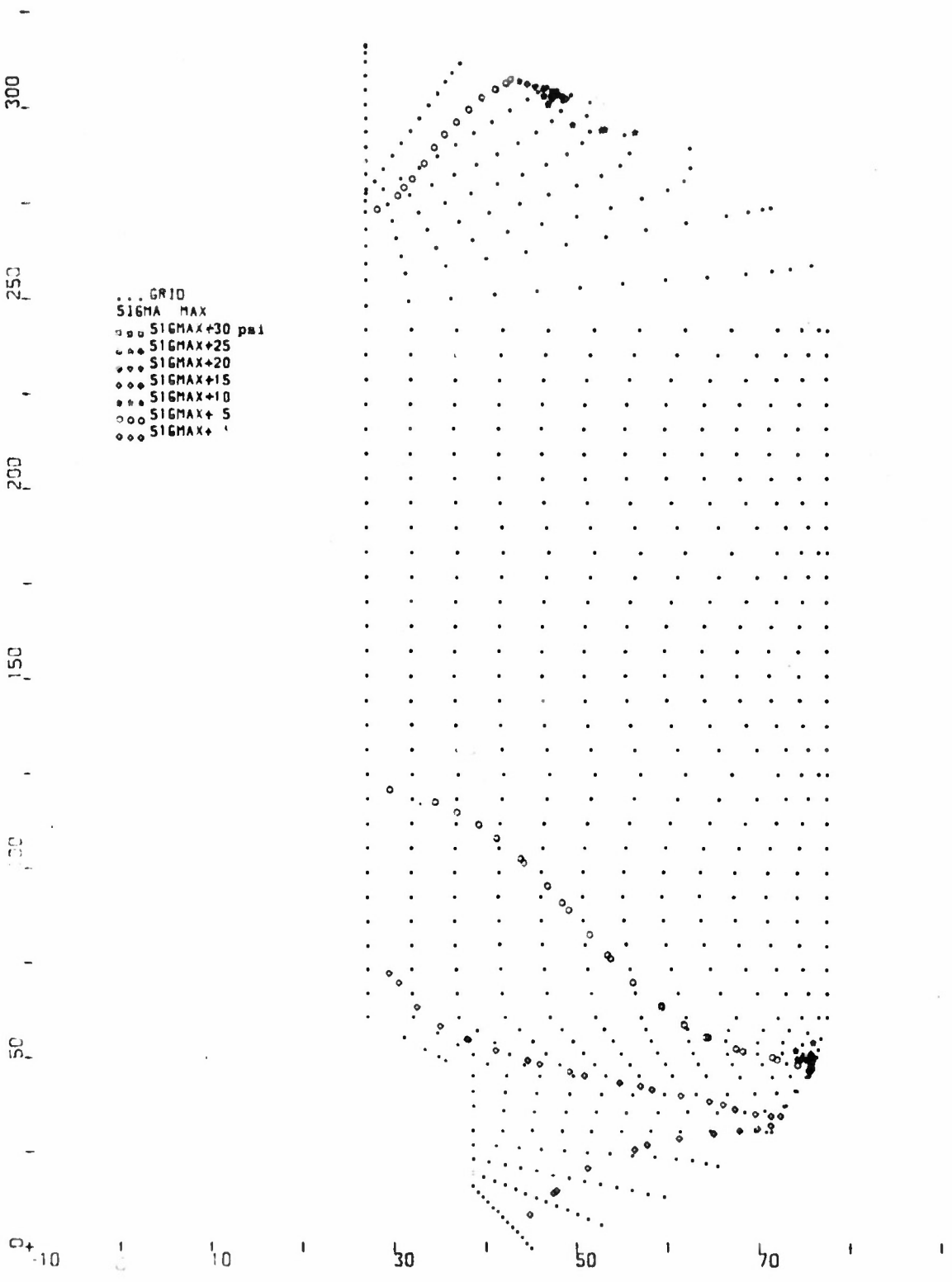

Figure 5-13. 156-9 Cure-Thermal Shrinkage Stress Analysis
Maximum Principal Stress (Sigma Max)

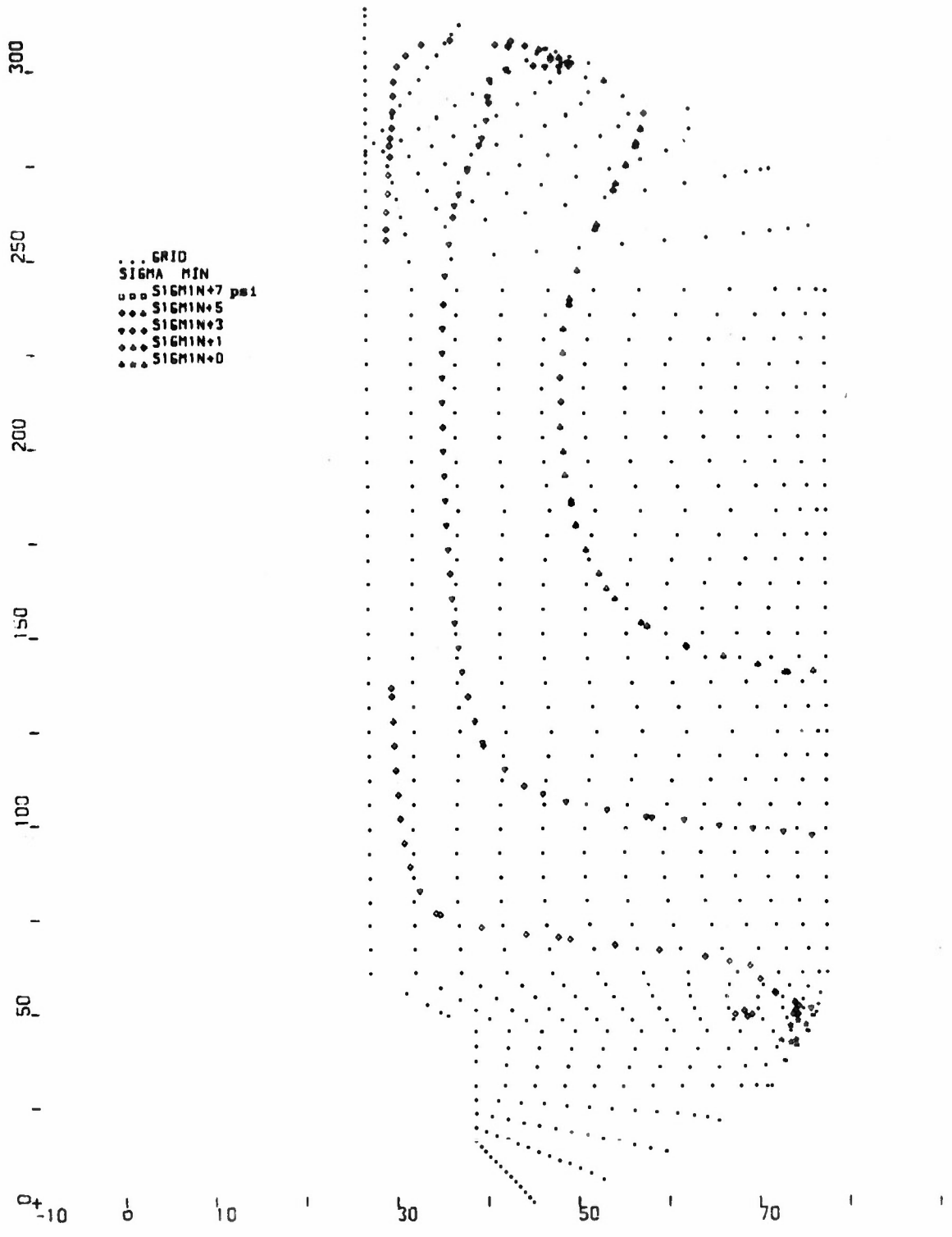

Figure 5-14. 156-9 Cure-Thermal Shrinkage Stress Analysis
Minimum Principal Stress (Sigma Min)

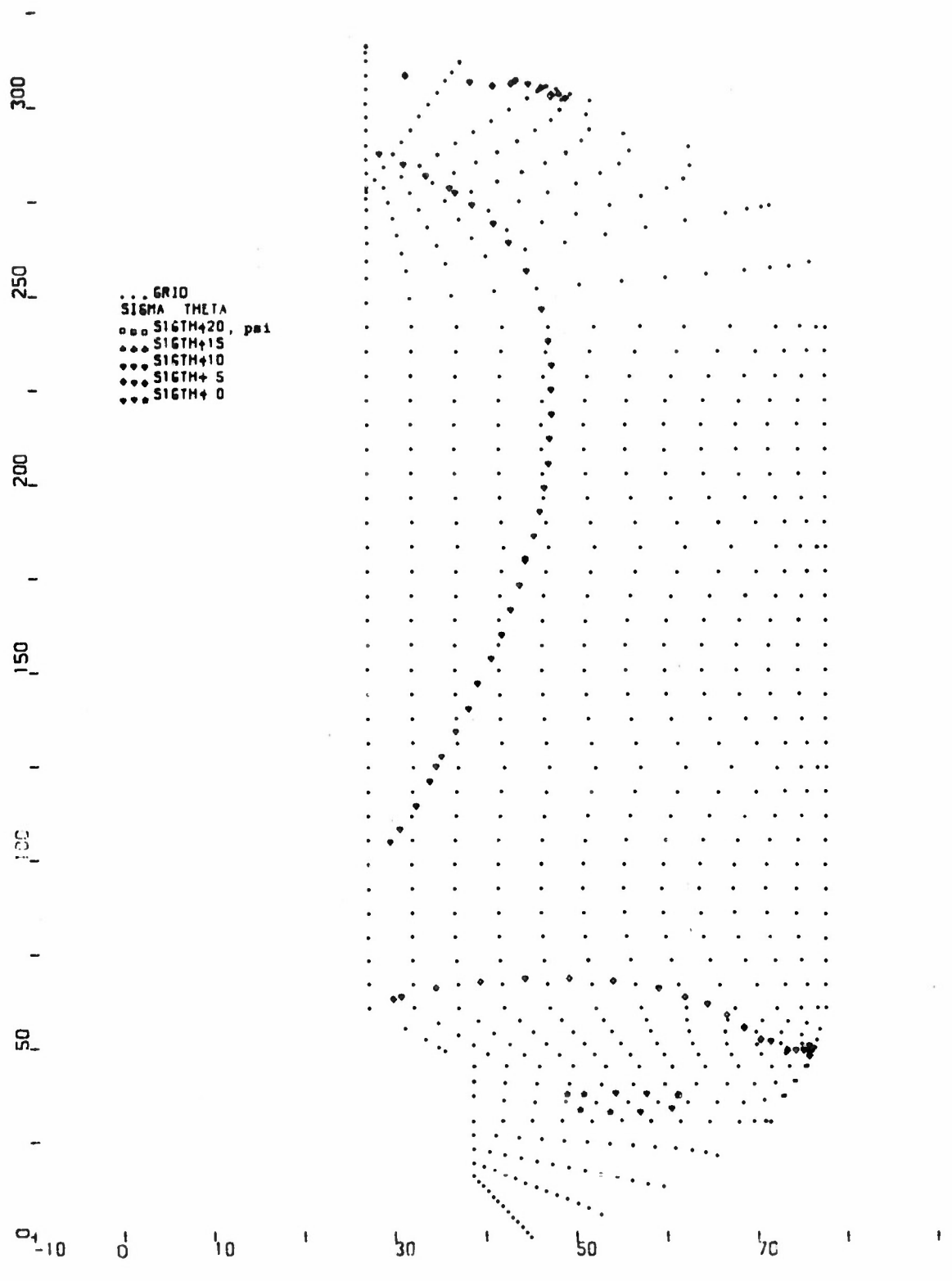

Figure 5-15. 156-9 Cure-Thermal Shrinkage Stress Analysis
Tangential (Principal) Stress (Sigma Theta)

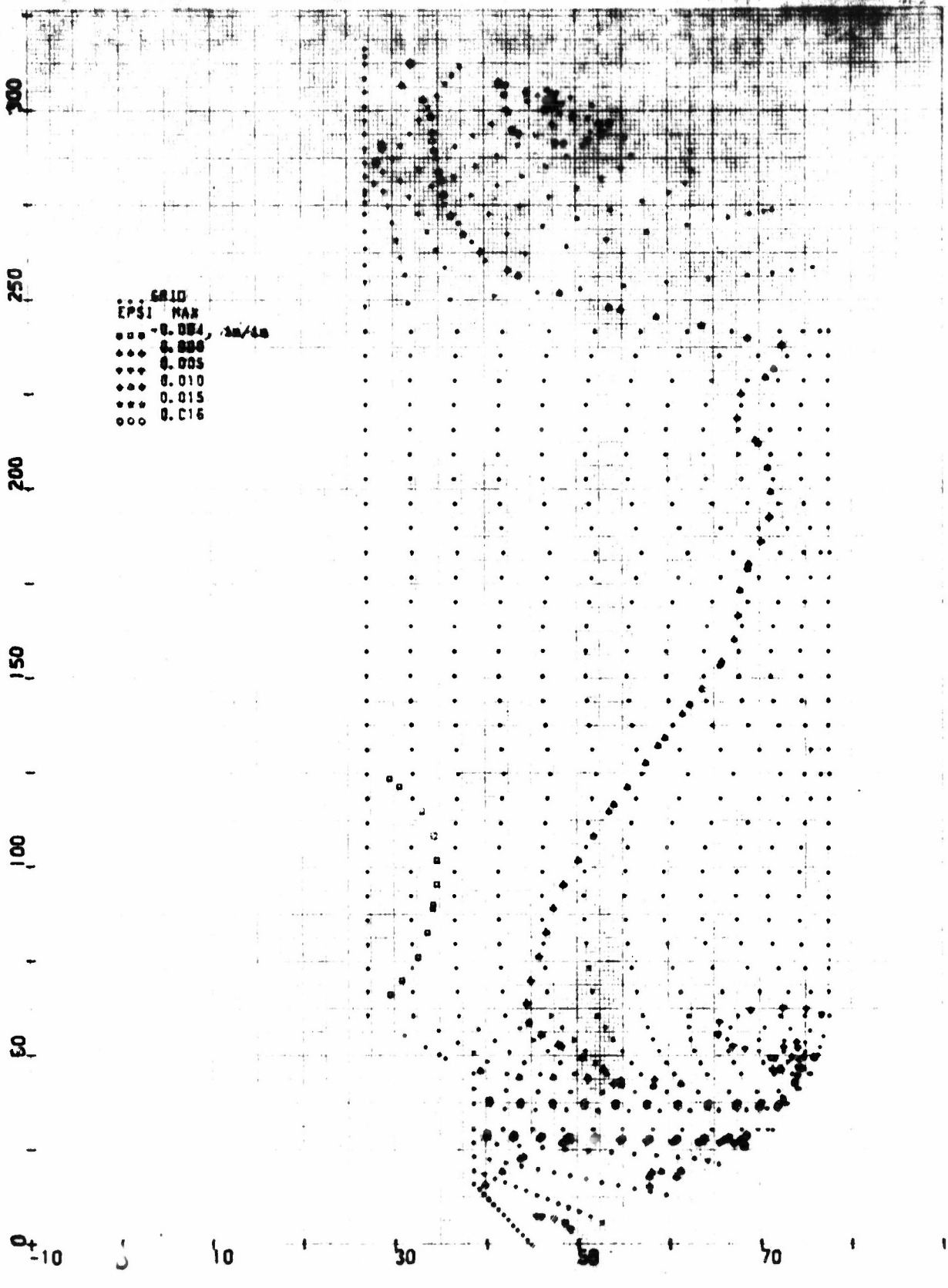

Figure 5-16. 156-9 Ignition Pressure 682 psi Stress Analysis
Maximum Principal Strain (EPSI Max)

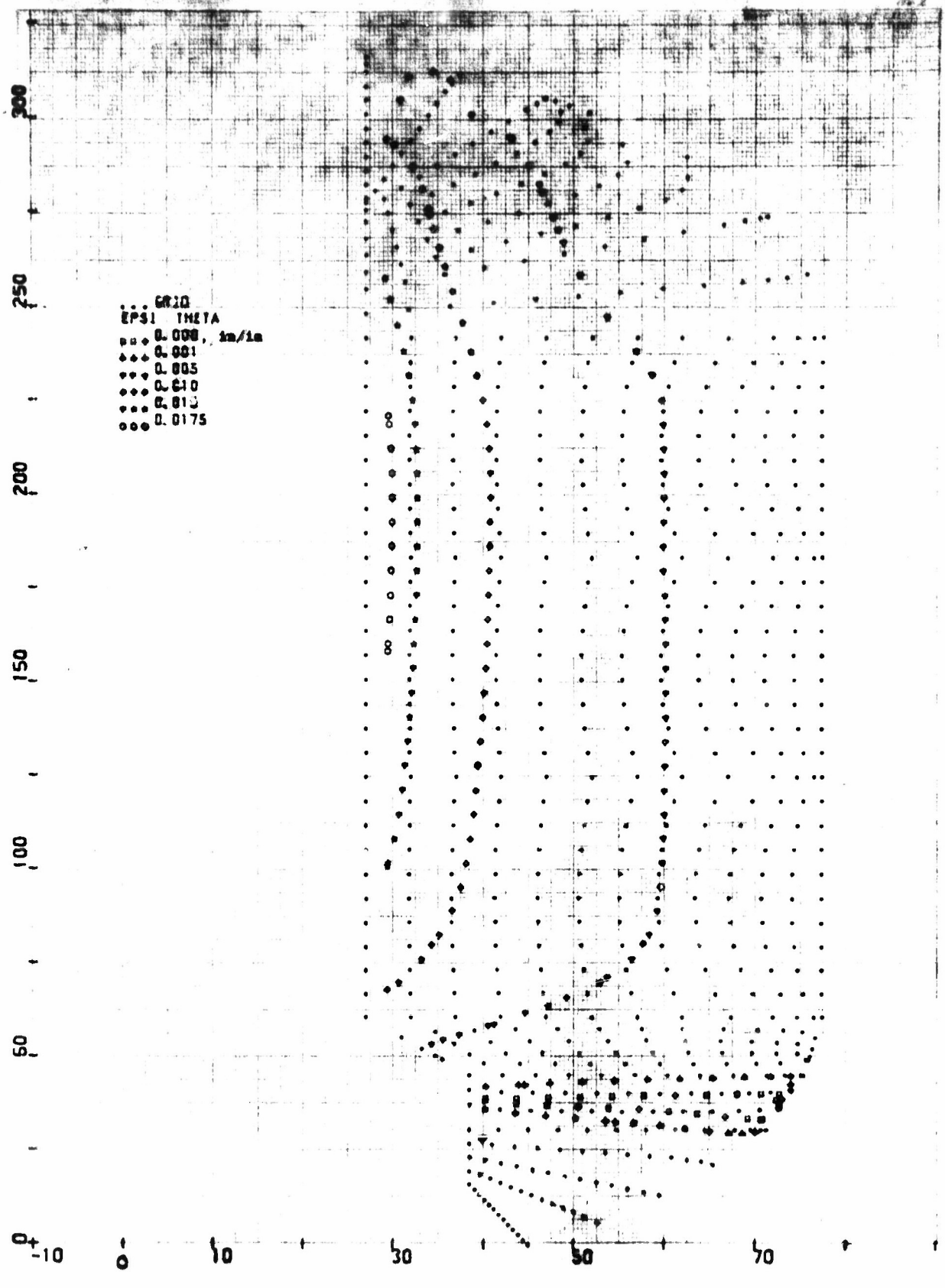

Figure 5-17. 156-9 Ignition Pressure 682 psi Stress Analysis
Tangential (Principal) Strain (EPSI Theta)

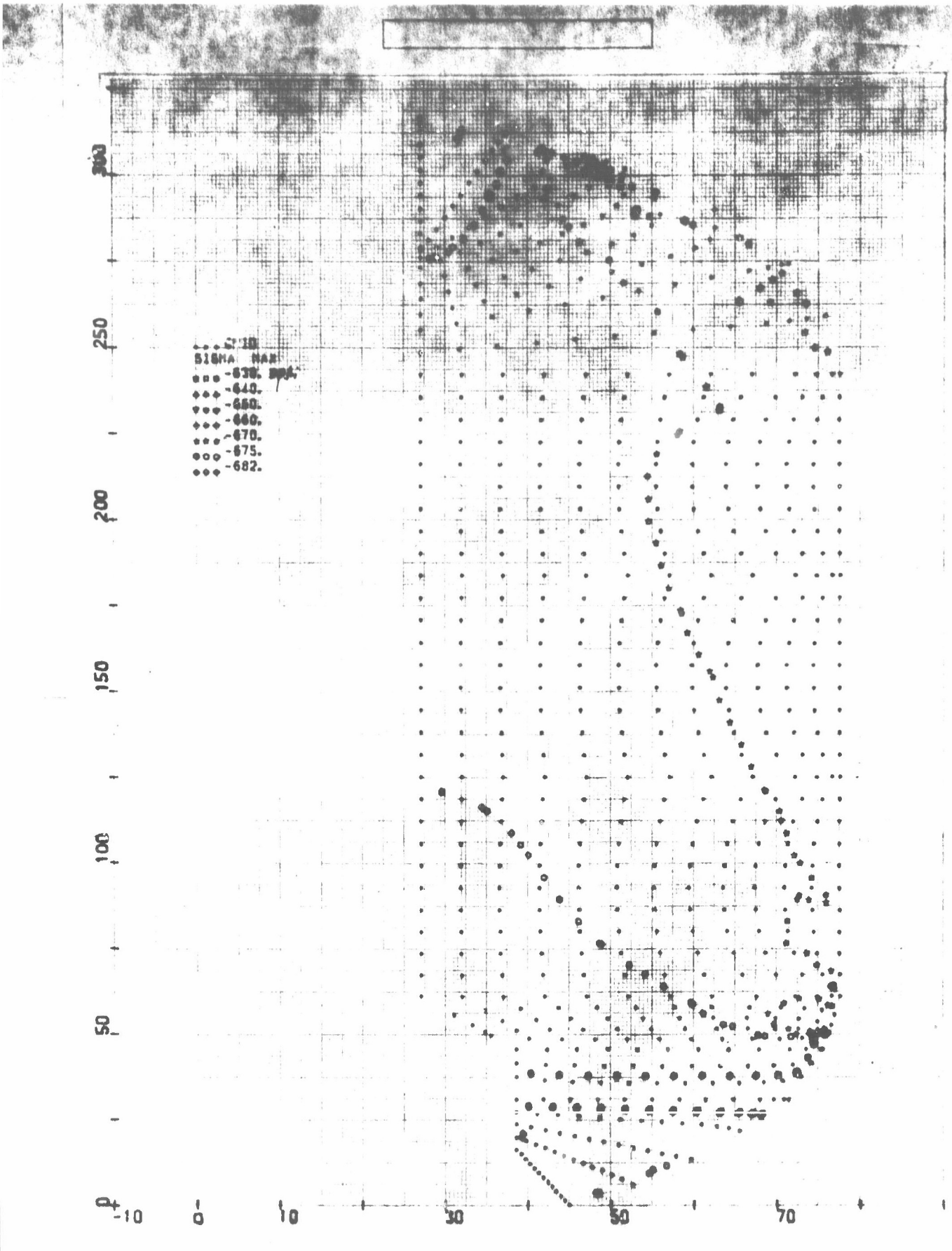

Figure 5-18. 156-9 Ignition Pressure 682 psi Stress Analysis
Maximum Principal Stress (Sigma Max)

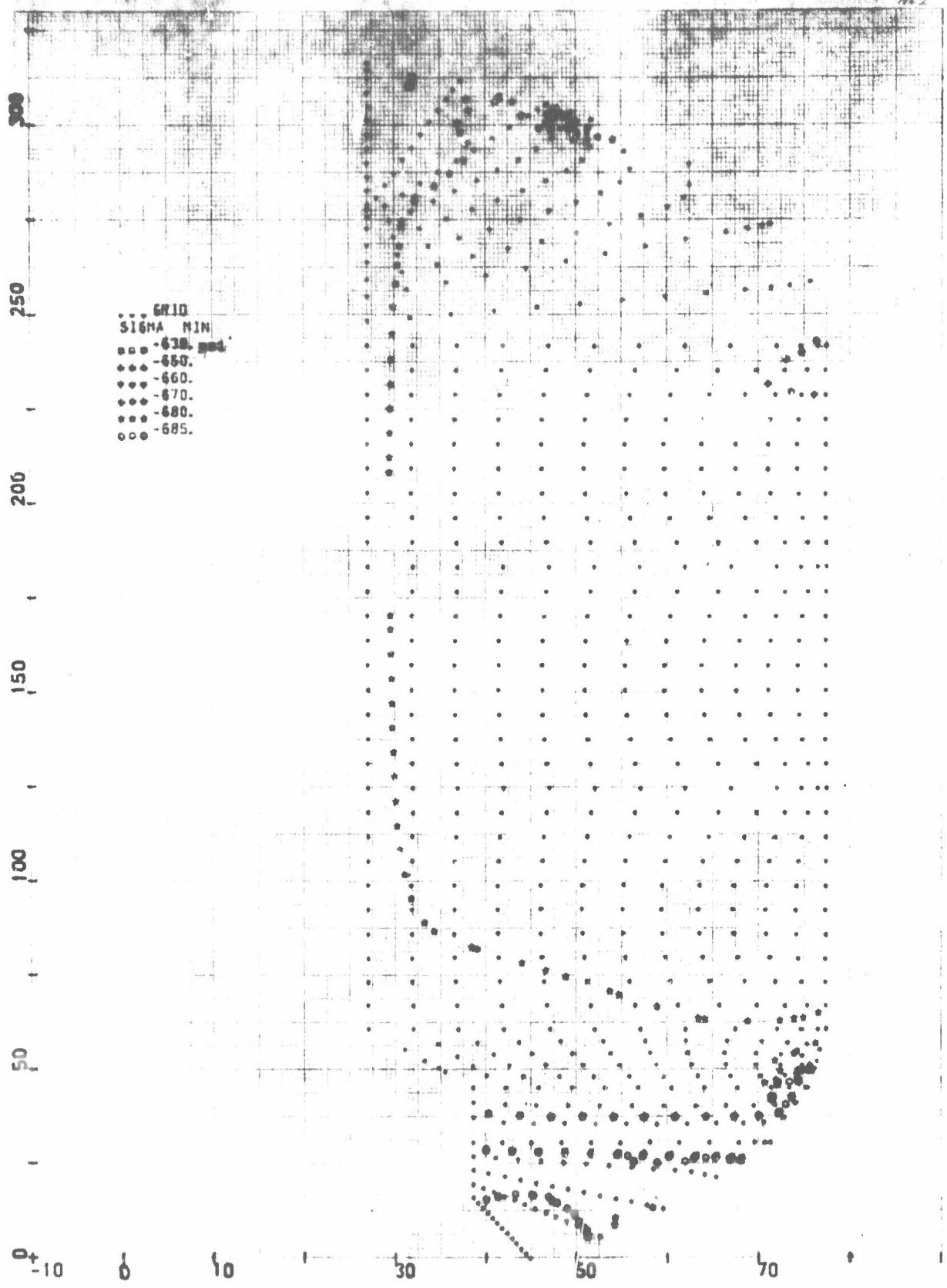

Figure 5-19. 156-9 Ignition Pressure 682 psi Stress Analysis
Minimum Principal Stress (Sigma Min)

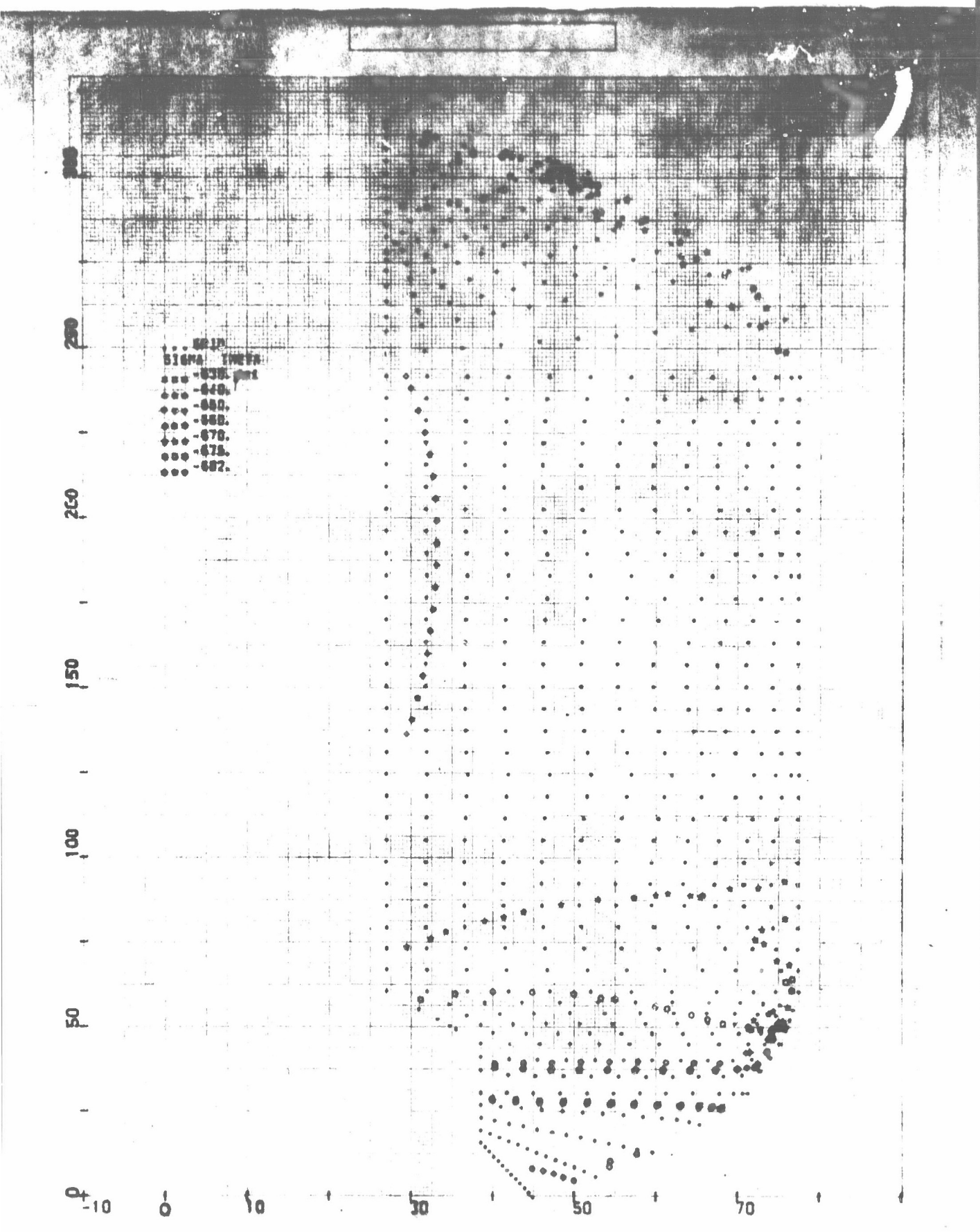

Figure 5-20. 156-4 Ignition Pressure 682 psi Stress Analysis
Tangential (Principal) Stress (Sigma Theta)

The dilatational and distortional failure boundaries, including the maximum induced grain stress-strain points, are shown in Figures 5-21 and 5-22. Figure 5-22 is the accumulation of cure and thermal shrinkage and pressure effects. These figures indicate that the induced stresses and strains never approach the respective boundaries. Table 5-3 further illustrates the inherent structural integrity of the 156-9 grain. The worst stress-strain points, the propellant capability, and the resulting margins of safety are shown. Margin of safety is defined as propellant capability divided by induced load less 1.0. The bases for determining safety margins may be stated as follows.

1. The path to the failure boundary will follow a constant stress line (hence, a maximum principal strain limit).
2. The path to the failure boundary will follow a constant strain line (hence, a maximum principal stress limit).
3. The failure limit lies at a point on the boundary where a constant percentage increase of both stress and strain has been used.

The latter statement attempts to establish a unified margin of safety for the stress-strain failure criteria. Since it results in generally lower margins than the other two, a limited condition is assumed. Prior to calculating the margin of safety (Table 5-3) the stress-strain capabilities are reduced by 21.8 percent and 17.6 percent, respectively. Statistically these have been determined to be the three sigma limits on the individual parameter batch to batch variations. Insufficient data precludes preparation of the three sigma limits on the failure boundary. The limited data examined to date indicate that on a unified basis the stress-strain boundary deviations will be smaller than either of those used.

d. Conclusions--From the foregoing, the 156-9 obviously has no grain structural behavior problems. With a least margin of safety as shown in Table 5-3, the grain is predicted to be extremely reliable.

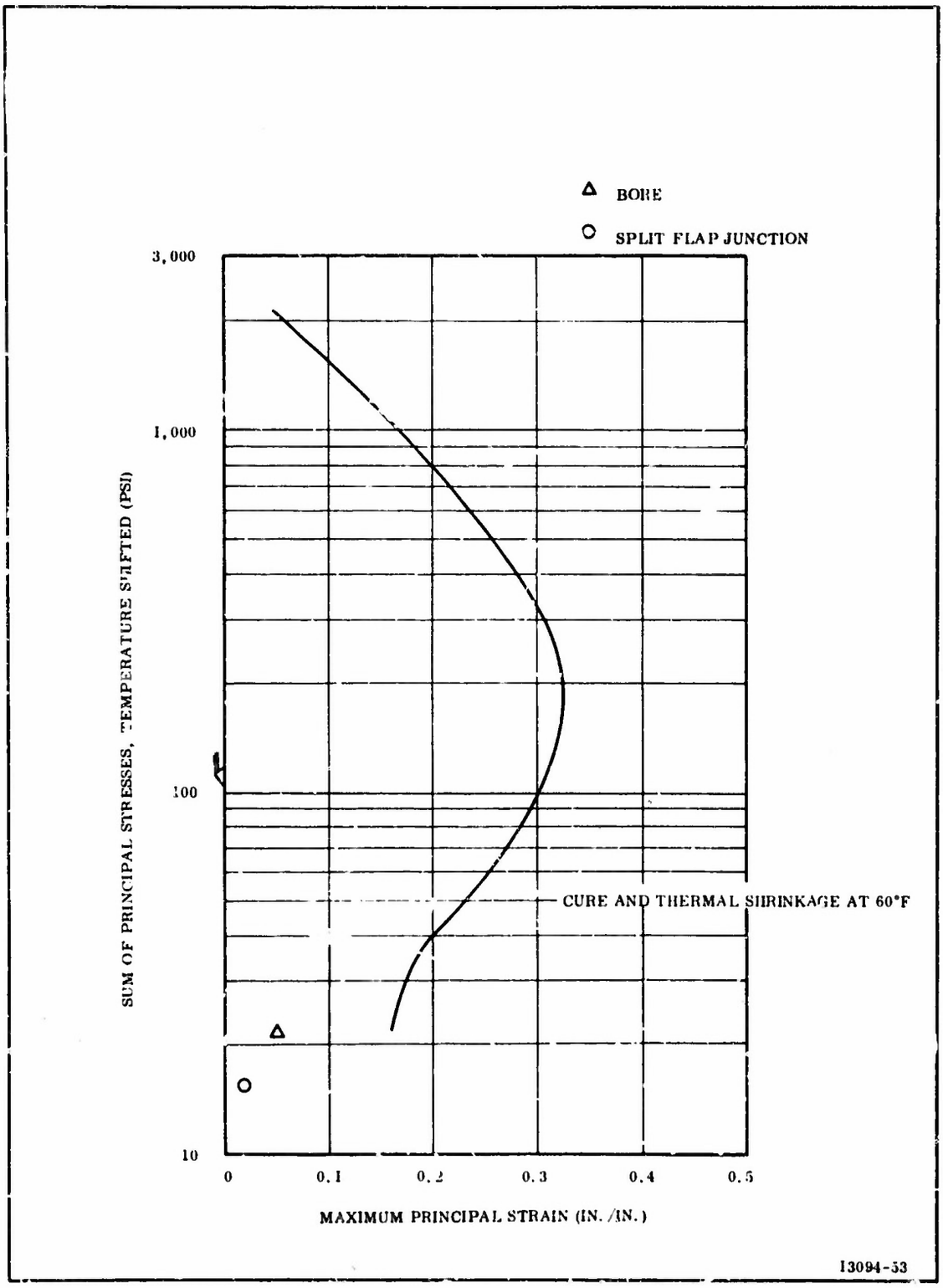

Figure 5-21. Dilatational Failure Boundary

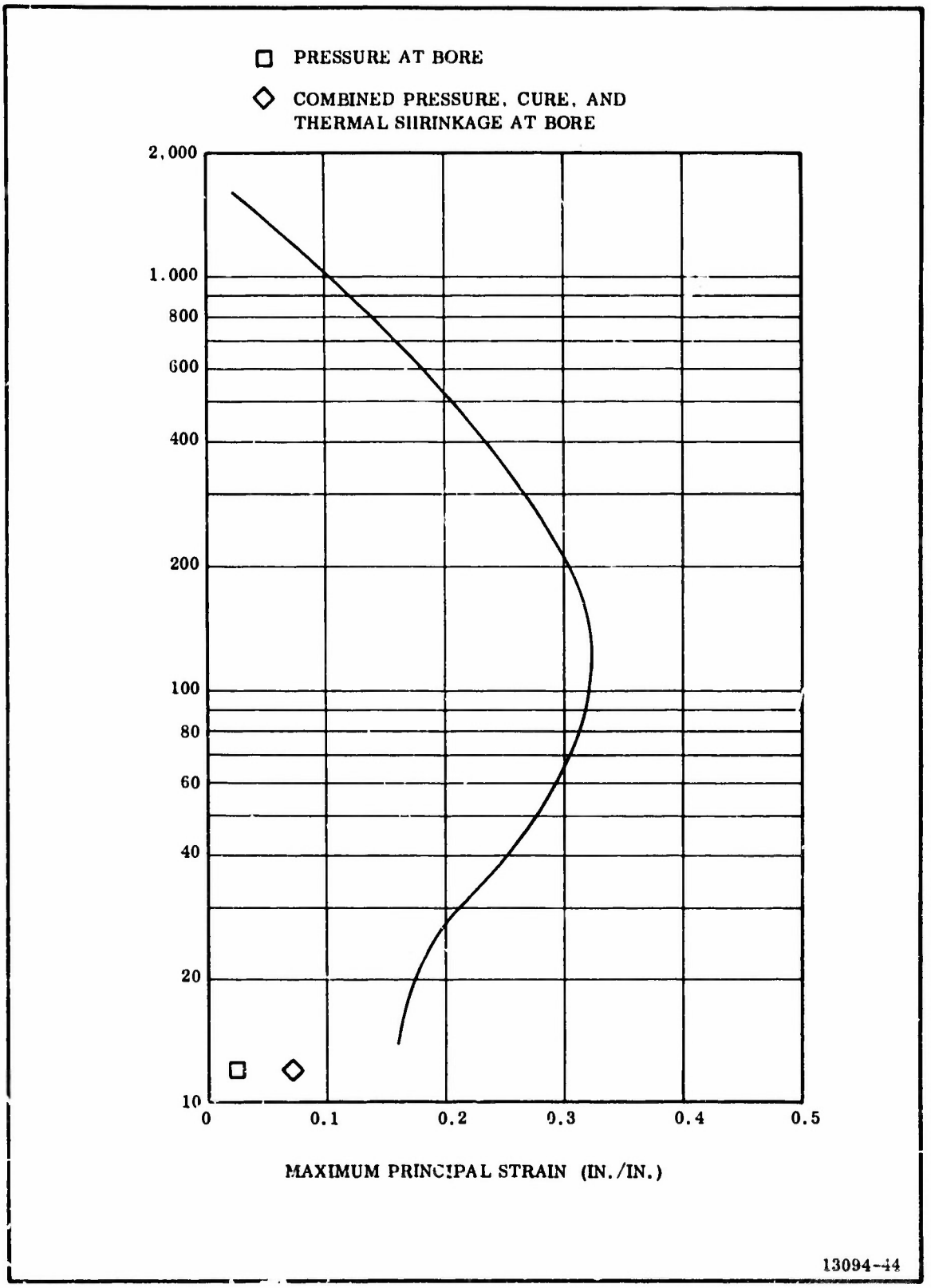

Figure 5-22. Distortional Failure Boundary

TABLE 5-3

WORST STRESS-STRAIN CONDITIONS AND FAILURE CRITERIA COMPARISON

Load	Location	Sum of Maximum Principal or Deviatoric Stress (psi)	Maximum Principal Strain (in./in.)	Propellant Capability			Margin of Safety*		
				1	2	3	1	2	3
1-Cure and Thermal Shrinkage to 60°F	Split Flap Case Junction	15.5	0.019	--	--	--	--	--	--
	Bore	22.0	0.050	0.16	2,100	--	1.72	73.0	--
2-Pressure, 682 psi	Split Flap Case Junction	8	0.012	--	--	--	--	--	--
	Bore	12	0.021	0.16	1,700	--	5.48	109.0	--
3-Combined Shrinkage and Pressure	Split Flap Case Junction	8	0.031	--	--	--	--	--	--
		12	0.07	0.16	1,200	0.175 30	0.87	77.0	1.00

*Propellant capability has been reduced 17.6 and 21.8 percent for strain and stress respectively before calculating margins. 1 is strain, 2 is stress, and 3 is combined stress-strain.

3. WEIGHT ANALYSIS

The 156-9 propellant grain is calculated to weigh 277,775 pounds. Ballistic performance will be repredicted when the actual propellant weight is determined.

SECTION VI

IGNITION SYSTEM DESIGN

A PYROGEN type head end ignition system loaded with TP-H1016 propellant (Figure 6-1) will be used to ignite the 156-9 motor.

Selection of the head end PYROGEN ignition system was based on proven performance and the availability of developed components which can be used to fabricate a reliable system for the proposed motor. Existing tooling from the MINUTEMAN, MACE, AF 156-1, and AF 156-8 motor programs required to fabricate this ignition system will be used to the greatest extent possible.

A. IGNITION SYSTEM DESCRIPTION

This ignition system will be identical to the AF 156-8 motor ignition system except for the method of adapting the ignition system to the motor (Figures 6-1 and 6-2).

The ignition system is composed of five main subassemblies.

1. Safety and Arming device.
2. Initiating system.
3. Booster PYROGEN igniter.
4. Adapter, booster igniter to motor.
5. Adapter, ignition system to motor.

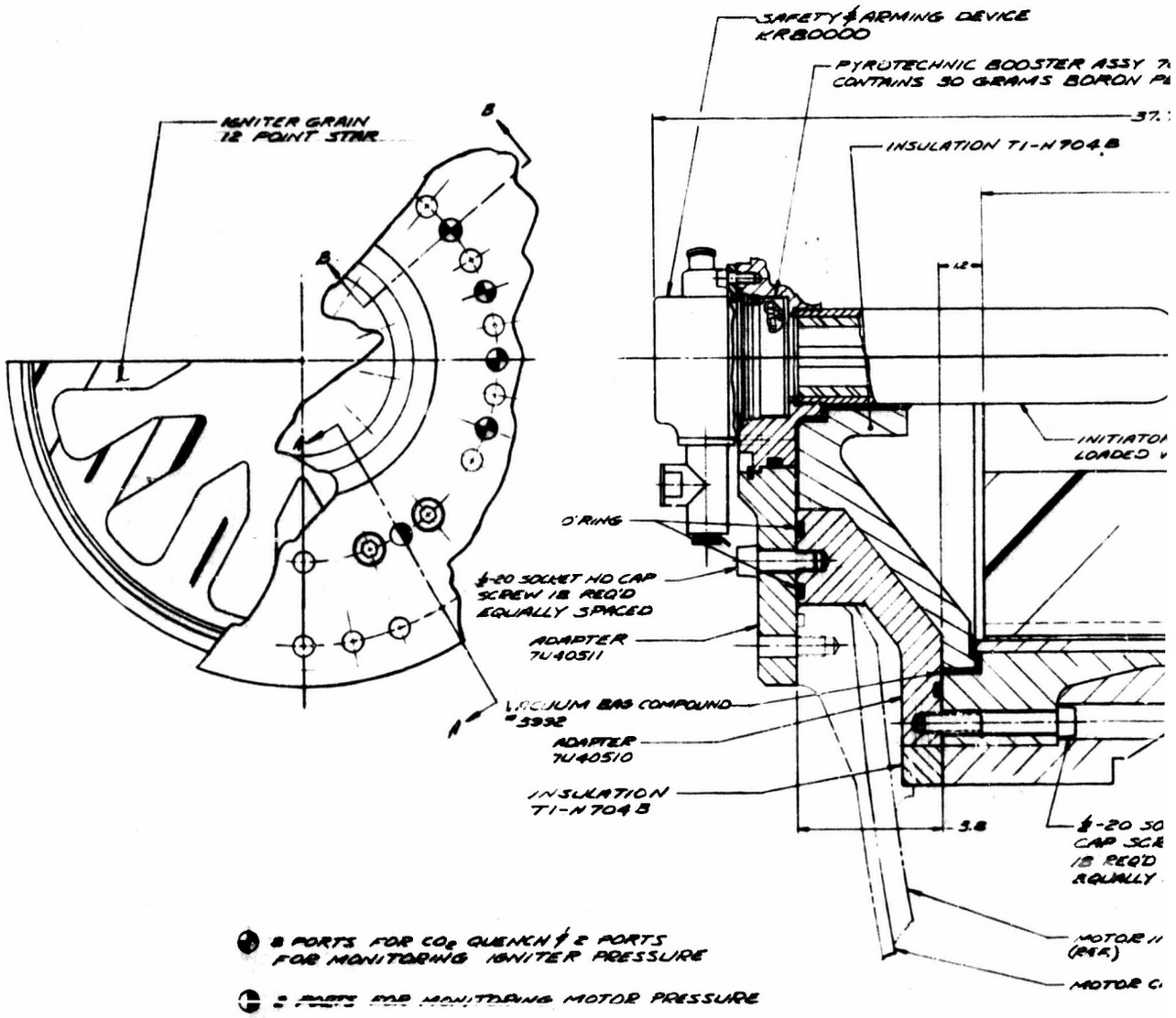
SAFETY & ARMING DEVICE KR80000
PYROTECHNIC BOOSTER ASSY 7
CONTAINS 30 GRAMS BORON P
IGNITER GRAIN 12 POINT STAR
INSULATION T1-N704B
O'RING
ADAPTER 7U40511
ADAPTER 7U40510
INSULATION T1-N704B
MOTOR
(REF.)
B PORTS FOR CO2 QUENCH & 2 PORTS FOR MONITORING IGNITER PRESSURE
PORTS FOR MONITORING MOTOR PRESSURE

DEVICE

IC BOOSTER ASSY 7U37347
0 GRAMS BORON PELLETS

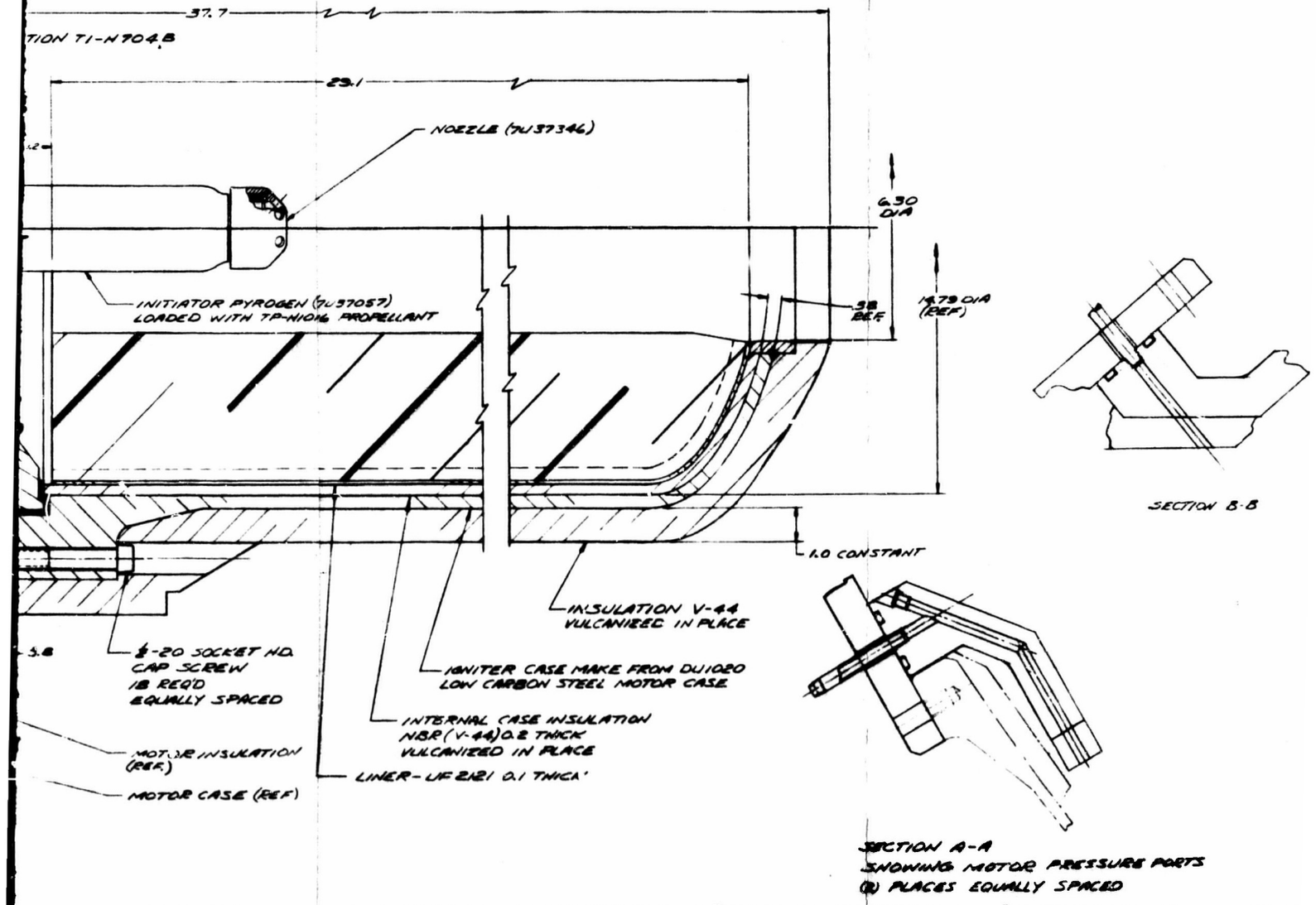

SECTION B-B

SECTION A-A
SHOWING MOTOR PRESSURE PORTS
(2) PLACES EQUALLY SPACED

Figu

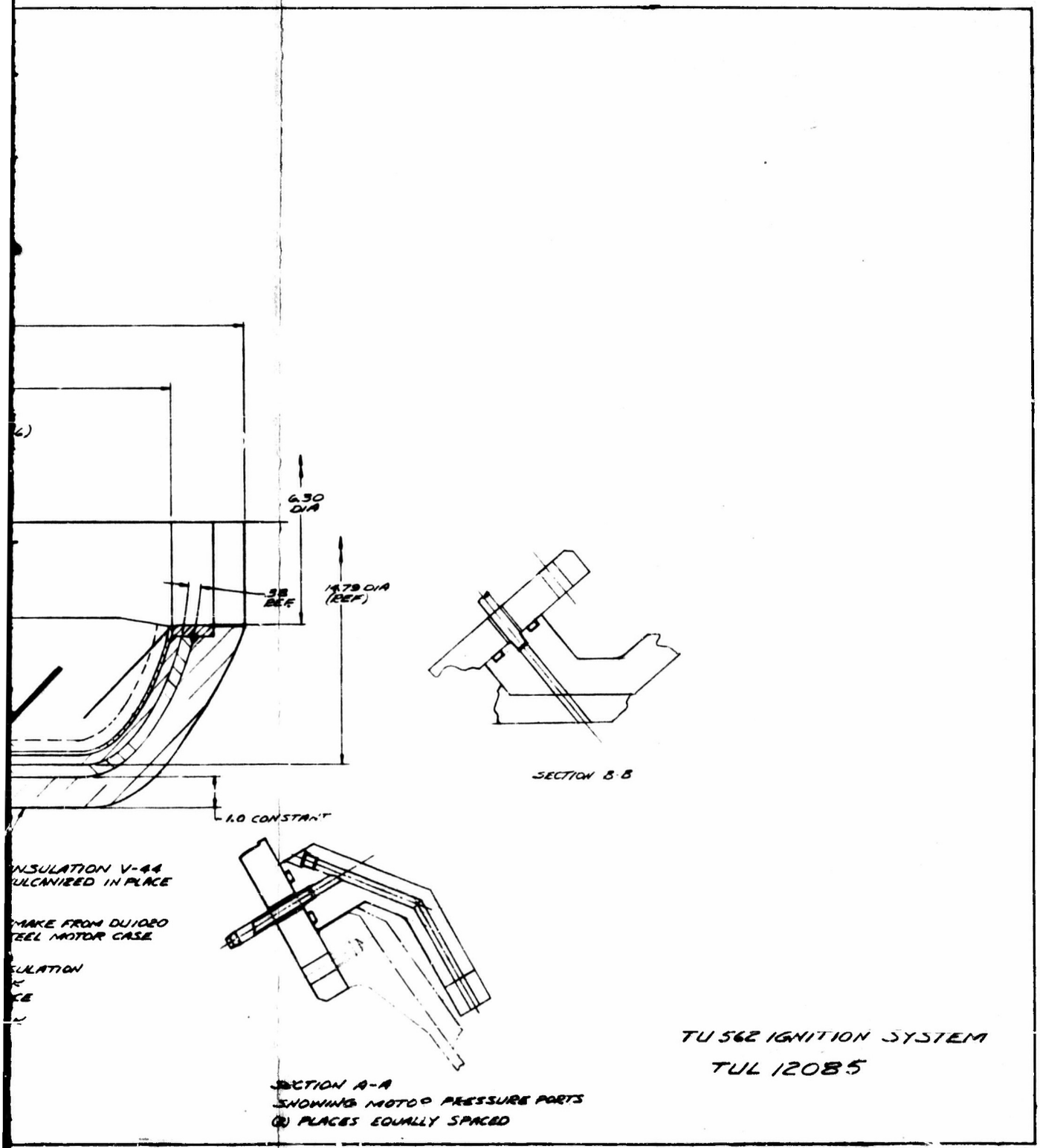

Figure 6-1. 156-9 Ignition System

3

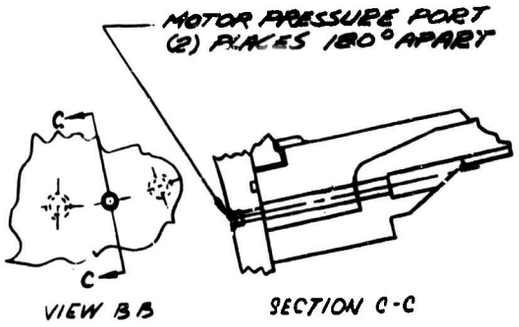

VIEW B-B

SECTION C-C

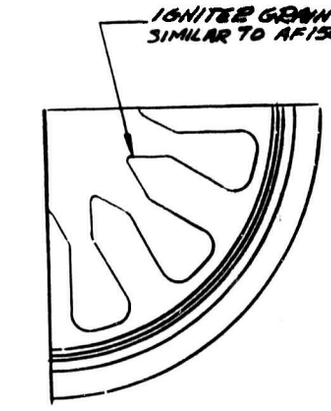

SECTION A-A

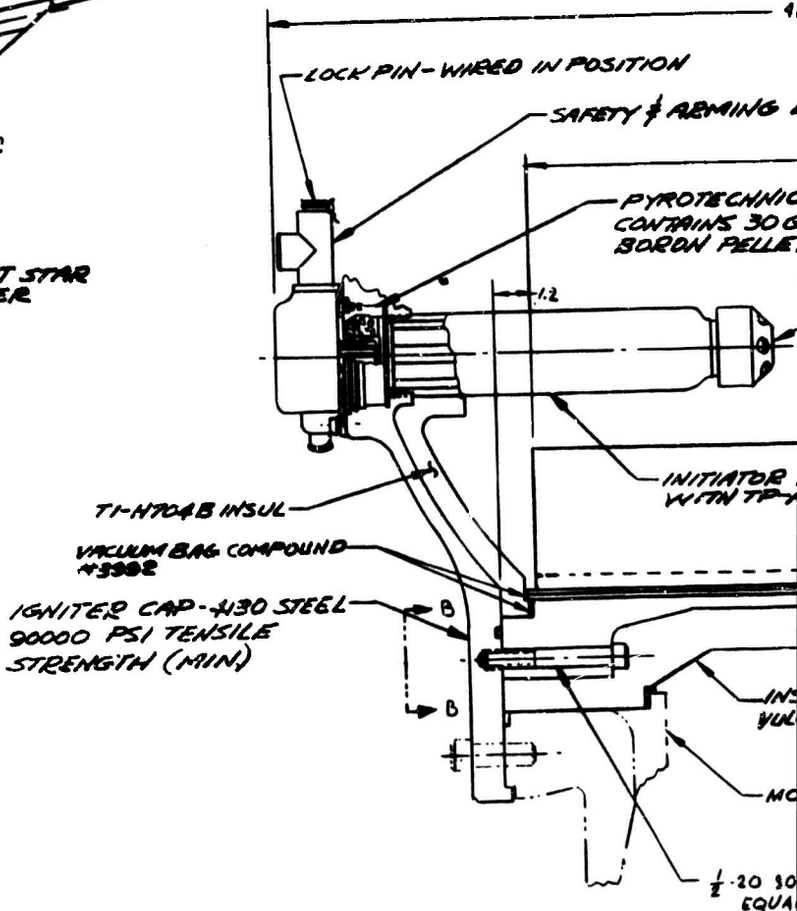

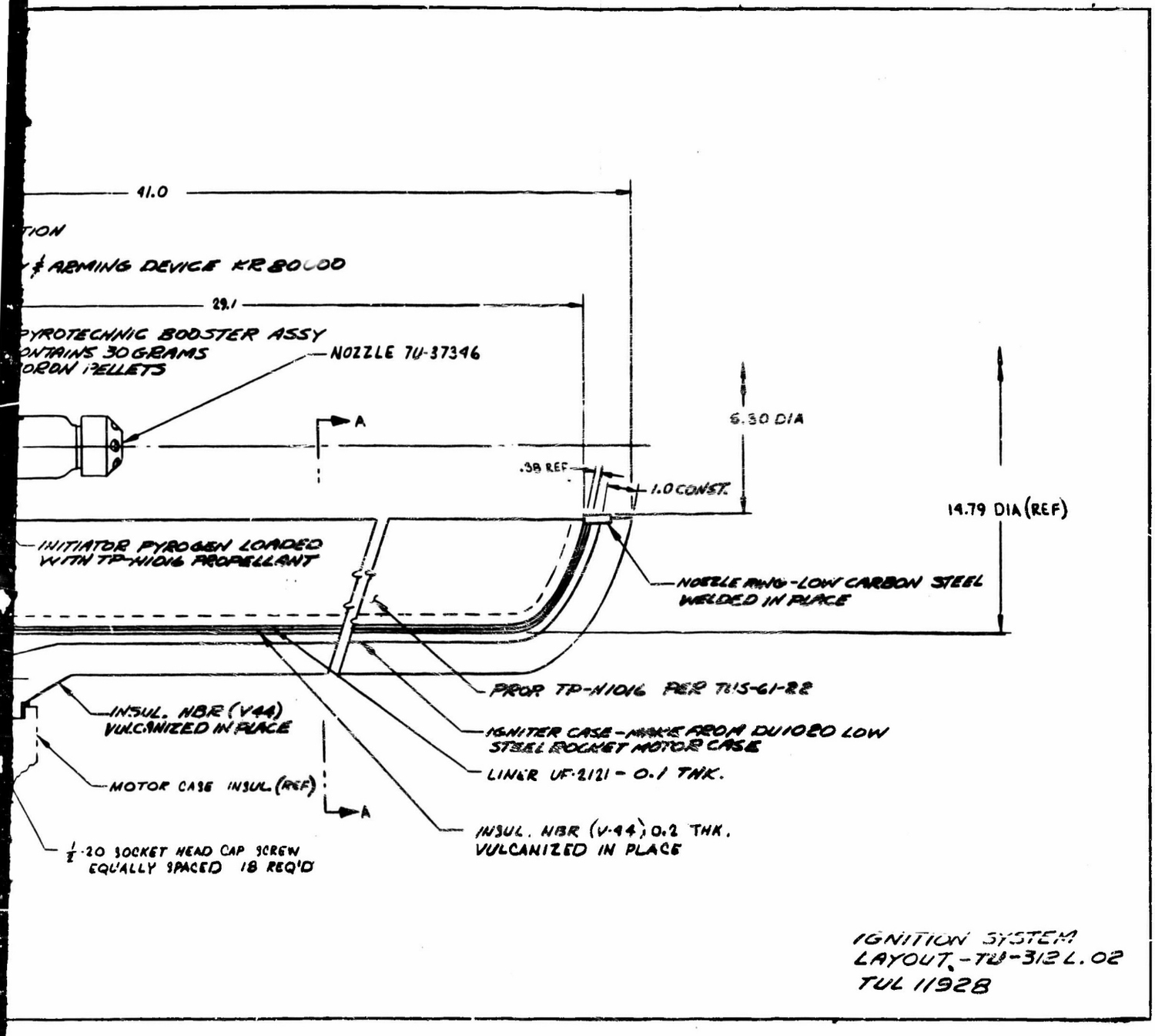

Figure 6-2. 156-8 Ignition System

1. SAFETY AND ARMING (S & A) DEVICE

The S & A device selected for the 156-9 ignition system is currently being used on the Stage I, II, and III MINUTEMAN motors. Thiokol developed this device for the Stage I motor ignition system and later it was standardized for all three stages. The S & A has been qualified to the latest Air Force requirements and over 2,500 have been produced for various development, qualification, flight test, and production programs.

Upon initiation, two ES-003 electrical squibs start the ignition train for the motor ignition sequence. In the safe position, the squibs are electrically shorted and mechanically isolated from the ignition train. The S & A device has a visual indicator, mechanical lockpin, separate connectors for the control and firing circuits, hermetic seals, and other safety features which minimize the possibility of inadvertent firing. A lockwire secures the lockpin in place to insure assembly of the S & A device to the PYROGEN igniter in the unarmed (safe) condition. The lockwire and lockpin must be removed manually before the device can be armed electrically. This feature satisfies the requirement that the S & A device cannot be installed in the motor while in the armed condition. This lockwire-lockpin arrangement was used on the S & A of the AF 156-7 rocket motor under Contract AF 04(695)-773, which had an identical safety requirement.

2. INITIATING SYSTEM

The initiating system consists of an adapter, pyrotechnic booster assembly and an initiating PYROGEN igniter.

a. Adapter--The initiating system adapter, which was made from low carbon steel, adapts the initiating PYROGEN igniter, pyrotechnic booster, and the S & A device into one integral assembly. This assembly is installed in the motor adapter and held in place with a beveled retaining ring. This method of installation has been

used successfully on the TU-500, a Thiokol sponsored motor static test.

b. Pyrotechnic Booster--The pyrotechnic booster provides the ignition train between the S & A device and the initiating PYROGEN igniter. It contains 30 gm of 2A boron-potassium nitrate pellets, and the container is identical to the design used on the Stage I MINUTEMAN and AF 156-1 motors.

c. PYROGEN Igniter--The initiating PYROGEN igniter for the 156-9 motor ignites the booster PYROGEN igniter. It is the same design as used to ignite the booster PYROGEN igniter for the AF 156-1 motor which was static fired at the Wasatch Division (Figure 6-3). Adequate ignition of the booster igniter grain configuration to be used in this system has been demonstrated using the multiple port nozzle design.

Loaded with TP-H1016 propellant (Stage I MINUTEMAN igniter propellant), the initiating PYROGEN igniter produces a mass discharge rate for booster igniter ignition of 3.5 lb/sec for approximately 0.3 second. The case length is 11.5 inches. The loaded case for this igniter was successfully tested five times before being used in the ignition system for the AF 156-1 motor. The case and grain designs were originally developed for the MACE ignition system.

3. BOOSTER PYROGEN

The booster PYROGEN igniter assembly consists of a modified rocket motor case, NBR external and internal insulation, UF-2121 liner, and TP-H1016 propellant. The grain is cast in the same 12 point star configuration used in the booster PYROGEN for the AF 156-1 motor. The igniter will operate at a pressure of 820 psia and provide a mass discharge rate of 156 lb/sec for approximately 0.6 sec after which pressure and mass flow drop off for a total burning time of approximately 1.1 seconds (Figure 6-4).

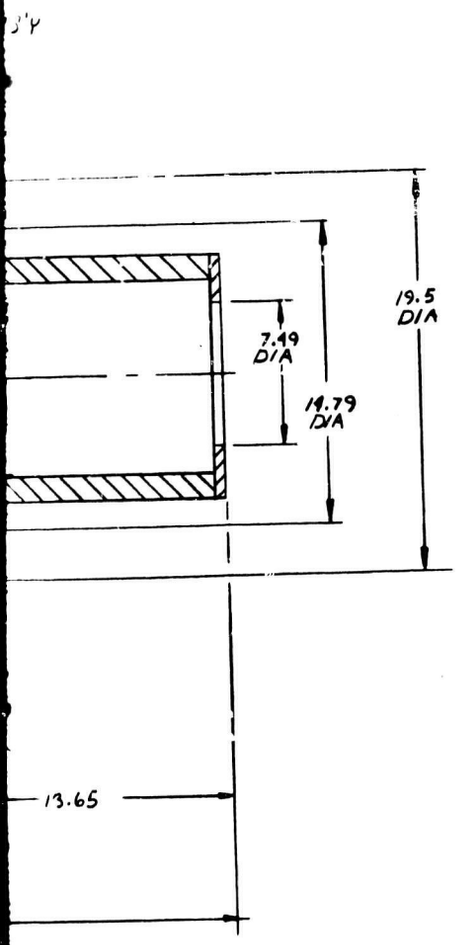

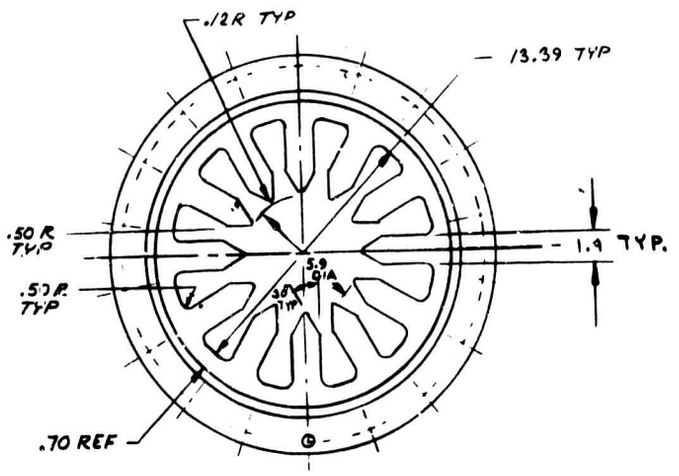

SECTION A-A

Figure 6-3. 156-1 Ignition System

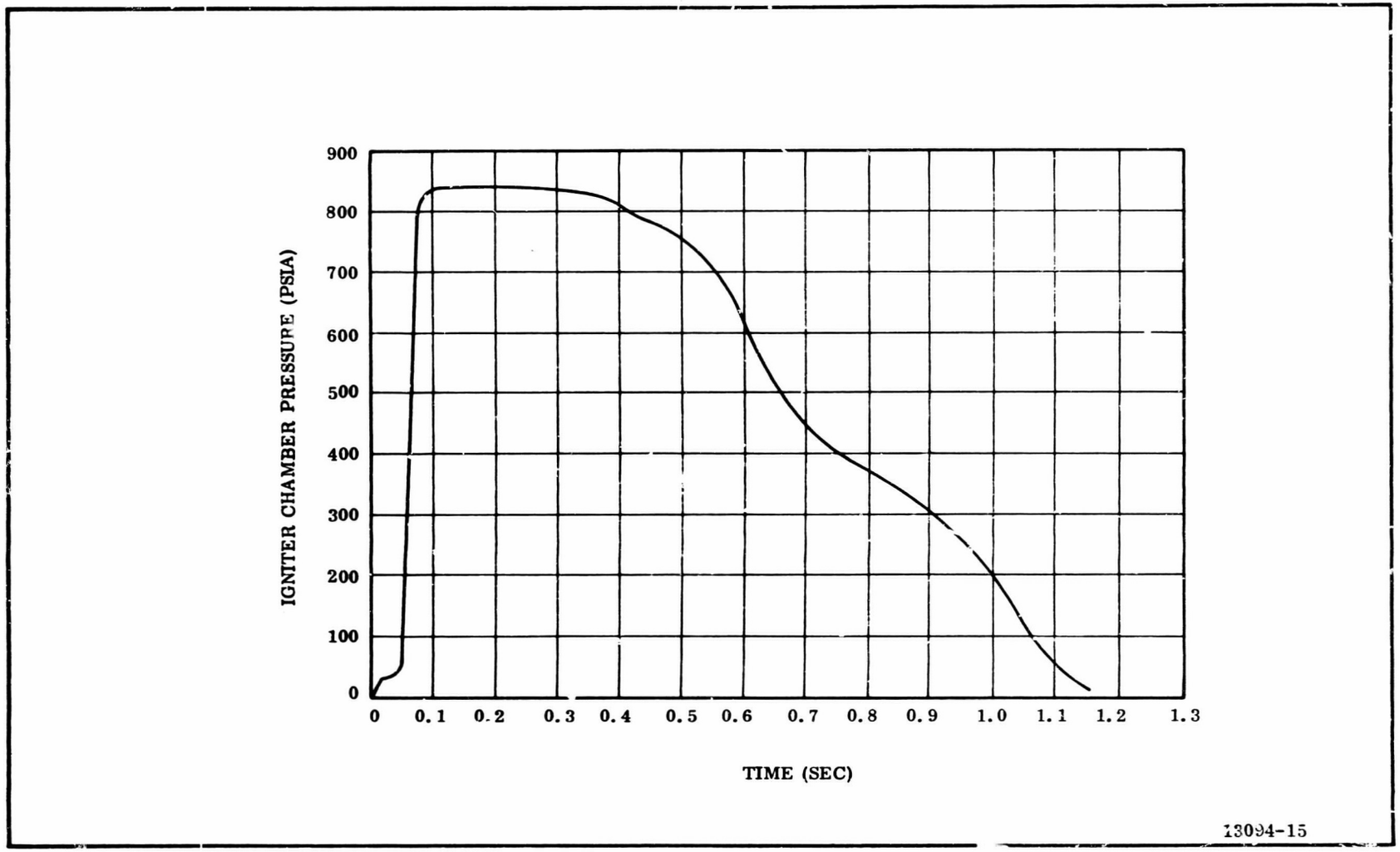

Figure 6-4. 156-9 Igniter Predicted Performance

At 820 psi, the booster PYROGEN igniter case will have a structural safety factor of 0.67 minute. The low carbon steel igniter case is 30 in. long and 15.5 in. in diameter. It will be fabricated by modifying an existing motor case by removing skirt and handling lugs. The head end dome will be modified by opening the port and welding in a low carbon steel ring to serve as the igniter nozzle. The selection of a steel case for the 156-9 igniter was based upon economic considerations rather than weight performance.

The steel case must be insulated internally and externally to prevent melting during the motor firing. Thermodynamic calculations indicate that 0.030 in. of insulation will prevent melting from the inside; however, to protect the bond of the external case insulation to the steel case, additional internal insulation is necessary. The proposed design will use 0.20 in. of NBR layup, vulcanized in place, and 0.10 in. of UF-2121 liner. This thickness controls the propellant web thickness to provide the required burning time and provide more than enough insulation on the internal surfaces to prevent bond failure of the external insulation.

4. ADAPTERS

a. Booster Igniter to Motor--The booster igniter adapter facilitates installation of the igniter loaded case assembly to the motor igniter adapter. Made from low carbon steel, this adapter permits installation of the booster igniter from the aft end of motor, down the propellant port, and through the motor polar boss where it interfaces with the motor ignition system adapter. The booster igniter adapter has ports that mate with the motor adapter and are used to monitor igniter pressure, motor pressure and the carbon dioxide quench system.

b. Ignition System to Motor--The adapter connecting the ignition system to the motor is made from low carbon steel. The booster assembly is attached to this motor adapter. The initiating system is attached to the motor adapter with a beveled retaining ring.

B. IGNITER BALLISTIC DESIGN AND MOTOR IGNITION TRANSIENT

The empirical PYROGEN igniter coefficient is the primary parameter used for determining the required size of a PYROGEN igniter. When the ratio of igniter mass flow rate (lb/sec) divided by the motor throat area (sq in.) is in the range of 0.15 to 0.25, satisfactory ignition will result. Thus, an approximate PYROGEN igniter motor mass flow rate can be established for a motor having specified nozzle dimensions. Usually, the values selected for the PYROGEN igniter coefficient have been in the range of 0.17 to 0.20. The proposed igniter has a mass flow rate of 158 lb/sec, which results in a coefficient of 0.168.

Motor ignition occurs sequentially through the action of a pyrotechnic charge and two PYROGEN igniters. The S & A device is electrically armed and two electrical squibs are initiated; the flame and pressure created by the squibs ruptures two diaphragms and ignites the booster assembly; the flame from the booster charge ignites the initiating PYROGEN igniter; and the initiating PYROGEN igniter exhaust gases ignite the booster PYROGEN igniter.

The ignition transient for the motor is made up of four relatively distinct time periods identified as follows.

1. Igniter response time.
2. Time to achieve motor pressure-igniter output equilibrium prior to motor propellant ignition.
3. Lag time or time between equilibrium pressure achievement and first ignition of motor propellant.
4. Flame spreading time or time from end of lag time until all surfaces of the motor grain have been ignited.

Thiokol has predicted the ignition transients expected for the 156-9 motor. The prediction includes an equilibrium calculation which begins at the end of lag time and ends upon achievement of motor equilibrium pressure. The prediction is based on the ballistic and physical characteristics of the 156-9 motor grain, the ignition parameter of the igniter, estimated time of first ignition, and flame spreading rates over all propellant surfaces in the motor. Motor pressure, thrust, mass flow rate, and surface area ignited, plus igniter pressure and mass flow rate are computed as functions of time.

The predicted chamber pressure transient for the 156-9 motor is illustrated in Figure 6-5. This prediction is based on the ignition system performance demonstrated by the AF 156-1 motor. The igniter pressure superimposed upon the motor pressure at equilibrium will not produce a pressure in excess of the motor MEOP. The maximum predicted ignition pressure of the motor is 715 psi.

The response time associated with igniting the AF 156-1 initiating PYROGEN was 0.038 second. The AF 156-1 booster PYROGEN took an additional 0.044 sec to achieve 75 percent of its first level operating pressure.

A time lapse of 0.080 sec between time zero and the first pressure rise in the main motor (igniter response time) resulted. Comparing the sizes of the AF 156-1 booster igniter and 156-9 PYROGEN igniter results predict igniter (156-9) ignition delay of 0.073 second.

The pressure produced by the igniter in the motor is approximated by the following formula.

$$P_c = \frac{M_i c^*}{A_t g}$$

where:

P_c = Equilibrium pressure (psia)

M_i = Igniter mass flow rate (lb/sec)

c^* = Igniter characteristic velocity (ft/sec)

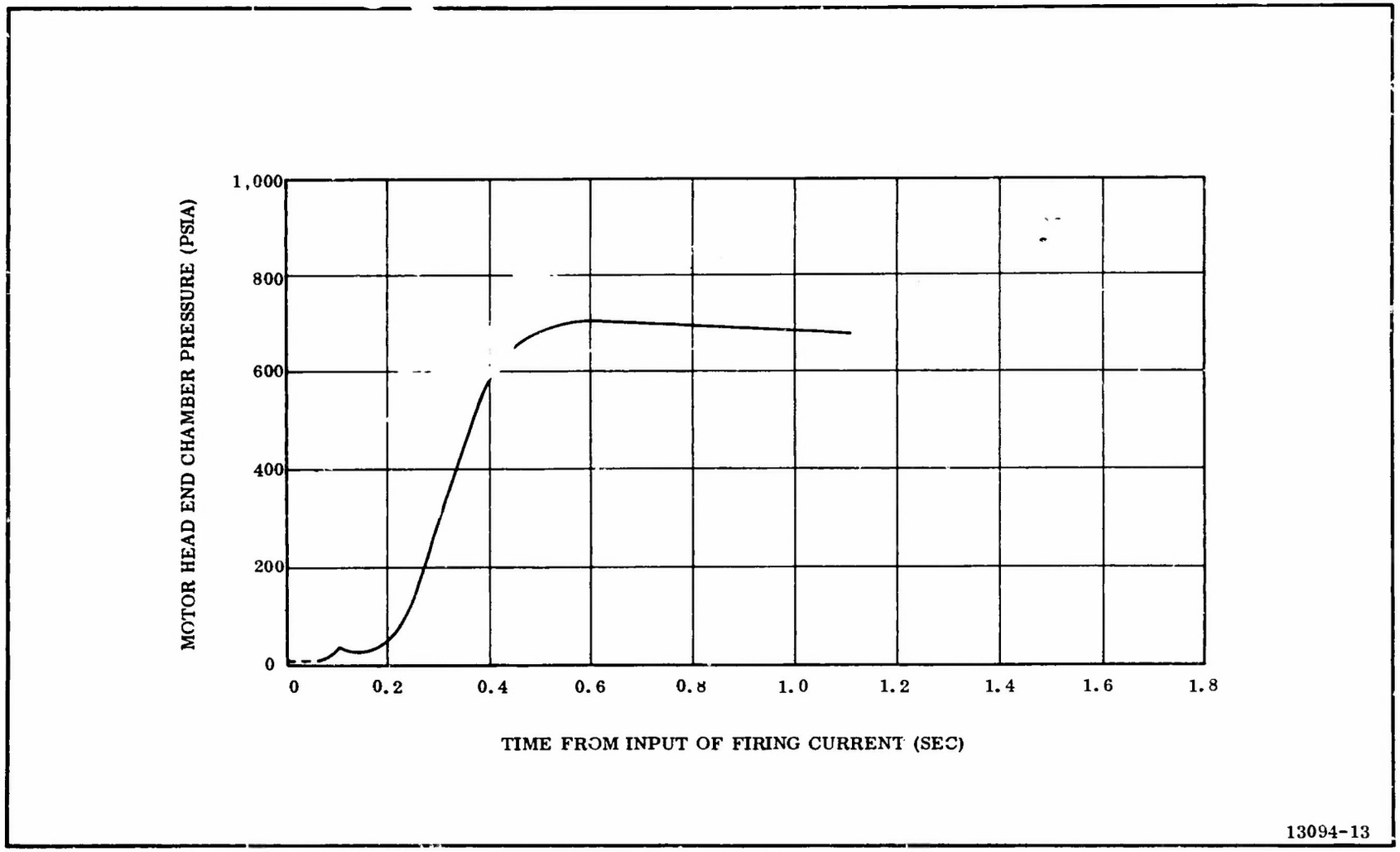

Figure 6-5. Predicted Pressure vs Time During Ignition Transient (Utah Conditions)

A_t = Motor throat area (sq in.).

g = Gravitational constant (ft/sq sec).

This equation represents an ideal condition and would logically predict higher than actual pressures. The actual pressures achieved during initial pressurization, however, are approximately 20 percent higher than predicted. The additional pressure is probably due to compression of the air in the motor by the igniter output before the column of air begins to flow through the nozzle. Including the 20 percent historical increase, the predicted motor chamber pressure produced by the igniter is 34.4 psia.

The time required to achieve equilibrium pressure is calculated using an equation derived by evaluating the relationships of igniter exhaust gas weight required to produce the equilibrium pressure and the time required by the igniter to produce the necessary weight of gas. This equation is:

$$t = \frac{L^*}{12C^* (\Omega)^2}$$

where:

t = Time to achieve equilibrium.

L* = Characteristic length (in.).

Ω = Function of propellant specific heat ratio.

C* = Characteristic exhaust velocity (ft/sec).

This relationship has been validated by plotting time to equilibrium as a function of L* from actual test data. The empirical and theoretical lines (Figure 6-6) are approximately parallel. The empirical and theoretical curves are different because the actual flame temperature in the motor chamber is less than the stagnation temperature and the igniter does not reach its full mass flow instantaneously. The L* value (874) gives a corresponding equilibrium time (Figure 6-6) of 0.037 second.

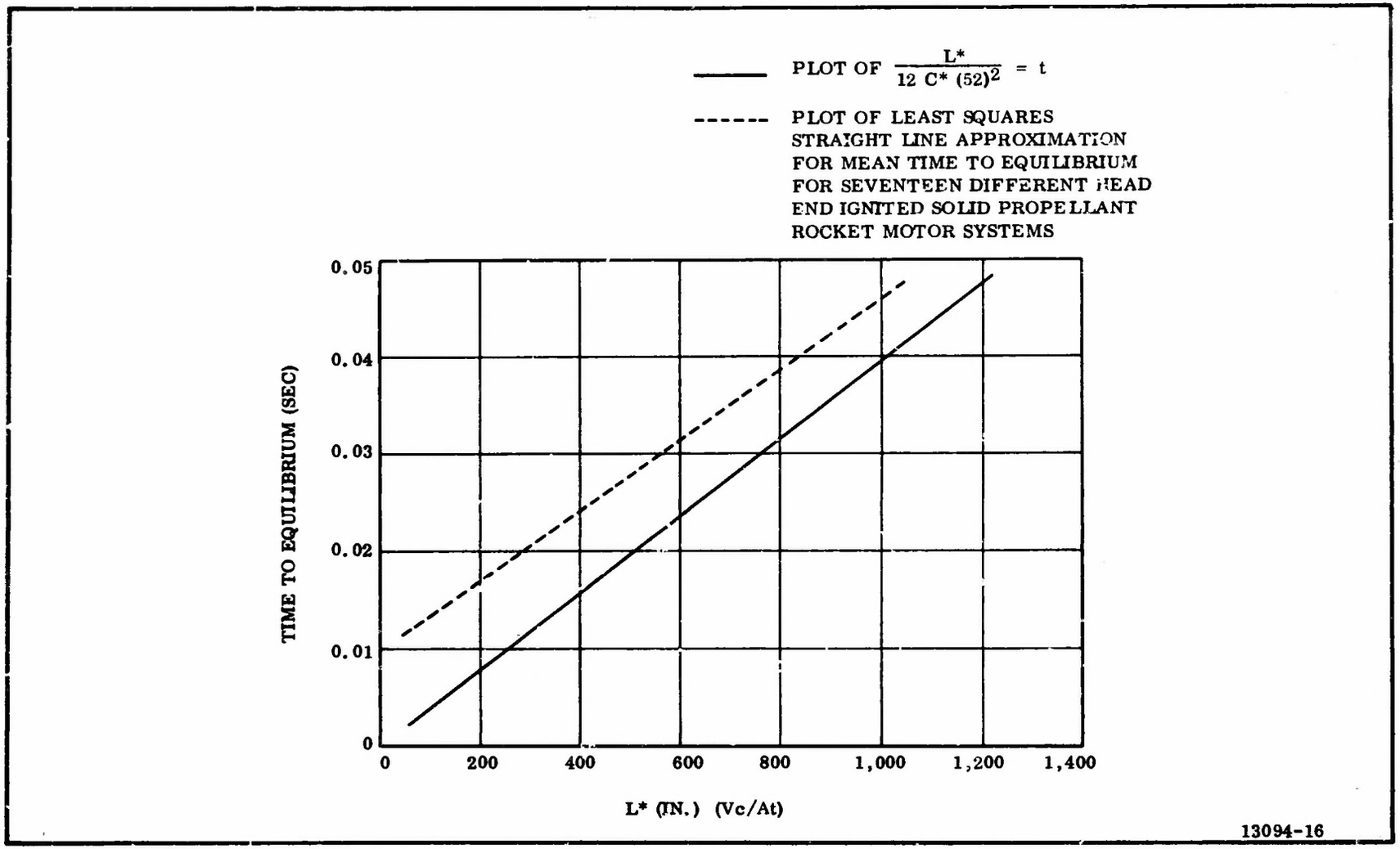

Figure 6-6. Time from First Motor Chamber Pressure Rise to Initial Equilibrium as Function of Motor Characteristic Length

Lag time is the time required for the igniter combustion products to heat the motor propellant at one spot on the surface above its autoignition temperature. For calculation purposes, this first point of ignition is located geometrically by a layout of igniter exhaust plume and the motor grain. The time to achieve the autoignition temperature is calculated by an equation which describes the heat transfer from a moving gas stream to an infinite plane. The equation generally takes the form of:

$$T = \frac{C_p \rho K (T_s - T_a)^2}{Q_T^2} \psi^2$$

where:

T = Lag time (sec).

C_p = Motor propellant heat capacity (Btu/lb-°F).

ρ = Motor propellant density (lb/cu ft).

K = Motor propellant thermal conductivity (Btu/hr-sq ft-°F).

T_s = Surface temperature of the propellant during steady state combustion (°R).

T_a = Ambient temperature of the propellant (°R).

Q_T = Heat flux rate (Btu/sq ft-sec).

ψ^2 = Constant, theoretically equal to $\pi/2$; in practice, ψ^2 approaches 1.

A method of calculating Q_T was presented by United Technology Center (UTC)* in which total heat flux, Q_T, is broken down into its radiative and convective components.

$$Q_T = Q_{RAD} + Q_{CONV}$$

where:

Q_{RAD} = Radiation heat flux.

Q_{CONV} = Convective heat flux.

*United Technology Center, Theoretical and Experimental Investigations of Ignition Systems of Very Large Solid Propellant Motors (U). Final Report, Contract AF 04(611)-7559; Sunnyvale, California; United Technology Center, May 1963; CONFIDENTIAL.

Radiative heat flux is calculated by the following equation.

$$Q_{RAD} = \sigma \epsilon (T_p^4 - T_a^4)$$

Where:

σ = Stephan Boltzmann radiation constant, 0.1714×10^{-8} Btu/hr-ft^2-°R^4.

ϵ = Emissivity of the igniter gases.

T_p = Igniter plume temperature (°F).

T_a = Propellant ambient temperature (°R).

UTC presented a figure from which emissivity could be taken as a function of port diameter and chamber pressure. For a diameter of 74 in. and a pressure of two atmospheres, the emissivity was found to be 0.135. Using a flame temperature of 5,220°R and an ambient temperature of 520°R, the radiation heat flux was found to be 172,000 Btu/hr-sq ft. UTC also presented a figure from which Q_{CONV} as a function of igniter mass flow rate and port diameter could be selected. For a port diameter of 74 in., Q_{CONV} is 65,000 Btu/hr-sq ft, giving a total Q_T of 237,000 Btu/hr-sq ft or 66 Btu/sq ft-sec.

For the 156-9 igniter, the lag time of 0.17 sec is primarily a result of the large free volume of the motor. The time lapse of the 156-9 motor propellant includes heatup time and the time of pressurization to equilibrium.

The flame spreading period covers the time from first ignition until all surfaces are ignited. Flame spreading rates are estimated from analysis of actual motor data. Rates vary from approximately 7,000 in./sec down the port to 250 in./sec down a stagnant slot. These rates vary with port diameter, flow directions, driving forces, etc., and must be selected with care for performance prediction. Based on predicted flame spreading rates of 250 in./sec down the slots, 5,000 in./sec down the main port, and 1,000 in./sec in the head end port, the ignition transient shown in Figure 6-5 was predicted. Table 6-1 shows the 156-9 igniter predicted performance.

TABLE 6-1

156-9 IGNITER PREDICTED PERFORMANCE

Characteristics	Value
Mass Flow Rate, first level 0.56 sec (lb/sec)	158
Burning Time (sec)	1.1
Maximum Operating Pressure (psia)	850
Average Operating Pressure, first level (psia)	820
Average Operating Pressure, second level (psia)	350
Ignition Delay, 10 percent P_{max} for Booster PYROGEN (sec)	0.050
Ignition Interval Booster PYROGEN T_o to 75 percent P_{max} (sec)	0.073
Motor Ignition Delay Time, T_o to 75 percent P_{max} (sec)	0.39
Maximum Motor Pressure at Ignition (psia)	715
Igniter Coefficient $\frac{lb\ sec}{sq\ in.}$	0.168

C. IGNITER INSULATION DESIGN

1. CASE INTERNAL INSULATION

The case internal insulation protects the igniter case from overheating during both igniter and motor firings and controls the web thickness of the propellant grain. The internal insulation consists of two 0.1 in. thick plies of asbestos filled NBR laid up and vulcanized in place. A 0.1 in. coating of UF-2121 liner is painted over the NBR to provide a high strength bond to the TP-H1016 propellant. The insulation-liner-propellant bond system concept has an extensive successful history at Thiokol.

2. CASE EXTERNAL INSULATION

The igniter case external insulation will prevent the steel case from melting during the motor firing, precluding the ejection of igniter case fragments. The external insulation consists of 1.0 in. of asbestos filled NBR laid up and vulcanized in place. The insulation thickness was calculated for the 156-8 motor which has an action time of 122 sec, compared to 66.6 sec for the 156-9 motor. To facilitate use of the same design without excessive engineering and manufacturing changes, the same external igniter insulation thickness will be used for the 156-9 as for the 156-8. The insulation thickness was calculated for the 156-8 based on a char rate of 5.5 mil/sec with a 1.5 safety factor. By comparison, the external insulation thickness for the 156-9 igniter is more than adequate.

3. IGNITER CAP INSULATION

The insulation applied to the adapter (Figure 6-1) will be TI-H704B. Thiokol has demonstrated TI-H704B insulation as the case insulation in four Stage I MINUTEMAN size motors, the ignition system insulation on a 120 in. diameter motor, and as the case insulation in the 156-1 motor. The insulation is a mastic material containing primarily HC binder, asbestos, and carbon black. It is most effective in areas of low gas velocity, and was selected as the PYROGEN igniter insulation because of its relatively low cost, ease of application to any configuration, and ability to cure at ambient temperature.

4. IGNITER INSULATION INTERFACES

Vacuum putty will be used to seal and provide thermal joints when assembling the initiator PYROGEN loaded case and the booster PYROGEN loaded case to the igniter cap (Figure 6-1). These parts are toleranced so that a minimum of 0.1 and a maximum of 0.25 in. of putty will be used at joint interfaces.

5. INSULATION INGREDIENTS, AND PHYSICAL AND THERMAL PROPERTIES

The composition of TI-H704B insulation is asbestos and carbon black filled HC polymer mastic material. The insulation formulation , specification SB-SP-365A, follows.

Ingredients	Weight Percent
Binders	45.0
Asbestos	30.0
Carbon Black	15.0
Diammonium Phosphate	10.0
	100.0

The physical and thermal properties of TI-H704B insulation are as follows.

Cured Density at 77 ± 3°F (g/cc)	1.30
Cured Thermal Properties	
Specific Heat (cal/g°C)	0.325
Thermal Conductivity (cal/cm/sec°C)	9.15×10^{-4}
Thermal Diffusivity (sq cm/sec)	2.35×10^{-3}

6. PHYSICAL AND THERMAL PROPERTIES OF IGNITER EXTERNAL INSULATION AND LINER

The physical and thermal properties of igniter external insulation (NBR) and igniter liner (UF-2121) have been described in the 156-9 motor insulation design report.

D. IGNITER WEIGHT ANALYSIS

The component weights for the PYROGEN igniter are listed below.

	Weight (lb)
Loaded Case Booster PYROGEN	
Case	260.8
External Insulation	87.6
Internal Insulation	13.306
UF-2121 Liner	4.1
TP-H1016 Propellant	131.9
Initiating PYROGEN	
Case	3.9
TP-H1016 Propellant	1.2
Nozzle	0.6

Booster Assembly	0.481
S & A Device	4.800
Adapter (7U40511)	51.425
Adapter (7U40512)	6.687
Insulated Adapter (7U40514)	113.153
Miscellaneous	11.23
TOTAL	691.176

E. IGNITION SYSTEM PROPELLANT

The propellant selected for use in the ignition system is designated TP-H1016. The composition, physical and ballistic properties and autoignition characteristics of this propellant are shown in the following tabulations.

1. TP-H1016 PROPELLANT

Constituent	Composition by Weight (Percent)
Ammonium Perchlorate	77
Aluminum Powder	2
HB and ERL*	18
Ferric Oxide	3

*The ratio of HB to ERL is determined from raw material standardization to achieve the desired physical properties.

2. PHYSICAL PROPERTIES

Item	Value	
	Minimum	Maximum
Density (lb/cu in.)	0.0599	0.0611
Maximum Stress (psi)	140	227

Item	Value Minimum	Maximum
Strain at Maximum Stress (in./in.)	0.20	0.33
Modulus of Elasticity (psi)	600	1,200

3. BALLISTIC PROPERTIES

Characteristic Velocity, C* (ft/sec)	4,945
Density ($lb/in.^3$)	0.0605
Exponent Burn Rate, n	0.44
Burn Rate at 1,000 psi (in./sec)	0.84

4. AUTOIGNITION

Temperature (°F)	Time (min)
390	60
408	40
445	20
496	10

F. IGNITION SYSTEM STRUCTURAL ANALYSIS

The ignition system booster igniter case, the adapters that integrate ignition system and adapt the igniter to the motor, the motor case polar boss, and the forward portion of the motor case were analyzed to determine structural integrity and compatibility. The following conditions were investigated to determine the most severe loading.

1. Booster igniter case pressurized to an ignition pressure of 1,100 psi (1.35 times average pressure) with motor unpressurized.
2. 156-9 motor pressurized to MEOP* (885) psi with booster igniter case at equilibrium pressure.

The analytical results are summarized in Figures 6-7 and6-8 . Margins of safety shown were calculated from the greatest stresses existing at the critical points of the structure and ultimate material strengths. A negative margin of safety is shown in condition 2 at the center of the adapter ring.

The stress is almost entirely due to bending moment and the computer program used is not programed to use an applicable 1.5 bending factor. But using a 1.5 bending factor, the following margin of safety exists.

$$1 - \frac{101,101}{(1.5)\ (90,000)} = 0.25$$

G. IGNITION BENCH TEST

The ignition system consists of components previously demonstrated in the AF 156-1 motor test. The only modification to the AF 156-1 igniter is that the booster PYROGEN igniter is somewhat shorter. Consequently, only minimal bench testing is required to verify components and performance. This testing will include the static firing of one complete igniter assembly with a rebuilt S & A device and without external insulation. This test will be conducted under the AF 156-8 program since 156-8 and 156-9 ignition systems are identical except for adapting to their respective motors. The primary objective of this test is to evaluate performance parameters such as igniter response time, igniter ignition delay, booster PYROGEN lag time, and booster PYROGEN pressures. Instrumentation will consist of pressure gages on the booster PYROGEN igniter.

*Actual MEOP (830) psi. The MEOP (885) psi value was derived at the time of preliminary design.

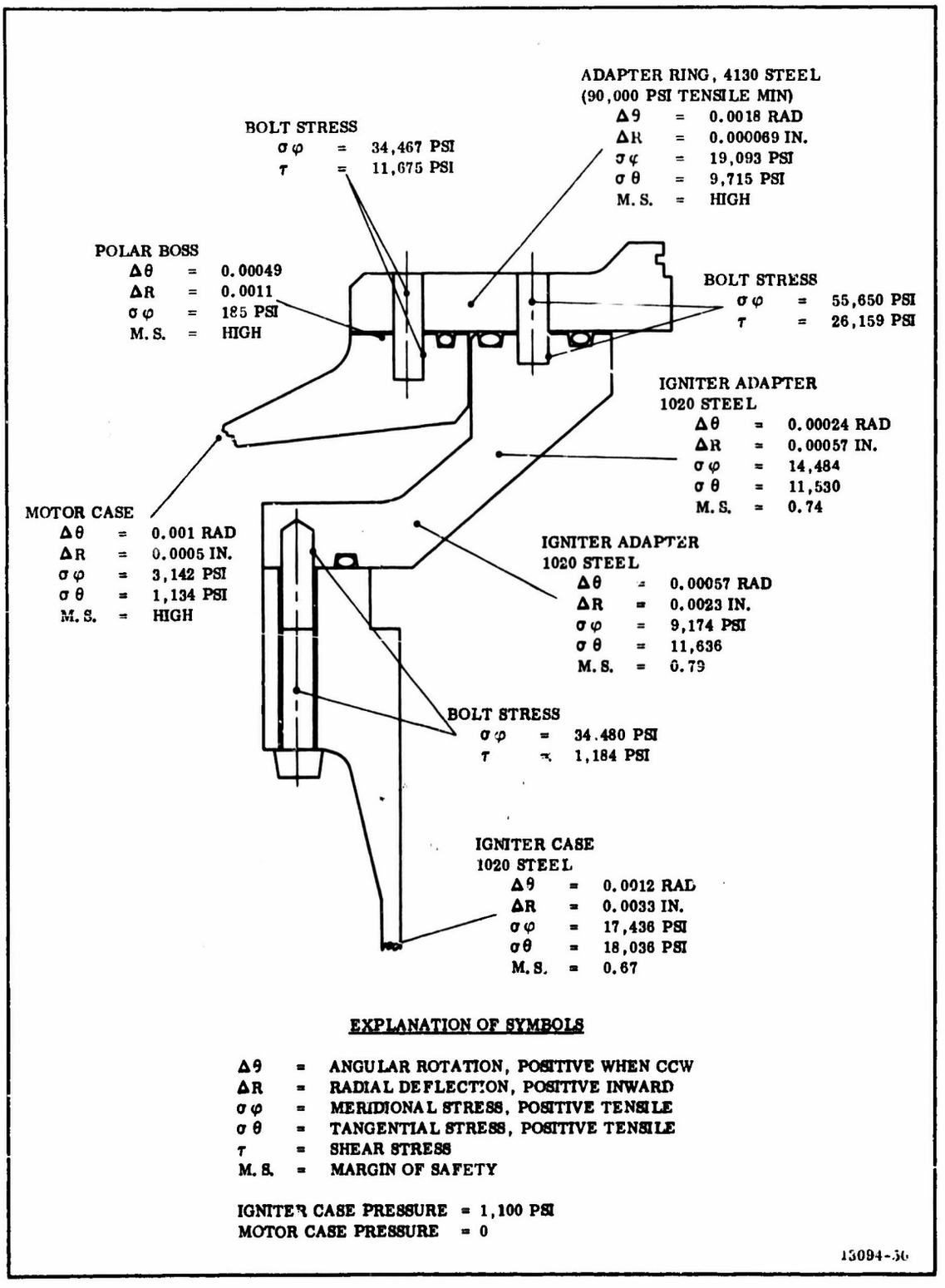

Figure 6-7. Summary of Structural Analysis, Condition 1

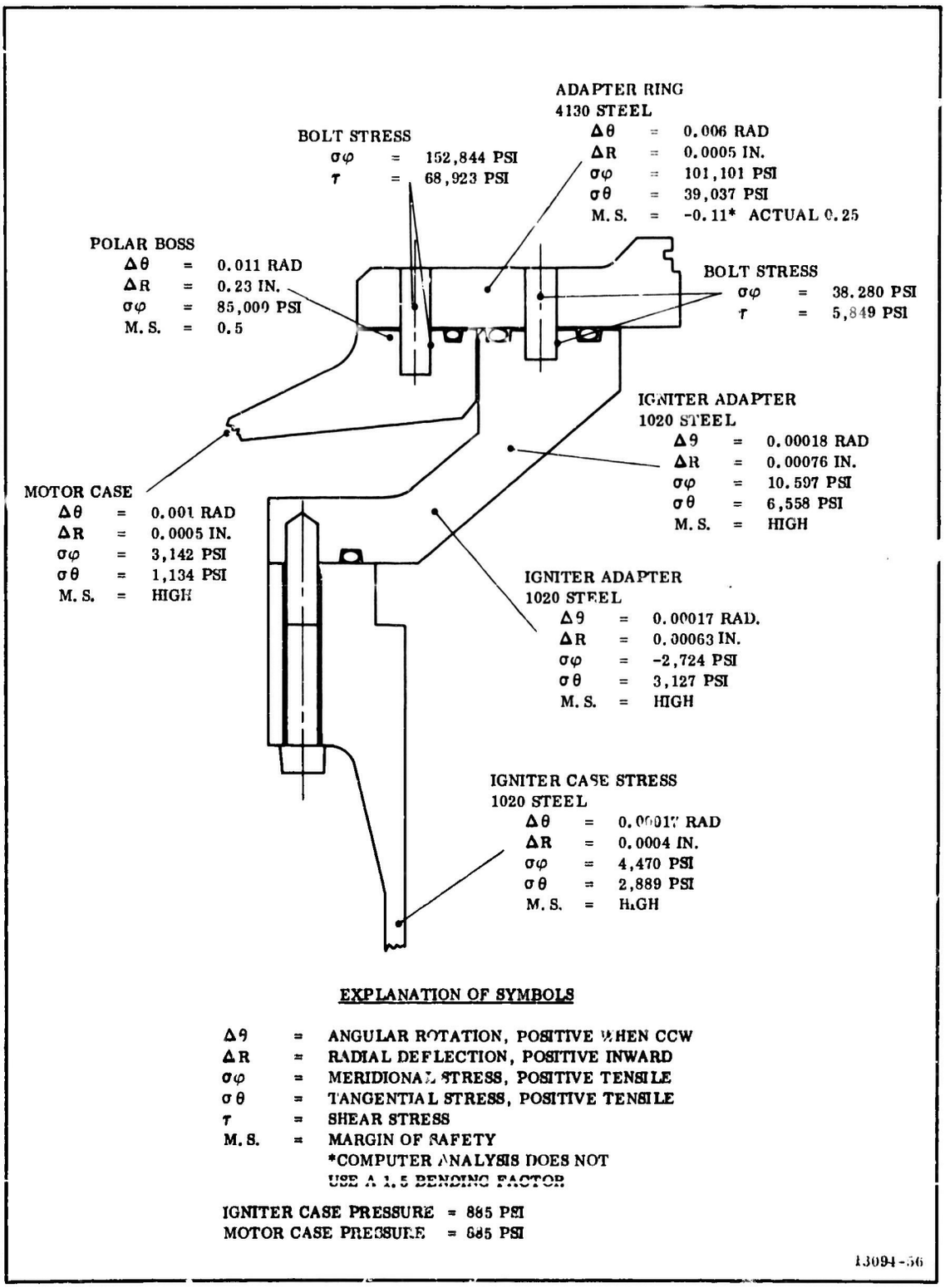

Figure 6-8. Summary of Structural Analysis, Condition 2

The 156-9 ignition system for the bench test will be temperature conditioned for a minimum of 12 hr at 80°F. The system will be static tested within 30 min after removal from conditioning. The ignition system will be installed in a delta test stand with pressure transducers installed to record igniter pressure. A documentary camera will be positioned to obtain photographic coverage of the static test. Pressure will be recorded as a function of time to provide data for analyzing igniter performance. After the igniter is tested, it will be examined for hot spots or any abnormalities. Still photographs will be taken before and after the static test.

SECTION VII

THRUST VECTOR CONTROL SYSTEM

The 156-9 thrust vector control system consists of two specially adapted linear hydraulic servoactuators operated by a ground hydraulic power supply and an external electronic control system. The actuators are standard heavy duty industrial units modified to allow mounting of the servovalves and position feedback transducers. The servovalves are three stage industrial units with a linear variable differential transformer (LVDT) position feedback on the third stage spool. The manifold provides straight through porting to one side of the actuator and two hydraulic lines to the other. A standard LVDT is mounted inside the piston rod to insure minimum exposure hazard and to minimize the length of the assembly. The servoactuator assembly is shown on Figure 7-1.

The actuators are mounted in a universal trunnion assembly to allow for actuation in the opposite direction for any inclined plane. The actuator trunnions are located on the head block to minimize structural loading in the actuator mounting brackets as well as to eliminate the tendency toward buckling when the rod is extended.

A. ACTUATOR DESIGN

The actuators are standard heavy duty industrial units modified to allow mounting of associated actuation system hardware. The cylinder is a Parker-Hannifin, Model KD-2HLST13. The cylinder has a 6 in. bore, a 7 in. stroke, a 2.5 in. bore diameter and an operating pressure of 3,000 psig. The units will be proof tested to 4,500 psig prior to use in the assembly. The actuator cylinder is shown in Figure 7-2.

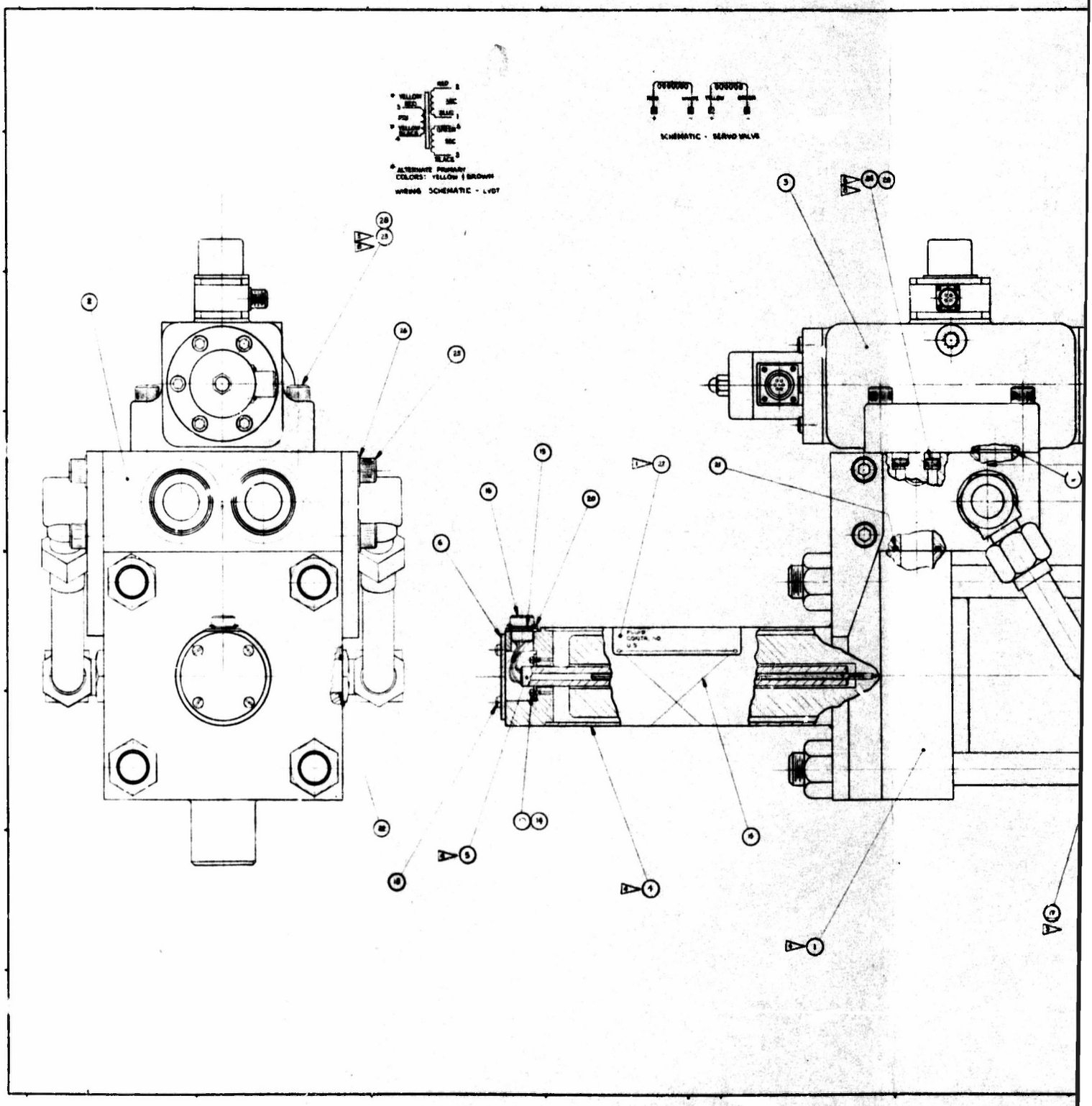
WIRING SCHEMATIC - LVDT
SCHEMATIC - SERVO VALVE

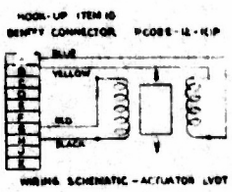

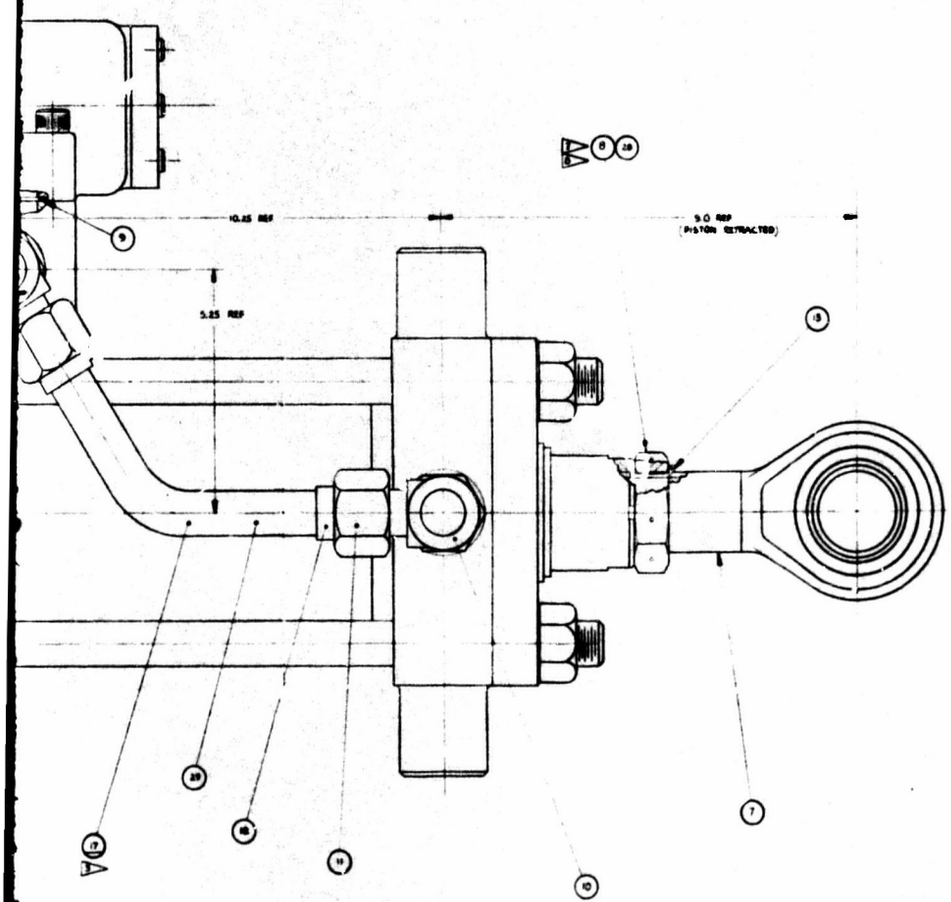

7U40505

Figure 7-

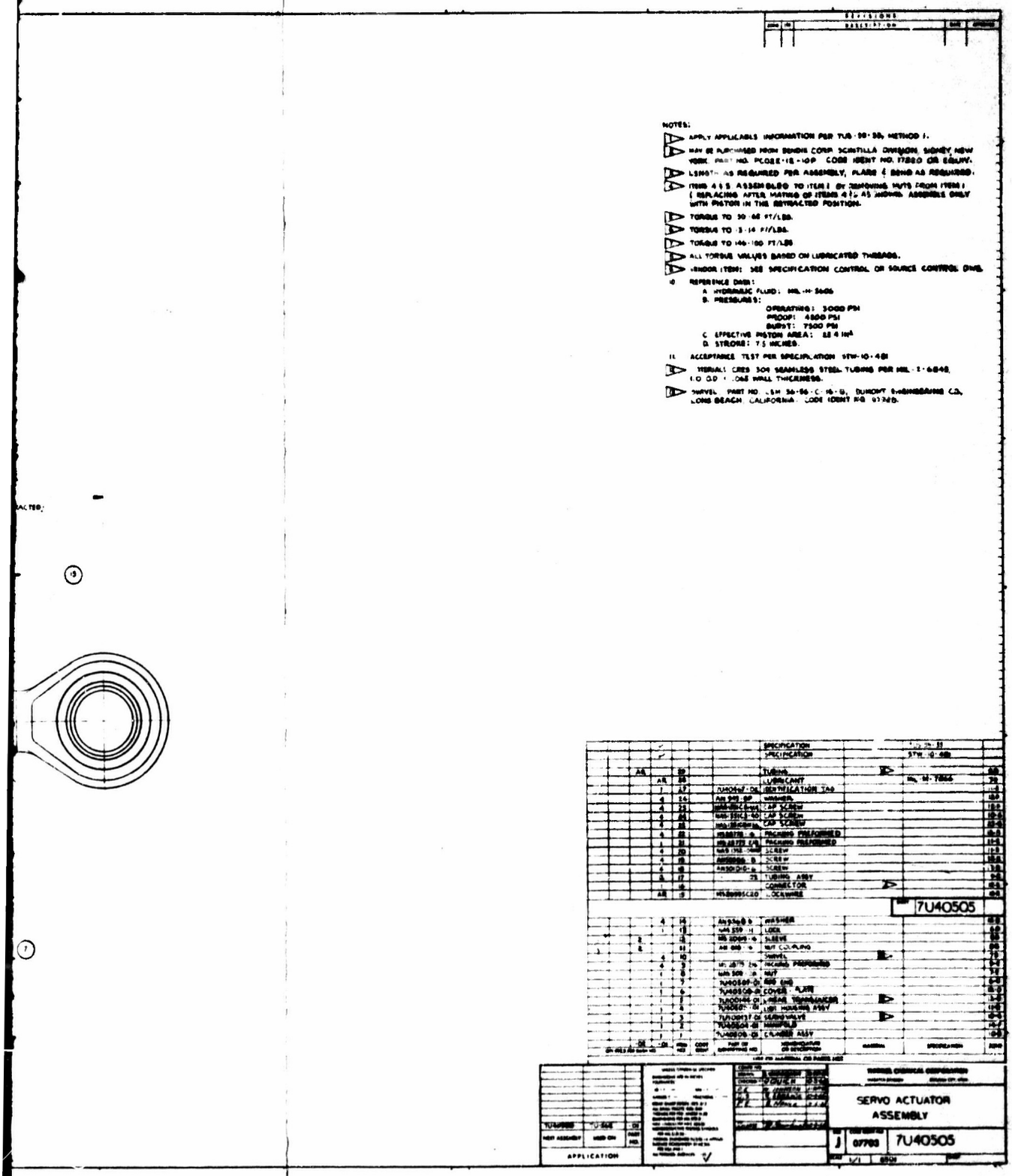

Figure 7-1. Servoactuator Assembly

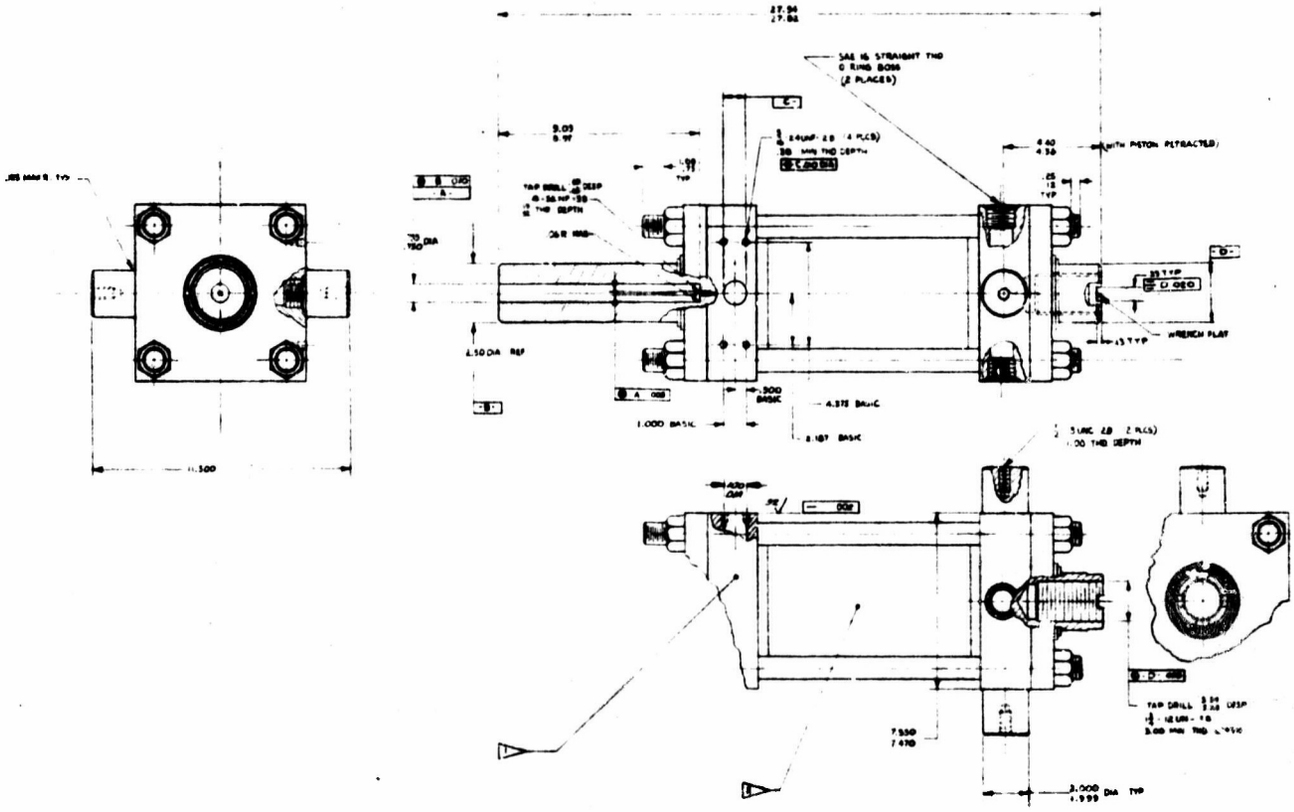

Figure 7-2. Act

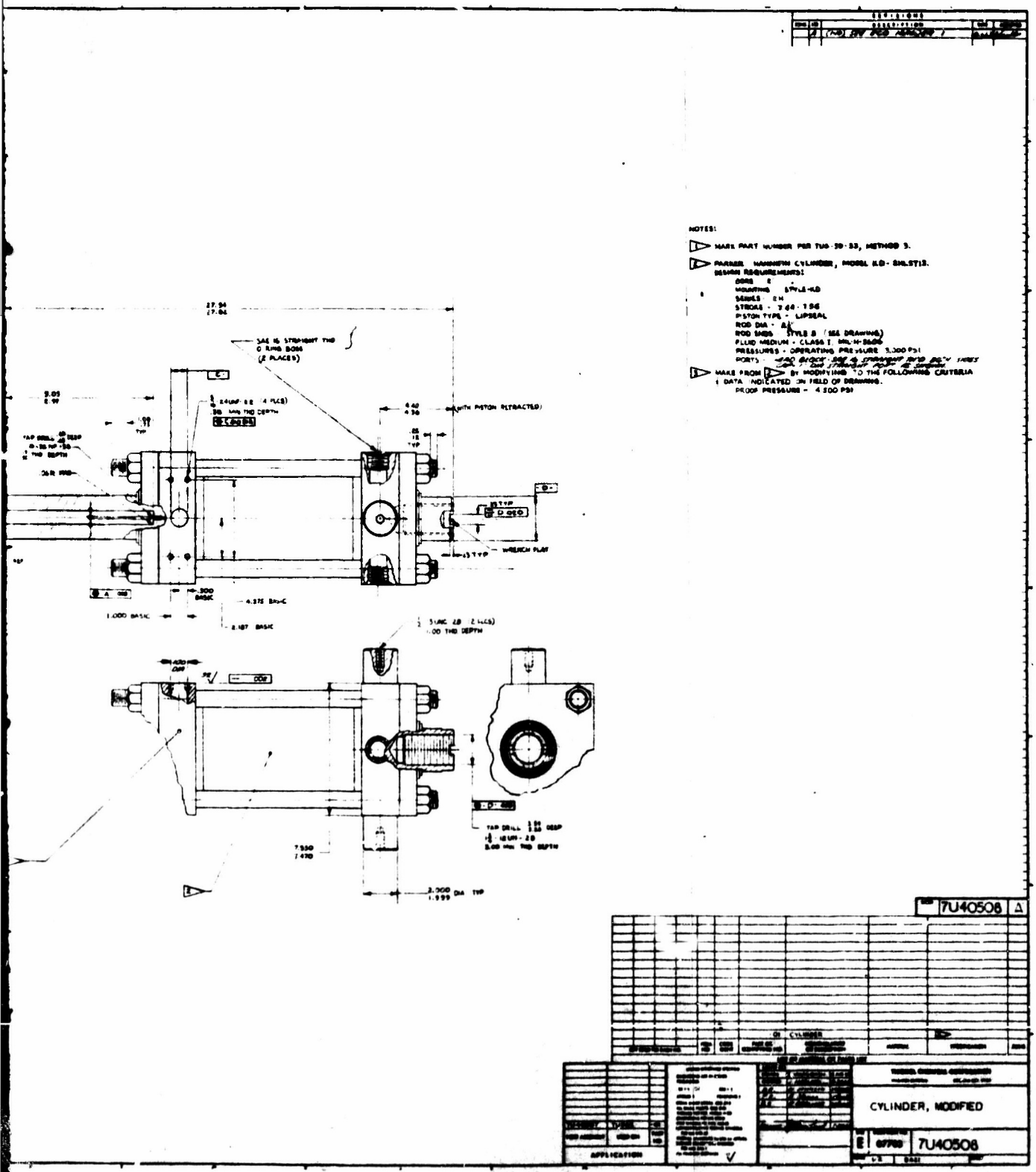

Figure 7-2. Actuator Cylinder

1. SERVOVALVE DESIGN

The servovalves are three stage industrial units with LVDT position feedback on the third stage spool. The servovalves are Dennison Model C-100. The valves are capable of operating at a temperature range of -65 to +275°F with a null shift per 100°F of 2 percent maximum. The rate of flow at 1,000 psi drop is 100 gpm with a null leakage at 3,000 psi of 3 gpm max and a flow linearity of at least 5 percent from 0 to 100 gallons per minute. The servovalve is shown on Figure 7-3.

2. TORQUE ANALYSIS

Calculated maximum torque about the nozzle pivot is shown in the following tabulation.

Dynamic Spring Torque	1,356,000 in.-lb
Seal Viscous Torque	256,000 in.-lb
Offset Torque	171,000 in.-lb
Gravitational Torque	186,000 in.-lb
Total Actuation Design Torque	1,963,000 in.-lb

Maximum values include a safety factor of approximately 1.5 over nominal values.

The inertial torque of 117,300 in.-lb has been neglected since it is always opposite in direction to the spring torque when deflections are large enough to make total torque an important design consideration. The viscous torque is also very conservative. It is calculated on the basis of a 1.25 cps sinusoidal actuation and would occur as the nozzle passes through null. At this time the spring torque, and therefore total torque, is low. If a triangular actuation program is used, the maximum viscous friction torque would be 63 percent of the listed value. The aerodynamic torque has been neglected since the location of the nozzle gimbal point makes it opposite in direction to the spring torque.

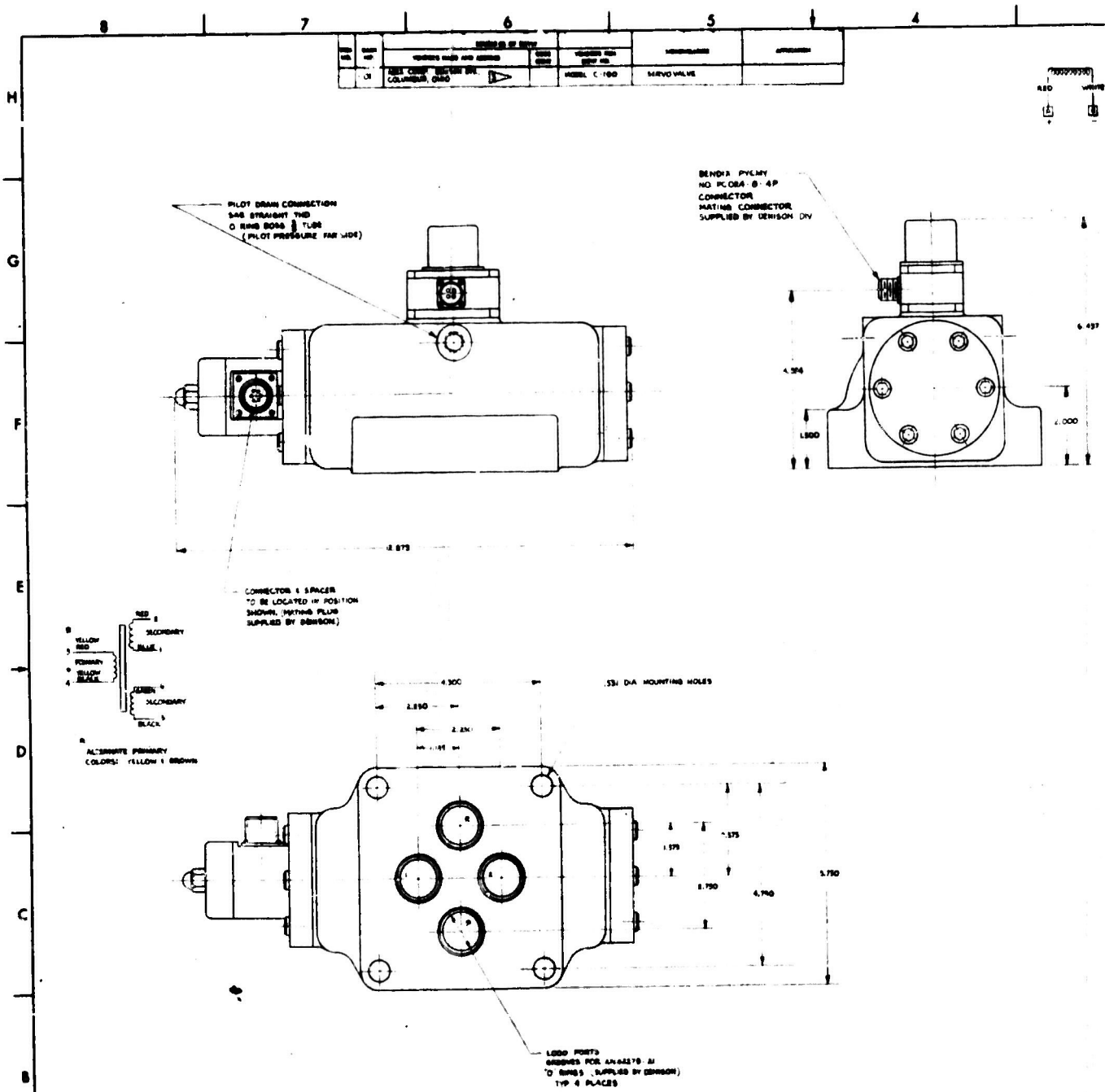
PILOT DRAIN CONNECTION
SAE STRAIGHT THD
O RING BOSS TUBE
(PILOT PRESSURE FAR SIDE)
BENDIX PYCMY
NO PC 084-8-4P
CONNECTOR
MATING CONNECTOR
SUPPLIED BY DENISON DIV
CONNECTOR & SPACER
TO BE LOCATED IN POSITION
SHOWN. (MATING PLUG
SUPPLIED BY DENISON)
.531 DIA MOUNTING HOLES
LEAD POSTS
O RINGS (SUPPLIED BY DENISON)
TYP 4 PLACES
MODEL C-100
SERVO VALVE

Fig

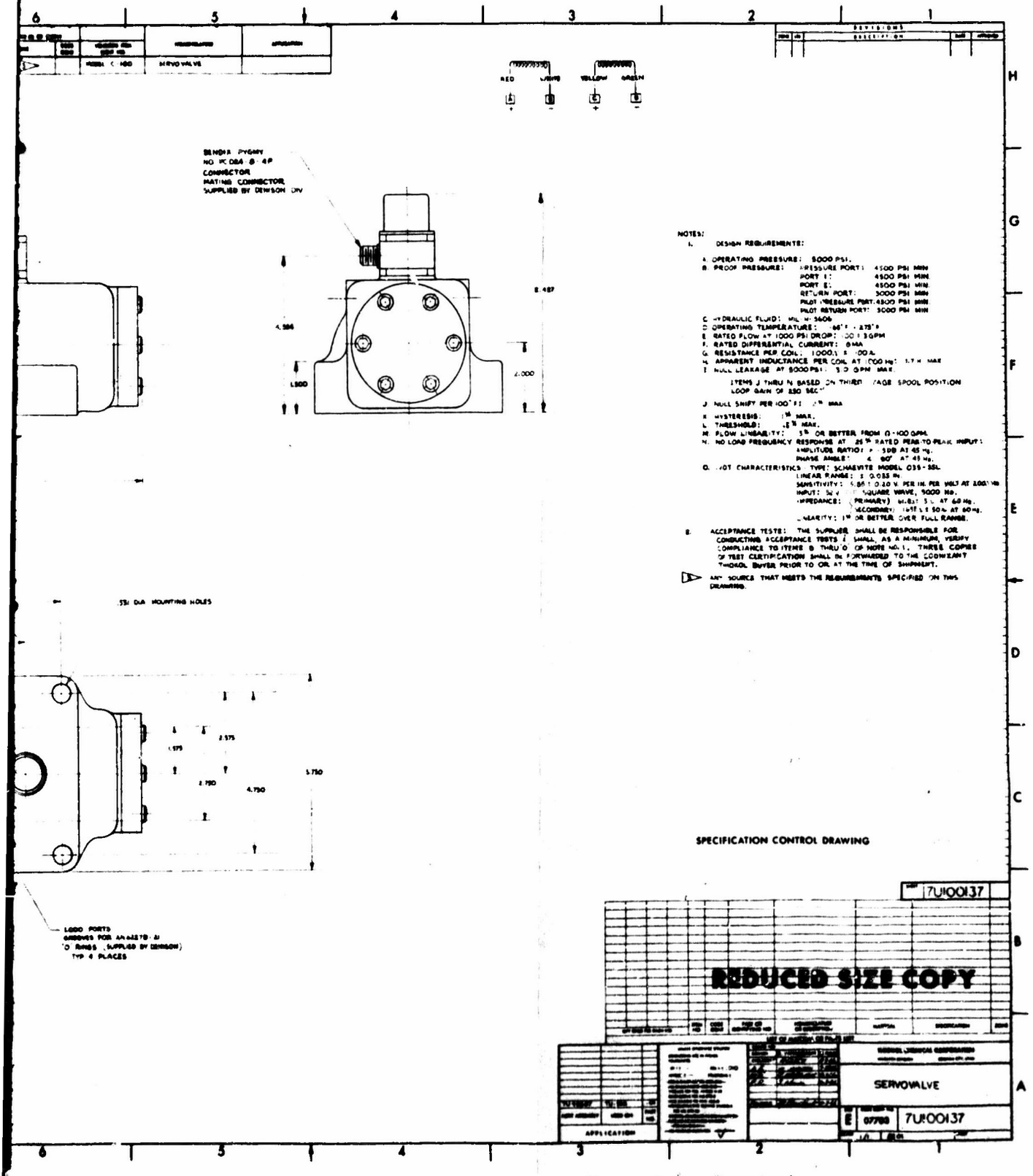

Figure 7-3. Servovalve

B. SYSTEM PERFORMANCE ANALYSIS

1. ACTUATION GEOMETRY

Due to the degree of nozzle submergence and the location of the seal pivot, it is impossible to use an ideal actuation geometry where the actuator is at right angles to the line connecting the pivot point and the clevis center at null. The degree of nonlinearity in the 156-9 is small, however, as evidenced by the following data.

Nozzle Position (deg)	Actuator Stroke (in.)	Lever Arm (in.)
0	--	48.66
-4	3.40	47.25
+4	3.44	49.44

2. ACTUATOR SIZE AND FORCE OUTPUT

The actuator must maintain a vector velocity of 20 deg/sec under maximum torque of 1,963,000 in.-lb. Assuming a pressure loss of 1,000 psi across the valve under maximum flow, the minimum required actuator effective area A_E is:

$$A_E = \frac{1,963,000 \text{ in.-lb}}{(47.25 \text{ in.})\ (2,000 \text{ psi})} = 20.8 \text{ sq in.}$$

The nearest industrial size is a 6 in. bore with a 2.5 in. rod.

$$A_E = \frac{\pi}{4}\ (6^2 - 2.5^2) = 23.4 \text{ sq in.}$$

Actuator dynamic torque = (23.4 sq in.)(2,000 psi) (47.25 in.) = 2,160,000 in.-lb.

Actuator stall torque = (23.4 sq in.) (3,000 psi) (47.25 in.) = 3,240,000 in.-lb.

Required actuator stroke was calculated from the actuation geometry to be 6.85 in. for ± 4 degrees. The selected stroke is 7.5 in., which corresponds to ± 4.38 degrees. This allows for sufficient overtravel to compensate for any shift in the pivot location, but is sufficiently short to prevent any possibility of contacting the nozzle stops.

3. RESPONSE STUDIES

Response studies were performed on an analog computer for the 156-9 gimballed nozzle system. The analysis used was the same as for previous designs and has been proven by the good correlation between computer results and actual firing data. Unlike the commonly used linearized analysis this analysis has no approximations for small inputs, so there were no input restrictions for these studies.

The computer predicted response of the nozzle system to a step input of 4 deg is shown in Figure 7-4 . Note that the system appears to be overdamped and there is no evidence of instability.

The system was designed to actuate at 20 deg per second. The system generates a maximum velocity of 28 deg per sec while responding to a 100 percent step. This system reaches 90 percent of maximum in 0.132 sec and 100 percent in 0.23 second.

The system's response to a 4 deg sine $2\pi(1.25)T$ input is shown in Figure 7-5. At this frequency (1.25 cps) the system lags by 9 deg and the attenuation is 0.2 db. The system's response to a triangle wave oscillating at a frequency of 1.25 cps, and an amplitude of 4 deg, is shown in Figure 7-6 . And response to a 2 deg amplitude square wave oscillating at 0.5 cps is shown in Figure 7-7 . The frequency response of the system for sine waves of 10 percent of maximum input amplitude is shown in Figure 7-8 Note that the -3 db point occurs at 10.7 cps.

Analog studies indicate that the 156-9 nozzle system exhibits stability for all expected conditions and is within contract performance specification.

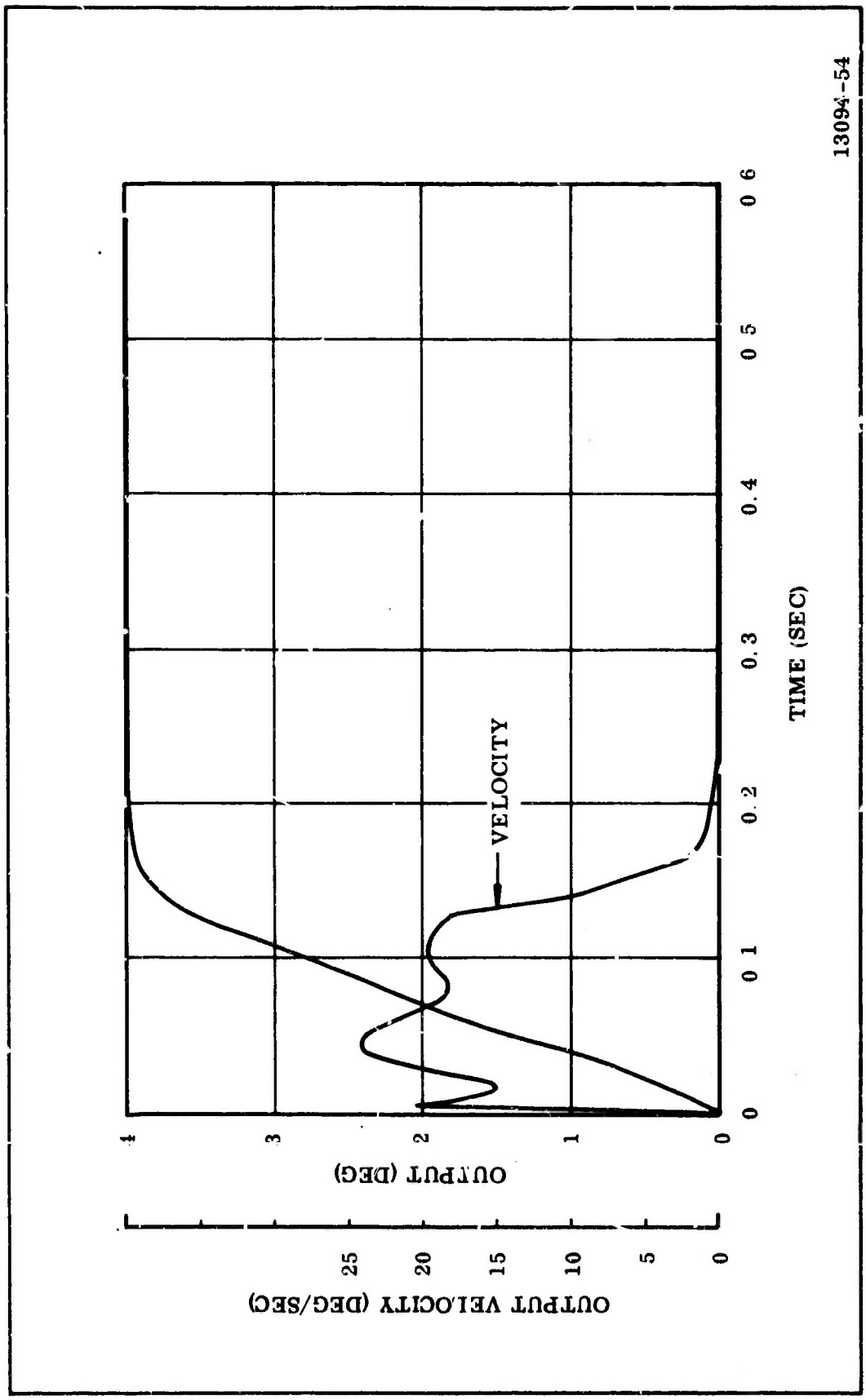

Figure 7-4. System Response to a 4 Deg Step

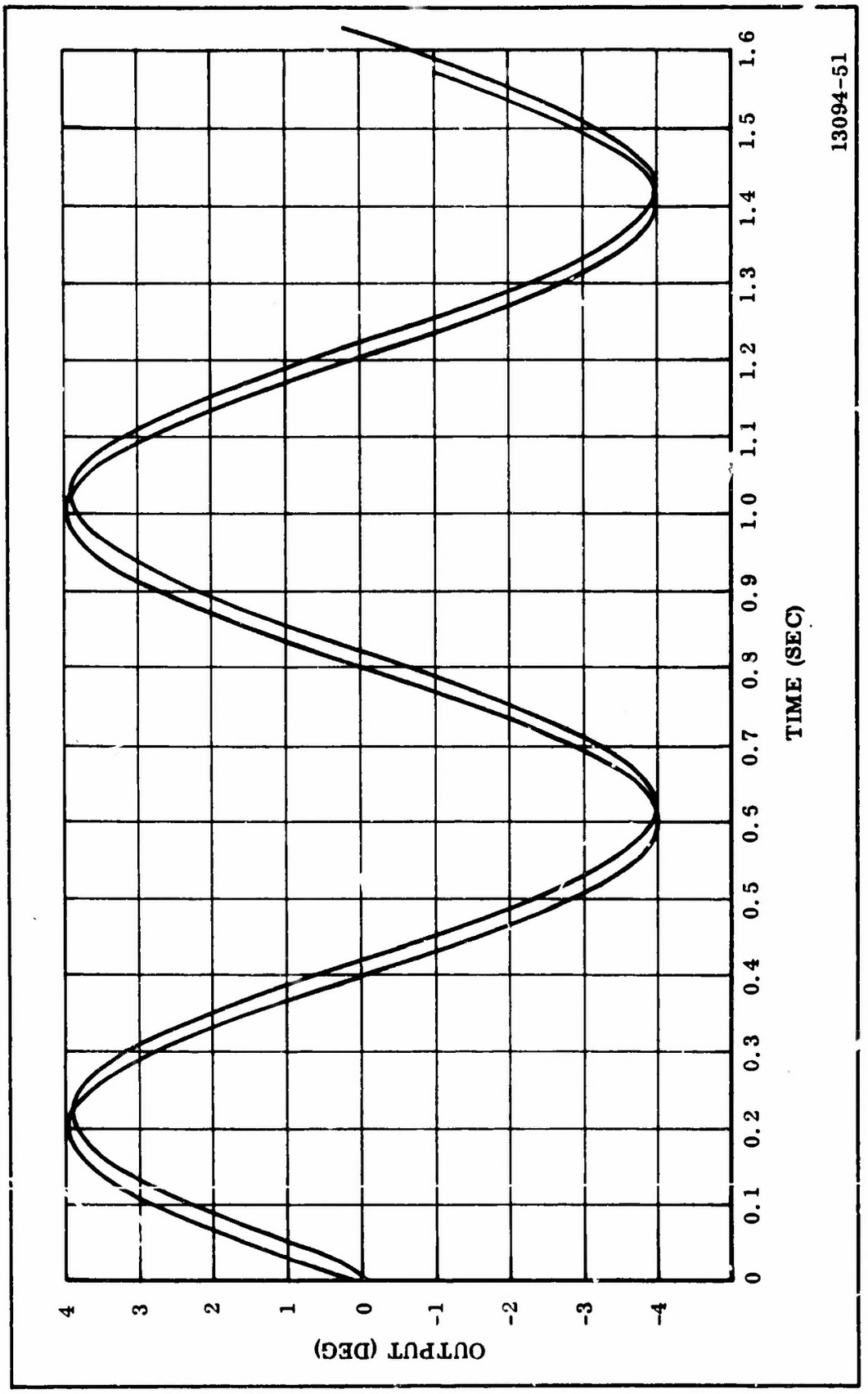

Figure 7-5. Response to a 1.25 CPS Sine Wave

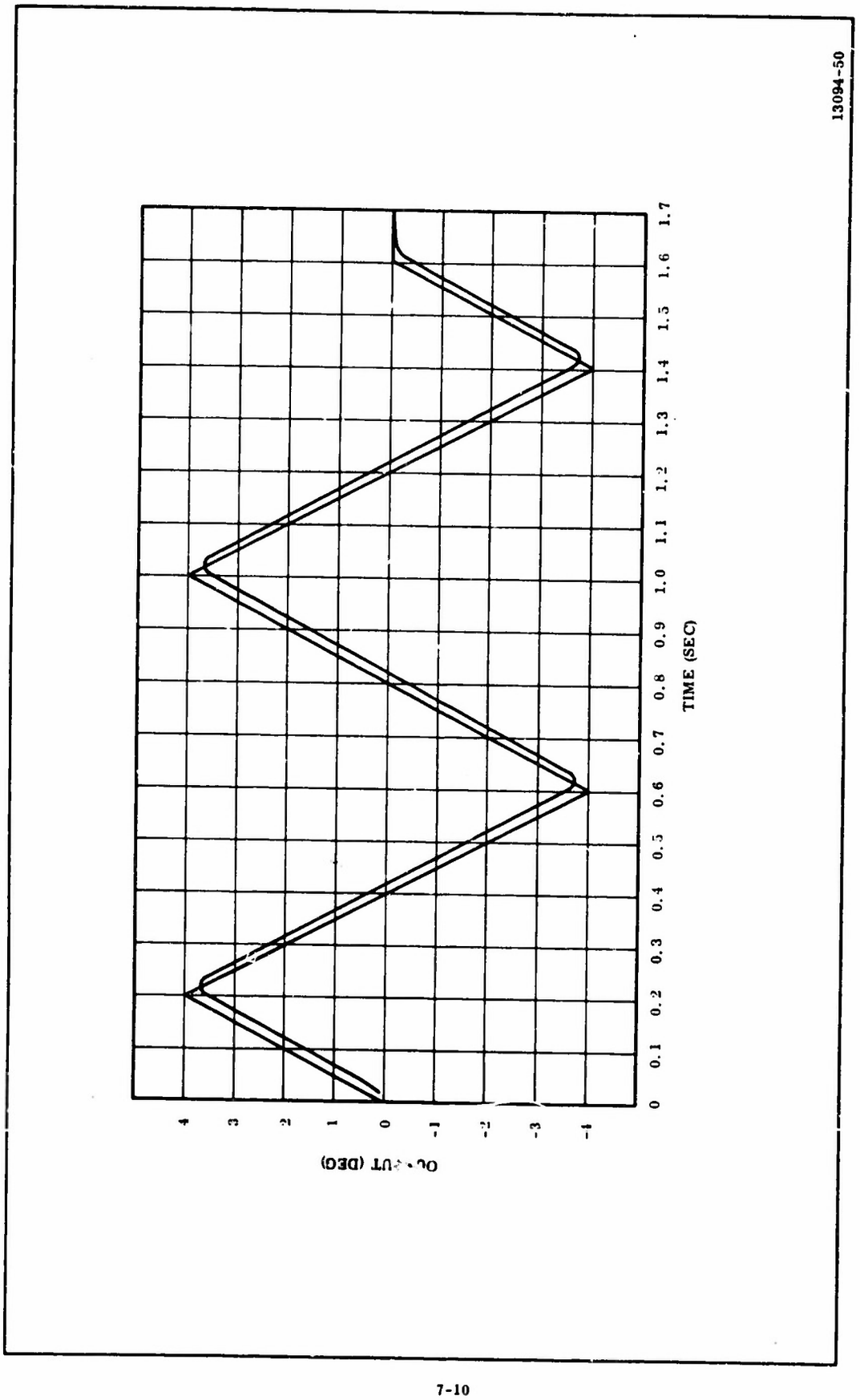

Figure 7-6. Response to a 1.25 CPS Triangle Wave

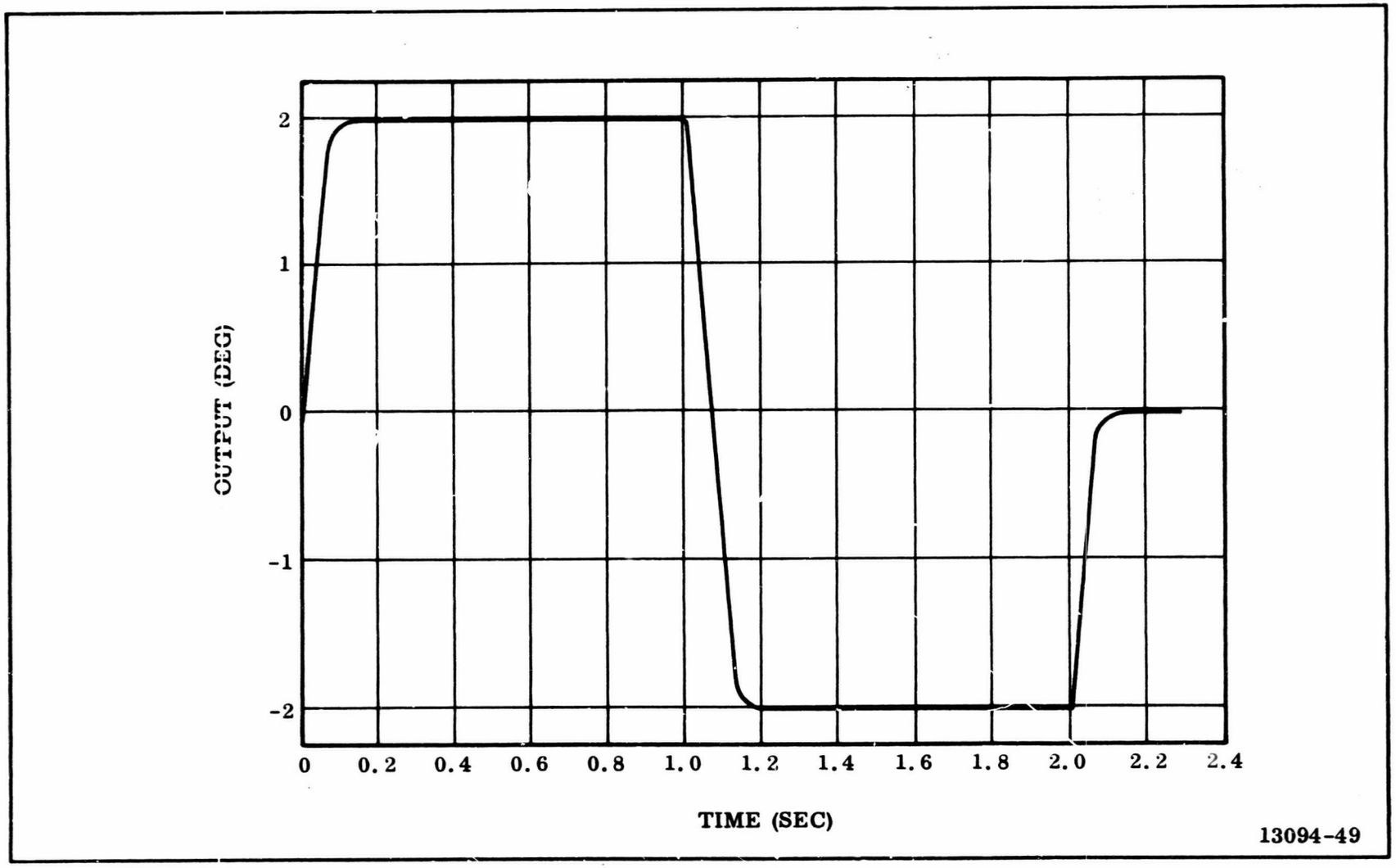

Figure 7-7. Response to a 0.5 CPS Square Wave

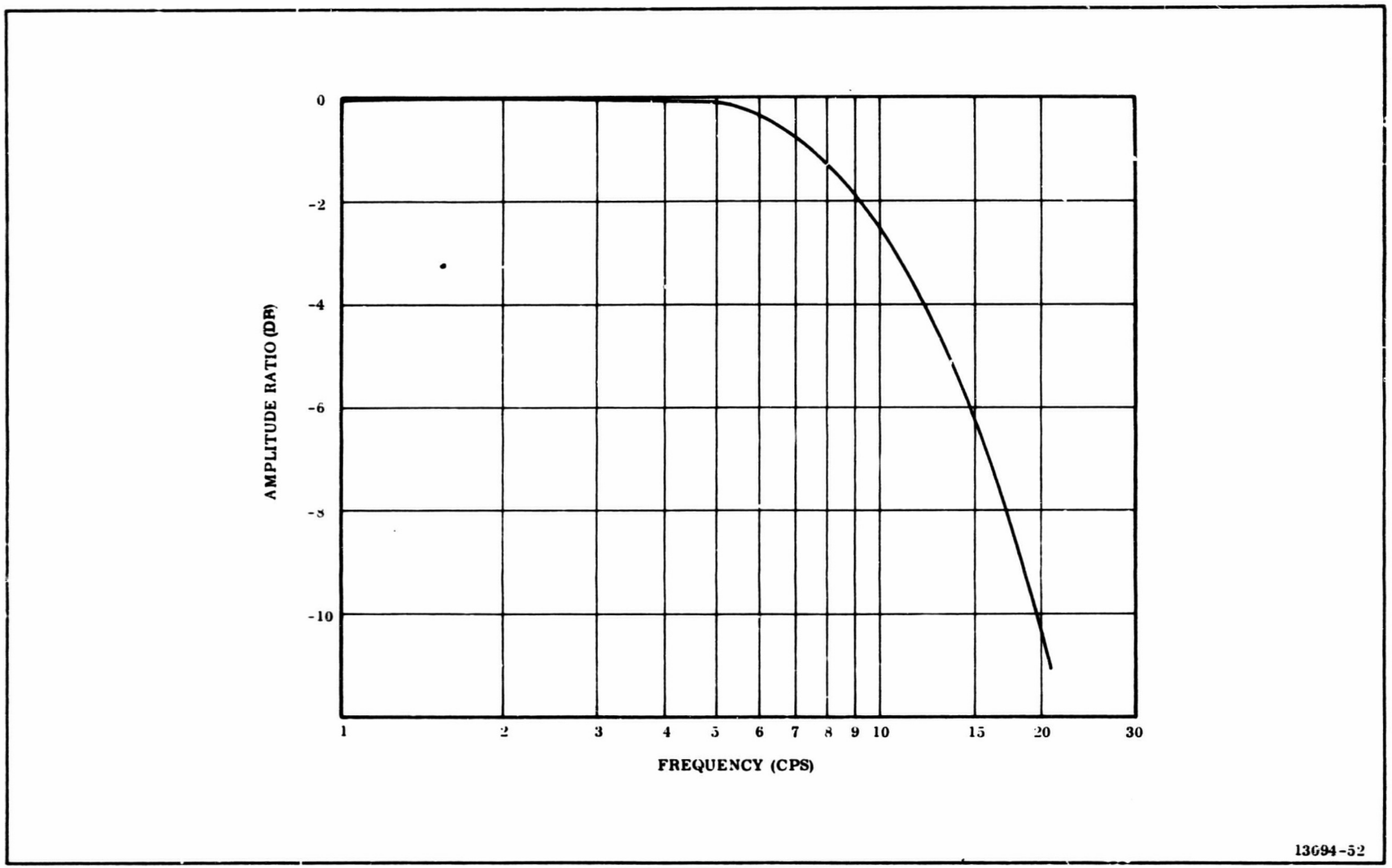

Figure 7-8. Frequency Response of 156-9 for 10 Percent of Maximum Input

C. WEIGHT ANALYSIS

The weight of each servoactuator assembly for the 156-9 motor is calculated to be 226 lb, with weight allocation among components as follows.

Item	Weight (lb)
Cylinder Assembly	128.5
Manifold	36.3
LVDT Housing Assembly	14.4
Cover Plate	0.2
Rod End	4.0
Servovalve	35.0
Linear Transformer	0.8
Miscellaneous	6.8
Total	226.0

D. HYDRAULIC SYSTEM

The hydraulic system schematic is presented in Figure 7-9. The ground power system was used previously for the 156-1 (TU-412) static test. It employs two pumps connected in parallel. Each of these units is capable of delivering 95 gpm at 3,500 psi. Since the maximum flow requirement is 105 gpm, either of the pumps could support the firing with no problem other than a slightly reduced vectoring rate.

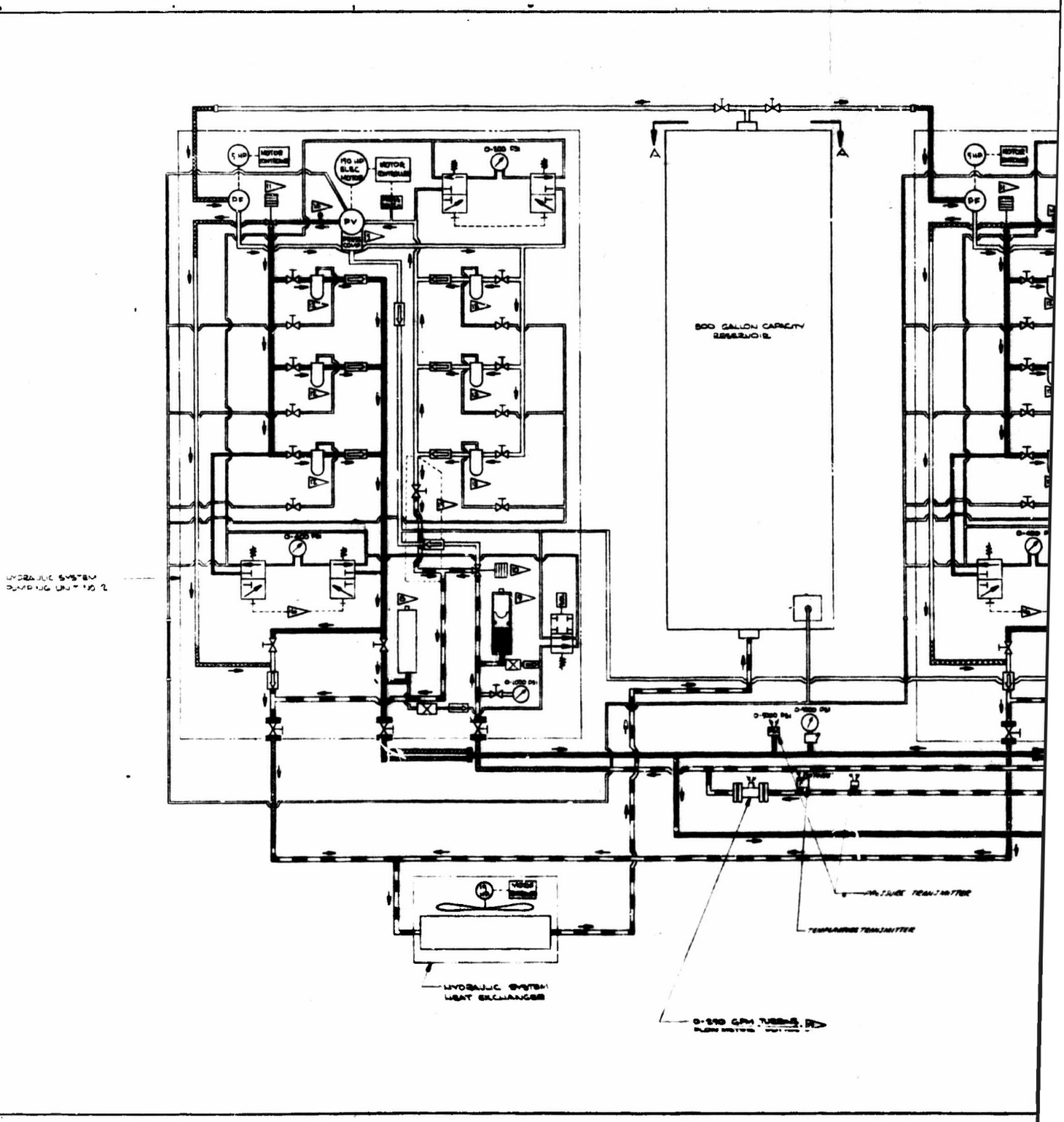
HYDRAULIC SYSTEM
PUMPING UNIT NO. 2
500 GALLON CAPACITY
RESERVOIR
HYDRAULIC SYSTEM
HEAT EXCHANGER

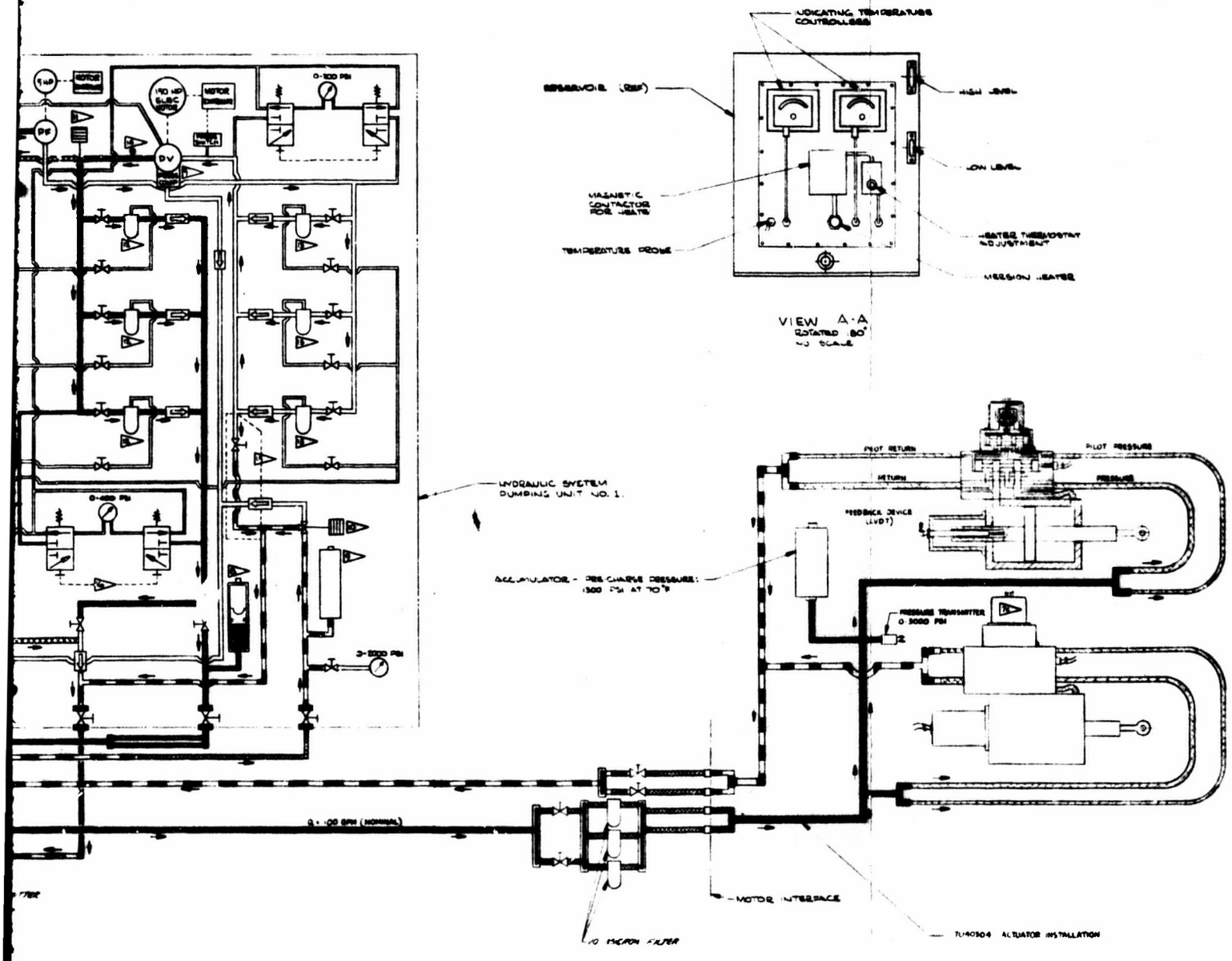

7U40587

Figure 7

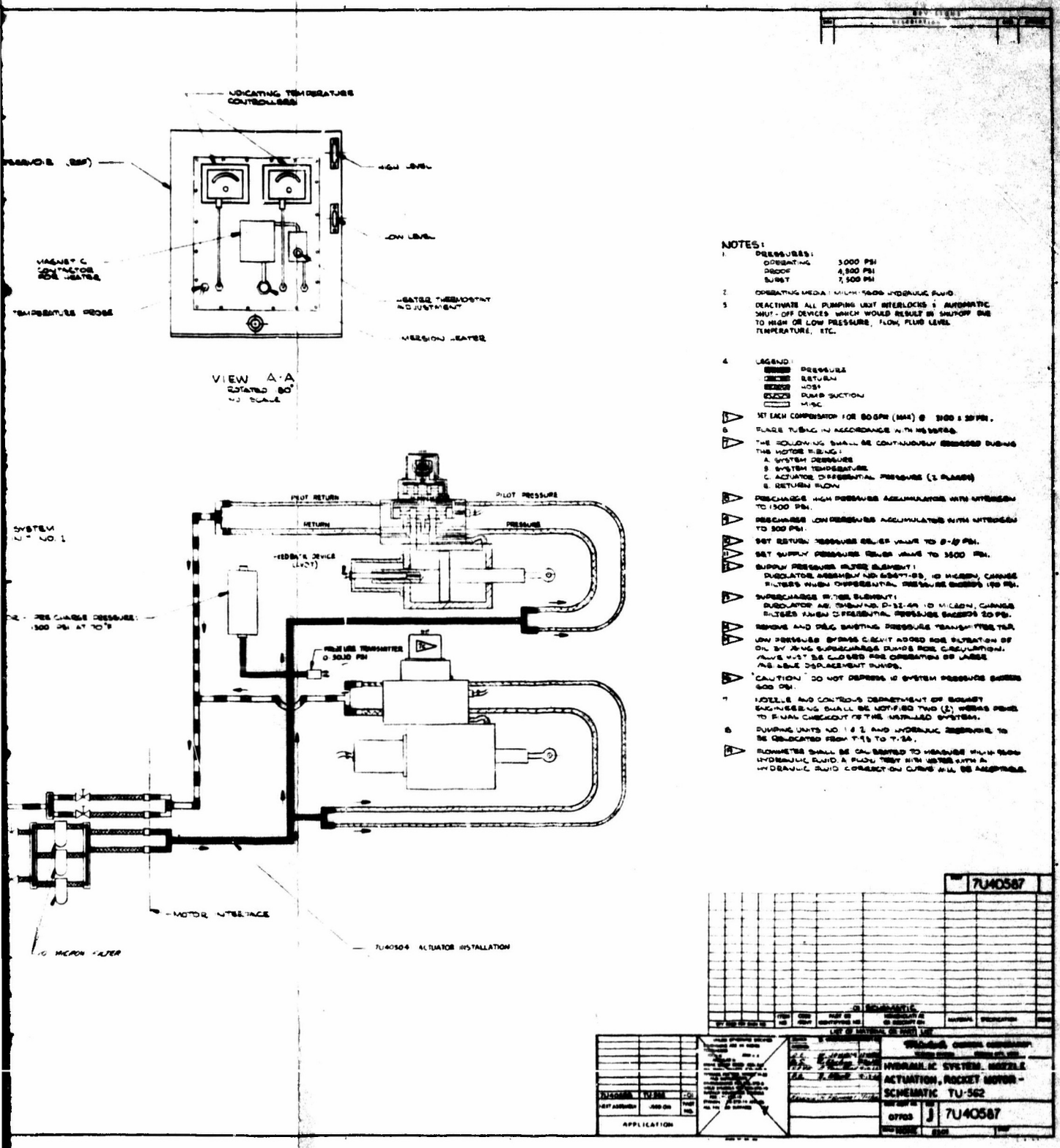

Figure 7-9. Hydraulic System Schematic

Motor-mounted equipment consists of the following.

1. Servoactuators
2. Accumulator
3. Manifold
4. System pressure transducer
5. Differential pressure transducers

Since this is not a flight system, the ground-to-motor interface manifold and the accumulator are mounted to the aft handling harness ring. Connections from the manifold to the servoactuators are by means of flexible hose.

The accumulator is included for compensation of any transients caused by sudden changes in flow demands.

All motor-mounted hydraulic lines are sized to keep the fluid velocity below 20 ft per sec to minimize line loss. The existing facility supply line, however, is 1.5 in. schedule 160 pipe in which the fluid velocity will be 24 ft per second. Calculated line loss over the 120 ft length of pipe and fittings approaches 250 psi at maximum flow. The exact line loss will be determined during system checkout by means of a system pressure transducer mounted on the motor. If necessary, system pressure can be set to a higher value to maintain 3,000 psi at the actuators during maximum flow conditions.

A 10-micron filter bank will be included in the ground hydraulic supply line as near as practical to the motor interface.

E. ELECTRICAL SYSTEM

A block diagram of the control system is shown in Figure 7-10. The TU-393 servocontrol unit provides all electronic components of the system, including LVDT excitation, demodulators, and servoamplifiers. Minor modifications include by-passing of the phase splitters, tying two demodulator outputs to one servoamplifier input, and changing feedback gain resistors.

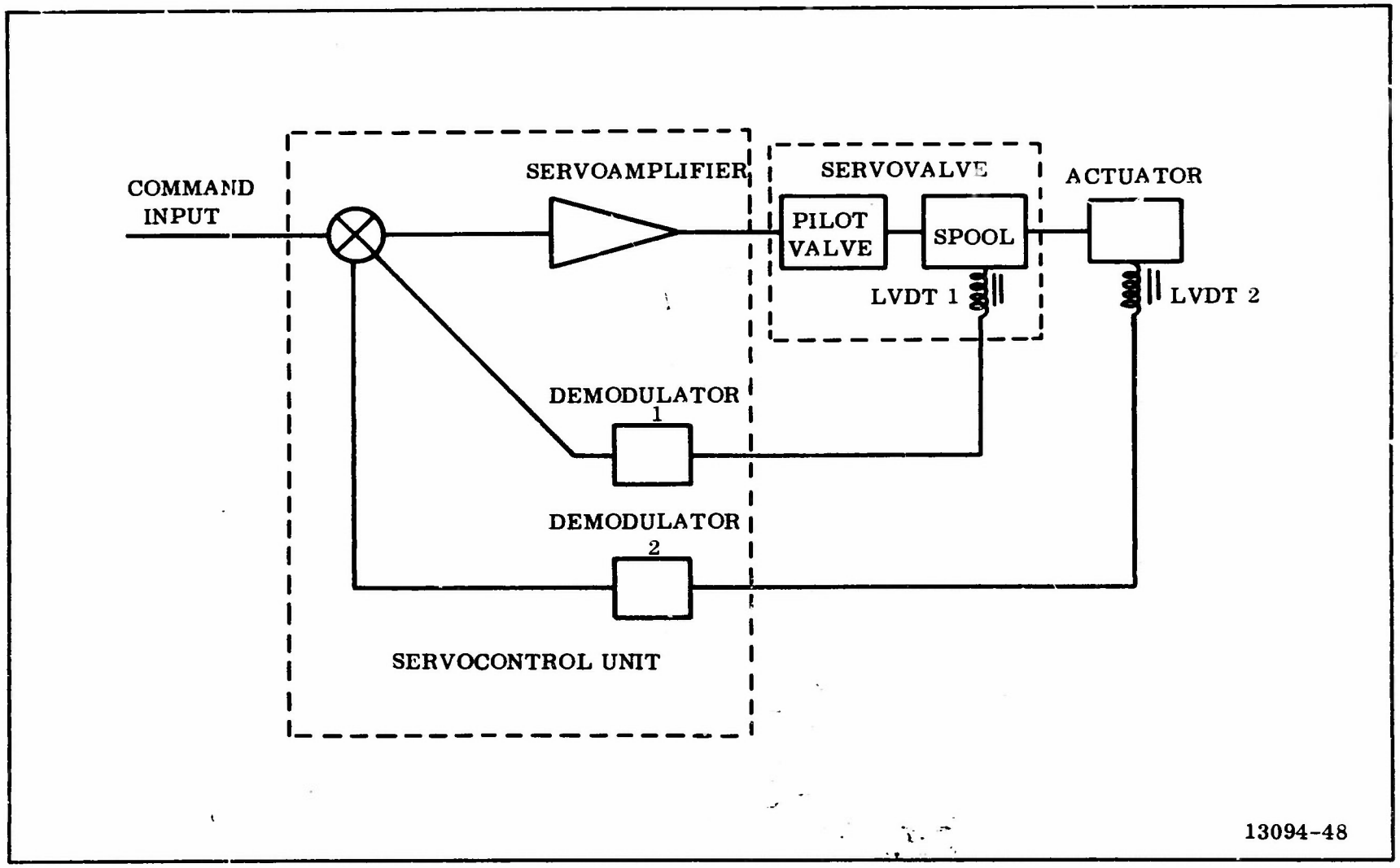

Figure 7-10. Servocontrol System

The three stage servovalve comes equipped with a Schaevitz 033-SSL transducer on the third stage spool. To verify operating characteristics of this transducer when excited with a 5 kc square wave, one of the units was received on consignment and checked out with the servocontrol unit electronics. Operation was satisfactory, and the scale factor under these conditions has been determined.

Feedback gain resistors have selected for nominal loop gains of 250 sec^{-1} in the minor loop and 50 sec^{-1} in the overall loop. The analog performance analysis shows this to provide a stable, high response system.

F. SYSTEM CHECKOUT

The servoactuators will be completely checked out by the fabrication and test vendor in accordance with specification STW-10-487. This testing includes a proof pressure test, leakage tests, transducer checks, and complete dynamic performance tests.

Because of the lack of pumping facilities, the only inhouse checkout will be performed in the test bay. This will consist of several complete simulated static tests using the entire hydraulic and electronic systems except that the actuators will not be attached to the motor. These tests will be used to adjust the servocontrol unit gains and to verify proper operation of the complete system. The hydraulic line loss under maximum flow will also be measured to determine the required no-flow system pressure setting.

After installation of the hydraulic system on the motor, a final dry run will be performed with the actuators disconnected from the clevises and rotated in the trunnion assemblies as necessary. This will constitute the final check on the actuation system prior to static test.

G. PLANNED DUTY CYCLE

The planned duty cycle is shown in Figure 7-11. This duty cycle produces a total side impulse of 1.37 percent of axial. The nozzle will be in the null position for 31.4 sec and will be vectored for 33.6 second. This duty cycle is still under study and is subject to revision.

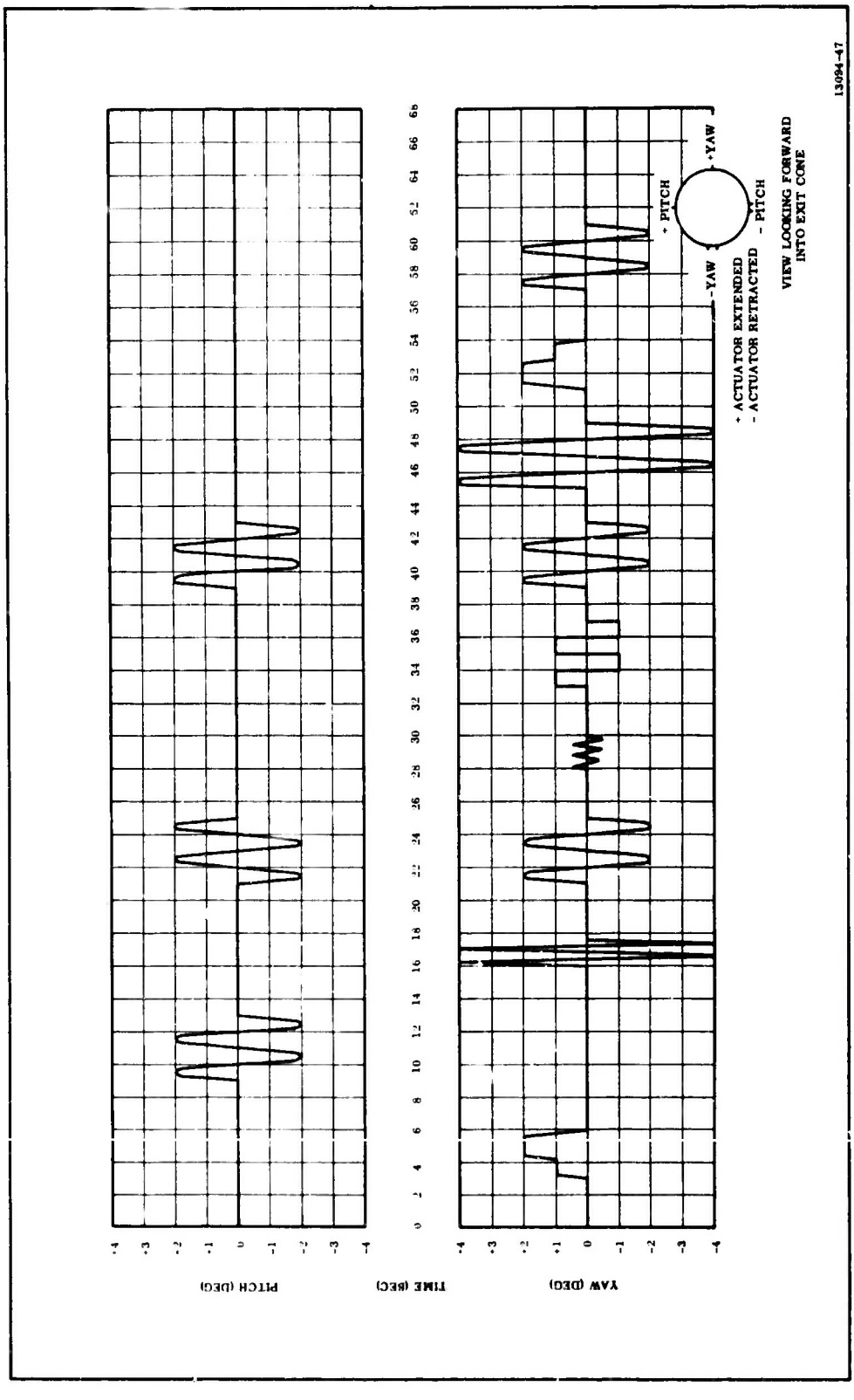

Figure 7-11. 156-9 Motor Duty Cycle

SECTION VIII

MOTOR FABRICATION

Processing of the 156-9 motor, which was scheduled to be initiated on 26 Sep, has not been started because of a delay in receipt of the GFE case.

SECTION IX

TOOLING

A. PROCESS TOOLING

In order to keep tooling cost at a minimum, as much use of existing tooling as possible has been planned. The majority of the new and modified tooling is required for propellant casting. Minor modifications to the handling equipment consists mainly of drilling and tapping holes in existing tooling to move brackets to accommodate a different case length. The design effort has been completed. Fabrication has started on all of the tooling with approximately 15 percent being completed. The vacuum casting fixtures arrangement shows the propellant casting tooling assembled for casting (Drawing 2U27972). The major modifications or new tools are described below.

1. CORE MODIFICATION, DRAWING 2U27994

To adapt the Lockheed Missile and Space Corporation core, Drawing T-11635, for casting propellant in the 156-9 motor, an aft end cover, a ring, and a cone section must be welded to the aft end. These items will form a portion of the coned section of the propellant grain and provide a means of positioning the slot formers. A locator ring and neoprene pad were placed on the forward end of the core to provide a vacuum seal against the insulation. The forward end was also drilled and tapped to accept a forward end core alignment stud.

2. CORE CAP, DRAWING 2U26010

The core cap bolts to the aft end cover of the modified core. It extends the core up to the aft end of the case and molds the major portion of the cored propellant grain.

3. CASTING DAM, DRAWING 2U27981

In order to net mold the propellant grain and eliminate machining of the propellant in the aft nozzle port, a casting dam was designed. During propellant casting the dam will be in a raised position allowing propellant to flow through the core cap out the aft nozzle port. After the motor has been filled with propellant, the casting dam will be remotely seated forming the remaining contour of the aft grain.

4. CASTING DAM SEATING AND REMOVAL TOOL, DRAWING 2U26028

Remote operation of the casting dam seating and removal tool is required because of the hazard involved. The tool consists of a framework and hydraulic ram. When actuated in the down direction it will force the casting dam downward in the aft propellant and seat the dam against the core cap. A reverse actuation, after propellant cure, will pop the casting dam free of the propellant grain.

5. VACUUM DOME ADAPTER, DRAWING 2U27973

To utilize the existing vacuum casting equipment which includes the vacuum dome used on the MINUTEMAN casting bells, an adapter was designed to mate the nozzle port flange to the vacuum casting bell dome. This adapter also serves as a nozzle port insulation mold during insulation installation.

6. SLOT FORMER, DRAWING 2U26005

The slot former is fabricated of urethane foam with a metal structure inside. The slot former is sectioned in pie shaped wedges allowing force to be selectively applied on the inner metal structure to remove the wedges after the propellant has been cured. Molds have been designed to form the segments during foaming operations.

7. ASTING HOPPER ADAPTER BASE, DRAWING 2U26038

Original plans were to use horizontal 300 gal. mixers for propellant casting. With the installation of a 600 gal. vertical mixer, however, a savings in propellant mixing and casting operations may be realized. To use the 600 gal. vertical mixer on this program an adapter to the 600 gal. casting hopper was designed and fabricated. This adapter mates to the 300 gal. hopper stand on the vacuum dome and to the stand supporting the 600 gal. casting hopper.

B. TEST TOOLING

1. COMPONENTS

Three types of tools are involved in the fabrication and test of this seal. They are simple drill rings for drilling bolt hole circles in metal rings, an assembly fixture or mold, and a test fixture.

a. Drill Rings--The drill rings are now being fabricated by Supreme Tool Co under subcontract from HITCO. These drill rings will be made available to the end ring machining vendor and used to drill the mating bolt hole patterns in the end rings. An additional drill fixture will be fabricated to drill the 40 holes around the periphery of the forward end ring, Part No. 7U40679-01.

b. Assembly Fixture--Thiokol designed two assembly fixtures. One was an open mold concept, Figure 9-1, and another was a closed mold concept, Figure 9-2. Either of these fixtures can be used but the closed fixture was selected on the basis of cost and schedule. A selection of the vendor has been made.

Prior to the design of these fixtures extensive tests were conducted in the materials laboratory which have determined the pressures at which rubber can be debulked cold or at elevated temperatures of 175°F. Maximum debulking pressures at which the spherical spacers will not damage the stainless steel shims have also been determined. The question of curing under pressure has also been investigated. This rubber formulation can be cured under pressure or without pressure, each giving the same physical properties. Because of the extensive tests we were able to consider an open mold approach. A contract to fabricate the assembly fixture will be negotiated with Reinhold by 25 December.

c. Test Fixture--Thiokol has designed a fixture in which to test the 156 in. flexible seal. This fixture (Figure 9-3) is now being fabricated by Lasker Boiler Works, Chicago, Illinois. The fixture provides two main features. With the -104 pin in place, the seal can be pressurized to pressures exceeding the planned motor MEOP. Thus the seal can be overpressurized without loading it in compression. This provides a test much more severe than would be encountered during firing. By removing the -104 pin and admitting pressure to the same cavity the seal will be subject to a blowout load similar to that achieved during static firing. The seal may be flexed through any duty cycle while in this mode.

All seals will be functionally tested in this fixture. The last Thiokol seal will be tested to an overpressure condition as well as flexed at a pressure equivalent to motor MEOP. Seal No. 2 will be tested to destruction.

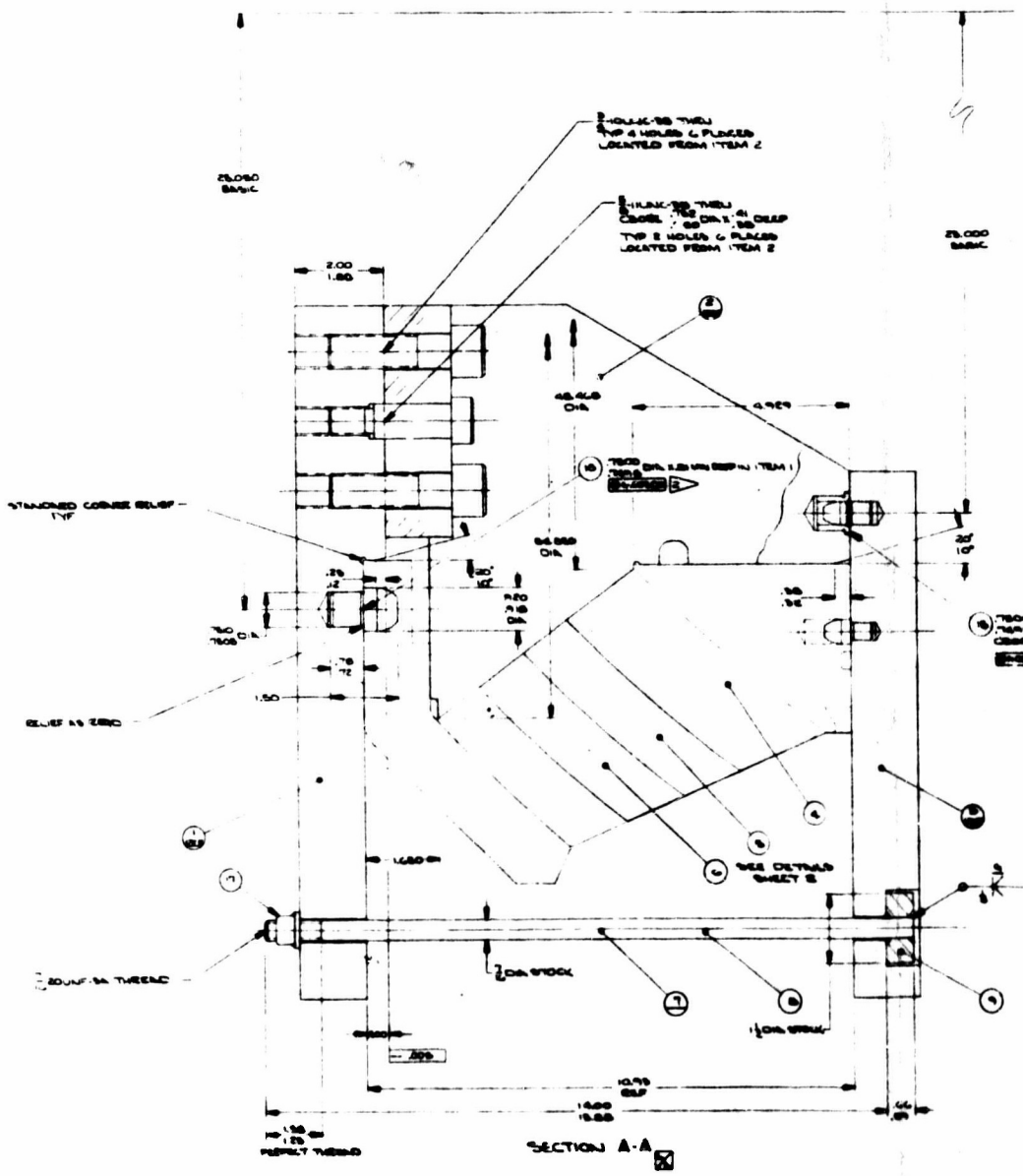

SECTION A-A

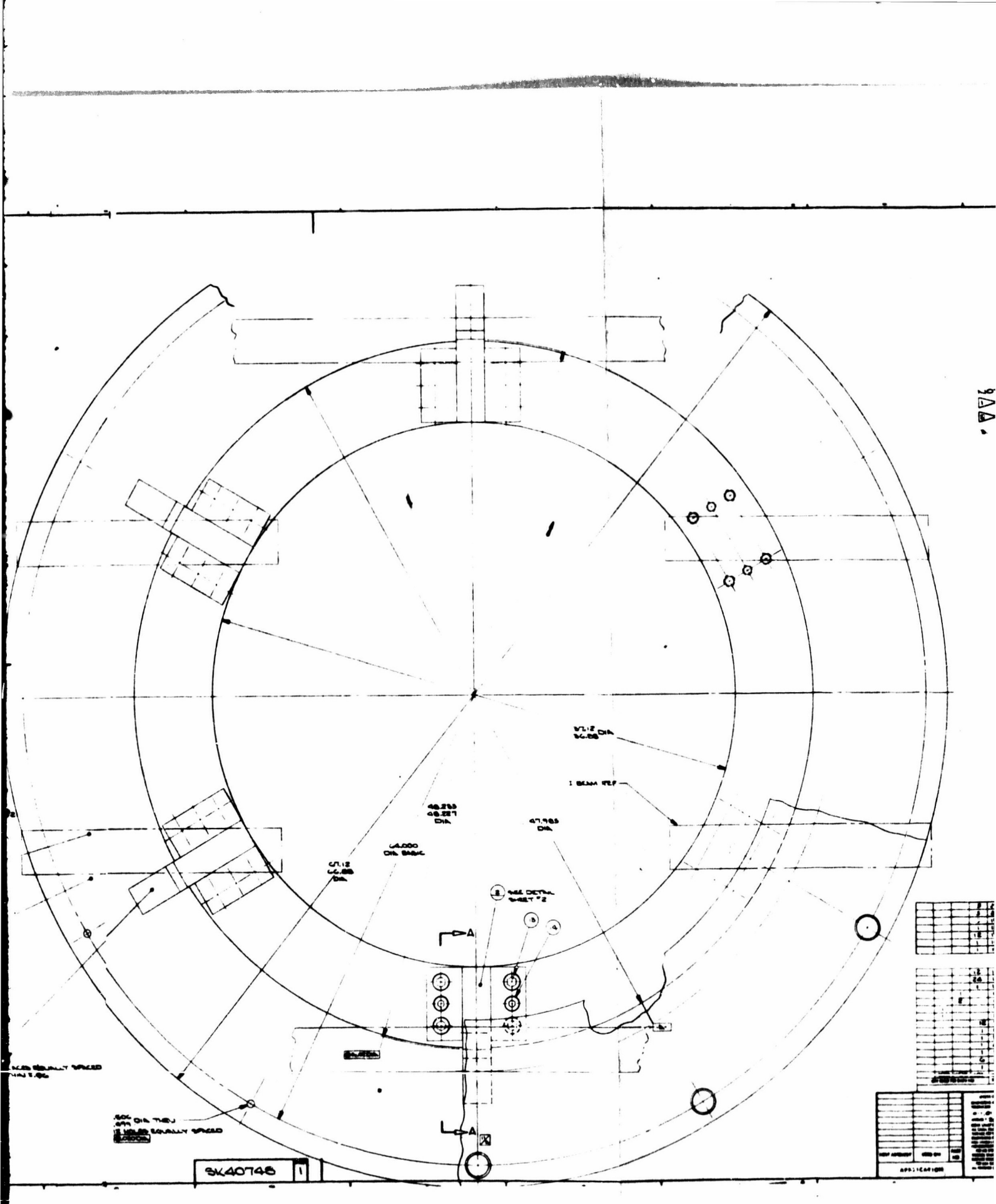

Figure 9-1. Flexible Seal As

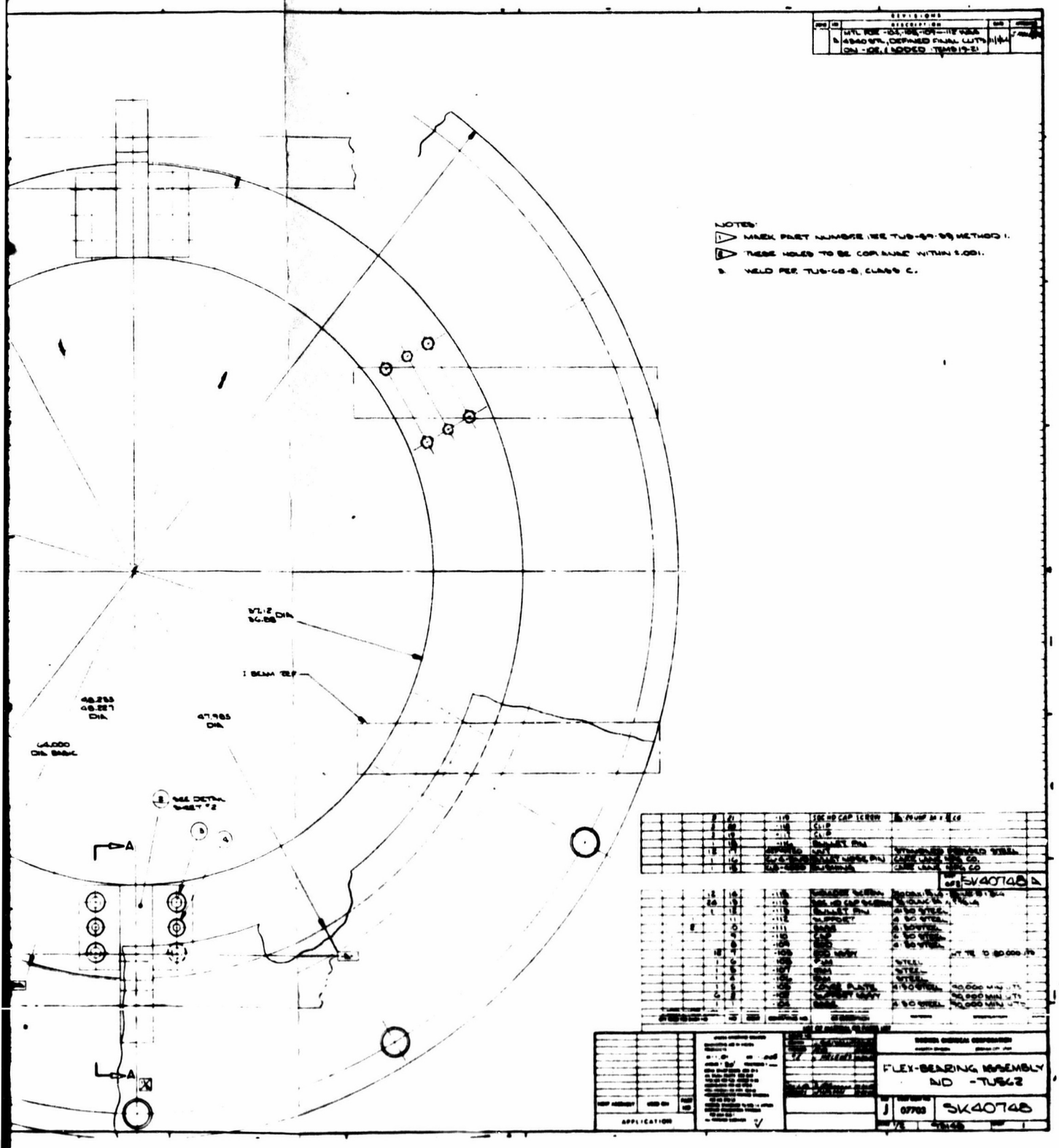

Figure 9-1. Flexible Seal Assembly Fixture (Open) (Sheet 1 of 2)

3

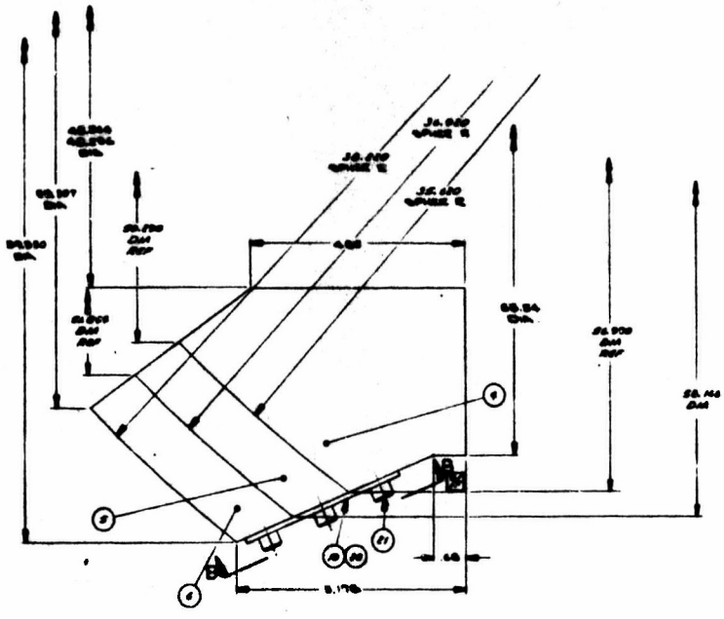

DETAIL OF ITEMS 4, 5 & 6
SCALE: 1/1

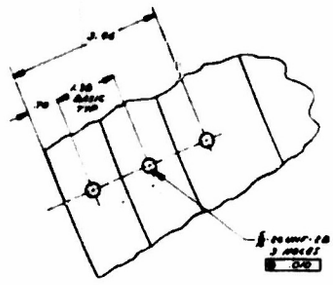

VIEW B-B
SCALE: NONE
TYP 3 PLACES NO ARROW
CLIP OMITTED FOR CLARITY

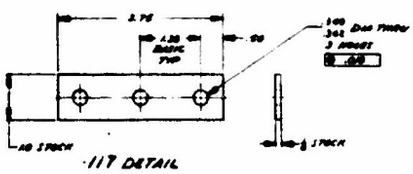

-117 DETAIL

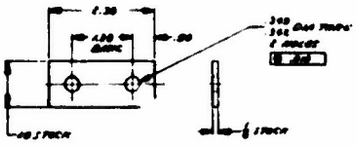

-118 DETAIL

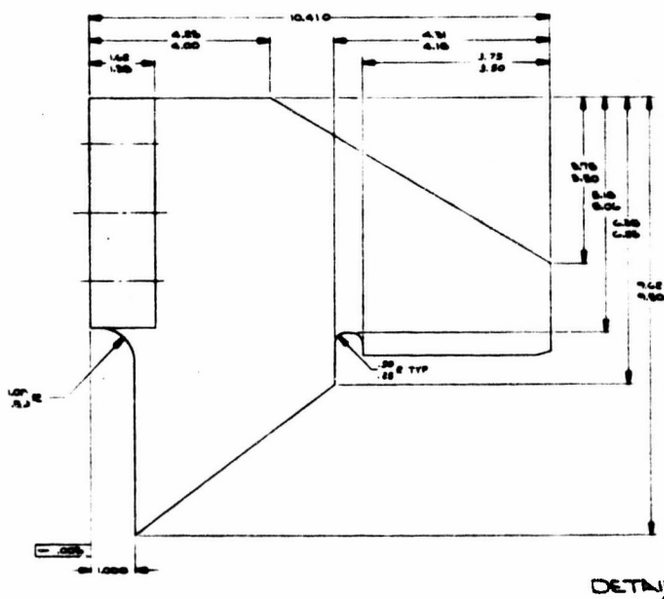

DETAIL OF ITEM 2
SCALE: 1/1

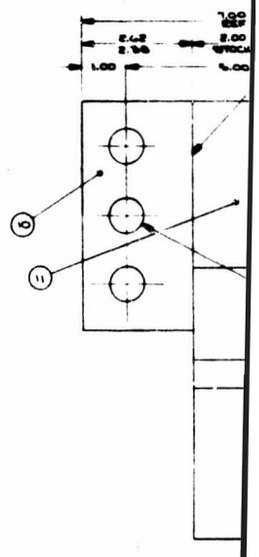

1

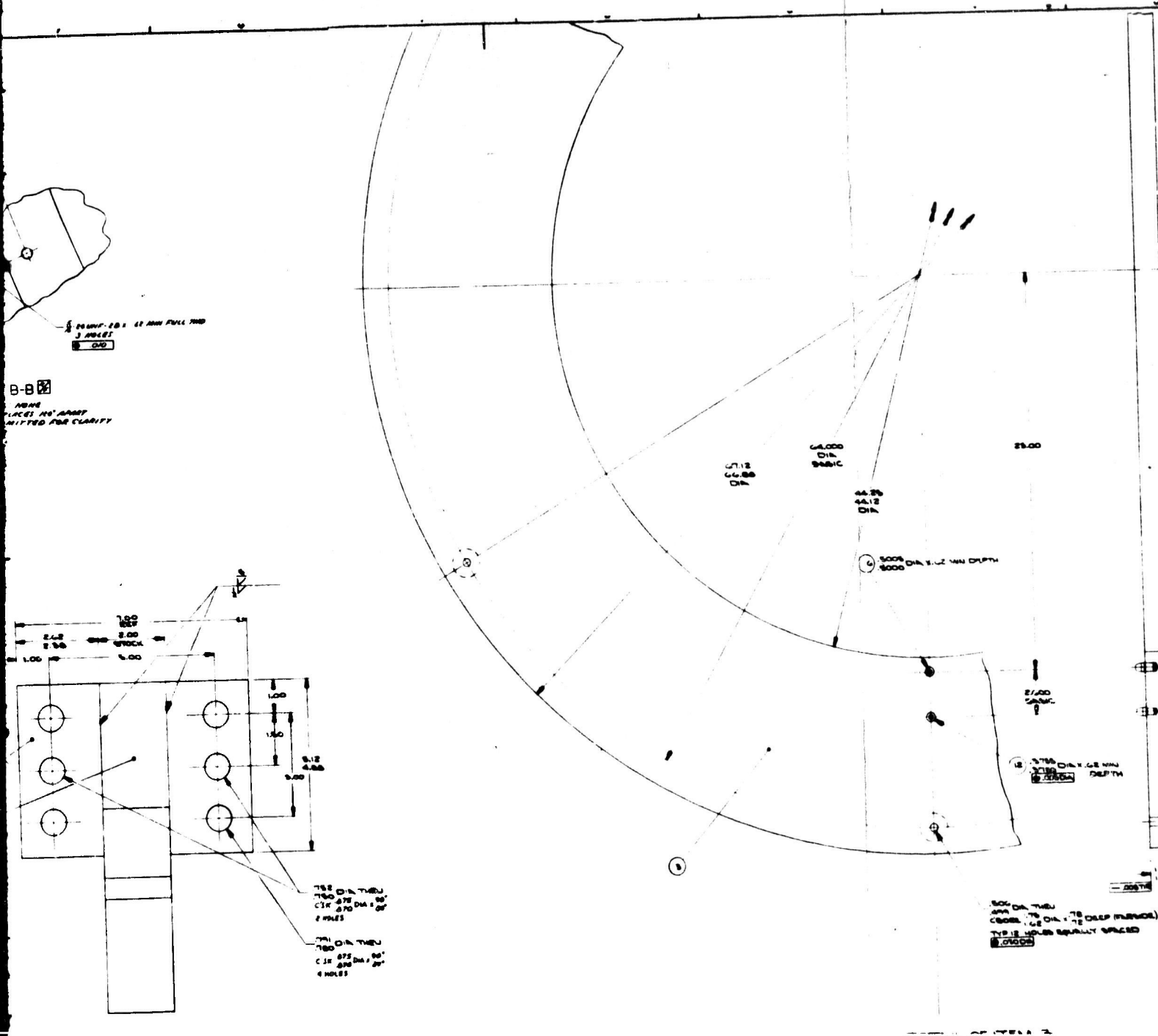

Figure 9-1. Fl

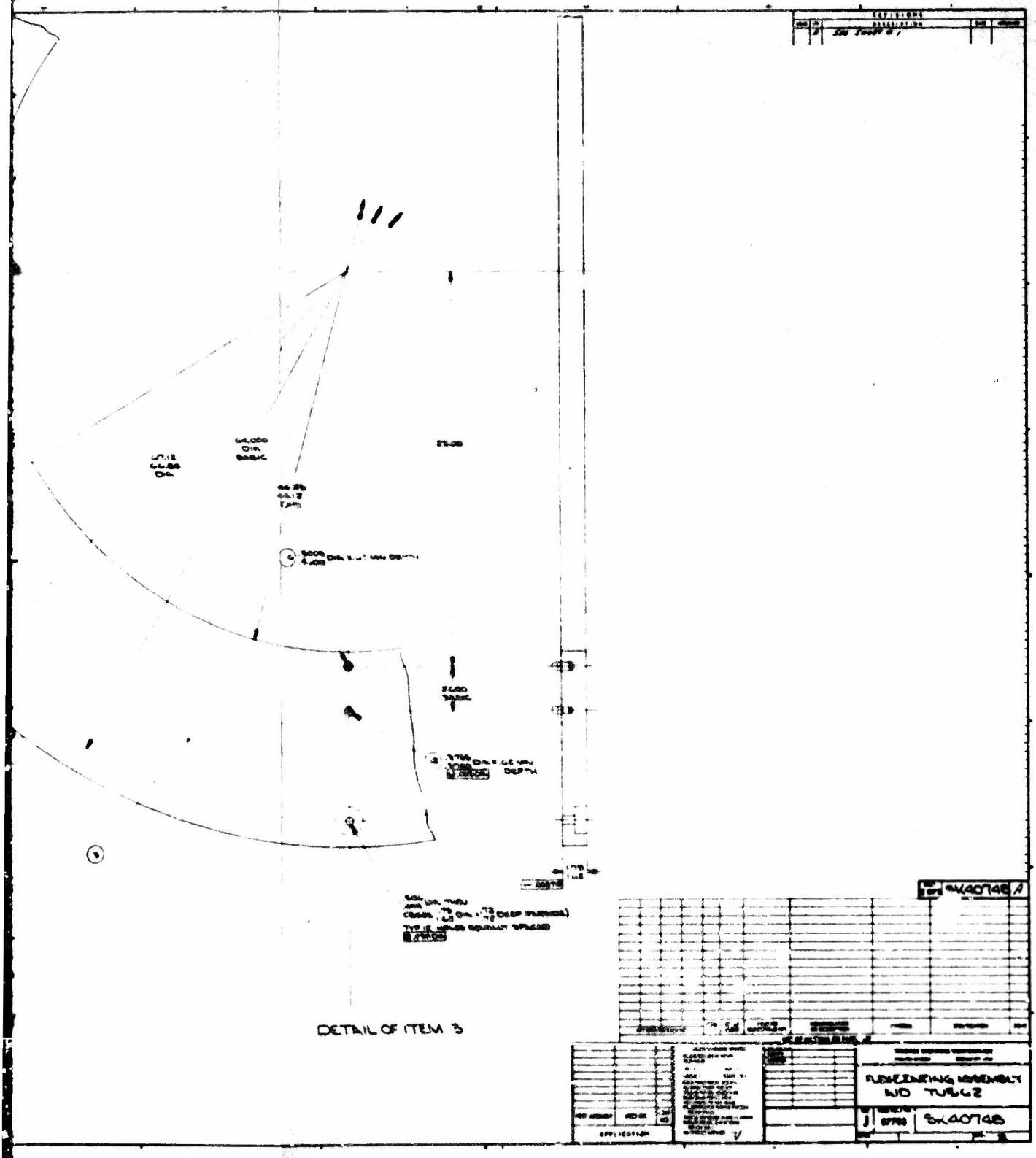

Figure 3-1. Flexible Seal Assembly Fixture (Open) (Sheet 2 of 2)

3

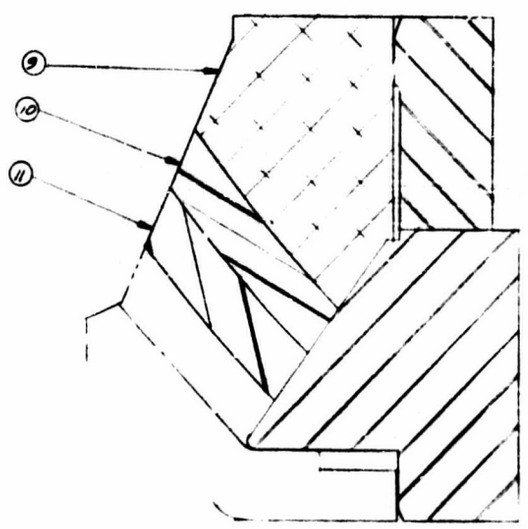

VIEW SHOWING USAGE OF TRACK 9, 10 & 11 IN DISMANTLING OPERATION

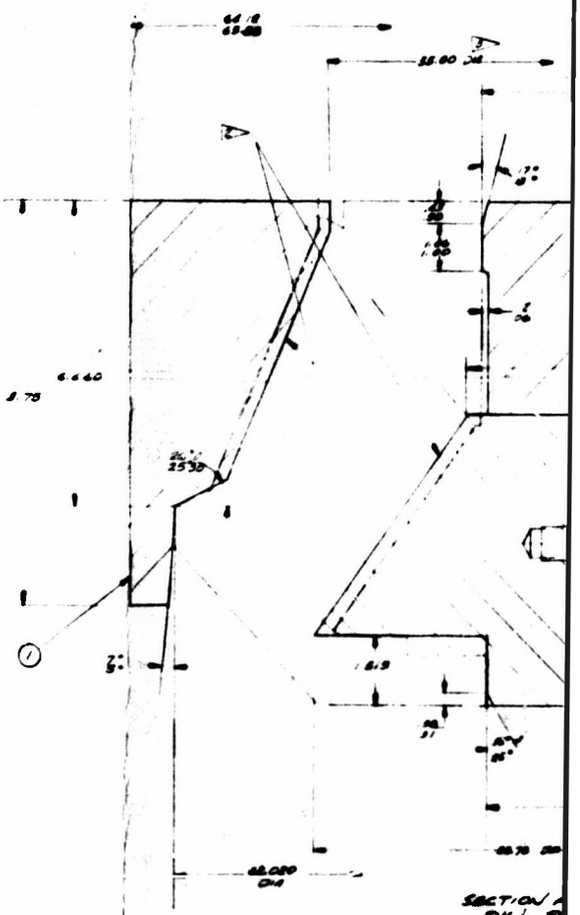

SECTION A
FULL SC

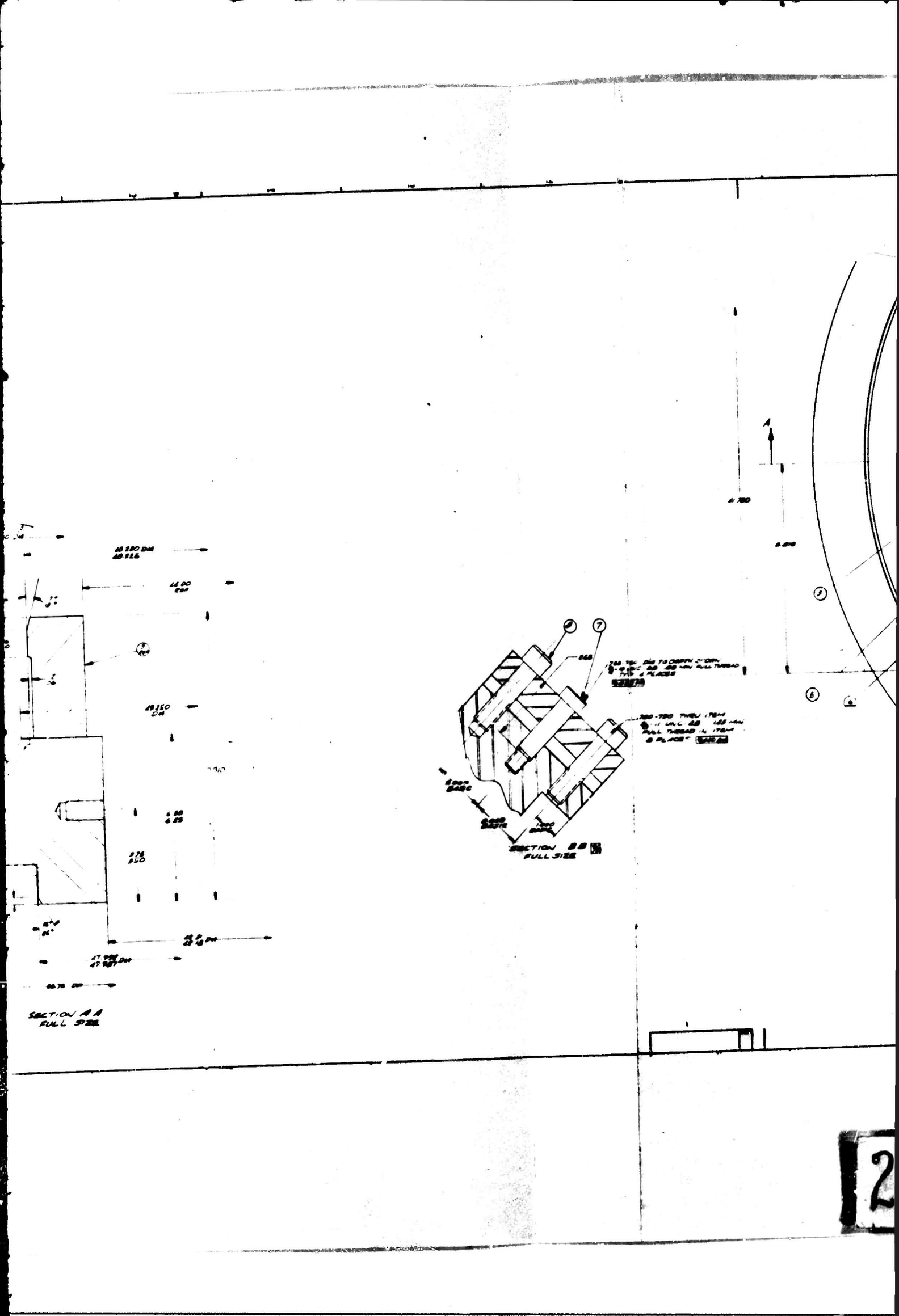
SECTION AA
FULL SIZE
SECTION BB
FULL SIZE

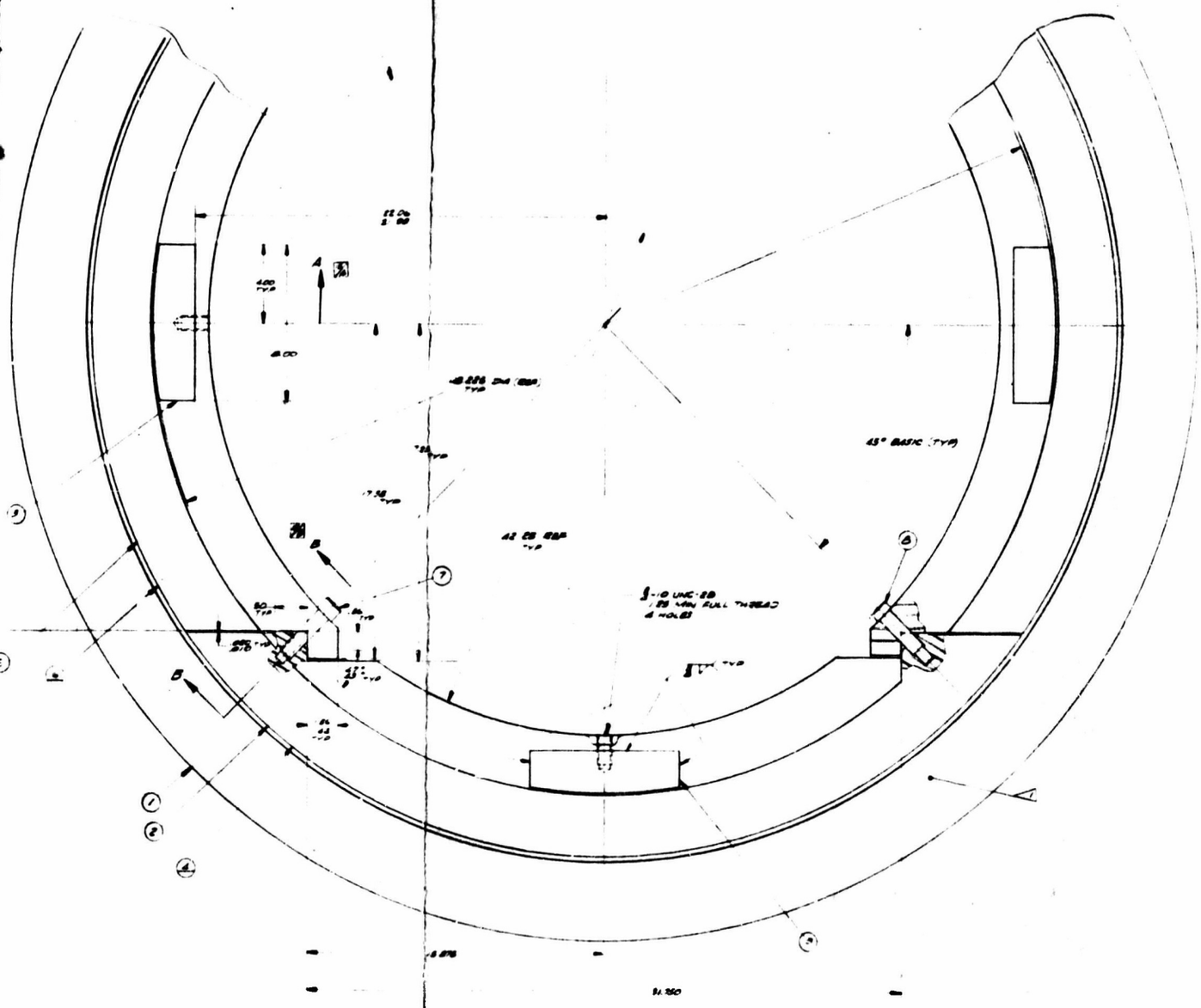

3

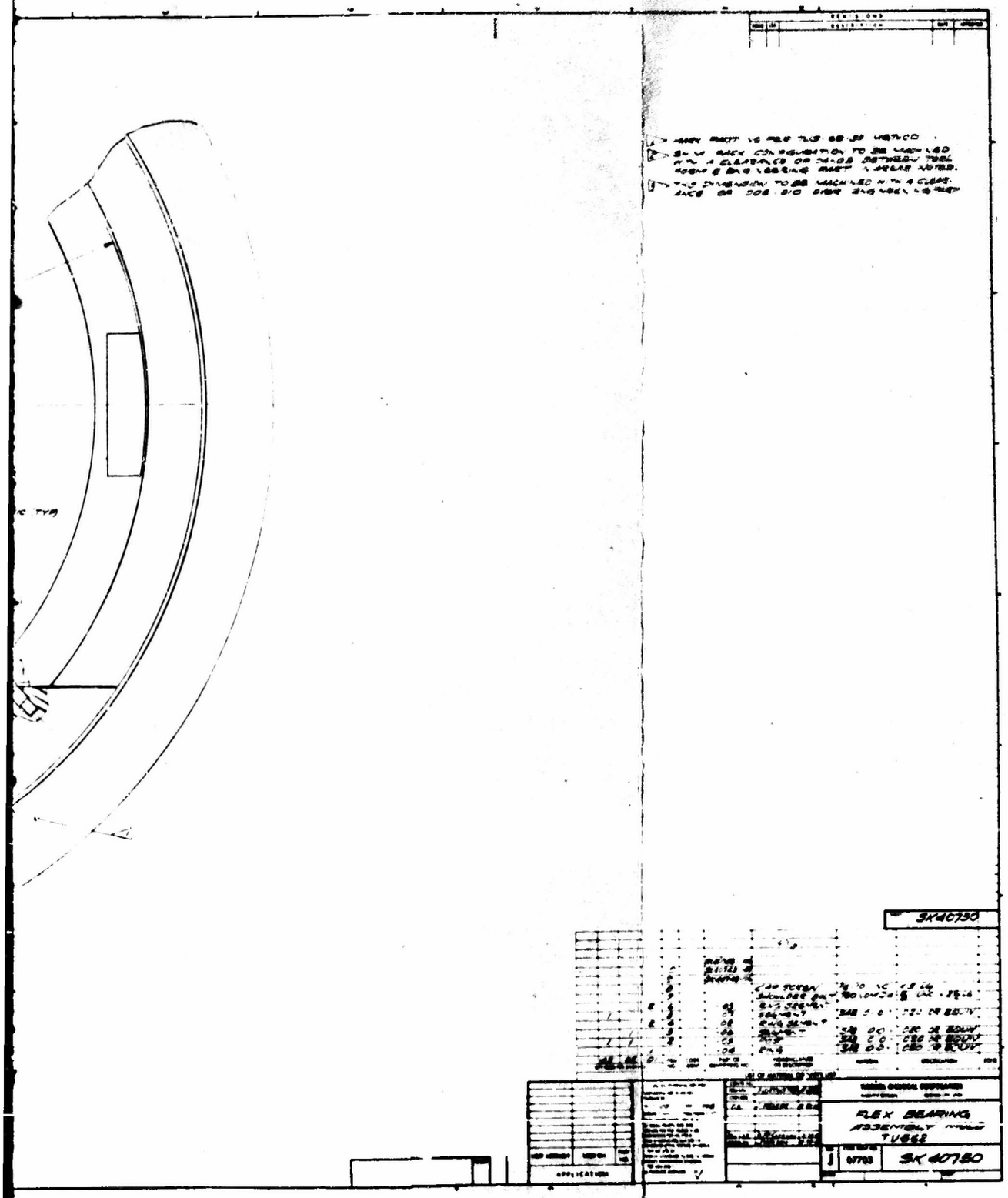

Figure 9-2. Flexible Seal Assembly Fixture (Closed Mold)

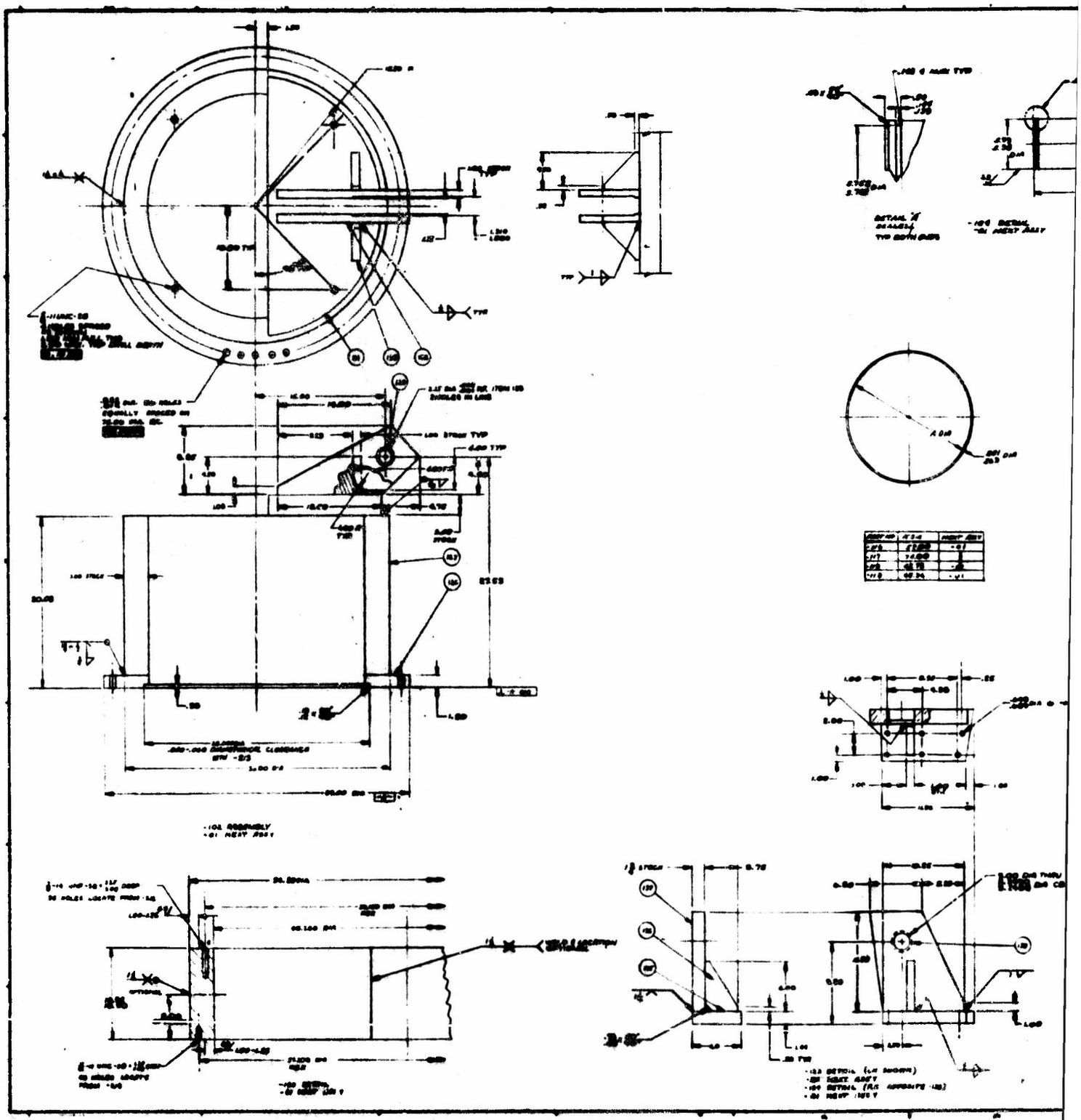

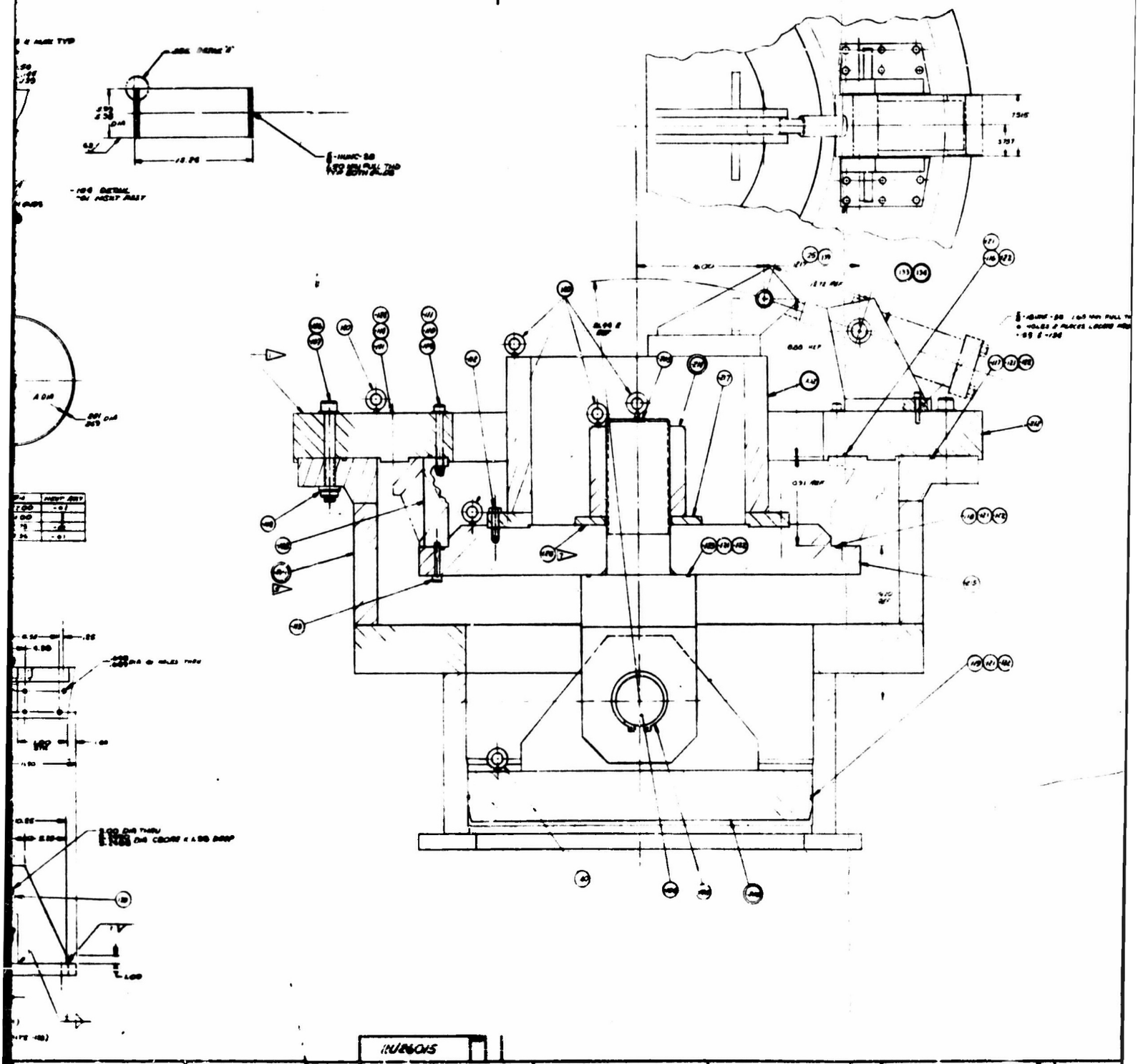

Figure

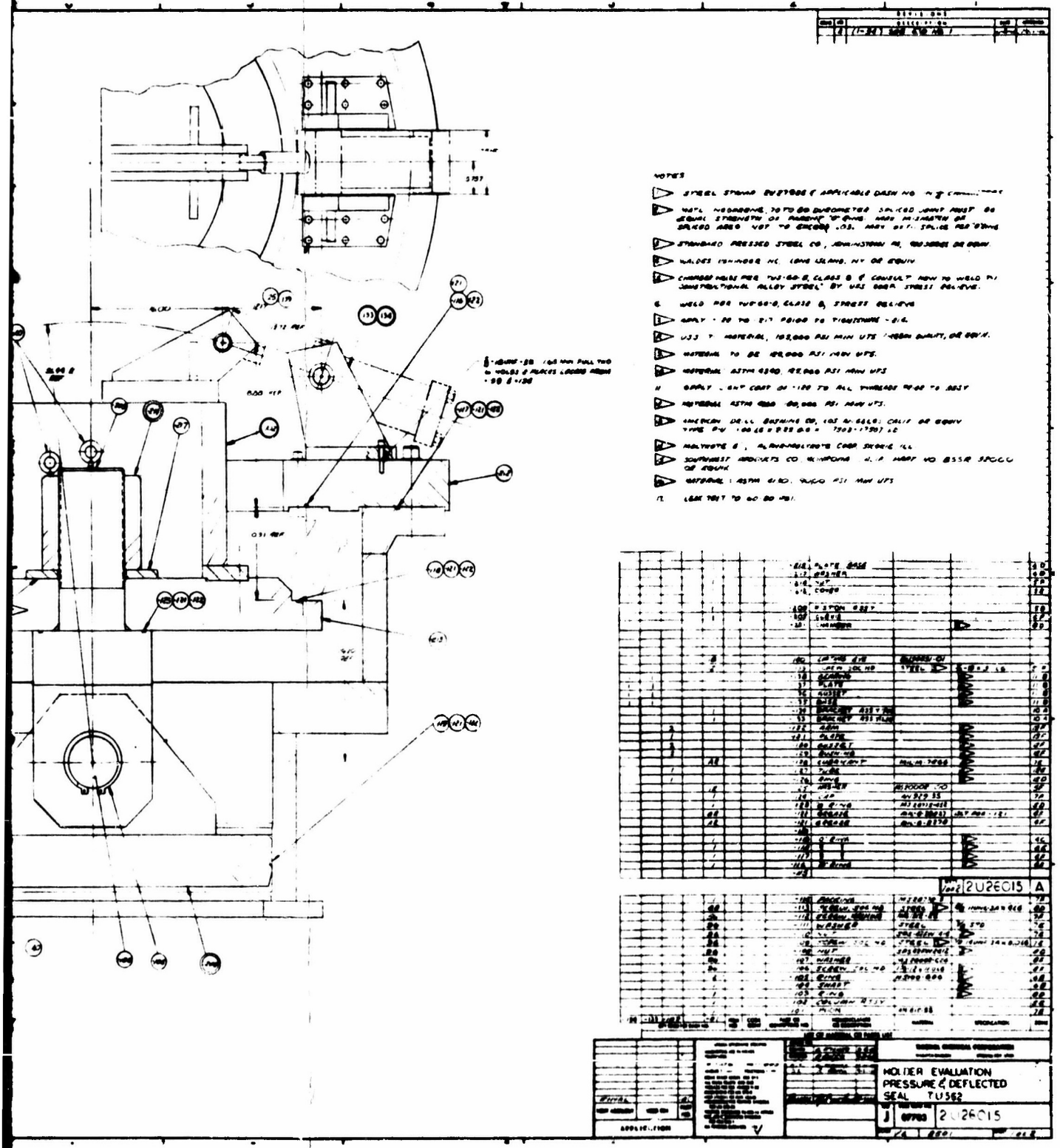

Figure 9-3. Flexible Seal Test Fixture (Sheet 1 of 2)

3

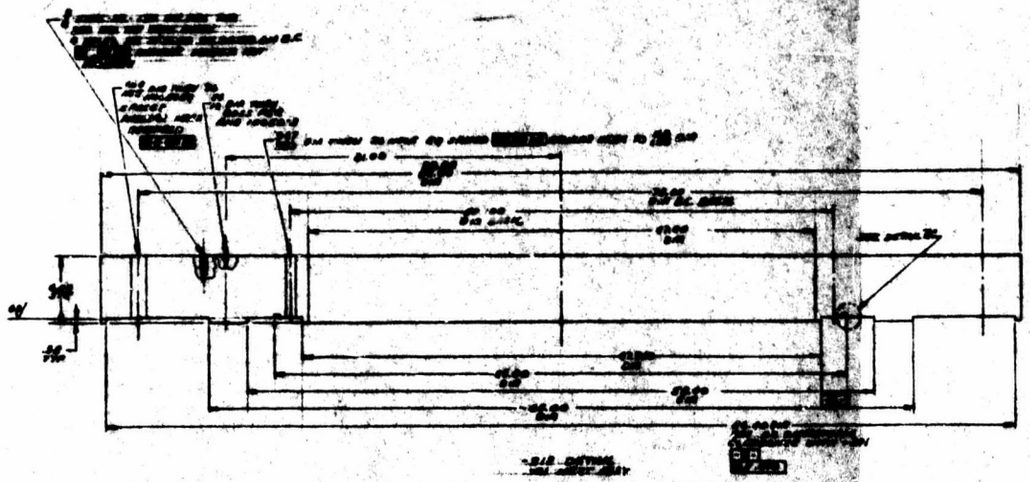

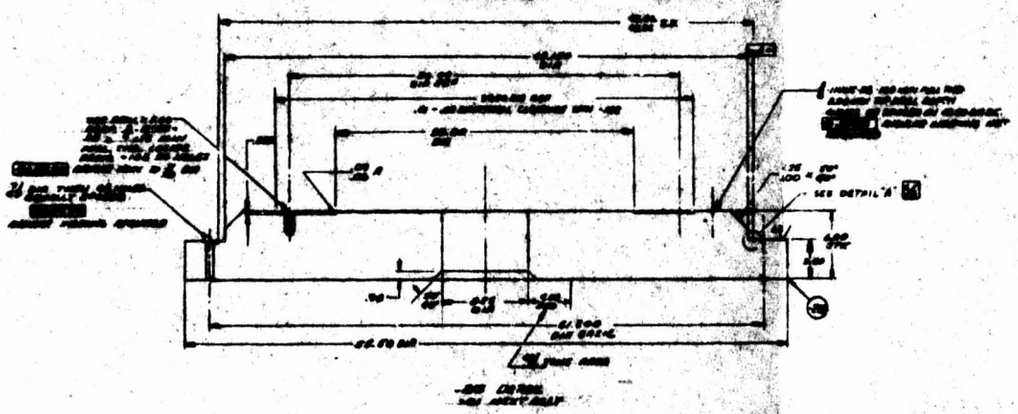

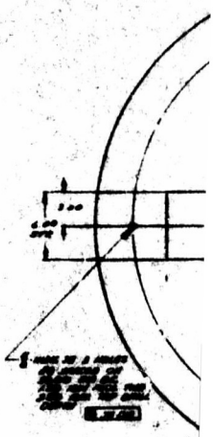

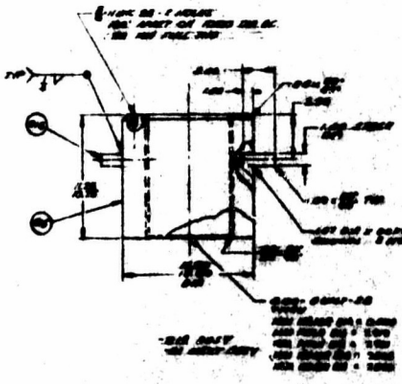

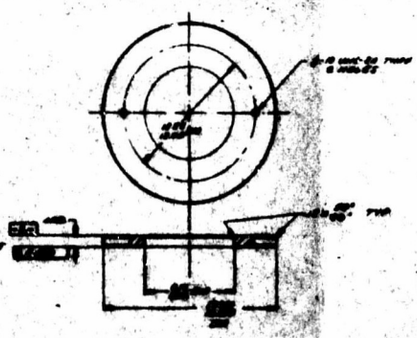

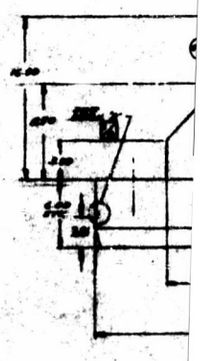

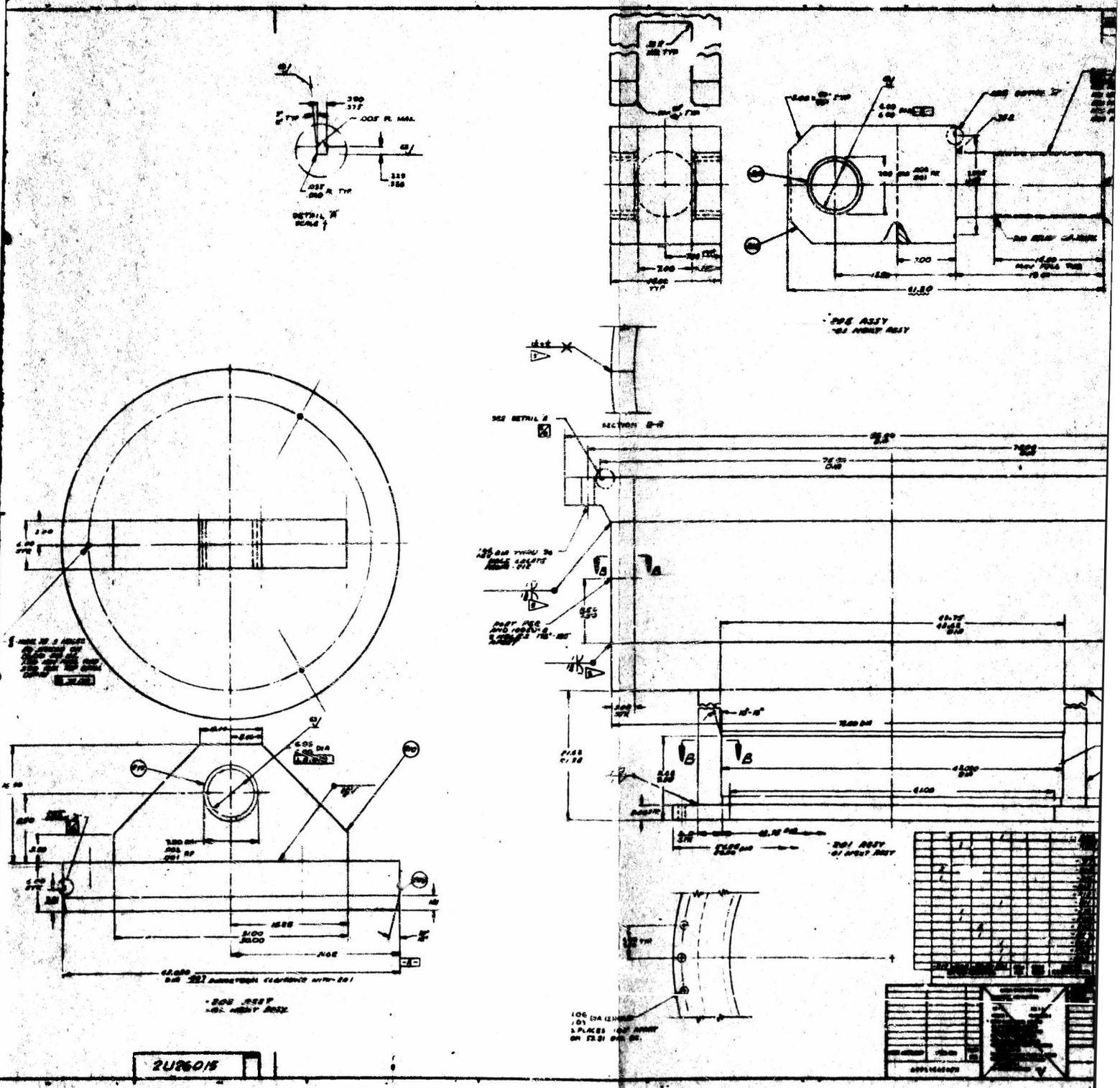

Figure 9-3. Flexible Seal T

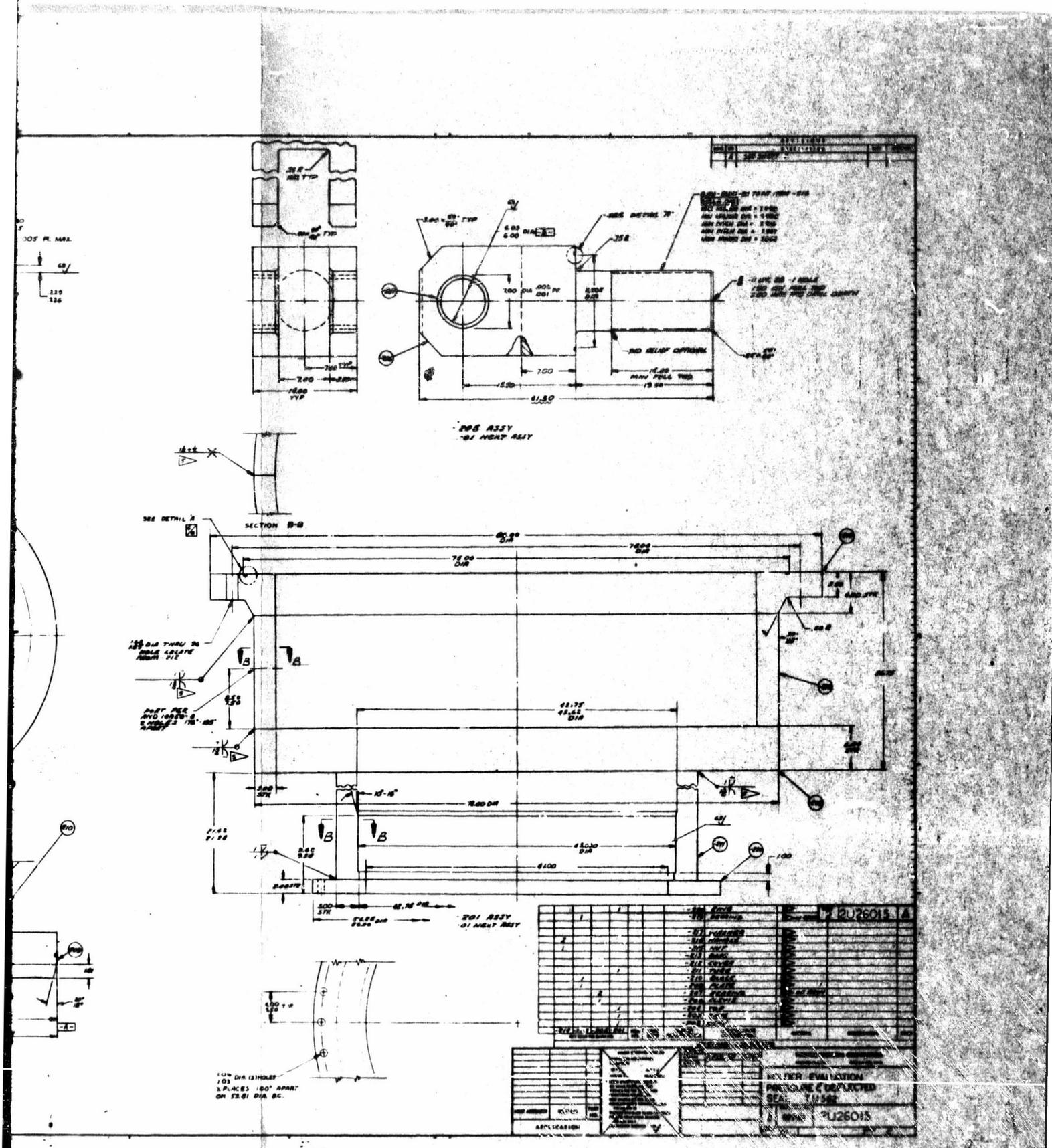

Figure 9-3. Flexible Seal Test Fixture (Sheet 3 of 2)

3

2. ACTUATION SYSTEM TEST FIXTURE

A servoactuator checkout fixture has been designed for use in simulating expected loads on the actuator. The fixture, shown in Figure 9-4 will be used to restrain the actuator during proof pressure and internal leakage tests. By completing operational checkout tests using the test fixture, only functional tests of the actuation system will be required after the servoactuators are installed on the motor.

3. ANTIFLIGHT SYSTEM

A motor restraint assembly to retain the motor in the test bay in case of motor malfunction will utilize a system of restraining cables. This system is similar in nature to restraining systems that are used throughout the solid propellant rocket industry. Excessive upward movement is restrained by three cable assemblies retained in light channel guides; axial restraint is provided by a tension-compression load train and four restraining cables fastened between the aft harness ring and the test bay.

4. POST TEST QUENCH SYSTEM

A head end carbon dioxide quench system is planned for use in extinguishing post fire insulation burning on the 156-9 motor test. It has been calculated that 2,030 lb of carbon dioxide will be required to cool the nozzle to ambient temperature and 1,950 lb of carbon dioxide will be required to cool the case insulation. This results in a total carbon dioxide requirement of 3,980 pounds. The carbon dioxide facility at Thiokol's test area has a weight capability of 8,000 pounds. Using the 300 psi facility carbon dioxide pressure, the quench system using the ports shown on Figure 6-1 will inject 2,000 lb of carbon dioxide into the motor in 2.5 min, 4,000 lb in 4.8 min, and the total 8,000 lb in 10 minutes. The carbon dioxide injection will start immediately after motor tailoff and will continue until 8,000 lb of carbon dioxide

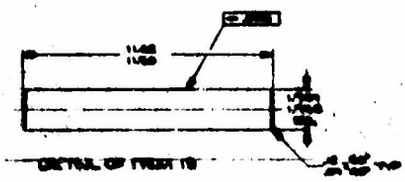

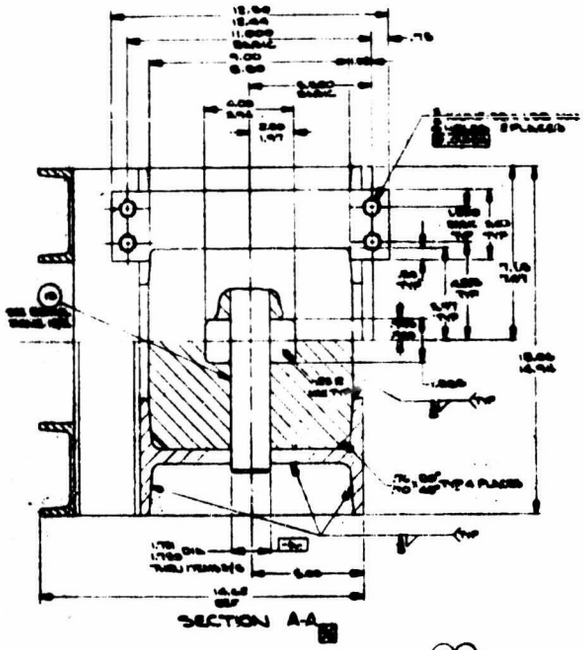
SECTION A-A

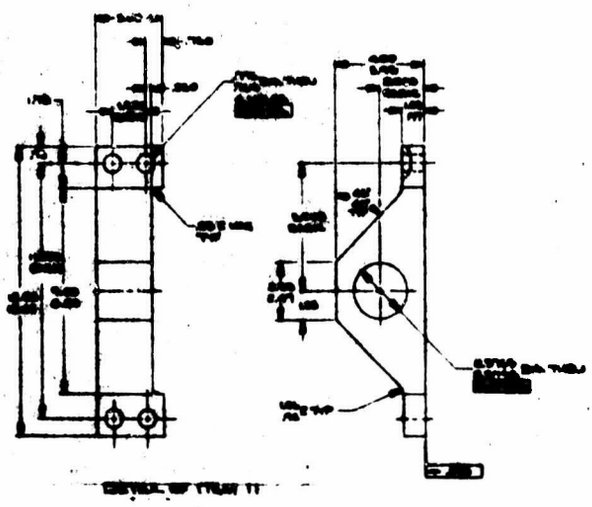

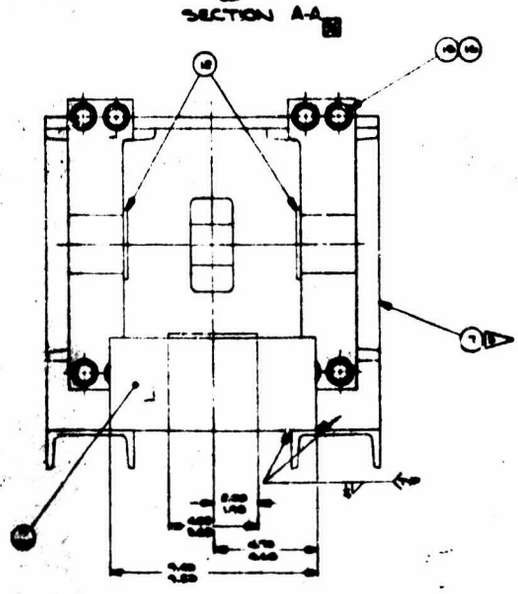

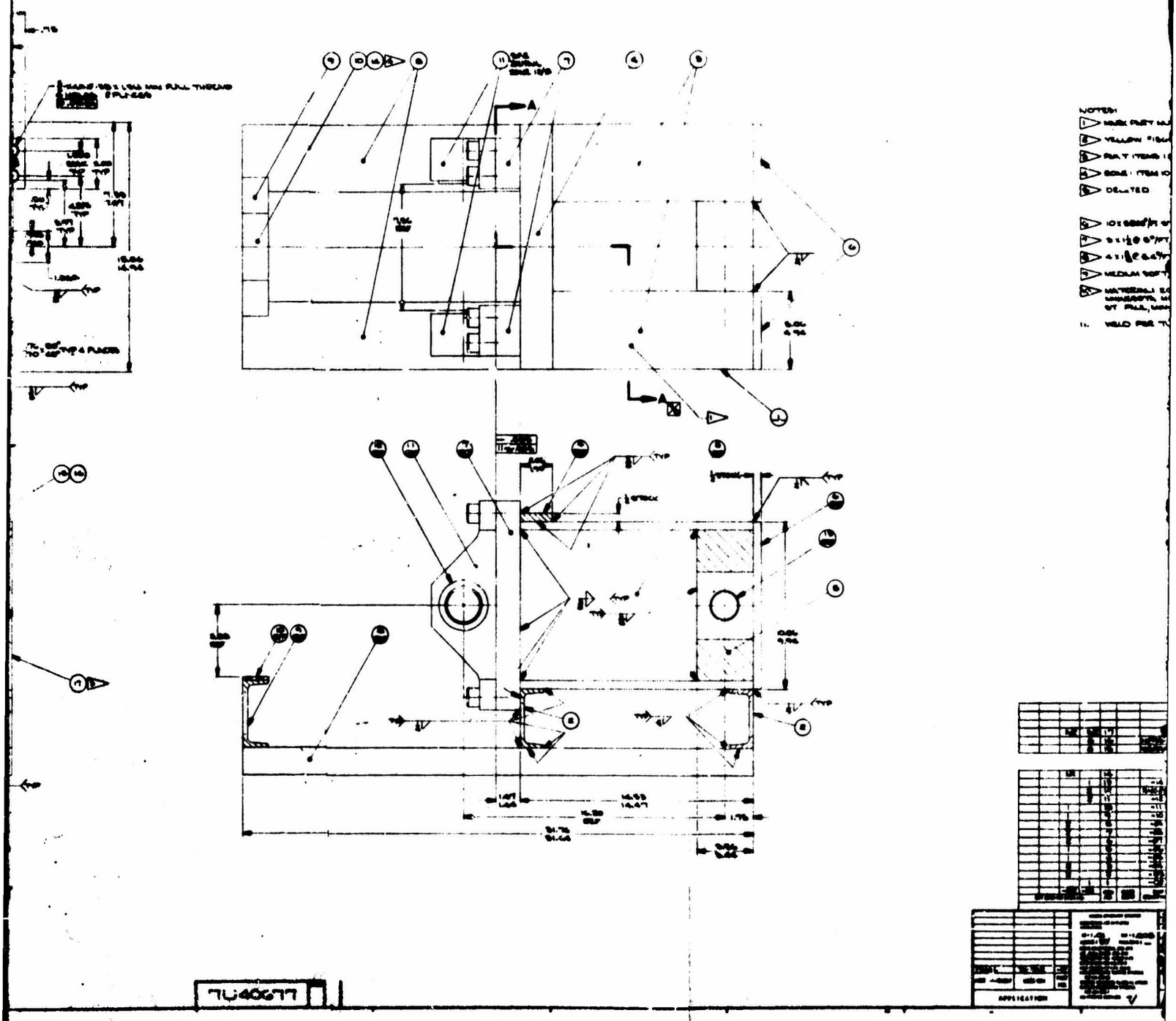

Figure 9-4. Sc

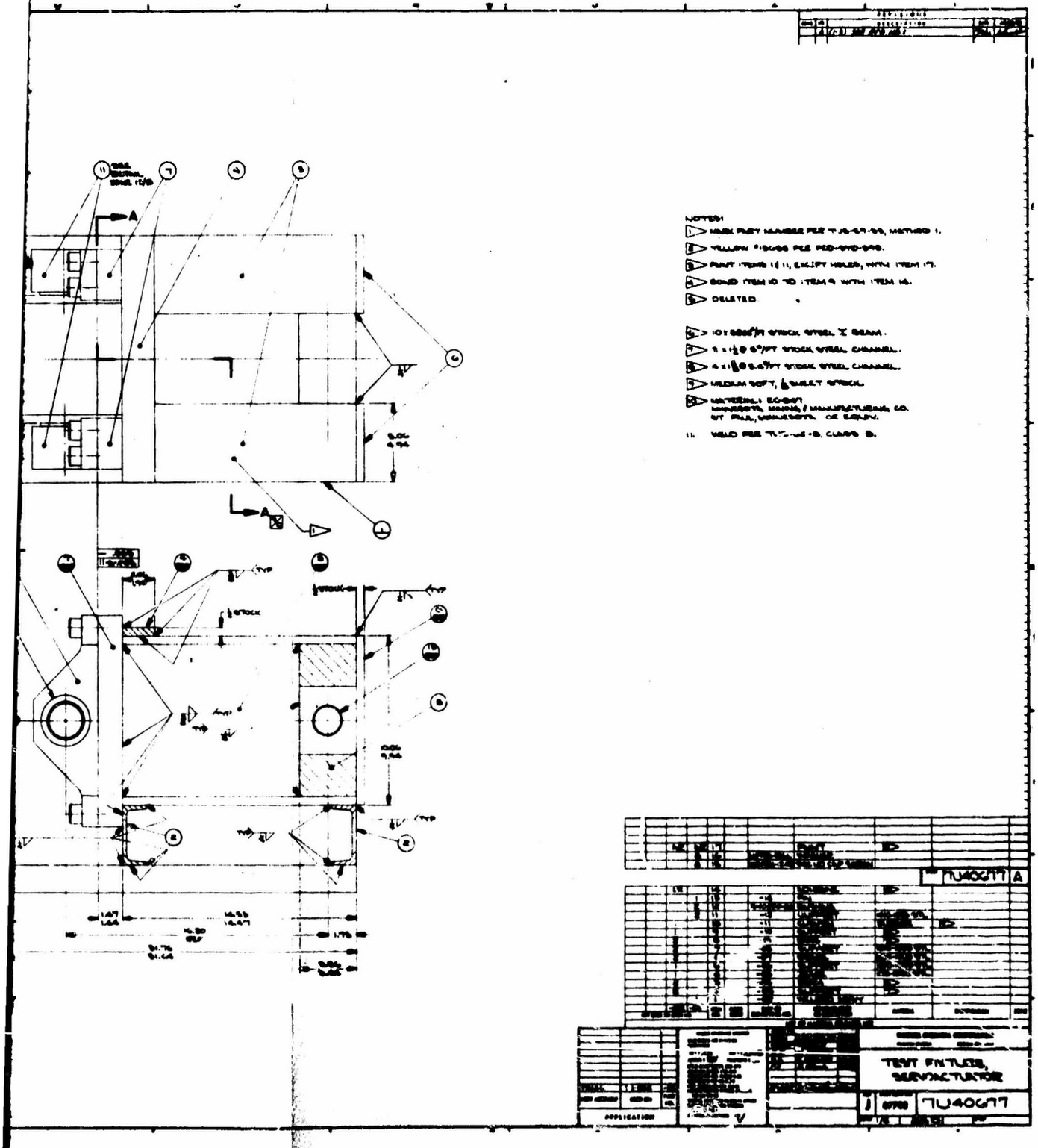

Figure 9-4. Servoactuator Test Fixture

3

have been injected into the motor. This system is similar to the quench system to be used on the 156-8 motor firing.

SECTION X

MOTOR TESTING

No motor test activities were scheduled during this reporting period.

SECTION XI

PROGRAM SCHEDULE

The period of performance covered by this report extends from 1 Jul through 31 Oct 1966. The contract provides for static testing the 156-9 demonstration motor within 240 days of the contract date. The program schedule (Figure 11-1) shows that the 156-9 motor will be tested on 7 Mar 1967. This schedule reflects actual performance through 31 Oct 1966 and planned performance through the remainder of the program.

A. ANALYSIS OF EFFORT ON MAJOR TASKS

1. MOTOR AND COMPONENT DESIGN

The following designs were submitted to the Air Force during this report period.

1. Motor Design
2. Nozzle Design
3. Insulation and Liner Design
4. Ignition System Design
5. Grain/Propellant Design
6. TVC Actuation System Design
7. Nozzle Material Design Change

2. NOZZLE AND SEAL FABRICATION

The 156-9 nozzle is being fabricated by H. L. Thompson Co (HITCO). All tooling is complete and fabrication is proceeding on schedule. Welding of steel parts is complete and final machining is in process.

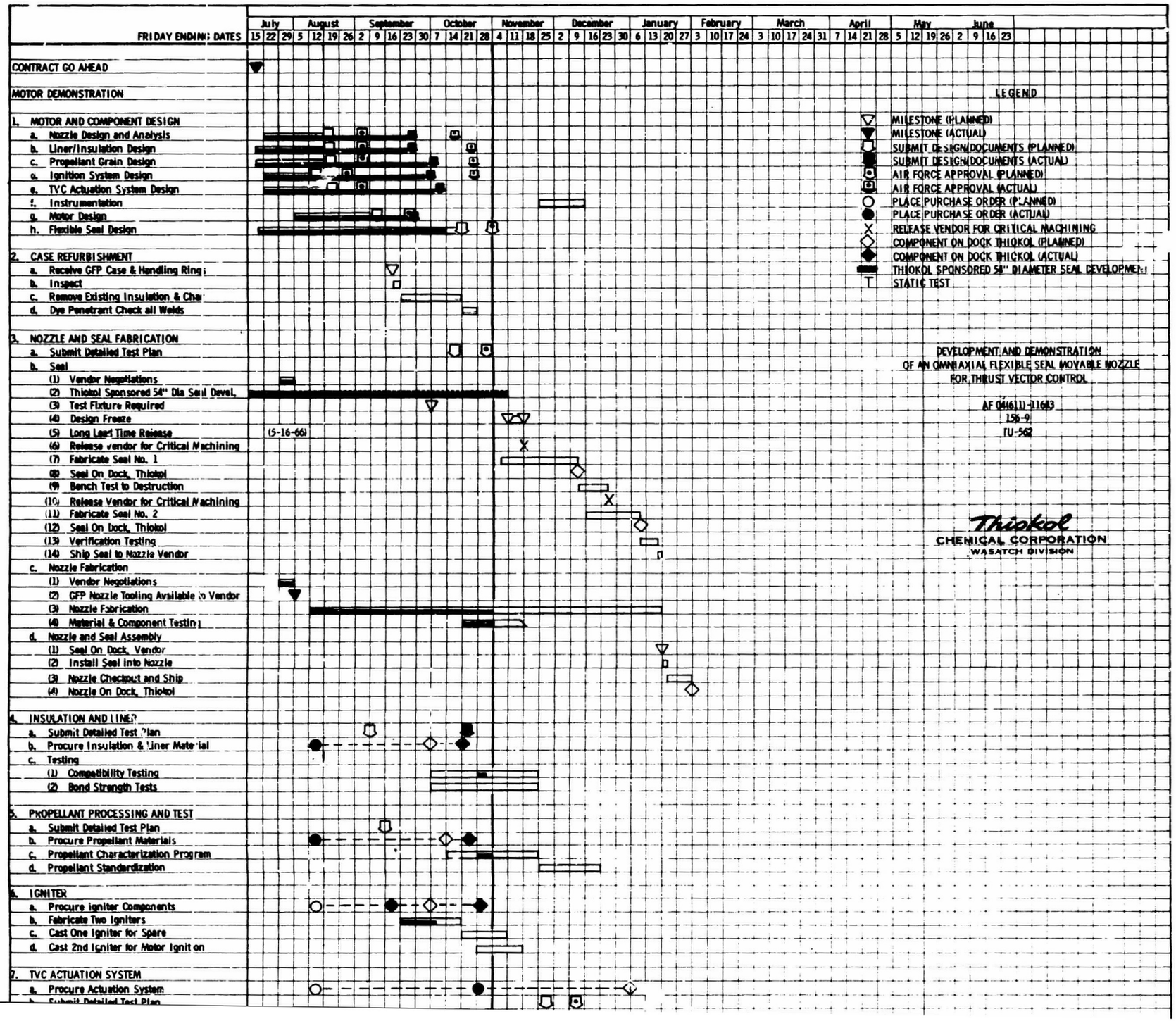
FRIDAY ENDING DATES
July 15 22 29
August 5 12 19 26
September 2 9 16 23 30
October 7 14 21 28
November 4 11 18 25
December 2 9 16 23 30
January 6 13 20 27
February 3 10 17 24
March 3 10 17 24 31
April 7 14 21 28
May 5 12 19 26
June 2 9 16 23
CONTRACT GO AHEAD
MOTOR DEMONSTRATION
1. MOTOR AND COMPONENT DESIGN
a. Nozzle Design and Analysis
b. Liner/Insulation Design
c. Propellant Grain Design
d. Ignition System Design
e. TVC Actuation System Design
f. Instrumentation
g. Motor Design
h. Flexible Seal Design
2. CASE REFURBISHMENT
a. Receive GFP Case & Handling Rings
b. Inspect
c. Remove Existing Insulation & Cha
d. Dye Penetrant Check all Welds
3. NOZZLE AND SEAL FABRICATION
a. Submit Detailed Test Plan
b. Seal
(1) Vendor Negotiations
(2) Thiokol Sponsored 54" Dia Seal Devel.
(3) Test Fixture Required
(4) Design Freeze
(5) Long Lead Time Release
(5-16-66)
(6) Release Vendor for Critical Machining
(7) Fabricate Seal No. 1
(8) Seal On Dock, Thiokol
(9) Bench Test to Destruction
(10) Release Vendor for Critical Machining
(11) Fabricate Seal No. 2
(12) Seal On Dock, Thiokol
(13) Verification Testing
(14) Ship Seal to Nozzle Vendor
c. Nozzle Fabrication
(1) Vendor Negotiations
(2) GFP Nozzle Tooling Available to Vendor
(3) Nozzle Fabrication
(4) Material & Component Testing
d. Nozzle and Seal Assembly
(1) Seal On Dock, Vendor
(2) Install Seal into Nozzle
(3) Nozzle Checkout and Ship
(4) Nozzle On Dock, Thiokol
4. INSULATION AND LINER
a. Submit Detailed Test Plan
b. Procure Insulation & Liner Material
c. Testing
(1) Compatibility Testing
(2) Bond Strength Tests
5. PROPELLANT PROCESSING AND TEST
a. Submit Detailed Test Plan
b. Procure Propellant Materials
c. Propellant Characterization Program
d. Propellant Standardization
6. IGNITER
a. Procure Igniter Components
b. Fabricate Two Igniters
c. Cast One Igniter for Spare
d. Cast 2nd Igniter for Motor Ignition
7. TVC ACTUATION SYSTEM
a. Procure Actuation System
LEGEND
MILESTONE (PLANNED)
MILESTONE (ACTUAL)
SUBMIT DESIGN/DOCUMENTS (PLANNED)
SUBMIT DESIGN/DOCUMENTS (ACTUAL)
AIR FORCE APPROVAL (PLANNED)
AIR FORCE APPROVAL (ACTUAL)
PLACE PURCHASE ORDER (PLANNED)
PLACE PURCHASE ORDER (ACTUAL)
RELEASE VENDOR FOR CRITICAL MACHINING
COMPONENT ON DOCK THIOKOL (PLANNED)
COMPONENT ON DOCK THIOKOL (ACTUAL)
THIOKOL SPONSORED 54" DIAMETER SEAL DEVELOPMENT
STATIC TEST
DEVELOPMENT AND DEMONSTRATION
OF AN OMNIAXIAL FLEXIBLE SEAL MOVABLE NOZZLE
FOR THRUST VECTOR CONTROL
AF 04(611)-11643
156-9
TU-562
Thiokol
CHEMICAL CORPORATION
WASATCH DIVISION

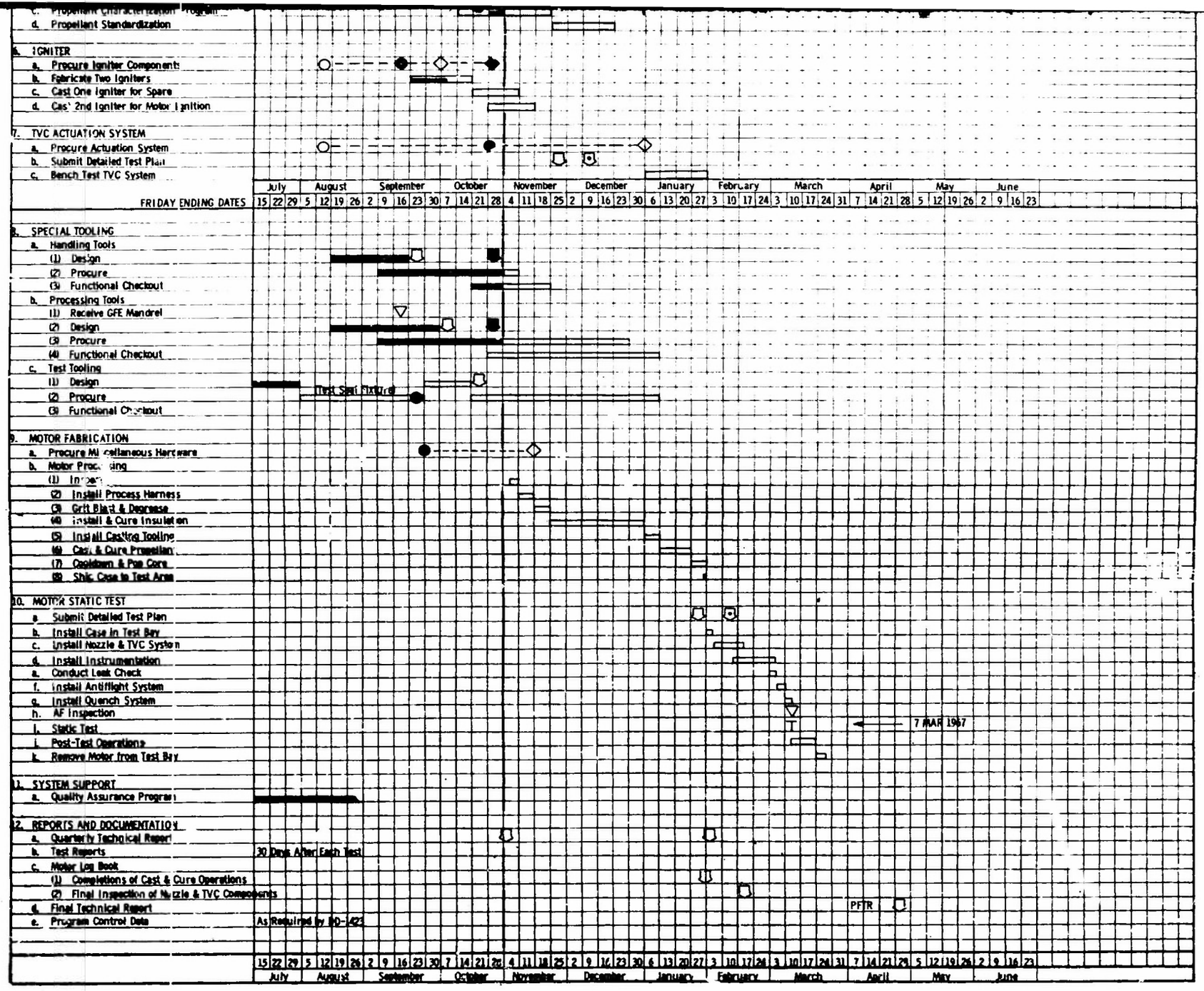

Figure 11-1. Program Schedule

Fabrication of the flexible seal was initially contracted to the Marlin-Rockwell Corporation (MRC). However, difficulties encountered by MRC in the rubber spray technique made it necessary to re-evaluate the seal fabrication. The MRC capability was found to be overloaded with the 156 in. size flexible seal in addition to work on the Stage III MINUTEMAN seal and the BSD 100 in. motor seal. The 156 in. seal contract with MRC was terminated during the week of 19 September. Reinhold Plastics has been contracted to assemble the seal under direct cognizance of Thiokol engineering personnel. Rubber and shim fabrication is in progress. The end ring forgings procured by MRC are available to this program and are being machined.

3. INSULATION AND LINER

All materials have been procured; the insulation and liner verification testing was initiated during this report period.

4. PROPELLANT PROCESSING AND TEST

All propellant materials have been procured; propellant characterization was initiated in October 1966.

5. IGNITION FABRICATION AND TEST

The ignition system long lead time items were ordered and fabrication was initiated during this report period.

6. TOOLING

Process tooling design is complete and procurement of all items has been initiated.

The test tooling design is 90 percent complete and procurement has been initiated for all completed items. The flexible seal test fixture design has been completed and this item is being fabricated.

7. PROGRAM COMPLETION

At the end of the report period, this program was 26.58 percent complete. Effort was initiated on all tasks as scheduled except for case refurbishment and motor processing.

B. WORK PROPOSED FOR THE NEXT REPORT PERIOD

In accordance with Exhibit B of this contract, AF 04(611)-11643, DD Form 1423, Sequence Number 70, the follcwing outline presents the work effort planned during the second quarter of the contract period of performance (November, and December 1966 and January 1967).

1. Motor and Component Design
   a. Submit flexible seal design.

2. Case Refurbishment
   a. Receive GFP case and handling rings.
   b. Case refurbishment.

3. Nozzle and Seal Fabrication
   a. Complete seal No. 1.
   b. Complete testing of seal No. 1.
   c. Complete fabrication of seal No. 2.

4. Insulation and Liner
   a. Complete compatibility testing.

5. Propellant Standardization

   a. Complete propellant characterization program.

   b. Complete propellant standardization.

6. Igniter

   a. Fabricate two igniters.

   b. Complete igniter testing.

7. TVC Actuation System

   a. Perform TVC actuation system bench testing.

8. Special Tooling

   a. Complete fabrication and checkout of handling tooling.

   b. Receive GFE mandrel.

   c. Continue test tooling design and fabrication.

9. System Support

   a. Continue quality assurance program.

10. Reports and Documentation

   a. Submit first quarterly report.

   b. Submit monthly contract status reports.

   c. Submit cost planning and appraisal charts.

Security Classification

DOCUMENT CONTROL DATA - R&D

(Security classification of title, body of abstract and indexing annotation must be entered when the overall report is classified)

1. ORIGINATING ACTIVITY (Corporate author) Thiokol Chemical Corporation Wasatch Division Brigham City, Utah 84302	2a. REPORT SECURITY CLASSIFICATION Confidential 2b GROUP 4

3. REPORT TITLE

Quarterly Technical Report No. 1
Development and Demonstration of an Omniaxial Flexible Seal Movable Nozzle for Thrust Vector Control (U)

4. DESCRIPTIVE NOTES (Type of report and inclusive dates)

Quarterly Technical Report (QTR) 11 Jul 1966 thru 31 Oct 1966

5. AUTHOR(S) (Last name, first name, initial)

C. G. Kennedy

6. REPORT DATE	7a. TOTAL NO. OF PAGES	7b. NO. OF REFS
November 1966	238	11

8a. CONTRACT OR GRANT NO.	9a. ORIGINATOR'S REPORT NUMBER(S)
b. PROJECT NO.	1166-13094
c.	9b. OTHER REPORT NO(S) (Any other numbers that may be assigned this report) TE2-237-11-6
d.	0416-64-1103 AFRPL-TR-66-315

10. AVAILABILITY/LIMITATION NOTICES Compliance with applicable security requirements is mandatory. In addition, this document may be further distributed by the holder only with the specific prior approval of: SSD (SSBS); Los Angeles Air Force Station, Air Force Unit Post Office, Los Angeles, California 90045

11. SUPPLEMENTARY NOTES	12. SPONSORING MILITARY ACTIVITY
N/A	Air Force Rocket Propulsion Laboratory Edwards California 93523

13. ABSTRACT

The primary objective of this program is the development and demonstration static test firing of an omniaxial flexible seal movable nozzle using a monolithic steel case, one million pound thrust class, 156 in. diameter motor, designated 156-9, as the test vehicle.

The flexible seal movable nozzle will consist of a fixed housing attached to the motor case and a movable housing interconnected by means of a flexible seal.

DD FORM 1 JAN 64 1473

Security Classification

14. KEY WORDS	LINK A		LINK B		LINK C	
	ROLE	WT	ROLE	WT	ROLE	WT
N/A						

INSTRUCTIONS

1. ORIGINATING ACTIVITY: Enter the name and address of the contractor, subcontractor, grantee, Department of Defense activity or other organization *(corporate author)* issuing the report.

2a. REPORT SECURITY CLASSIFICATION: Enter the overall security classification of the report. Indicate whether "Restricted Data" is included. Marking is to be in accordance with appropriate security regulations.

2b. GROUP: Automatic downgrading is specified in DoD Directive 5200.10 and Armed Forces Industrial Manual. Enter the group number. Also, when applicable, show that optional markings have been used for Group 3 and Group 4 as authorized.

3. REPORT TITLE: Enter the complete report title in all capital letters. Titles in all cases should be unclassified. If a meaningful title cannot be selected without classification, show title classification in all capitals in parenthesis immediatel. following the title.

4. DESCRIPTIVE NOTES: If appropriate, enter the type of report, e.g., interim, progress, summary, annual, or final. Give the inclusive dates when a specific reporting period is covered.

5. AUTHOR(S): Enter the name(s) of author(s) as shown on or in the report. Enter last name, first name, middle initial. If military, show rank and branch of service. The name of the principal author is an absolute minimum requirement.

6. REPORT DATE: Enter the date of the report as day, month, year; or month, year. If more than one date appears on the report, use date of publication.

7a. TOTAL NUMBER OF PAGES: The total page count should follow normal pagination procedures, i.e., enter the number of pages containing information.

7b. NUMBER OF REFERENCES: Enter the total number of references cited in the report.

8a. CONTRACT OR GRANT NUMBER: If appropriate, enter the applicable number of the contract or grant under which the report was written.

8b, 8c, & 8d. PROJECT NUMBER: Enter the appropriate military department identification, such as project number, subproject number, system numbers, task number, etc.

9a. ORIGINATOR'S REPORT NUMBER(S): Enter the official report number by which the document will be identified and controlled by the originating activity. This number must be unique to this report.

9b. OTHER REPORT NUMBER(S): If the report has been assigned any other report numbers *(either by the originator or by the sponsor)*, also enter this number(s).

10. AVAILABILITY/LIMITATION NOTICES: Enter any limitations on further dissemination of the report, other than those imposed by security classification, using standard statements such as:

(1) "Qualified requesters may obtain copies of this report from DDC."

(2) "Foreign announcement and dissemination of this report by DDC is not authorized."

(3) "U. S. Government agencies may obtain copies of this report directly from DDC. Other qualified DDC users shall request through _____."

(4) "U. S. military agencies may obtain copies of this report directly from DDC. Other qualified users shall request through _____."

(5) "All distribution of this report is controlled. Qualified DDC users shall request through _____."

If the report has been furnished to the Office of Technical Services, Department of Commerce, for sale to the public, indicate this fact and enter the price, if known.

11. SUPPLEMENTARY NOTES: Use for additional explanatory notes.

12. SPONSORING MILITARY ACTIVITY: Enter the name of the departmental project office or laboratory sponsoring *(paying for)* the research and development. Include address.

13. ABSTRACT: Enter an abstract giving a brief and factual summary of the document indicative of the report, even though it may also appear elsewhere in the body of the technical report. If additional space is required, a continuation sheet shall be attached.

It is highly desirable that the abstract of classified reports be unclassified. Each paragraph of the abstract shall end with an indication of the military security classification of the information in the paragraph, represented as *(TS), (S), (C), or (U)*.

There is no limitation on the length of the abstract. However, the suggested length is from 150 to 225 words.

14. KEY WORDS: Key words are technically meaningful terms or short phrases that characterize a report and may be used as index entries for cataloging the report. Key words must be selected so that no security classification is required. Identifiers, such as equipment model designation, trade name, military project code name, geographic location, may be used as key words but will be followed by an indication of technical context. The assignment of links, rules, and weights is optional.